HETEROGENEOUS CATALYSIS IN SUPERCRITICAL FLUIDS: THE ENHANCEMENT OF CATALYTIC STABILITY TO COKING

BY

FAIZA HASSAN

A thesis submitted to

The University of Birmingham

for the degree of

DOCTOR OF PHILOSOPHY

Department of Chemical Engineering

School of Engineering

The University of Birmingham

May 2011

UNIVERSITY OF
BIRMINGHAM

University of Birmingham Research Archive

e-theses repository

This unpublished thesis/dissertation is copyright of the author and/or third parties. The intellectual property rights of the author or third parties in respect of this work are as defined by The Copyright Designs and Patents Act 1988 or as modified by any successor legislation.

Any use made of information contained in this thesis/dissertation must be in accordance with that legislation and must be properly acknowledged. Further distribution or reproduction in any format is prohibited without the permission of the copyright holder.

ABSTRACT

Catalytic deactivation caused by coking was studied in ZSM5 and zeolite Y catalysts during the isomerisation of 1-hexene under sub and supercritical conditions.

The effects of varying temperature and pressure, from 220–250 °C and 10-70 bar respectively, on conversion and coke deposition were studied in both zeolites. TGA, DRIFTS, nitrogen sorption isotherms for fresh and coked catalysts and catalyst acidity measurements were compared.

In ZSM5 the catalyst was stable for 96 hours. TGA and DRIFTS results show coke deposits were mainly polyolefinic and the amount decreases considerably from 18.8 wt% in the subcritical region to 10 wt% in the supercritical region. In zeolite Y, decay in conversion was observed with the rate of deactivation being slower at supercritical conditions at 235 °C and 40 bar. Naphthalene hydrogenation on NiMo/γ-Al_2O_3 catalyst was also studied. The effect of temperature, pressure, varying naphthalene feed concentration and operating in sub and supercritical conditions were studied. Coke deposit decreased by 38 wt% in the supercritical region. SC CO_2 (T_c 31.04 °C, P_c 73.8 bar) was also used to re-activate the coked catalysts. This resulted in recovering 93% of the catalytic activity and 37% of the coke was effectively extracted by SC CO_2.

To my mother: Dr. Maryan Qasim. You are my courage, inspiration and hero.

To my father: Abdulaziz Hassan. You are my secure foundation.

To my husband: Abdiaziz E. Yusuf. You are my best friend and my rock.

To my siblings: Abbas, Zahra, Aisha, Rawdah and Ahmed. Thank you for being such a great loving and supportive family.

Acknowledgments

This thesis would not have been completed without the assistance and help of several individuals.

First and foremost, I would like to express my gratitude to my supervisor Dr. Joe Wood for his continuous support during my Ph.D study and research. I would like to thank him for his patience, enthusiasm and guidance at all times during the research and writing of this thesis. Without him, this thesis would not have been written or completed.

I would also like to thank my co-supervisor, Dr. Bushra Al-Duri for her continuous support and advice.

I would also like to thank Dr. Jiawei Wang for his immense support during the research.

Contents

LIST OF FIGURES

Figure 4.1. Calculated phase boundary for the isomerisation and oligomerisation reaction mixture in the first 24 hour: a) 235 ºC 10 bar; b) 235 ºC 40 bar; c) 235 ºC 70 bar; d) 220 ºC 40 bar; e) 250 ºC 40 bar. Symbols o represents the calculated critical points. Symbols x represent the reaction conditions.

Figure 4.2. 1-hexene conversion against time at 235 ºC and 10, 40 and 70 bar for 96 hours on stream.

Figure 4.3. a) Yield of isomers at 235 ºC and 10, 40 and 70 bar; b) yield of dimers at 235 ºC and 10, 40 and 70 bar; c) yield of trimers at 235 ºC and 10, 40 and 70 bar.

Figure 4.4. 1-Hexene conversion against time at 40 bar and 220, 235 and 250 ºC.

Figure 4.5. a) Yield of isomers against time at 40 bar and 220, 235 and 250 ºC; b) yield of dimers at 40 bar and 220, 235 and 250 ºC; c) yield trimers at 40 bar and 220, 235 and 250 ºC.

Figure 4.6. 1-Hexene conversion against time at 235 ºC, 10 bar and 40 bar.

Figure 4.7. Typical TGA and DTG profile of coked catalyst. The weight loss was divided into three stages based on DTG profile; a) room temperature – 200 ºC; b) 200 – 410 ºC; c) 410 – 1000 ºC.

Figure 4.8. DRIFTS spectra of the fresh catalyst and coked catalyst. a) 4000 – 600; b) 3800 – 3300; c) 3800 – 3700; d) 3000 – 2800; e) 1600 – 1000 cm^{-1}. The

dotted lines are for the fresh catalyst and the solid lines are for the coked catalyst.

Figure 4.9. XRD data for fresh (solid line) and coked samples run at 235 ºC and 10 bar (dashed line), 40 bar (dot-dash line) and 70 bar (dotted line) for 96 hours.

Figure 4.10. Nitrogen adsorption isotherms for fresh (solid line) and coked samples (□) run at 235 ºC and a) 10 or b) 40 bar for 8 hours,0.5g catalyst bed. Also shown are isotherms for coked samples (♦) where each point has been multiplied by a constant factor of a)1.38 and b)1.15.

Figure 4.11. Nitrogen adsorption isotherms for fresh (solid line) and coked

samples (□) run at 235 ºC and a) 10; b) 40; c) 70 bar for 96 hours, 10g catalyst bed. Also shown are isotherms for coked samples (♦) where each point has been multiplied by a constant factor of a)1.05 and b)1.3.

Figure 4.12 TPD spectra for catalyst coked at 235 ℃, 10 bar

Figure 5.1 a) 1-hexene conversion, on zeolite Y, versus time on stream at 40 bar and 220 ℃, 235 ℃, 250 ℃ after 6 hours on stream; b) Selectivity towards iC_6 and C_{12} on zeolite Y and ZSM5 at 220 ℃, 235 ℃, 250 ℃ after 6 hour on stream.

Figure 5.2. 1-hexene conversion, on zeolite Y, versus time at 235 ℃ and 10, 40 and 70 bar at 6 hour on stream. The data was fitted by Equation 5.1.

Figure 5.3. a) Selectivity towards iC_6 and C_{12}, on zeolite Y and ZSM5 at 235 ℃ and 10, 40 and 70 bar at 6 hour on stream; b) Effect of pressure on conversion of 1-hexene at 2 hours on stream on zeolite Y at 235 ℃.

Figure 5.4. TGA data for zeolite Y coked at 10 and 40bar after 6 hour on stream.

Figure 5.5 DRIFTS spectra of fresh and coked zeolite Y catalyst after 6 hour on stream at 235 ℃ and either 10 bar or 40 bar, (a) 4000-500 cm^{-1}, (b) 3800-3300 cm^{-1}, (c) 3000-2800 cm^{-1}, (d) 1750-1000 cm^{-1}.

Figure 5.6. Reversible regions of nitrogen adsorption isotherms for fresh (□) catalyst, and for spent catalysts (zeolite Y) after 6 hour on stream at 235 ℃ and, either 10 bar (+) or 40 bar (×). The solid lines are fits of the experimental data to two-component Langmuir and BET composite isotherm models as described in the text.

Figure 5.7. TPD spectra of fresh zeolite Y and coked zeolite Y at 235 ℃, 10 bar, 6 hour on stream with and without tertbutylamine and total free acidity

Figure 5.8 1-hexene conversion versus time at 235 ℃, 10 bar or 40 bar, 6 hour on stream in zeolite Y and ZSM5.

Figure 5.9. (a) Cis/trans-2-hexene ratio over zeolite Y and ZSM5 versus conversion of 1-hexene, (b) 3-Hexene/2-hexene ratio over zeolite Y and ZSM5 versus conversion.

Figure 6.1. HYSYS ternary VLE plots. a) at 300 ℃ and 80 bar; b) at 280 ℃ and 80 bar; c) at 250 ℃ and 80 bar.

LIST OF TABLES

NOMENCLATURE

X	Conversion (%)
k, k_0, k_1, k_2	Deactivation rate constant (h^{-1})
t	Time (h)
C, X_0	Constants
M_t	Amount of sorbate taken (cm^2/g)
M_∞	Equilibrium sorption (cm^2/g)
D	Fickean diffusion coefficient (cm^2/s)
a	Radius of the zeolite crystallite (μm)
β	Time constant
P_0	Steady state partial pressure (Pa)
P	Pressure at time t (Pa)
D_0	Intrinsic diffusion coefficient (cm^2/s)
$\theta = n_a/n_a^0$	Fractional saturation of the adsorbent
n_a	Amount adsorbed (cm^2/g)
n_a^0	Maximum amount adsorbed (cm^2/g)
D_0^*	Pre-exponential factor (s^{-1})
E_a	Activation energy (J/mol)

R	Gas constant (KJ/mol K)
T	Temperature (K)
x_i	Mole fraction of the ith component
a_i and b_i	Pure substance parameters in PR-EOS
k_{ij}	Binary interaction parameter for the (i,j) pair
Conv	Conversion (%)
Y_i	Isomers, dimers, and trimers (wt%)
C_i^0 and C_i	Initial and the final weight concentrations for compound i (%)
r	Reaction rate (mol/g_{cat}h)
F	Molar flow rate of the reactant (mol/s)
m_{cat}	Catalyst weight (g)
w_{200}	Weight of the sample at 200 ℃ (g)
w_{1000}	Weight of the sample at 1000 ℃ (g)
A_1, A_2	Peak area of desorption (TCD signal)
w_1, w_2	Sample weight for desorption (g)
c	Percentage coke (%)
V_{bed}	Volume of the catalyst bed (m^3)

ε_b	Bed voidage

CHAPTER 1

INTRODUCTION

1.1. Background and motivation

Catalyst deactivation is the loss of catalytic activity or selectivity over time and it is a continuing problem of great concern in the practice of industrial catalytic processes (Bartholomew, 2001). The time scales for catalyst deactivation can vary from seconds to years but it is inevitable that all catalyst will decay. There are many paths for catalyst deactivation and coking is one of the major paths (Bartholomew, 2001).

Coking refers to the deposition of non-volatile and usually undesirable organic compounds, which are formed during operation, onto the catalyst surface. The deposition of these compounds onto the catalyst surface results in the loss of catalyst activity due to the blockage of active sites and/or pores. This hinders the passage of reacting molecules from the bulk fluid outside the catalyst to the active sites within the catalyst pellets (Bartholomew, 2001).

Coke precursors have relatively low volatilities and can therefore form and build up on catalyst surfaces. At the relatively low subcritical densities and low solvent power of the gas-phase reacting mixtures the coke precursors are left behind on the catalyst surface and these precursors then undergo further reactions to consolidated graphite-like carbon (Baiker, 1999).

The use of supercritical fluids (SCFs) as reaction media can improve the solvating power of the reaction mixture. A fluid is termed supercritical when its temperature and pressure exceed the critical temperature and critical pressure

and at this point the liquid and vapour become one single phase (Baiker, 1999). Many of the physical properties of a supercritical fluid are intermediate between those of a liquid and a gas and SCFs have shown higher solubility than corresponding gases for heavy organics which may act as catalyst blocking agents and thereby deactivate catalysts and promote coking (Baiker, 1999). This deactivation may be suppressed by changing the working conditions from gas-phase to dense supercritical medium (Subramaniam, 2001). Furthermore enhanced diffusivities can accelerate the transfer of coke from the internal and external catalyst surface making the regeneration of catalysts deactivated by coking possible (Subramaniam, 2001).

Tiltscher *et al*. (1981) reported the possibility to regenerate heterogeneous catalysts by removing coke with SCFs in 1981 and since then the maintenance and reactivation of heterogeneous catalysts in SCFs have attracted a lot of interest. Saim and Subramaniam (1991), Subramaniam and McCoy (1994; 1995), Ginosar and Subramaniam (1995) and Clark and Subramaniam (1996; 1998; 1999) conducted extensive studies of catalytic 1-hexene isomerisation under supercritical conditions over the past decade and developed models for the associated catalyst deactivation issues. The results confirm that optimum conditions with maximum catalyst activity and effectiveness factor exist in the near-critical region.

1.2. Aim of the work

The purpose of this study was to investigate the alleviation of catalyst coke deposition by adopting SCFs as reaction media and to compare the effect of operating conditions in conventional reaction medium and supercritical fluid medium.

Zeolite ZSM5 and Y type catalysts were selected to study coke deposition during 1-hexene isomerisation. Comparisons are drawn between the different coking behaviours and acidity of ZSM5 and zeolite Y at sub and supercritical conditions. The effects of operating in supercritical fluid medium were also investigated during the hydrogenation of naphthalene on a pre-sulphided NiMo catalyst supported on alumina. The effects of temperature, pressure, H_2/naphthalene ratio in sub and supercritical conditions were studied and suitable conditions to maximise the catalyst lifetime are recommended.

Changes to the catalyst pore structure have also been studied in ZSM5, zeolite Y and NiMo catalyst samples. Tests were carried out to determine how the catalyst pore structure changed between the fresh unused catalyst, and the catalyst used under sub and supercritical conditions. The characterisation methods used include:

- Thermogravimetric analysis (TGA) used to determine the amount of coke deposited on the catalysts where the weight change in the catalysts during oxidation was measured.

- Diffuse Reflectance Infrared Fourier Transform Spectra (DRIFTS) used to investigate the nature of the active species and nature of coke deposits on the catalyst.
- X-ray diffraction (XRD) used to provide information regarding the chemical nature of the active phase and crystallinity of the catalyst.
- Temperature programmed desorption (TPD) used to analyse the acidity of the zeolite catalysts.
- Nitrogen adsorption-desorption isotherms, where the isotherms obtained from the adsorption measurements provided information on the surface area, pore volume, and pore size distribution of the catalyst samples.

Overall, the work in this project explores the advantages of using supercritical fluids to help remove coke from the catalyst surface in catalysts of an acidic nature such as zeolites. The greater solvating powers of supercritical fluids compared to gases and liquids and their potential in delaying catalyst deactivation is reported. The potential of using supercritical fluids in a multi component system is also explored in this work. Conditions to maximise the catalyst life time are reported as well as new data that add to previously published work.

1.3. Thesis layout

The work reported in this thesis is introduced in Chapter 1. In Chapter 2 a literature review which covers heterogeneous catalysis, catalyst deactivation issues, catalyst coking, the effect of SCFs on coking behaviour and on

minimizing coking is presented. The experimental design and operating procedures are covered in Chapter 3 with a discussion of the analytical tools used in this work. Chapter 4 contains the results of 1-hexene isomerisation over ZSM5 catalyst and Chapter 5 reports the results of 1-hexene isomerisation over zeolite Y catalyst. The hydrogenation of naphthalene is reported in Chapter 6 and a conclusion and future work recommendations are made in Chapter 7.

1.4. Publications

Publications resulting from work in this thesis are listed below, and copies are provided in Appendix 8.1.

1.4.1. Journals

1. F. Hassan, J. Wang, B. Al-Duri, S.P. Rigby, P.Chigada and J. Wood. Zeolite Y and ZSM5 Catalyst Deactivation During 1-Hexene Isomerization In Supercritical Fluids (2011). Industrial and Engineering Chemistry Research (Accepted for publication, Industrial and Engineering Chemistry Research, April 2011).

2. J. Wang, F. Hassan, J. Wood, B. Al-Duri, S.P. Rigby and P.Chigada (2009). Coke Formation and Characterization During 1-Hexene Isomerisation and Oligomerisation over H-ZSM5 Catalyst under Supercritical Conditions. *Industrial and Engineering Chemistry Research*, 48 (17), 7899-7909.

1.4.2. Conference presentations

1. F. Hassan, J. Wang, B. Al-Duri, S.P. Rigby, P.Chigada and J. Wood (2009). ZSM5 and Zeolite Y Catalyst Deactivation During 1-Hexene

Isomerisation in Supercritical Fluids. 8th World Congress of Chemical Engineering, Montreal, Canada, September 2009. Oral presentation.

2. F. Hassan, J. Wang, J. Wood, B. Al-Duri, S.P. Rigby and P.Chigada (2008). Studies of ZSM5 Catalyst Deactivation During 1-Hexene Isomerisation in Supercritical Fluids. IChemE Catalysis Subject Group Student Conference, Bath University, November 2008. Oral presentation.

CHAPTER 2

LITERATURE REVIEW

2.1. Introduction

2.1.1. Introduction to catalysis

The term ‘catalysis’ was introduced in 1835, and since then the concept of catalysis has evolved greatly (Fogler, 2006). Catalysis can be defined as ‘the change of the rate of chemical reactions under the action of certain substances’ (Boreskov, 2003). A catalyst is the substance that speeds up the rate of a reaction, by lowering the activation energy, without being consumed in the reaction (Fogler, 2006). They preserve their composition throughout the chemical reaction and are not wasted in the course of the catalysis. Furthermore, catalysts can speed up the reaction in a more selective manner which allows chemical processes to work more efficiently and with less waste (Fogler, 2006). This makes catalysts of great importance in industrial applications (Boreskov, 2003).

Catalysts are important in petroleum refining, large scale and fine chemicals production, pharmaceutical and food industries as well as having environmental applications (Boreskov, 2003). It is estimated that 90% of all commercially produced chemical products involve the use of a catalyst at some stage in their manufacture and that the sales of process catalysts were over $3.5 billion in the United States alone in 2007 (Fogler, 2006).

Since their discovery catalysts composition and chemical structure have become extremely varied. In industry many combinations of compounds are available and the most common materials used as catalysts are metals and oxides of various kinds (Bowker, 1998).

Most catalysts have three types of components; active component, support and promoters. The active components of the catalyst are usually metals and are responsible for the principal chemical reaction (Winterbottom and King, 1999). The catalyst support has many functions such as maintaining a high surface area for the active component which helps to disperse small quantities of valuable metals over a large surface area. There are many types of catalyst support but the most commonly used are alumina, silica, zeolite and carbon supports (Winterbottom and King, 1999). The catalyst promoter results in desirable activity, selectivity and stability effects. An example of catalyst promoter is in the ammonia synthesis process where the catalyst consists of iron doubly promoted by alumina and potassium to stabilise the surface planes of the catalyst (Winterbottom and King, 1999).

In industry, the catalysts used can range from zeolites to metallic catalysts and from activated carbon to different compounds like oxides, sulphides and halides. Other more complex catalysts consist of metal complexes with organic ligands or polyatomic compounds of protein nature such as enzymes (Boreskov, 2003). Some catalysts, such as enzymes, are only active with respect to a narrow group of reactions while other catalyst, such as those of an acid nature like zeolites, can catalyse a wide range of reactions ranging from isomerisation, hydrolysis, alcohol dehydration and alkylation (Boreskov, 2003).

Table 2.1 summarises some industrially important reactions and the type of catalysts used.

Table 2.1. Types of reactions and representative catalysts (taken from Fogler, 2006).

Reactions	**Catalysts**
Halogenation-dehalogenation	$CuCl_2$, AgCl, Pd
Hydration-dehydration	Al_2O_3, MgO
Alkylation-dealkylation	$AlCl_3$, Pd, zeolites
Hydrogenation-dehydrogenation	Co, Pt, Cr_2O_3, Ni
Oxidation	Cu, Ag, Ni, V_2O_5
Isomerisation	$AlCl_3$, Pt/Al_2O_3, zeolites

2.1.2. Introduction to heterogeneous catalysis

Catalytic processes can be classified as homogeneous or heterogeneous. In homogeneous catalysis the reactants and catalyst form one phase whereas in heterogeneous catalysis the reactants and catalyst are in different phases (Baiker, 1999). In heterogeneous catalysis the reactants, usually in gas or liquid-phase, flow through and adsorb onto a solid catalyst (Bowker, 1998). The reaction takes place and the reactants desorb and are taken downstream while the catalyst remains unchanged. As the catalyst and reactants are present in

different phases this makes mass and heat transfer through phase boundaries a necessary requirement for reaction (Baiker, 1999). The physical and chemical processes that take place in heterogeneous catalysis are illustrated in Figure 2.1 and are as follows:

1. Diffusion of gaseous reactant A from bulk gas-phase to the gas-liquid interface.
2. Absorption of A at the gas-liquid interface and ensuing diffusion to the liquid bulk phase.
3. Diffusion of reactants from bulk liquid-phase through stagnant fluid film surrounding solid catalyst particle.
4. Diffusion of reactants into porous network of the catalyst.
5. Adsorption of reactant.
6. Surface reaction.
7. Desorption of products.
8. Diffusion of products through porous network to outer surface of the catalyst.
9. Diffusion of products through boundary layer into bulk fluid.

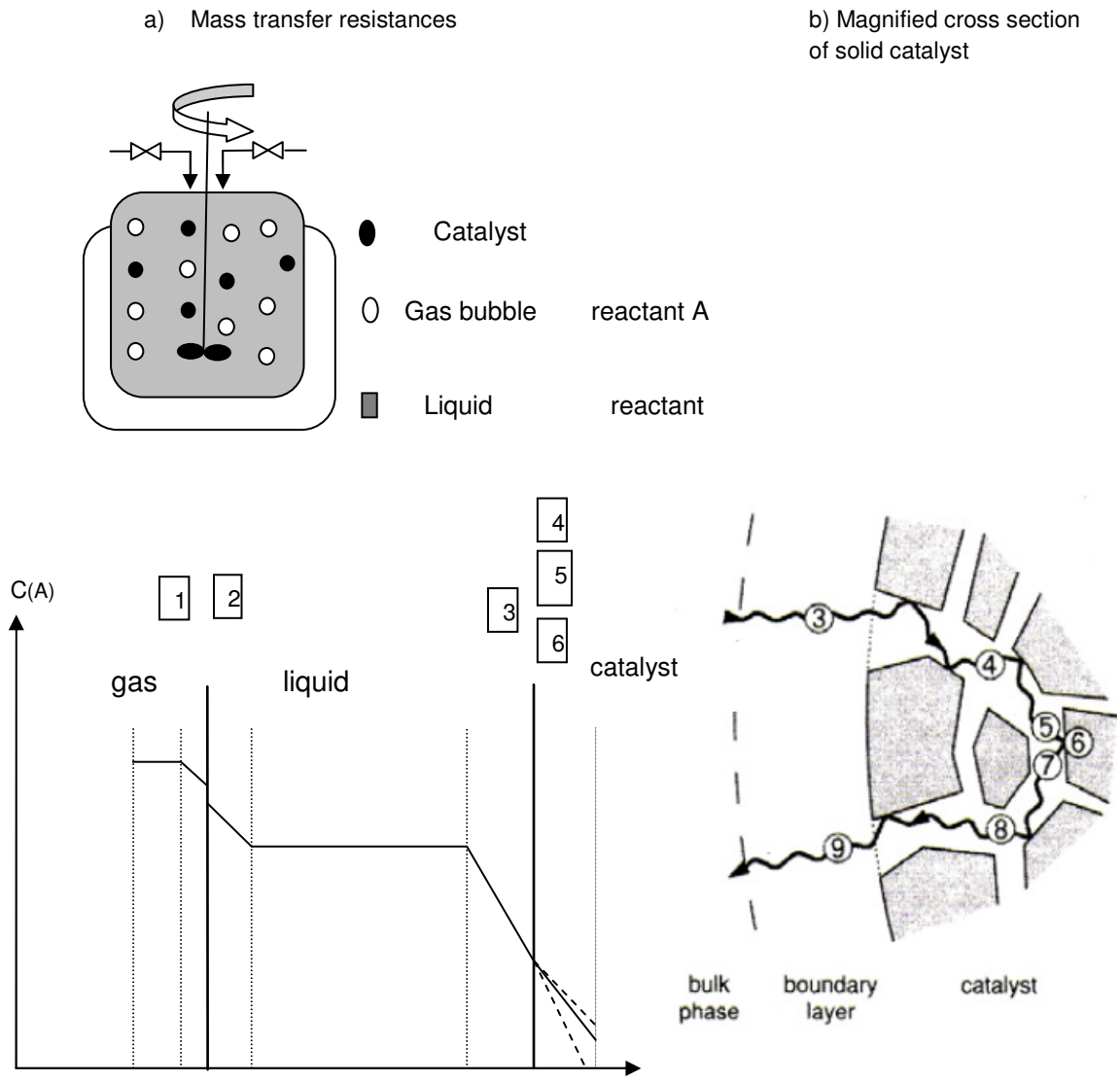

Figure 2.1. Sequence of physical and chemical steps occurring in heterogeneous catalytic gas-liquid reaction. a) Section of the reactor content consisting of a gas bubble and a solid catalyst particle and mass-transfer boundary layers at subcritical conditions; b) A magnified cross section of the catalyst particle. A concentration profile of reactant A is depicted on the bottom. (taken from Baiker, 1999). The physical and chemical processes taking place between 1, 2, 3, 4, 5, 6 are described on the previous page, 30.

2.2. Catalyst deactivation

The loss of catalytic activity and or selectivity over time is a continuing problem of great concern in the practice of industrial catalytic processes. Costs to

industry for catalyst replacement and process shutdown total billions of dollars per year, thus developing ways to prolong the catalyst life time has become at least as important as controlling the activity and selectivity of the catalyst (Froment, 1982).

It is inevitable that all catalysts will decay over time however the rate at which this occurs for a given catalyst and reaction depends greatly on reaction conditions such as temperature, pressure and reactant composition (Bartholomew, 2001). Whilst catalyst deactivation is inevitable for most processes, it can occur slowly in a well-controlled process and some of its immediate effects could be avoided, postponed or even reversed (Bartholomew, 2001). It is therefore very important to research deactivation issues such as rate and reaction conditions to aid the development, design and operation of commercial processes.

Much research has gone into the causes and mechanisms of catalyst deactivation. Many books (Hughes, 1984; Oudar and Wise, 1985; Butt and Petersen, 1988), comprehensive reviews (Bartholomew, 1984; Anderson and Boudart, 1984; Farrauto and Bartholomew, 1997; Bartholomew, 2001) and proceedings of international symposia (Hegedus and McCabe, 1980; Denny and Twigg, 1980; Bartholomew and Butt, 1991; Guisnet and Magnoux, 1994; Bartholomew and Fuentes, 1997; Cerqueira *et al.*, 1999; Masuda *et al.*, 1999) have been written on this topic.

There are many paths by which a catalyst can deactivate either through chemical, mechanical or thermal degradation (Bartholomew, 2001). The main

mechanisms of deactivation have been grouped into five main paths by Bartholomew (2001) and are summarised in Table 2.2. These are poisoning, fouling, thermal degradation, vapour-solid and/or solid-solid reactions and attrition or crushing.

Table 2.2. Summary of mechanisms of catalyst deactivation (Bartholomew, 2001).

Mechanism	**Type**	**Brief definition**
Poisoning	Chemical	Strong chemisorptions of species on catalytic sites which block sites for catalytic reaction.
Fouling/coking	Mechanical	Physical deposition of species from fluid phase onto catalytic surface and in catalyst pores.
Thermal degradation	Thermal	Thermally induced loss of catalytic surface area, support area and active phase support.
Vapour formation	Chemical	Reaction of gas with catalyst phase to produce volatile compounds.
Vapour-solid and solid-solid reactions	Chemical	Reaction of vapour, support or promoter with catalytic phase to produce inactive phase.
Attrition/crushing	Mechanical	Loss of catalytic material due to abrasion, loss of internal surface area due to mechanical induced crushing of catalyst particle.

Poisoning of a catalyst occurs due to the strong chemisorption of reactants, products or impurities on catalytic active sites which leads to the blocking of adsorption sites and changes in the geometric and electronic properties of the catalyst surface (Bartholomew, 2001). Figure 2.2 (taken from Bartholomew, 2001) illustrates the poisoning of metal surface by sulphur during the hydrogenation of ethylene. Poisoning occurs in many reactions including cracking; hydrogenation and Fischer-Tropsch synthesis and it can be either reversible or irreversible depending on the strength of poison adsorption. It is better to prevent poisoning of the catalyst rather than attempting to remove the poison from the catalyst afterwards. Poisoning can be prevented through purification of the reactant stream by means of scrubber or guard beds (Bartholomew, 1994).

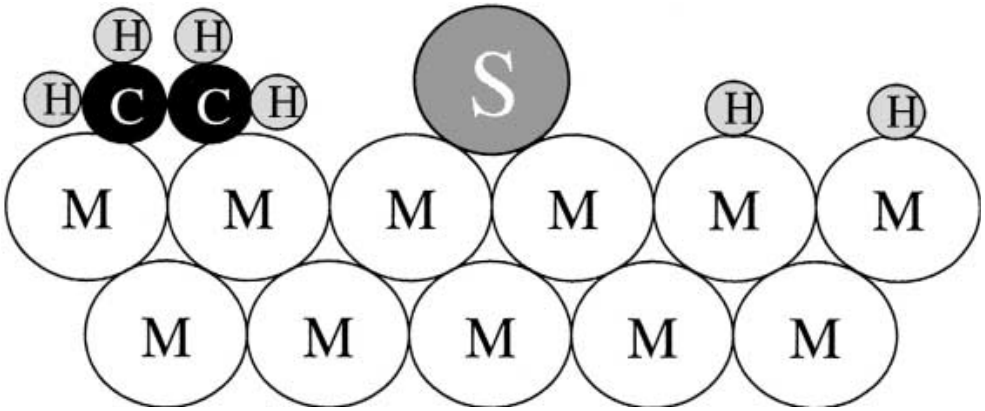

Figure 2.2. Conceptual model of poisoning by sulphur atoms of a metal surface during ethylene hydrogenation (Bartholomew, 2001).

Sintering or aging of the catalyst occurs due to the loss of active surface area resulting from prolonged exposure to high gas-phase temperatures (Fogler, 2006). Sintering is a thermally induced deactivation of catalysts resulting in a)

the loss of catalytic surface area due to crystallite growth of the catalytic phase (see Figure 2.3), b) the loss of the support area due to support collapse, c) the loss of catalytic surface area due to pore collapse on crystallites of the active phase (Farrauto and Bartholomew, 1997). Sintering processes take place at high reaction temperatures (above 500 ℃) and the presence of water vapour generally accelerates the process. An example of a process causing catalyst deactivation through sintering is the reforming of heptanes over platinum on alumina catalyst (Fogler, 2006).

Sintering is irreversible or difficult to reverse (Bartholomew, 2001). It is slow at moderate reaction temperatures and the key to preventing sintering processes is to maximise catalytic activity enough to enable operation at temperatures low enough that sintering rates are negligible (Bartholomew, 1994).

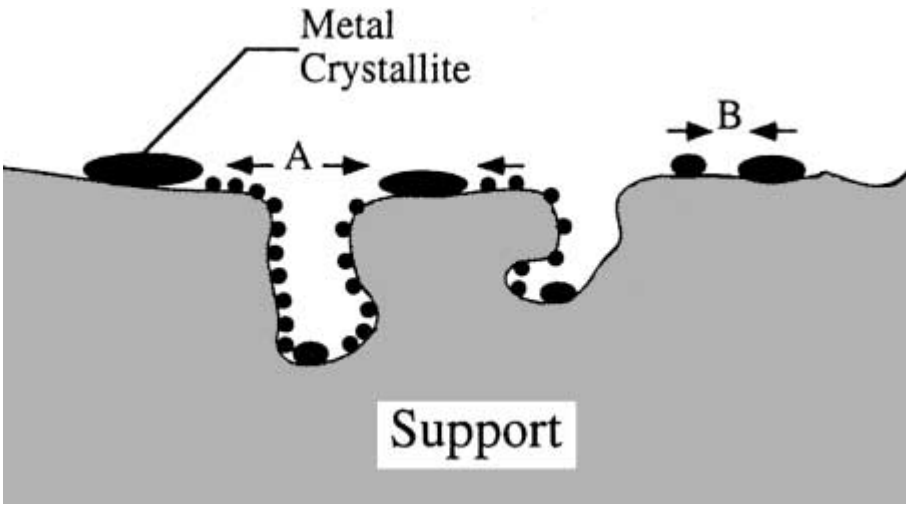

Figure 2.3. Two conceptual models for crystallite growth due to sintering by (A) atomic migration or (B) crystallite migration (taken from Bartholomew, 2001).

Mechanical failure of a catalyst can occur in different forms such as the crushing of catalyst due to a load or attrition (size reduction or breakup of

catalyst to produce fines) (Bartholomew, 2001). This is a common problem in fluid or slurry beds where erosion of catalyst particles occurs due to high fluid velocity and many commercial catalysts are vulnerable to mechanical failure because of the manner in which they are formed (Pham *et al.*, 1999). Ways in which to increase the resistance of catalysts to mechanical failure or attrition have been discussed in literature and Bartholomew (2001) made a detailed review.

2.3. Catalyst fouling or coking

Fouling or coking is the most common deactivation process in heterogeneous catalysis (Absi-Halabi *et al.*, 1991) and refers to the physical deposition of species from the fluid phase onto the catalyst surface (Bartholomew, 2001). Coke is produced by decomposition or condensation of hydrocarbons onto catalyst surfaces and its chemical structure varies depending on reaction type, catalyst type and reaction conditions (Bartholomew, 1982). Typically coke consists of polymerised heavy hydrocarbons, however coke forms may vary from high molecular weight hydrocarbons to primarily carbons such as graphite, depending upon the conditions under which the coke was formed and aged (Bartholomew, 1982). The deposition of coke onto the catalyst surface results in the loss of catalyst activity due to blockage of the active sites and/or pores and in more extreme cases it can result in the disintegration of the catalyst particles and plugging of the reactor voids (Albright and Baker, 1982).

The rate at which coke is accumulated in a given reaction under given conditions can vary significantly with catalyst structure and support as well as the nature of the reactants and products of the reaction (Guisnet and Magnoux, 1994; Karge, 1991). For example, linear alkanes and monoaromatics have a slow coking rate compared to alkenes and polyaromatics (Guisnet and Magnoux, 1994). This is because alkenes form highly reactive species while polyaromatics strongly adsorb on catalyst acid sites and thereby deactivating the catalyst (Guisnet and Magnoux, 1997). The rate of coking also depends on the operating conditions such as temperature and pressure. Higher temperature favours side reactions which lead to coke formation (Guisnet and Magnoux, 1997) and higher pressure generally favour the formation of higher molecular weight olefins (Quann *et al.*, 1998) and thus the rate of coking increases with reaction temperatures and pressures.

Menon (1990) classified catalytic reactions which are accompanied by coke formation as coke-sensitive or coke-insensitive. In coke-sensitive reaction, unreactive coke is deposited on active sites leading to activity decline. In coke-insensitive reactions relatively reactive coke precursors are formed on the active sites and are removed by gasifying agents such as hydrogen. Based on this classification it can be argued that the structure and location of coke are more important than its quantity in affecting catalytic activity. Examples of coke-insensitive reactions include Fischer–Tropsch synthesis, catalytic reforming, and methanol synthesis while catalytic cracking and hydrogenolysis; on the other hand, are examples of coke-sensitive reactions (Menon, 1990).

2.3.1. Mechanisms of coking reaction

The mechanism of coke formation depends on the catalyst type and is different for metal or metal oxides, sulphide catalysts and zeolites (Butt and Petersen, 1988). The mechanisms of coke formation and carbon deposition on metal catalysts from carbon monoxide and hydrocarbons are illustrated in Figures 2.4 and 2.5. Both Figures were taken from Bartholomew (1982).

Figure 2.4 shows that CO dissociates on metals to form Cα, an adsorbed atomic carbon; Cα can react to Cβ, a polymeric carbon film. The more reactive, amorphous forms of carbons formed at low temperatures (e.g. Cα and Cβ) are converted at high temperatures over a period of time to less reactive, graphitic forms.

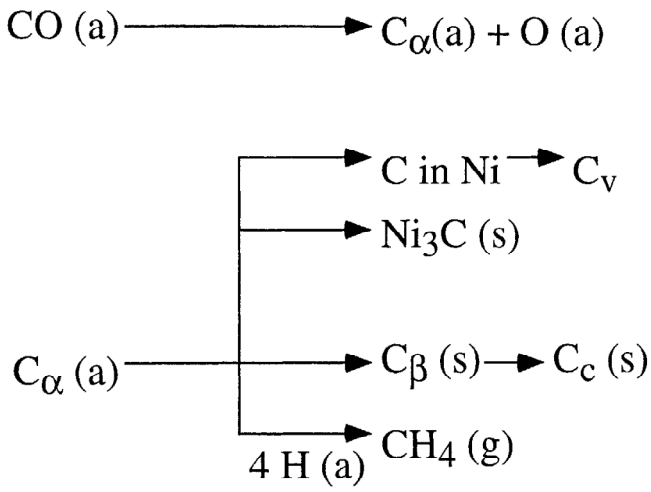

Figure 2.4. Formation, transformation and gasification of carbon on nickel (a, g, s refer to adsorbed, gaseous and solid states, respectively) (Bartholomew, 1982).

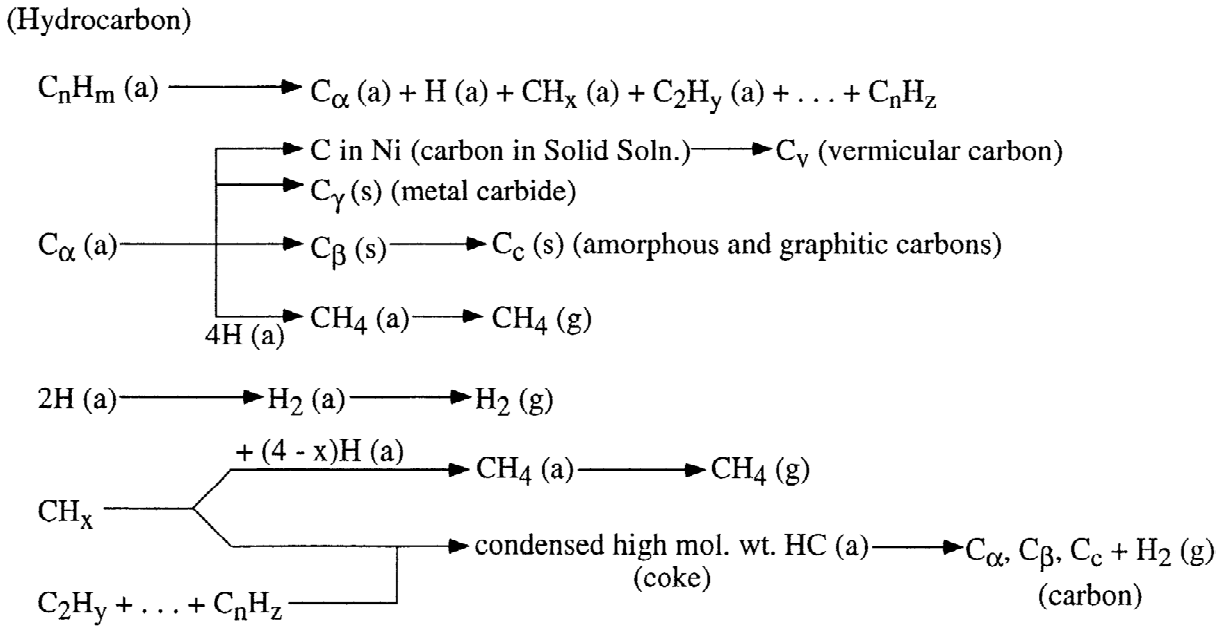

Figure 2.5. Formation and transformation of coke on catalyst metal surfaces (a, g, s refer to adsorbed, gaseous and solid states, respectively); gas-phase reactions are not considered (Bartholomew, 1982).

Coke formation on oxide and sulphide catalysts is a result of cracking reactions involving coke precursors such as olefins and aromatics being catalysed by acid sites (Gates *et al.*, 1979). Carbocation intermediates formed on catalytic acid sites further undergo dehydrogenation and cyclization reactions and react further to form higher molecular weight polynuclear aromatics which condense as coke (Naccache, 1985). This condensed coke may then deposit on catalytic and/or non catalytic surface area's (Menon, 1990).

Olefins, benzene and benzene derivates are all coke precursors; however the reactivity for coke formation is structure dependant (Appleby *et al.*, 1962). A study showed that the amount of coke deposited on a silica/alumina catalyst at 500 ℃ was 0.06, 3.8, 12.5 and 23 wt% for benzene, naphthalene, fluoranthene

and anthracene respectively (Appleby *et al.*, 1962). This indicates that the order of reactivity to coke increases from normal alkanes to branched alkanes to olefins to aromatics to polynuclear aromatics.

Figure 2.6 shows reactions of alkenes and aromatics leading to coke formation on oxide and sulphide catalysts. In Figure 2.6, reactions 1 – 3 show the polymerisation of olefins, reactions 4 – 8 show the cyclization from olefins, reactions 9 – 14 show the chain reaction formation of polynuclear aromatics which then condense as coke on the catalyst surface. The polynuclear carbocations shown in reactions 10 – 13 have a high stability and can therefore continue to grow on the surface for a long time before a termination reaction occurs through the back detonation of a proton (Bartholomew, 2001). Figure 2.6 was taken from Bartholomew (2001).

a. Polymerization of Olefins

Step 1: Reaction of olefin with Brønsted acid to form secondary carbenium ion:

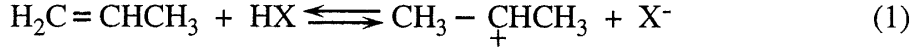

(1)

Step 2: Condensation reaction of a C_3 carbocation with a C_3 olefin to form a condensed, branched C_6 product with a carbenium ion:

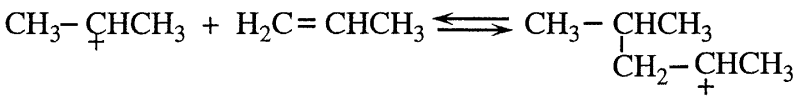

(2)

Step 3: Reaction of carbenium ion with Brønsted base to form olefin:

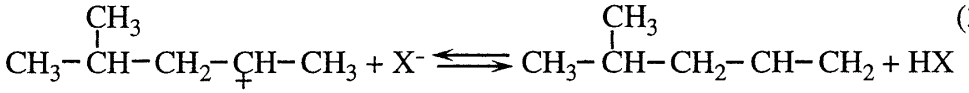

(3)

b. Cyclization from Olefins

Step 1: Formation of an allylic carbocation ion by reaction of a diene with a primary carbocation ion:

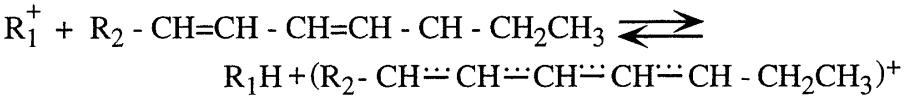

(4)

Step 2: Reaction of an allylic carbocation ion with a Brønsted base to form a triene:

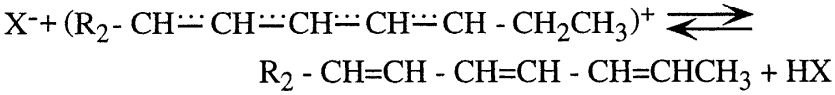

(5)

Step 3: Cyclization of a triene to form a substituted cyclohexadiene:

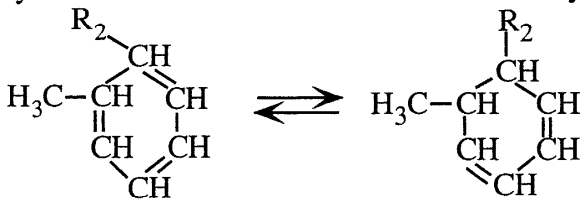

(6)

Step 4: Formation of a tertiary carbocation ion:

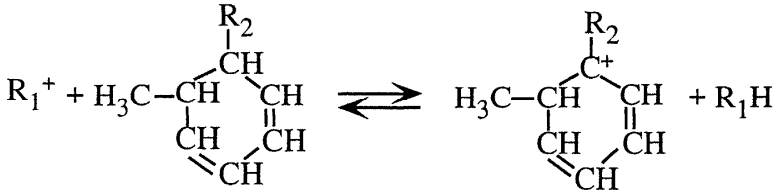

(7)

Step 5: Reaction of a tertiary carbocation ion with Brønsted base to form substituted benzene:

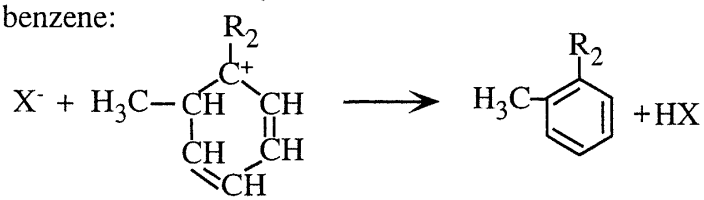

(8)

c. Formation of Polynuclear Aromatics from Benzene

Step 1: Initiation (protonation of benzene):

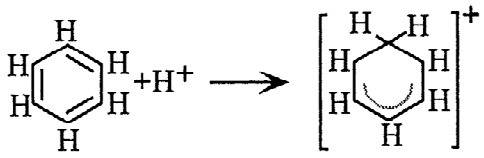

(9)

Step 2: Propagation (condensation reaction of carbocation with benzene followed by H abstraction):

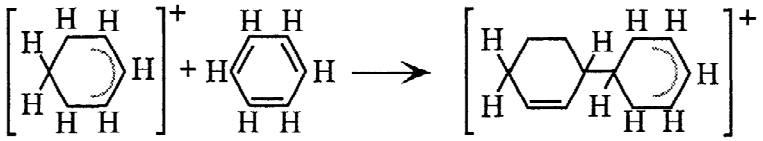

(10)

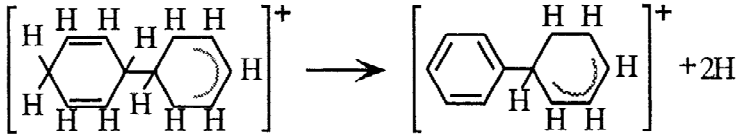

(11)

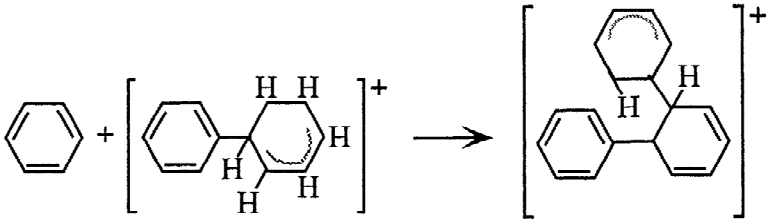

(12)

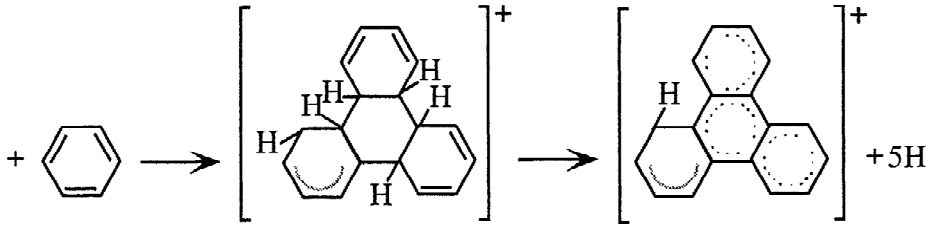

(13)

and so forth.

Step 3: Termination (reaction of carbocation with Brønsted base):

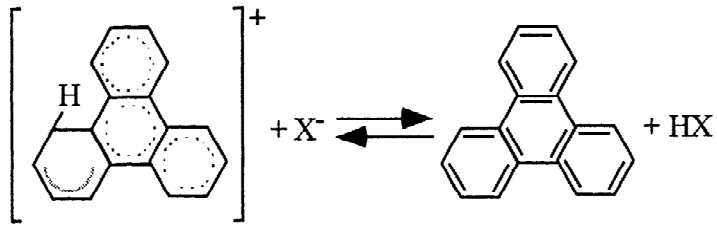

(14)

Figure 2.6. Coke-forming reactions of alkenes and aromatics on oxide and sulphide catalysts. a) Polymerisation of alkenes; b) Cyclization from alkenes; c) Formation of polynuclear aromatics from benzene (Bartholomew, 2001).

Figure 2.7 shows a model of coking where the coke encapsulates and plugs the pores of a supported metal catalyst. As coke is formed on the catalyst surface it can chemisorb strongly as a monolayer or physically adsorb in multilayers resulting in blocked access of reactants to catalyst surface sites (Rostrup-Nielsen and Trimm; 1977). Coke formation on the catalyst can also hinder the diffusion of reactants and/or products from the active site due to the decreasing pore size (Trimm, 1977). Furthermore coke can plug micro- and meso-pores blocking the access of reactants to many crystallites inside these pores (Trimm, 1983). Finally, in extreme cases, coke can build up to levels which stress and fracture the support material and cause the disintegration of catalyst pellets and plugging of reactor voids (Batholomew, 1982).

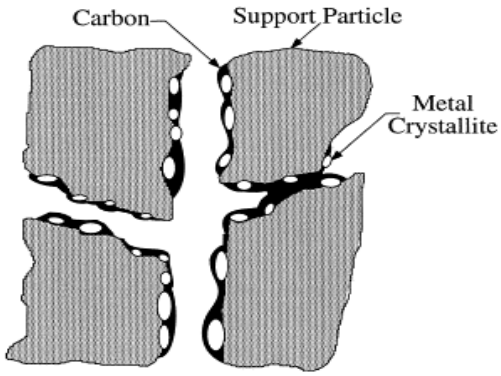

Figure 2.7. Conceptual model of fouling, crystallite encapsulation and pore plugging of a supported metal catalyst due to carbon deposition (taken from Bartholomew, 2001).

2.4. Catalyst deactivation kinetics

When studying catalyst deactivation, reaction kinetics are divided into two categories; nonseparable and separable kinetics (Fogler, 2006). In non-

separable kinetics the activity and kinetics cannot be separated and deactivation is described by a mechanism composed of several steps whereas in separable kinetics it is possible to study catalyst decay and reaction kinetics independently (Fogler, 2006).

Fogler (2006) summarises several examples of reactions with decaying catalysts and their decay laws. Such reactions are linear, exponential, hyperbolic and reciprocal power reactions with decays orders of zero, first or second order. Different types of deactivation lead to a certain type of decay law, for example one of the most commonly used decay laws for sintering is second order while poisoning and coking can lead to zero, first as well as reciprocal order decay (Farrauto and Bartholomew, 1997). Below is a brief summary of these decay laws and a more detailed explanation can be found in Fogler (2006).

For a reaction with a linear zero order decay the rate law is given as:

$$X = 1 - k_0 t \tag{2.1}$$

Where X is the conversion, k_0 is the deactivation rate constant and t is time.

Examples where such decay equation is used is the conversion of para-hydrogen on tungsten when poisoned with oxygen.

For a reaction with exponential first order decay the decay law is given as:

$$X = e^{-k_1 t} \tag{2.2}$$

Where X is the conversion, k_1 is the deactivation rate constant and t is time.

Examples where such decay equation is used include ethylene hydrogenation on copper catalyst poisoned with CO, paraffin dehydrogenation on $CrAl_2O_3$, cracking of gas oil and vinyl chloride monomer formation.

For a hyperbolic reaction with second order decay the decay law is given as:

$$\frac{1}{X} = 1 + k_2 t \quad (2.3)$$

Where X is the conversion, k_2 is the deactivation rate constant and t is time.

Examples where such decay equation is used include vinyl chloride monomer formation, cyclohexane dehydrogenation on Pt/Al_2O_3 and isobutylene hydrogenation on nickel.

In this work, the coking reaction was assumed to be first order with the resulting deactivation leading to an exponential decay in conversion (Fogler, 2006). The deactivation observed in this work was fitted by the following equation (Wang *et al.*, 2009):

$$X = C + X_0 e^{-kt} \quad (2.4)$$

Where X is the conversion, C and X_0 are constants, k is the deactivation rate constant and t is time in hours. This is further discussed in Chapters 4, 5 and 6.

2.5. Zeolite catalysts

Zeolites are crystalline silicates and aluminosilicates linked through oxygen atoms, producing a three-dimensional network containing channels and cavities of molecular dimensions (Corma, 2003). Zeolites are useful catalysts in a large

variety of reactions ranging from cracking, isomerisation, alkylation and polymerisation. They have been used as cracking catalysts since the early sixties and their importance has grown in the past decade. They also offer new opportunities in the chemical and fine chemicals field (Corma, 2003).

Zeolites possess a unique micro-porous structure, which allows the ability to discriminate reactants and products by size and shape (Corma, 2003). Zeolites and zeolite related materials have a large number of available structures ranging from very narrow pore systems to pores large enough to process heavy molecules (Guisnet and Magnoux, 1997). Zeolites have the ability to control the geometry of the structure and its composition, as well as the capability to act as host for a variety of guests with catalytically attractive properties such as transition metal ions or complexes (Guisnet and Magnoux, 1994). Zeolites are also easily modified through a range of procedures from ion exchange to hydrothermal treatments or chemical vapour deposition, so that their properties are tailored to the particular application needed (Corma, 2003).

2.5.1. Geometry of zeolite catalysts

Zeolites possess well defined pore structures within which most active sites are located and access to the cavities is possible through voids of various sizes (Ribeiro *et al.,* 1995). This geometrical property of zeolites, also known as shape selectivity, allows it to be shape and size selective in catalytic molecular re-arrangements and is a major factor in their application (Ribeiro *et al.*, 1995).

In shape selective catalysis there is an interaction between the shape, size and configuration of reactants, transition states and products and the dimension, geometry and tortuosity of the channels and cages of the zeolite catalyst. Csicsery and Rabo (Ribeiro *et al*., 1995) categorised the shape-selectivity of zeolites into three main effects:

1. Reactant selectivity. As illustrated in Figure 2.8a, this occurs when some of the feed molecules are too bulky to diffuse through the zeolite pores and thus are prevented from reacting further. As is illustrated in Figure 2.8a reactant *i* can diffuse through the zeolites pores whereas reactant *ii* is a branched molecule and therefore too bulky to diffuse through the zeolite pores. Therefore reactant *ii* would be prevented from reacting further.
2. Product selectivity. Figure 2.8b shows this effect, where a certain bulky product molecules cannot diffuse through the zeolite pores. An example of product selectivity of zeolite catalysts is during the production of para-aromatic compounds on ZSM5 based catalysts (Ribeiro *et al.,* 1995). Figure 2.8b illustrates a para-aromatic easily diffusing out of the zeolite pores whereas an ortho-aromatic remains in the pores due to diffusional limitations.
3. Restricted transition state selectivity. In this type of selectivity, certain reactions are prevented from occurring as some transition state in the reaction pathway requires more space than is available in the zeolite void volume (Ribeiro *et al.,* 1995). This plays an important role in the deactivation by coking as certain coke precursor molecules cannot form in certain zeolite pores. An example where such an effect takes place is in the isomerisation of xylenes on ZSM5 where transalkylation is almost absent due to the restriction

on the formation of bimolecular complexes in the narrow pores of ZSM5 (Ribeiro *et al.,* 1995).

a)

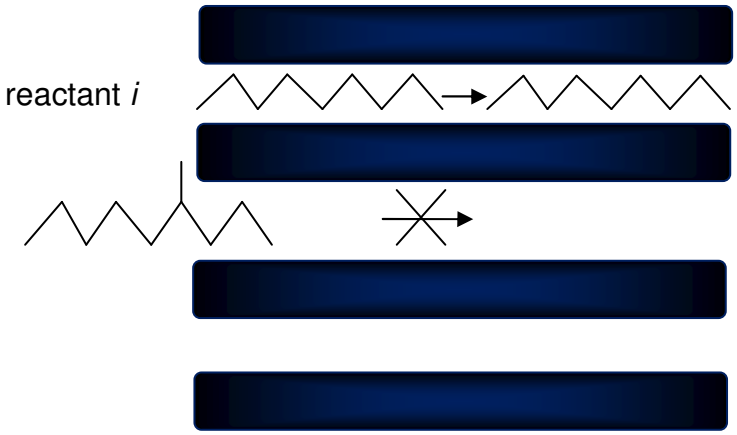

b)

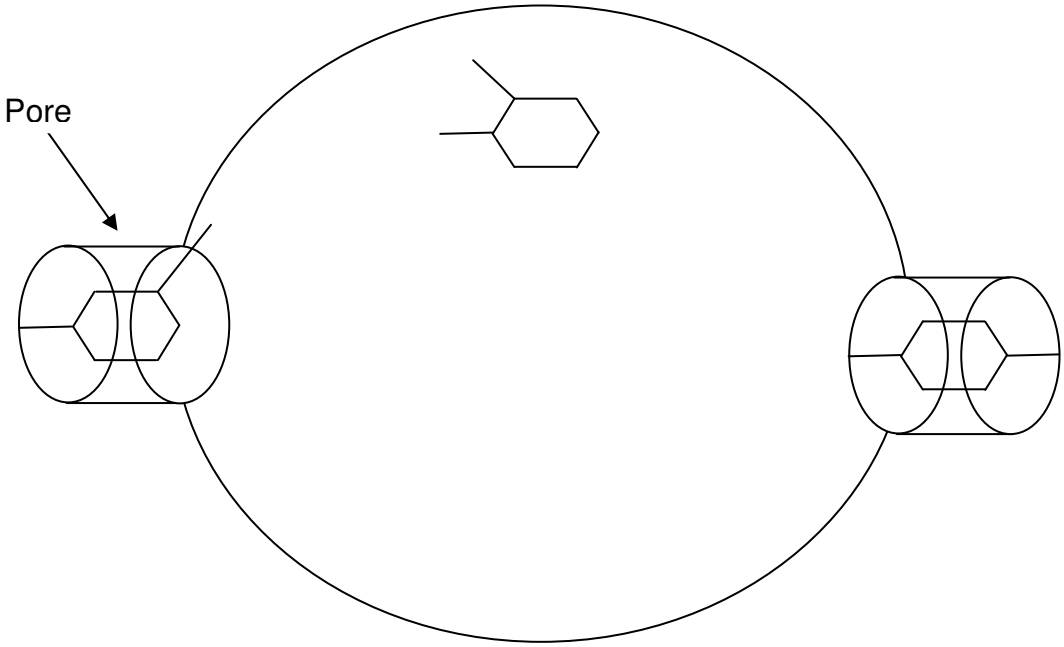

Figure 2.8. Shape selective catalysis. a) Reactant selectivity; b) Product selectivity (Figure taken from Ribeiro *et al.,* 1995).

Ribeiro *et al.* (1995) wrote an extensive review on the structure-activity relationship in zeolites and reviewed other smaller molecular shape-selectivity effects; however such detail is beyond the scope of this review.

On the basis of pore structure; Y type, ZSM5 and mordenite are three important zeolites from the catalytic and industrial point of view (Guisnet and Magnoux, 1997) and in this research ZSM5 and zeolite Y were selected to study. Zeolite Y belongs to the faujasite class of zeolites and possesses a three dimensional 12-membered-ring pore system. It belongs to the group of large pore zeolites and its pore system consists of supercages (spherical cages). These have a diameter of 1.3 nm connected tetrahedreally with four neighbouring cages through windows with a diameter of 0.74nm as is illustrated in Figure 2.9a (Abbot and Wojciechowski, 1984).

ZSM5 has pore structures and dimensions which are significantly different from those in faujasites. ZSM5 belongs to the group of pentasils and has much smaller pores (5.3 Å – 5.6 Å) compared to zeolite Y (7.4Å) (Abbot *et al*, 1985). Figure 2.9b shows that ZSM5 has a 10-membered oxygen ring with pores of uniform dimensions. ZSM5 shows high shape-selectivity in catalytic reactions as its channel diameter is approximately in the dimensional range of aromatic molecules (Ribeiro *et al.*, 1995). These geometrical constraints pose a restriction on the formation of any large polynuclear hydrocarbons which are responsible for coking (Ribeiro *et al.,* 1995). Due to its shape selectivity, acidity and low coke formation ZSM5 and ZSM5 based catalysts have become a success in industrial applications (Bartholomew, 2001).

a)

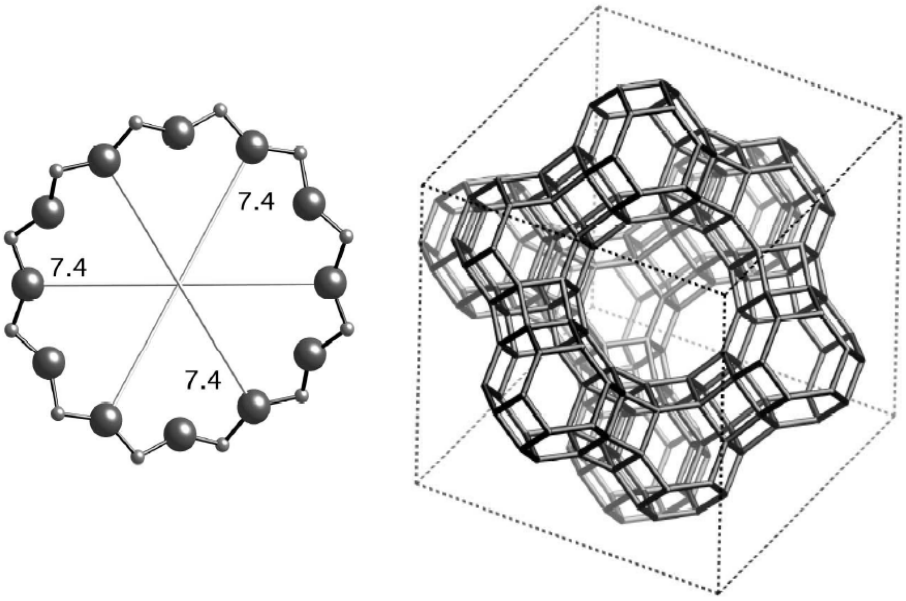

b)

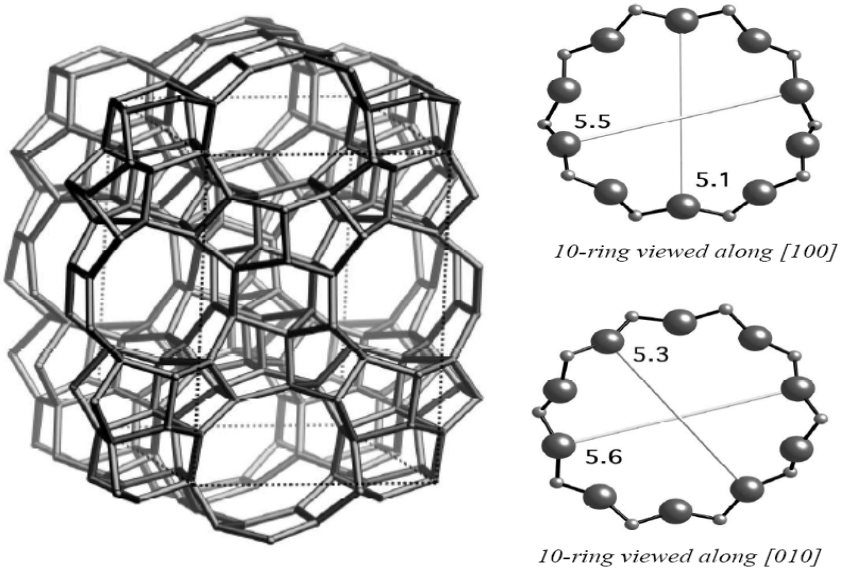

Figure 2.9. a) Zeolite Y catalyst structure; b) ZSM5 catalyst structure (Figure taken from Baerlocher *et al.*, 2001).

2.5.2. Diffusion in zeolites

The diffusion in zeolites differs from the molecular and Knudsen diffusion regimes and is referred to as configurational diffusion (Ribeiro *et al.,* 1995).

Configurational diffusion is characterised by very small diffusivities (10^{-8} – 10^{-14} cm^2/s), strong dependence on the size and shape of the guest molecules, high activation energies (10 – 100 kJ/mol) and strong concentration dependence (Roque-Malherbe *et al.*, 1995). In configurational diffusion, a small change in molecule to pore size relationship can induce a very large change in the diffusion coefficient (Ribeiro *et al.,* 1995). An example is the hydrogenation of trans-butene-2 over platinum-zeolite catalyst. The size difference between the cis and trans isomer is 2 Å, whereas the diffusivity of trans-but-2-ene is 200 times larger than that of cis-2-butene (Ribeiro *et al.,* 1995).

Roque-Malherbe *et al.* (1995) studied the diffusion of aromatic molecules of different sizes within the pores of H-ZSM5, H-Beta and H-MCM-22 zeolites using Fourier Transform Infrared Spectroscopy (FTIR) technique. H-Beta zeolite is a tri-directional high silica zeolite formed by 12-membered ring channels; H-MCM-22 has a pore system that consists of two independent sets of 10-membered ring opening pores (Roque-Malherbe *et al.*, 1995).

Roque-Malherbe *et al.* (1995) obtained the Fickean diffusion coefficient from the following Equation 2.5.

$$\frac{M_t}{M_\infty} = 1 - \frac{3D}{\beta a^2}\left[1 - \left(\frac{v\beta a^2}{D}\right)\cot\left(\frac{v\beta a^2}{D}\right) + \frac{6\beta a^2}{\pi D}\sum(exp - \frac{(Dn^2\pi^2 t)}{a^2})/2\left(n^2\pi^2 - \frac{\beta a^2}{D}\right)\right] \quad (2.5)$$

Where M_t is the amount of sorbate taken at time t, M_∞ is the equilibrium sorption value, D is the Fickean diffusion coefficient, a is the radius of the zeolite crystallite and β is a time constant which describes the evolution of the sortive partial pressure in the dead space of the IR cell:

$$P = P_0 (1-\exp(-\beta t)) \quad (2.6)$$

Where P_0 is the steady state partial pressure and P is the pressure at time t.

Roque-Malherbe *et al.* (1995) corrected the obtained Fickean diffusion coefficient, D, to obtain the intrinsic diffusion coefficients, D_0, with Equation 2.7 below.

$$D_0 = D (1-\theta) \quad (2.7)$$

Where $\theta = n_a/n_a^0$ is the fractional saturation of the adsorbent, n_a is the amount adsorbed and n_a^0 is the maximum amount adsorbed.

The intrinsic D_0 for benzene, toluene and ethylbenzene in H-ZSM5, H-Beta and H-MCM-22 catalyst, was calculated with Equation 2.5 using the uptake they measured in the FTIR spectrometer and corrected by Equation 2.7. The intrinsic diffusion coefficient, D_0, values are given in Table 2.3 (taken from Roque-Malherbe *et al.*, 1995).

Table 2.3. Intrinsic diffusion coefficients (D_0 x 10^9 cm^2/s) of benzene, toluene and ethylbenzene in H-ZSM5, H-Beta and H-MCM-22 at 127 ℃ (Roque-Malherbe *et al.* 1995).

D_0			
Sortive	**H-ZSM5**	**H-Beta**	**H-MCM-22**
Benzene	8	8.2	1.4
Toluene	6	10	1.6
Ethylbenzene	5	2.5	1.2

Roque-Malherbe *et al.* (1995) then calculated the activation energy (E_a) and pre-exponential factor (D_0^*) using the Eyring equation below in Equation 2.8.

$$D_0 = D_0^* \exp\left(-\frac{E_a}{RT}\right) \quad (2.8)$$

Where D_0 is the intrinsic diffusion coefficient, D_0^* is the pre-exponential factor, E_a is the activation energy, R is the gas constant and T is the temperature.

Table 2.4. Diffusional activation energies and pre-exponential factors for the diffusion of benzene, toluene and ethylbenzene in H-ZSM5, H-Beta and H-MCM-22 (taken from Roque-Malherbe *et al.*, 1995).

Zeolite	**Sortive**	**10^4 D_0^*(cm^2/s)**	**E_a (J/mol)**
H-ZSM5	Benzene	0.3	28
	Toluene	0.05	21
	ethylbenzene	0.2	26
H-Beta	Benzene	2.2	32
	Toluene	3.3	36
	Ethylbenzene	9	41
H-MCM-22	Benzene	0.004	19
	Toluene	0.024	26
	Ethylbenzene	0.006	20

Overall Roque-Malherbe *et al.* (1995) concluded that diffusion of aromatic hydrocarbons in silica acid zeolites is not related to strong adsorption. Benzene, toluene and ethylbenzene can move freely in the frameworks of H-ZSM5 and H-Beta catalyst. Other aromatic hydrocarbons such as m-xylene and o-xylene move slowly in H-ZSM5 and freely in H-Beta frameworks. For H-MCM-22 the diffusion process is not as rapid as H-ZSM5 or H-Beta and this was explained by the presence of big cavities with four entrance windows, where the aromatic hydrocarbon molecule spends a residence time higher than in a straight or sinusoidal channel (Roque-Malherbe *et al,*. 1995).

2.5.3. Acidity of zeolite catalysts

Acidity can be achieved in zeolites because of the charge balance in the zeolitic frameworks where aluminium exists in tetrahedrally coordinated silicon structures which require the existence of compensating cations that are located in the porous system of the structure (Ribeiro *et al.*, 1995).

To evaluate the acidity of a zeolite in relation to a particular application; several parameters such as the structure, the total number of Brønsted (proton donor) and Lewis (electron pair acceptor) sites, the strength and distribution of these sites as well as the location of these sites has to be taken into account (Guisnet and Magnoux, 1994). Lewis acid sites have an influence on the strength of the Brønsted acid sites through an inductive effect where the Lewis sites increase the strength of the Brønsted acid sites and in turn result in an enhancement of the catalytic activity (Ribeiro *et al.,* 1995). Furthermore, the catalytic activity per

strong acid site and the acidity of the Brønsted sites is dependent on the chemical composition of its environment such as the Si/Al ratio (Ribeiro *et al.,* 1995). Generally an increase in the Si/Al ratio results in a decrease in the total number of acid sites as well as an increase in strong Brønsted acid sites (Ribeiro *et al.*,1995).

Acidity can be introduced by cations ion exchange through a) ion exchange with NH_4^+ followed by calcination to produce the proton form of the zeolite, b) the hydrolysis of ion-exchanged polyvalent cations followed by partial dehydration and c) the reduction of metal ions to a lower valency state (Humphries *et al.*, 1993).

Figure 2.10 shows the treatment of zeolite Y with ammonium salts, followed by calcination, which decomposes the NH_4^+ ion to NH, gas and H^+ (Humphries *et al.*, 1993). In the zeolite the proton bonds with oxygen atoms in the lattice to form –OH groups and in this form the zeolite can transfer a proton to an adsorbed hydrocarbon. These active sites are also known as Brønsted acid sites (Szostak, 1991).

Lewis acid sites can be formed by further dehydroxylating (eliminating water) Brønsted acid sites at temperatures in excess of 500 ℃ (Ribeiro *et al.*, 1995) as is shown in Figure 2.11. Both Figures 2.10 and 2.11 were taken from Humphries *et al.* (1993).

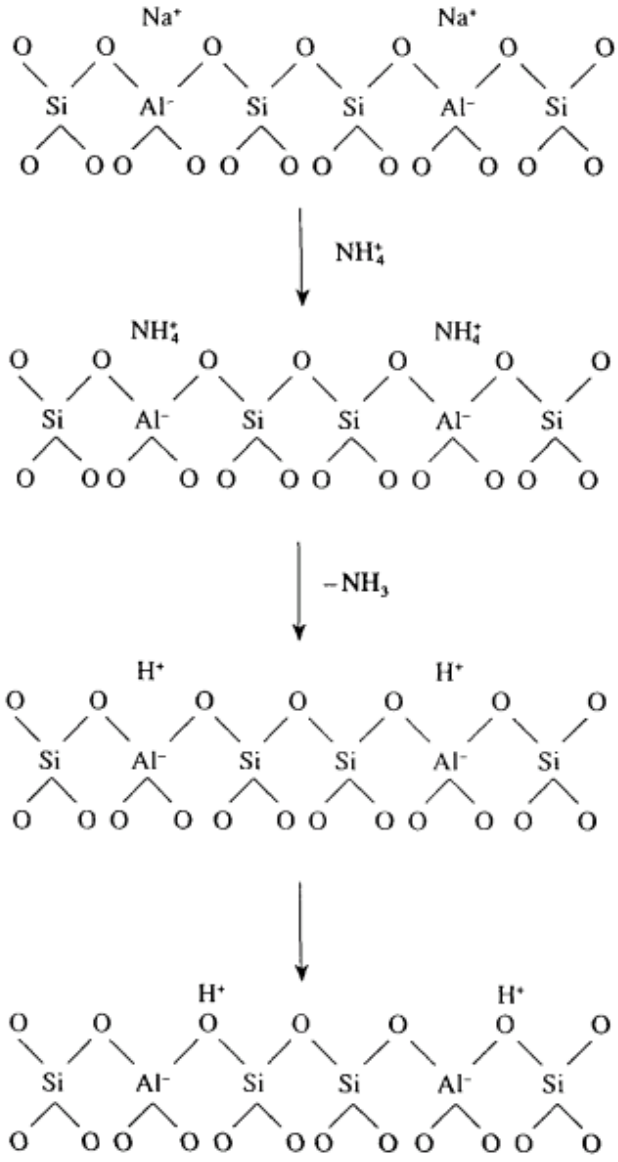

Figure 2.10. The formation of Brønsted acid sites in zeolite Y (Humphries *et al.*, 1993).

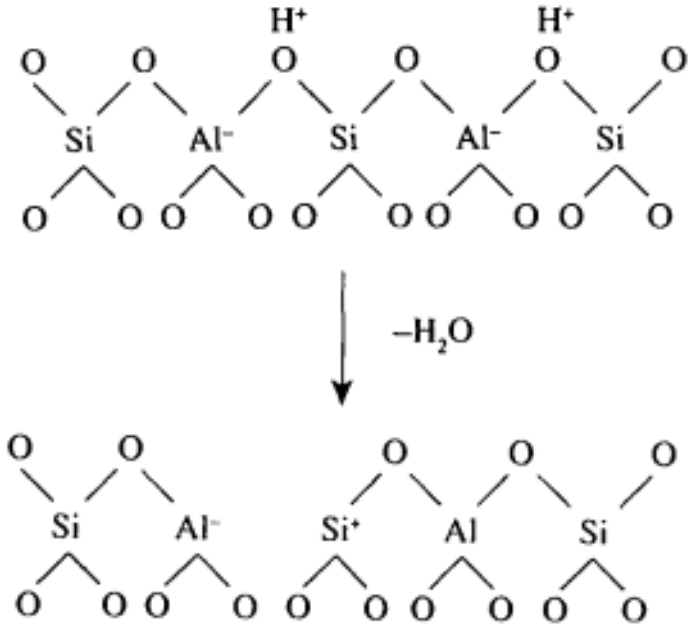

Figure 2.11. The formation of Lewis acid sites from Brønsted acid sites (Humphries *et al.*, 1993).

Ward (1968) studied the effect of the calcination temperature on the acidic character of zeolite Y by spectrum of chemisorbed pyridine. Ward (1968) reported that Brønsted acidity increases as the calcination temperature is increased from 300 ℃ to 425 ℃. This then remains constant up to calcination temperatures of 600 ℃ after which it declines sharply as the temperature is increased to 800 ℃. Lewis acidity remains weak and constant until the calcination temperature reaches 550 ℃; this then increases rapidly as the Brønsted acidity decreases (Ward, 1968). Ward (1968) reported that the elimination of water leads to the creation of one Lewis acid site from every two Brønsted acid site.

As a result, in this work NH_4-ZSM5 and zeolite Y were converted to the proton form by calcinations at 500 ℃ to maximise Brønsted acidity.

The acidity of H-ZSM5 catalyst has been reported to be between 0.48 – 0.66 mmol/g whereas the acidity of zeolite Y was reported to be between 0.62 – 0.96 mmol/g (Salguero *et al.*, 1997; Minchev *et al.*, 1989). Choudhary (Ribeiro *et al.*, 1995) compared the acidity for several zeolites and stated that according to the amount of strong acid sites; H-Y and H-M are more acidic than H-ZSM8 which is more acidic than H-ZSM5 which in turn is more acidic than H-ZSM11.

2.5.4. Coking in zeolites

Coking is one of the main causes of zeolite catalyst deactivation (Guisnet and Magnoux, 1994) and many studies (Rollmann and Walsh, 1979; Guisnet and Magnoux, 1989; Grotten *et al.*, 1992; Bellare and Dadyburjor, 1993; Uguina *et al.*, 1993; Guisnet and Magnoux, 1994; Li *et al,*. 1994) have focused on coke formation during hydrocarbon reactions in zeolites. The studies have shown that zeolite catalyst deactivation by coking is mainly due to a) acid sites coverage and/or b) pore blockage.

In zeolites, coking can lead to great loss of activity and the two main factors, which play an important role in coking are the pore size and acidity of the zeolite (Bartholomew, 2001). Coke formation involves bimolecular reactions such as condensation and hydrogen transfer between bulky molecules. Due to the size of certain zeolite pores, such as ZSM5, these coke forming processes are limited (Guisnet and Magnoux, 1994). Bartholomew (2001) reported that the

yield to coke in fluid catalytic cracking is 0.4% for ZSM5 catalyst with pore diameters of 0.53 – 0.56 nm compared to 2.2% for Zeolite Y catalyst with pore diameters of 0.72 nm.

The rate and extent of coke formation is also influenced by the acid strength density of the catalyst. For any fixed pore diameter, the coking rate increases with increasing acid site density. This is because the average acid site density has an important role to play in the balance between monomolecular and bimolecular reactions (Bartholomew, 2001). For example in Y type catalyst, an increase in the acid site density results in an enhancement to coke selectivity (Ribeiro *et al.*, 1995).

The deactivating effect of coke molecules is also influenced by acidity. For example, H-ZSM5 has acid sites of identical strength, hence the greater coke content the greater the deactivation effect (Guisnet and Magnoux, 1997). In contrast, zeolite Y type has acid sites of different strengths; hence the strong and most active acid sites are deactivated first, which results in a large deactivating effect at even small coke contents (Guisnet and Magnoux, 1997).

Guisnet *et al.* (1997) reported the composition and mode of formation of coke in zeolite catalysts. Guisnet *et al.* (1997) distinguished between coke formed at low and high reaction temperatures. At low reaction temperature (120 ℃), the H/C ratio of the coke compounds was close to that of the reactants indicating that this is a result of condensation reactions. Coke formed on HY, H-ZSM5 and 5A zeolites from propene at 120 ℃ were branched aliphatic or alicyclic hydrocarbons with no aromatics observed. Olefin oligomerisation was the main

reaction involved in the formation of these compounds and most of these coke compounds were located inside the zeolite pores. At higher reaction temperatures of 450 ℃, Guisnet *et al.* (1997) found that the composition of coke did not depend on the reactants. At 450 ℃ in H-ZSM5 catalyst, methylpyrenes were the main coke components formed from propene, toluene and a propene-toluene mixture.

After the formation of coke molecules they are retained inside the zeolite pores or on the outer surface of the crystallites as the coke molecules are not volatile enough under the operating conditions. Guisnet *et al.* (1997) also report that the retention of coke molecules in zeolites depends on the difference between the size of the cavities and the size of the pore apertures and that the greater the difference between the two the easier it is for coke molecules to get trapped.

In zeolites, a large number of active sites are located in the inner pores. If the access of the reactants to these pores is limited or blocked then it results in very pronounced deactivation effect of the coke molecules. At low coke content, the active sites located in the cavity or at the channel intersection are deactivated in both ZSM5 and Y type zeolite (Guisnet and Magnoux, 1989). At higher coke content, coke molecules located on the outer surface of the crystallites block pores. Figure 2.12 illustrates four possible modes of H-ZSM5 catalyst deactivation by coke deposits.

Magnoux and Guisnet (1989) argue that at low coke coverage (below 2 wt%) and high operating temperatures acid site poisoning is the main dominating deactivation cause; while at high reaction rates, low temperatures and high

coke coverage pore blockage is the main deactivation cause. Thus they conclude that pore size and pore structures are likely to be more important than acid strength and density under typical commercial process conditions (Guisnet and Magnoux, 1997).

Regeneration of zeolite catalyst is generally done through oxidative treatment at high temperatures, which could have a detrimental effect on the catalyst such as dealumination or degradation (Guisnet and Magnoux; 1994). Generally to minimise the deactivating effect of coke molecules, it is important to select zeolite catalysts with suitable pore structure which are tri-dimensional without trap cavities such as H-ZSM5 and Y type (Guisnet and Magnoux, 1997). It is also important to adjust the acidity so that it is homogeneous in strength and distribution (Batholomew, 2001).

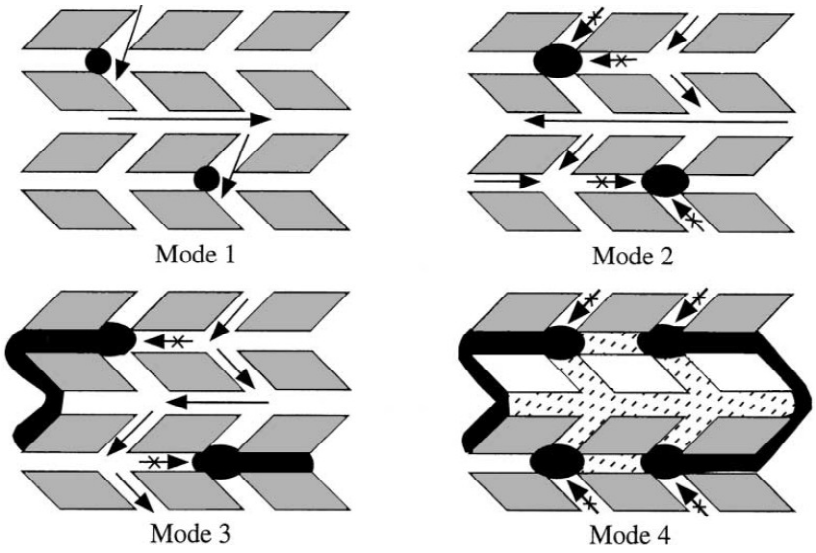

Figure 2.12. Schematic of the four possible modes of deactivation by carbonaceous deposits in H-ZSM5: (1) reversible adsorption on acid sites, (2) irreversible adsorption on sites with partial blocking of pore intersections, (3) partial steric blocking of pores, and (4) extensive steric blocking of pores by exterior deposits (taken from Guisnet *et al.*,1997).

2.6. Supercritical fluids

A fluid is termed supercritical when it exists at a temperature and pressure exceeding its critical temperature (T_c) and critical pressure (P_c) (Clifford, 1999). At this point the liquid and vapour phase become one single phase (Baiker, 1999).

Figure 2.13 illustrates the phase diagram for pure carbon dioxide. The areas where CO_2 exists as a gas, liquid, solid or a supercritical fluid can be seen in Figure 2.13. The curve in Figure 2.13 shows where two phases coexist in equilibrium. At the triple point, the three phases coexist. By moving upwards along the curve; increasing both pressure and temperature; the gas becomes denser as the pressure rises and the liquid becomes less dense due to thermal expansion. Eventually the densities of the two phases become identical. This means that the distinction between gas and liquid disappears and the liquid and vapour phase become one single phase (Savage *et al.*, 1995). When a supercritical fluid is used as a solvent then the critical point of the pure solvent is usually referred to as supercritical rather than that of the mixture. Therefore a mixture with a supercritical fluid is not necessarily in a single phase (Baiker, 1999).

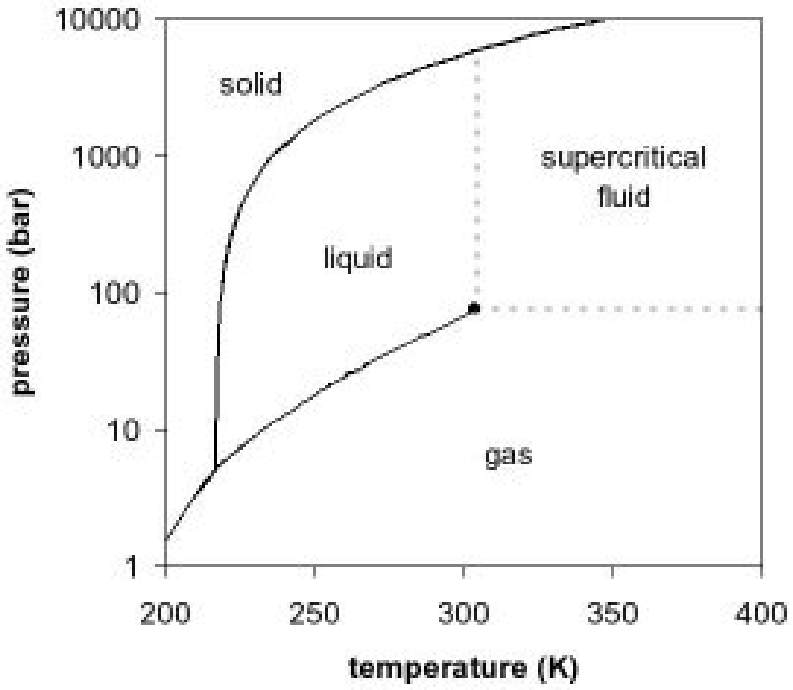

Figure 2.13. Phase diagram of carbon dioxide (New world encyclopedia, 2011).

2.6.1. Properties of SCFs

Table 2.5 (taken from Baiker, 1999) shows a comparison between the physical properties of liquids, gases and SCFs. Many of the properties of SCFs are an intermediate between those of a liquid and gas. Table 2.5 shows that the density of a supercritical fluid is approximately two orders of magnitude higher than the density of a gas but is less than half of the density of a liquid. Table 2.5 also shows that viscosity of SCFs is at least an order of magnitude lower than that of a liquid whereas the diffusivity is an order of magnitude higher than those of liquids. This means that the liquid like density of SCFs enables materials to be dissolved to a much higher level than what can be expected in an ideal gas-phase situation. This allows temperature and pressure to be used as variables to control the solubility and separation of a solute. In addition; transport

properties depend on diffusivity and viscosity, which means that in SCFs the diffusion of a certain species will occur much faster than in liquid-phase (Schneider, 1994; Baiker, 1999).

SCFs also have a unique property of pressure sensitive density, so the density can be adjusted from that of a vapour to that of a liquid as the pressure is adjusted (Reid *et al.*, 1988; Baiker, 1999). In addition, small changes in pressure will result in large changes in density, in the vicinity of the critical point, and hence materials solubility (Peters, 1994; Baiker, 1999). Changes in temperature will also lead to changes in the density and solubility of materials. These characteristics provide the opportunity to engineer the reaction environment by manipulating the pressure and temperature.

Table 2.5. Comparison between the physical properties of liquids, gases and SCFs (Baiker, 1999).

Physical quantity	**Gas (ambient)**	**Supercritical fluid (T_c, P_c)**	**Liquid (ambient)**
Density (kg/m^3)	0.6 – 2	200 – 500	600 – 1600
Dynamic viscosity (mPas)	1-0.3	0.01 – 0.03	0.2 – 3
Kinematic viscosity (10^6 m^2/s)	5 – 500	0.02 – 0.1	0.1 – 5

In heterogeneous catalysis; reactions are generally controlled by the rate of diffusion of the reactants into the catalyst pores, as the reactants and catalyst are present in different phases (Härröd *et al.*, 2001). The use of SCFs, in heterogeneous catalysis, is advantageous as it provides enhanced diffusion rates compared to liquids as well as providing the additional advantage of eliminating the gas-liquid resistance, as is shown in Figure 2.14 (taken from Härröd *et al.*, 2001), and therefore resulting in enhanced mass and heat transfer under supercritical conditions (Clifford *et al.*, 1999).

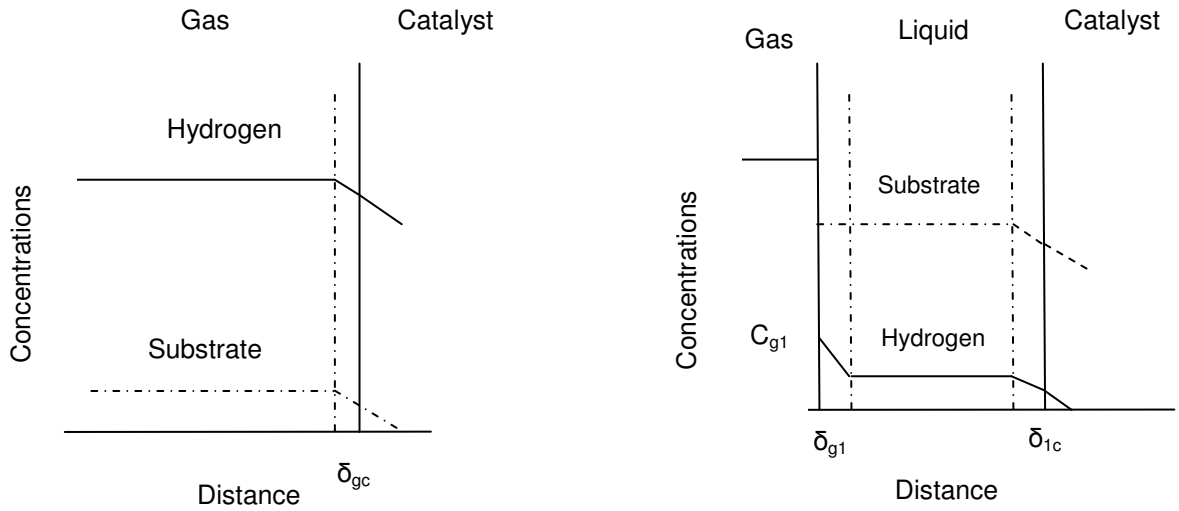

Figure 2.14. a) General concentration profiles in a gas-phase hydrogenation; b) General concentration profile in gas-liquid-phase hydrogenation (Härröd *et al.*, 2001)
--- Substrate; ___ Hydrogen; δ_{gc} Stagnant film layer at the gas – solid catalyst interface; δ_{g1} Stagnant film layer at the gas – liquid interface; δ_{1c} Stagnant film layer at the liquid – solid catalyst interface; c_{g1} Equilibrium conc. of H_2 in the liquid.

The enhanced heat transfer also prevents the formation of local overheating spots which can occur in exothermal reactions in the gas-phase (Baiker, 1999). Good wetting of the surface or in the pores can also be expected in supercritical

conditions as the surface tensions at solid surfaces are extremely small (Ekart *et al.*,1993). SCFs have shown local density enhancement, clustering or molecular charisma (Eckert and Knutson, 1993) which gives rise to interesting solvating effects not found in liquid mixtures. SCFs are more compressible and have larger free volume compared to liquids which means that the attractive forces can move into energetically favourable locations (Brennecke *et al.*, 1990). This in turn results in the formation of non uniform spatial distribution of solvent molecules about a solute molecule. This can affect the selectivities and rates of chemical reactions through physical and chemical mechanisms (Eckert and Chandler, 1997). Furthermore, the reduced viscosity of SCFs combined with the efficient mass and heat transfer properties allows the use of continuous flow systems (Baiker, 1999). Overall SCFs can be used as solvents or reactants providing many advantages summarised as:

- The control of phase behaviour, elimination of gas-liquid and liquid-liquid mass transfer resistances.
- The enhanced diffusion rate in reactions controlled by external diffusion.
- Enhanced heat transfer and reaction rates.
- Improved selectivity for certain products and easier product separation.
- Improved catalyst lifetime by extraction of deactivating deposits.
- Tunability of solvent properties by pressure and co-solvents.
- Process intensification.

The critical temperature and pressure for different fluids used in reactions at supercritical conditions are listed in Table 2.6. The data were taken from Reid *et al.*, (1987) (Clifford *et al.*, 1999).

The most frequently used SCFs in reactions are CO_2 and water. CO_2 is a supercritical fluid when it is above its critical point (T_c 31.04 °C and P_c 73.8 bar) (Health and safety executive, 2011). Supercritical CO_2 and water have different applications but both are non-flammable, non toxic and environmentally compatible (Boreskov, 2003). Water has a relatively high critical point whereas CO_2 has a critical temperature near ambient conditions. This makes supercritical CO_2 one of the most frequently applied SCFs. Higher reaction rates as well as improved selectivity are achieved in supercritical CO_2 and this has attracted the interest of industry. For example, Thomas Swan and Co. Ltd. have operated a 800 t/a test facility to perform heterogeneously catalysed reactions in Sc CO_2 since 2002 (Boreskov, 2003).

Table 2.6. Substances useful as SCFs, with parameters from Reid *et al.* (1987) (Baiker, 1999).

Substance	**Critical temperature, T_c (K)**	**Critical pressure, P_c (bar)**
Carbon Dioxide	304	74
Water	647	221
Ethane	305	49
Ethene	282	50
Propane	370	43
Xenon	290	58
Ammonia	406	114
Nitrous Oxide	310	72
Fluoraform	299	49

2.6.2. Coking behaviour at supercritical conditions

The main reason for coke build up in porous catalysts is the relatively low volatilities of the coking precursors that are formed on the catalyst surface (Saim and Subramaniam, 1990). At the relatively low subcritical densities and low solvent power of the gas-phase reacting mixtures the coke precursors are left behind on the catalyst surface. These precursors then undergo further reaction to consolidated coal-like carbon (Baptist and Subramaniam, 1992).

SCFs have shown higher solubility than corresponding gases for heavy organics hence the use of SCFs as a reaction media should improve the solvent power of the reaction mixture (Baiker, 1999). The enhanced solubility of heavy organics results in the coke precursors that are formed on the catalyst surface being extracted by the supercritical solvent, therefore less coke deposits on the catalysts pores (Saim and Subramaniam, 1990). The catalyst deactivation rate can be reduced at supercritical conditions because freshly formed coke precursors are simultaneously extracted by the supercritical solvent. Nevertheless complete reactivation of a catalyst by supercritical solvent is not possible as the larger coke molecules are difficult to re-dissolve (Manos and Hofman, 1991).

2.6.3. SCFs effect on transport properties

SCFs offer higher diffusion coefficients compared to liquids and the elimination of inter phases which can exist in multi component systems (Baiker, 1999). This results in significantly enhanced mass transfer under supercritical conditions.

The coefficient of self diffusion represents the limiting form of the coefficient of binary diffusion (Lee and Thodos, 1983). Lee and Thodos (1983) reported that self diffusivity can be calculated using Equation 2.9.

$$\frac{D\delta}{T_R} = \frac{0.77*10^{-5}}{\rho_R} \qquad (2.9)$$

Where δ is the self diffusivity modulus, D is self diffusivity (cm^2/s), T_R is the reduced temperature (T/T_c), ρ_R is the reduced density (ρ/ρ_c) The relationship in Equation 2.9 is valid for reduced densities ranging up to ρ_R equal to 1.0.

The self diffusivity modulus, δ, is defined as:

$$\delta = \frac{M^{0.5}}{P_c^{0.5}\, v_c^{5/6}} \qquad (2.10)$$

where M is the molecular weight, P_c is the critical pressure in atm, v_c is the critical volume in $cm^3/gmol$. At higher densities of ρ_R above 1.0 then the following Equation 2.11 describes the self diffusivity behaviour (Lee and Thodos, 1983).

$$\frac{D_\delta}{T_R} * 10^5 = (0.7094G + 0.1916)^{2.5} \quad \text{for } (0 < G < 1.0) \qquad (2.11)$$

Where δ is the self diffusivity modulus, D is the self diffusivity, T_R is the reduced temperature (T/T_C), G is the normalized density-temperature modulus. Equation 2.11 assumes values of: $D_\delta/T_R = 0.0161 * 10^{-5}$ at G = 0 and $D_\delta/T_R = 0.77 * 10^{-5}$ at G = 1.0. The application of Equation 2.11, for dense fluid states, is limited to G values equal to or smaller than 1.0. For G values above 1.0 Equation 2.9 becomes applicable (Lee and Thodos, 1983).

Both Equation 2.9 and 2.11 produce the relationship given in Equation 2.12 at the critical point for self diffusivity values.

$$D_c = \frac{0.77 * 10^{-5}}{\delta} \qquad (2.12)$$

These correlations can be used to predict self diffusivities over the complete range of conditions from dilute and dense gaseous state to the saturated and compressed liquid region of fluids (Lee and Thodos, 1983).

2.6.4. Equation of state and phase behaviour

It is important to have knowledge of the boundaries of the single-phase supercritical region. For a pure fluid, identification of the supercritical region is straightforward however for multi component systems this can be more difficult as the location of the phase border curves in pressure-temperature-composition space (Baiker, 1999). In multi component systems, the composition changes with time (batch reactor) or location (continuous fixed bed reactor) which means that the critical point changes with time or location in reactor (Baiker, 1999). Experimentally determined data are not available for all mixtures but the critical properties of a mixture can be determined by using predicting software's using equations of state.

Equations of state describe the state of matter under a given set of physical conditions (Johnston *et al.*, 1989). It provides a relationship between two or more state functions such as temperature, pressure, volume or internal energy (Baiker, 1999). Equations of state are useful in describing properties of fluids, mixtures of diverse components and solids. They can be applied over wide ranges of temperature and pressure and can also be used to calculate vapour-liquid, liquid-liquid and supercritical fluid-phase equilibrium (Baiker, 1999).

Several equations of state have been developed. The van der Waals equation of state was the first equation to describe the properties of fluids over a wide range of pressures and predict vapour-liquid coexistence (Schaink and Venema, 2007).

The van der Waals equation of state is an improvement on the ideal gas law; however it is not sufficiently accurate for critical properties and phase equilibria calculations (Baiker, 1999). The Redlich-Kwong equation of state improved the accuracy of the van der Waals equation by introducing temperature dependence for the attractive term (Law and Lielmezs, 1984). The Redlich-Kwong equation of state is accurate for predicting molar volumes of pure substances (Baiker, 1999). However, calculations of the properties of mixtures and predictions of vapour-liquid equilibrium using this model are not very accurate (Baiker, 1999). Soave (Fuller, 1976) further improved the equation.

Peng and Robinson (Xu and Sandler, 1987a) proposed additional modifications to more accurately predict the vapour pressure, liquid density and equilibria ratios. The Peng-Robinson and Soave-Redlich-Kwong equations are widely used in industry (Kabadi and Danner, 1985). The advantages of these equations are that they can accurately and easily represent the relation among temperature, pressure and phase compositions in binary and multicomponent systems (Baiker, 1999). They only require the critical properties and acentric factor for the generalised parameters and good phase equilibrium correlations can be obtained (Xu and Sandler, 1987b). However, the success of these modifications is restricted to the estimation of vapour pressure (Fuller, 1976). The calculated saturated liquid volumes are not improved and are invariably higher than experimental measurements (Fuller, 1976).

In this work, the critical point of the reaction mixture was obtained from the Aspen HYSYS software using the Peng-Robinson equation of state, Equation

2.13, for the physical property package. The *Tc, Pc, ω* (the acentric factor) and binary interaction parameters, which are required to calculate parameters *a* and *b*, were taken from HYSYS library. The van der Waals mixing rule, Equations 2.14 and 2.15, was used. The accuracy of these calculations was evaluated by calculating the critical properties and phase diagram of a benzene-ethane system. This was then compared to values and diagrams found in the literature. The results obtained are very similar to those in the literature and have been summarised in Appendix 8.2.

$$P = \frac{RT}{v-b} - \frac{a}{v(v+b)+ b(v-b)} \quad (2.13)$$

$$a = \sum_i \sum_j x_i x_j \, (a_i a_j)^{0.5}(1 - k_{ij}) \quad (2.14)$$

$$b = \sum_i x_i b_i \quad (2.15)$$

Where x_i is the mole fraction of the *i*th component; a_i and b_i are the pure substance parameters in PR-EOS; and k_{ij} is the binary interaction parameter for the (*i*,*j*) pair.

2.6.5. Reactions in SCFs

A wide range of catalytic reactions have been conducted in supercritical conditions and some of the main reactions are summarised in Figure 2.15.

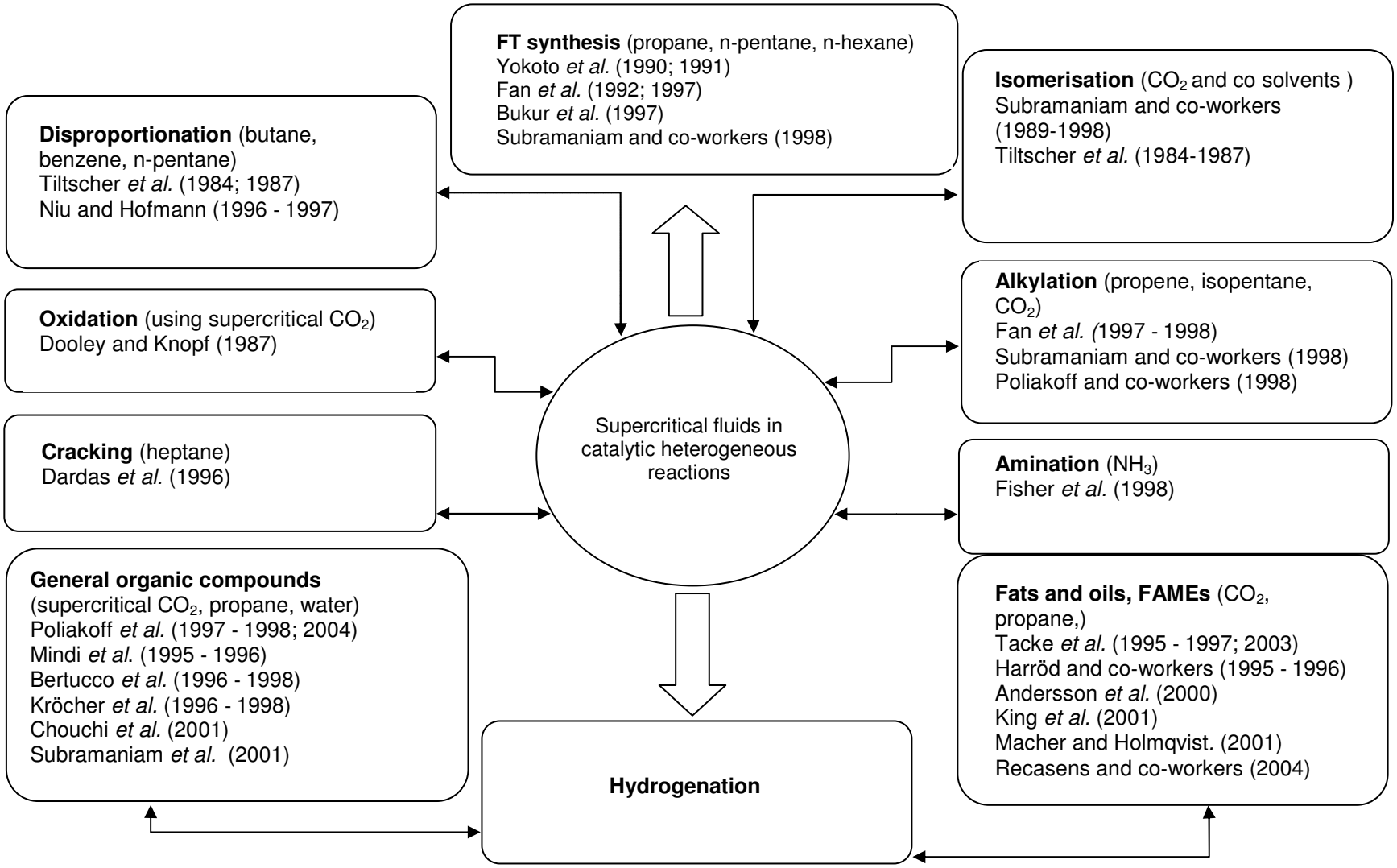

Figure 2.15. Summary of reactions in supercritical fluids.

Li Fan *et al*. (1997) studied the alkylation of isopentane with isobutene and isobutene with isobutene on a zeolite Y catalyst during gas-phase (140 ℃, 35 bar), liquid-phase (125 ℃, 50 bar) and supercritical (140 ℃, 50 bar) conditions. No supercritical solvent was used but rather the reaction mixture was at supercritical conditions. Li Fan *et al.* (1997) reported that reactions carried out in supercritical conditions showed a higher catalyst activity and longer catalyst life time compared to the gas or liquid-phase reactions. The activity of the catalyst declined to zero in both the gas and liquid-phase reactions as the amount of olefins in the feed increased to 15 mmol/g.cat whereas in supercritical conditions the deactivation was suppressed and the conversion remained almost at 100%. This was attributed to the ability of SCFs to extract *in situ* and transport the high molecular weight olefins responsible for coking and thereby extending the catalyst life time (Li Fan *et al.*, 1997).

Gao *et al.* (1996; 1997) studied the deactivation of zeolite Y catalyst during the alkylation of benzene with ethylene under both supercritical and liquid-phase reactions as well as under supercritical CO_2 solvent. Gao *et al.* (1996; 1997) reported that operating in supercritical mode results in a significantly slower catalyst deactivation and improved selectivity to ethylbenzene due to the suppression of the formation of undesired xylenes. The authors attributed the slower deactivation of the catalyst to higher solubility and enhanced diffusivity of polynuclear aromatic compounds in supercritical reaction mixture and supercritical CO_2 solvent. The higher product selectivity to ethylbenzene was due to the faster removal of the product from the catalyst surface in SCFs which

prevented it from further isomerising in a consecutive reaction step to form xylenes (Gao *et al.*, 1996; 1997).

Clark and Subramaniam (1998) investigated the alkylation of isobutene/1-butene in supercritical, gas-phase and liquid-phase reaction conditions. By using a molar excess of supercritical CO_2, alkylation was performed at supercritical conditions at temperatures lower than the critical temperature of isobutene (T_c 135 °C), which resulted in steady, alkylate production for nearly 2 days on stream. Without supercritical CO_2 the higher temperatures (above 135 °C) required for supercritical operation would favour cracking and coking reactions. The alkylate yield was between 5 – 10% and the conversion of 1-butene was 20% in supercritical CO_2 solvent at reaction conditions of 140 °C, 60.7 bar for 30 hours on stream. Although the yield and conversion were relatively low compared to conventional alkylate yields of above 70% and conversions of 100%, the steady alkylate production, using supercritical CO_2, in itself is a significant result. The authors concluded that CO_2 based fixed bed solid acid alkylation shows promise as a possible environmentally safer option compared to conventional alkylation which uses liquid acid (Clark and Subramanium, 1998).

Fischer *et al*. (1999) investigated the effect of pressure, in the range of 50 – 135 bar, on the conversion and product selectivity during the amination of amino-1-propanol with ammonia over a CoFe catalyst at 195 °C. The authors reported a large change in product selectivity from 4% to 40% to the desired product of 1,3-diaminopropane in the near critical region of ammonia and the changes observed in conversion were very small (Fischer *et al.*, 1999).

Dardas *et al.* (1996) studied n-heptane cracking using *in situ* cylindrical reflectance infrared technique (CIR-IR) at temperatures between 200 – 475 ℃ and pressures of 200 - 500 psi (13.7 - 34.4 bar). The critical properties of n-heptane are 267 ℃ and 397 psi (27.3 bar). The authors reported that *in situ* CIR-IR showed an increase in heptane concentration within the pores of zeolite Y during the cracking of heptane. The results showed that at subcritical conditions (475 ℃ and 200 psi) 75% of the terminal silanols and 60% of Brønsted acid sites disappeared whereas at supercritical conditions (475 ℃ and 450 psi) the catalyst only lost 40% of terminal silanols and 33% of the Brønsted acid sites. Furthermore n-heptane conversion increased from 17% to 23% as the reaction conditions changed from sub to supercritical. The results also showed that new spectral bands appeared between 3500 – 3100 cm^{-1} corresponding to the interactions of the acid sites with the reactant and products (paraffin and olefins). The authors concluded that coke forms in the supercages and silanols on the external surface of the catalyst and that supercritical heptane dissolved part of the coke that covers the catalyst acid sites and clogs the micro-pore openings of the zeolite which results in a partial regeneration of the deactivated catalyst (Dardas *et al.*, 1996).

Tiltscher *et al.* (1984) studied the disproportionation of 1,4-diisopropylbenzene under gas-phase and supercritical conditions on a zeolite 13-NaHX catalyst in an internal differential reactor. Benzene and n-pentane were used as diluents to lower the critical temperature of the reaction mixture. During this reaction, the reactant is of medium volatility (210.3 ℃ T_{bp}) and two main products are formed; cumene with a relatively low volatility (152 ℃ T_{bp}) and 1,3,5-

triisopropylbenzene with a relatively higher volatility (237 °C T_{bp}). In the gas-phase, the reaction product solution contains large amounts of the low volatility product (cumene) whereas the higher volatility product (1,3,5-triisopropylbenzene) remains and accumulates on the catalyst surface resulting in a fast decline of the catalyst activity. The authors reported that when supercritical conditions are used, an increase in the higher volatility product was observed in the liquid product outlet indicating that SCFs enhanced the desorption of the adsorbed product due to its increased dissolution power. Tiltscher *et al.* (1984) suggested that this effect of SCFs can be used to prolong catalyst life time and to direct the product selectivity of the reaction.

Niu and Hofmann (1995a, b; 1996; 1997a, b) demonstrated the significant power of SCFs for the *in-situ* regeneration of coked zeolite Y catalyst in the disproportionation of ethylbenzene. Deactivation and coke removal kinetics were derived from experimental data for the same reaction over a Y-faujasite catalyst (Niu and Hofmann, 1995). Niu and Hofmann (1996) demonstrated that the coke deposition profiles were dependent upon the physico-chemical properties of the catalysts used, and made comparisons between the behaviour of US-Zeolite Y, H-ZSM5 and H-mordenite. Further studies of deactivation kinetics (Niu and Hofmann, 1997) and coke extraction using SCFs (Niu and Hofmann, 1997) led to greater understanding of the catalyst aging and regeneration processes.

Fischer-Tropsch (FT) synthesis has also been studied in supercritical conditions. FT can synthesize higher hydrocarbons in the liquid fuel range from synthesis gas (CO and H_2) and involves an exothermic gas-phase reaction

(Baiker, 1999). A problem that occurs in FT synthesis is the condensation of higher hydrocarbons within the catalyst pores during the reaction, which results in a loss of catalyst activity (Baiker, 1999). Operations in the liquid-phase can mitigate this problem due to the improved heat transfer and better solubilitites of higher hydrocarbons; however reactions in the liquid-phase suffer from mass transfer limitations and a lower overall reaction rate as a result (Baiker, 1999). This means that SCFs can be of great benefit in FT synthesis as they combine the desirable gas-like diffusivity and liquid-like solubilities.

Bukur *et al.* (1997) investigated the effect of process conditions on olefin selectivity during FT synthesis in supercritical propane compared to conventional FT synthesis using a fixed bed reactor with precipitated iron catalyst. The authors reported that the total olefin selectivity was independent of reaction temperature in the range of 235 – 265 ℃. The authors also reported that supercritical conditions resulted in a higher selectivity towards olefin and a decrease in 2-olefin selectivity compared to subcritical conditions. The authors attributed this to the lesser occurrence of undesired secondary reactions of high molecular weight R-olefins in supercritical conditions due to the higher diffusivities and desorption rate of R-olefin in the supercritical propane conditions. Minder *et al.* (1995) studied the enantioselective hydrogenation of ethyl pyruvate using supercritical ethane on a platinum alumina catalyst modified with cinchonidine. The authors reported that in SCFs a reduction in reaction time by a factor of 3.5 was observed, in a batch reactor, compared to experiments in liquid toluene solvent under similar conditions. In both supercritical ethane and liquid toluene similar levels of enantiometric excess

(ee) were achieved at similar reaction conditions. However in supercritical ethane, an increase in catalyst/reactant ratio showed a slight increase in ee compared to a considerable decrease in ee in liquid toluene solvent due to mass transfer limitations at higher catalyst/reactant ratios. The authors concluded that this showed the possible application of supercritical fluid conditions in heterogeneous enantioselective catalysis and that tuning of the supercritical solvent properties to influence the structure of the diastereomeric transition complexes and thus controlling the enantio differentiation needs further research.

SCFs have also been applied in heterogeneous catalytic oxidation reactions as both the hydrocarbon reactant and oxygen can exist in one single phase in supercritical conditions which allows the tuning of the amount of oxygen present at the catalyst surface (Baiker, 1999). Furthermore operating in supercritical conditions can affect the reaction pathway and can minimise losses in the yield of partial oxidation products (Baiker, 1999).

SCFs can also be used to lower the operating temperature of reactions such as pyrolysis (Subramaniam and McHugh, 1986). The advantage of using SCFs is improved yields, selectivity, easier product separation and the carbon formation that occurs at high temperatures in pyrolysis can be minimised in SCFs (Subramaniam and McHugh, 1986). An example of a reaction at high temperature is the thermal degradation of cellulose and chitinin. The degradation temperatures in the pyrolysis of these polysaccharirdes are very high and it is necessary to remove the primary products from the reaction zone as soon as they are formed to avoid secondary reactions which can result in

strong carbon formation (Subramaniam and McHugh, 1986). The yield and product distribution are affected by the very high operating temperatures. These problems can be overcome by reacting cellulose in the presence of supercritical acetone in a flow reactor (Subramaniam and McHugh, 1986). Köll and Metzger (1978) reported that the use of supercritical acetone as reaction medium results in 98% of extraction, less carbon formation and better yield (38.8% compared to 28.1% yield) at temperatures lower than those used in conventional pyrolysis.

2.6.6. The isomerisation of 1-hexene

The isomerisation of 1-hexene was one of the first reactions to be studied under supercritical conditions (Baiker, 1999). This reaction is suitable as a model reaction because olefins such as 1-hexene are direct coke precursors and the critical properties of 1-hexene are moderate and permit investigations over a wide range of pressures, temperatures and densities (Wang *et al.,* 2009).

The reaction network is summarised in Figure 2.16. 1-Hexene is isomerised into trans-2-hexene, cis-2-hexene and 3-hexene and the products are formed through a system of complex parallel and consecutive reactions as is illustrated in the reaction mechanism in Figure 2.16. Trans isomers are thermodynamically more stable than cis isomers, however the cis isomer is kinetically favoured at higher pressures due to steric effects (Abbot *et al.,* 1985). Tiltscher and Hofmann (1981) reported that the initial cis/trans ratio cannot be influenced by variation of temperature at low pressure and in a gas-phase reaction. Under liquid-phase the products remain longer on the surface, which favours the thermodynamically more stable trans isomer. Whereas in the supercritical

phase the cis isomer is kinetically favoured due to its enhanced desorption in supercritical phase conditions. This results in the cis/trans ratio increasing with pressure (Tiltscher and Hofmann, 1981).

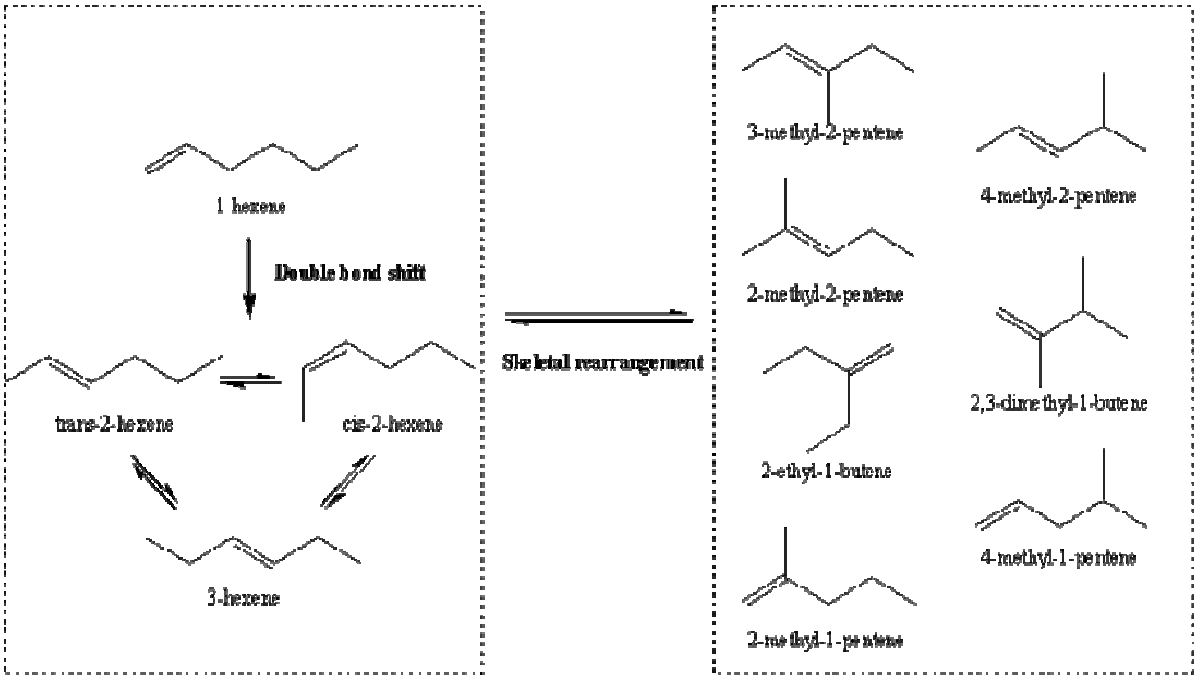

Figure 2.16. Reaction network of 1-hexene isomerisation (Wang *et al.*, 2009).

Tiltscher *et al.* (1981) reported that coked catalyst can be reactivated *in situ* by adjusting the pressure and temperature of the reaction so that the reacting medium is in the supercritical state. They demonstrated their technique for the catalytic isomerisation of 1-hexene on Al-metal shell catalyst and γ/Al_2O_3 catalyst. The authors investigated temperatures and pressures between 45 °C to 250 °C and 15 bar to 500 bar. The authors used a high pressure differential recycle reactor and demonstrated SCFs reactivation for three different modes of

deactivation. Their results show that in the gas-phase, the deactivation process occurs parallel with the reaction and that deactivation is caused by side reactions which produce low volatile oligomers ($C_{12} – C_{30}$) which build up on the catalyst surface causing coking. The oligomers can be removed by increasing the pressure of the reaction mixture to 500 bar which is well above the critical point. As a result, the conversion levels are restored to the values obtained before coking. Tiltscher *et al.* (1984) also observed that if the high pressure was maintained, there was a two fold increase in the overall conversion and a 30% increase in cis/trans-2-hexene ratio. The catalyst activity was maintained at similar levels to pre-coking results after 12 hours on stream. They conclude that catalyst reactivation can occurs at more moderate pressures of 50 – 150 bar.

Tiltscher *et al.* (1984) also studied a second deactivation mode by adding a small amount of finely dispersed MoS to act as catalyst coking substance. They showed that by operating in the mixture critical region the catalyst activity can be maintained and trace amounts of catalyst coking substances can be solubilised by the supercritical reaction mixture. This shows that catalyst coking by low volatile impurities can be controlled by operating in the supercritical region.

In the third deactivation mode reported by Tiltscher *et al.* (1984), a dilute solution of pyridine in 1-hexene was used to deactivate the acid sites of the catalyst over 12 hours on stream. Tiltscher *et al.* (1984) reported that the catalyst can be reactivated by operating in the supercritical regions and the catalyst poison is removed and precipitated from the product solution as pyridinium chloride. However, in general non-polar hydrocarbon SCFs are not

expected to solubilise inorganic or organic salts. Subramaniam and McHugh (1986) state that in this case supercritical 1-hexene could remove pyridinium chloride because it was only necessary to solubilise parts per million of this salts to reactivate the catalyst.

Saim and Subramaniam (1990) conducted studies of catalytic 1-hexene isomerisation in a continuous stirred tank reactor. They studied the thermodynamical constraints of the system by analysing the phase and reaction equilibrium. They reported that at subcritical densities, there was no coke extraction and hence 1-hexene conversion decayed with time. At low to moderate supercritical densities, the coke formation rate increased without any significant increase in coke extraction rates. At relatively high densities the enhanced solubilities of the coke compounds in the reaction mixture led to increased 1-hexene conversions and a slower decay of conversion with time. They reported that in subcritical densities the catalyst weight increased by 26%, which was attributed to depositing coke. They also found that at supercritical densities this value was reduced by a third.

Clark and Subramaniam (1996) investigated the effect of feed impurities on catalyst deactivation on a platinum alumina catalyst during 1-hexene isomerisation. The authors reported that with untreated 1-hexene feed at 280 °C and 1 bar, the catalyst deactivated in 10 hours and the coke lay down was 11% with great surface area and pore volume loss. This was due to the presence of organic peroxides, in the feed, which decompose to form free radicals that catalyse the formation of hexane oligomers. Increasing the pressure to 70 bar (supercritical), with untreated feed, resulted in the coke deposit decreasing to

5% and a slower deactivation for the catalyst. The authors suggested this decrease in percentage coke deposit is due to the *in situ* extraction of coke by the supercritical reaction mixture. With pre-treatment of the feed, a slower deactivation at 1 bar and a total coke deposit of 1% was observed. At 70 bar (supercritical) and with feed pre-treatment, there was a steady catalyst activity that persisted throughout 42 hours on stream. There was no measurable coke deposit or loss in surface area of the catalyst.

The authors conclude that SCFs can mitigate coke build up in porous catalysts by extracting the coke compounds *in situ* and transporting them out of the catalyst pores. This in turn results in extending and prolonging the catalyst life time. Pre-treatment of the feed allows SCFs to more easily balance the coke precursor's formation and extraction rate.

Clark and Subramaniam (1999) studied the reaction kinetics for 1-hexene isomerisation and reported a first order isomerisation to cis and trans hexane isomers with an activation energy of 109 kJ/mol. The authors reported that optimum conditions with maximum catalyst activity and effectiveness factor exist in the near critical region.

2.7. Hydrogenation processes

2.7.1. General conditions of hydrogenation processes

Hydrogenation is a major type of chemical processes performed in many different areas such as petrochemicals, fine chemicals, food and the pharmaceutical industry (Härröd *et al.*, 2001). In hydrogenation processes,

hydrogen and the substrate are mixed and brought into contact with either a heterogeneous or homogeneous catalyst (Baiker, 1999). Heterogeneous hydrogenation processes are carried out in the gas-phase or gas-liquid-phase.

In gas-phase hydrogenation, the transport properties are good and it is possible to have enough hydrogen at the catalyst surface (Härröd *et al.*, 2001). However gas-phase hydrogenation is only possible for small molecules as larger molecules will form a liquid under the reaction conditions (Härröd *et al.*, 2001). Under gas-liquid-phase hydrogenation, hydrogen is mixed with the liquid substrate and mass transfer from the gas to the liquid-phase limits the reaction rate. Furthermore hydrogen has a low solubility in organic liquids. Figure 2.14 showed the mass transfer resistance in liquid-gas hydrogenation systems in comparison with gas-phase hydrogenation systems. Figure 2.14 has been placed below for ease of reference.

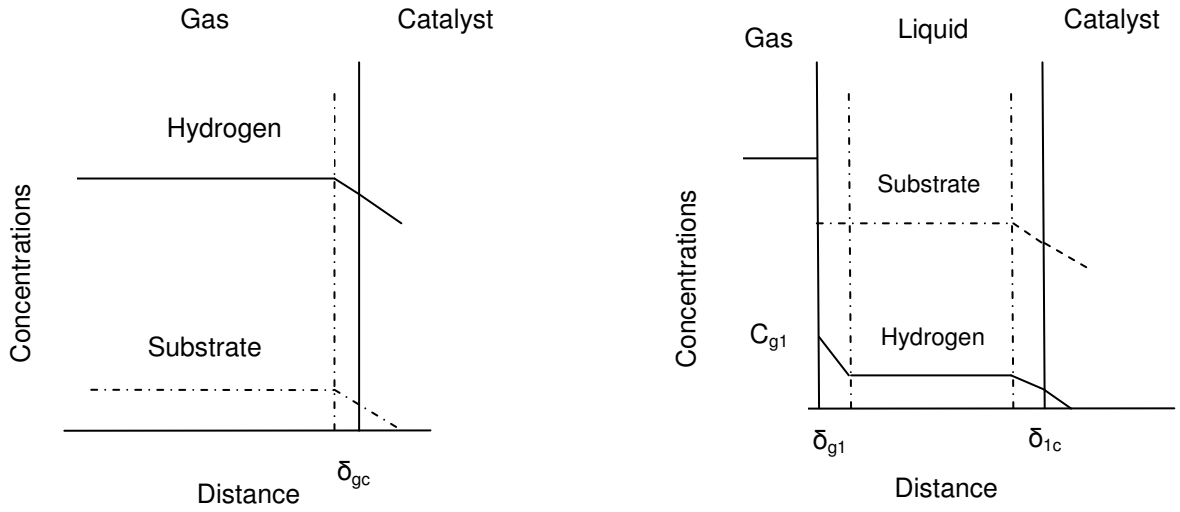

Figure 2.14. (page 41) a) General concentration profiles in a gas-phase hydrogenation; b) General concetration profile in gas-liquid-phase hydrogenation (Härröd *et al.*, 2001). --- Substrate; ___ Hydrogen; Δ_{gc} Stagnant film layer at the gas – solid catalyst interface; Δ_{g1} Stagnant film layer at the gas – liquid interface; Δ_{1c} Stagnant film layer at the liquid – solid catalyst interface; Δ_{g1} Equilibrium conc. of H_2 in the liquid.

The pressure of the system affects both gas and gas-liquid-phase reactions. In gas-phase hydrogenation, an increase in pressure increases the reactant concentration, which results in an increase in reaction rate. In gas-liquid-phase hydrogenation; increasing the pressure results in an increase in hydrogen solubility in the liquid (Baiker, 1999). For example, in vegetable oils hydrogen solubility is 2 mol% at 3 bar compared to a solubility of 20 mol% at 100 bar (Härröd *et al.*, 2001). The increased hydrogen solubility results in an increased mass transport and increased reaction rates. Pressure can also affect the product selectivity in both gas and gas-liquid-phase hydrogenation, for example in the partial hydrogenation of oils the trans isomer product is reduced in favour of the cis isomer product with increasing hydrogen pressure (Härröd *et al.*, 2001).

The temperature used in hydrogenation processes is mainly determined by the type of catalyst used and the formation of side products (Härröd *et al.*, 2001). Generally, an increase in temperature results in an increase in reaction rate as predicted by the Arrhenius equation (Härröd *et al.*, 2001). The temperature can also influence the product selectivity, for example an increase in temperature in the hydrogenation of oils leads to an increase in the formation of trans-fatty acids (Härröd *et al.*, 2001). Increasing the temperature also has an influence on side reactions such as polymerisation and coke formation. Hence the temperature has to be balanced between achieving the required reaction rates, equilibrium and avoiding side reactions. In conventional hydro-treating processes, a reaction temperature above 350 ℃ is typical (Rautanen e*t al.*, 2002) and higher pressure of hydrogen is required to offset the limitation of thermodynamic equilibrium conversion at high temperatures.

In hydrogenation processes mass transport resistances between gas and liquid-phase can be eliminated by adopting supercritical conditions (Figure 2.17; taken from Härröd *et al.*, 2001). Hydrogen has a solubility that is an order of magnitude larger, at a given pressure, in SCFs compared to organic solvents (Baiker, 1999). SCFs such as CO_2, propane, ethane have been used as solvents in several hydrogenation reactions including the hydrogenation of fats and oils (Baiker, 1999).

The phase behaviour of a system depends on the composition, pressure and temperature. It is very important to understand the influence of these parameters on the phase behaviour. Sometimes a process can be moved from the gas-phase or gas-liquid-phase by either increasing the temperature or

pressure respectively. However this is only practical if the substrate and product have a critical point in the range of possible reaction conditions. If the range of is not practical then single phase conditions can still be achieved by the use of a solvent such as supercritical CO_2 (Härröd *et al.*, 2001).

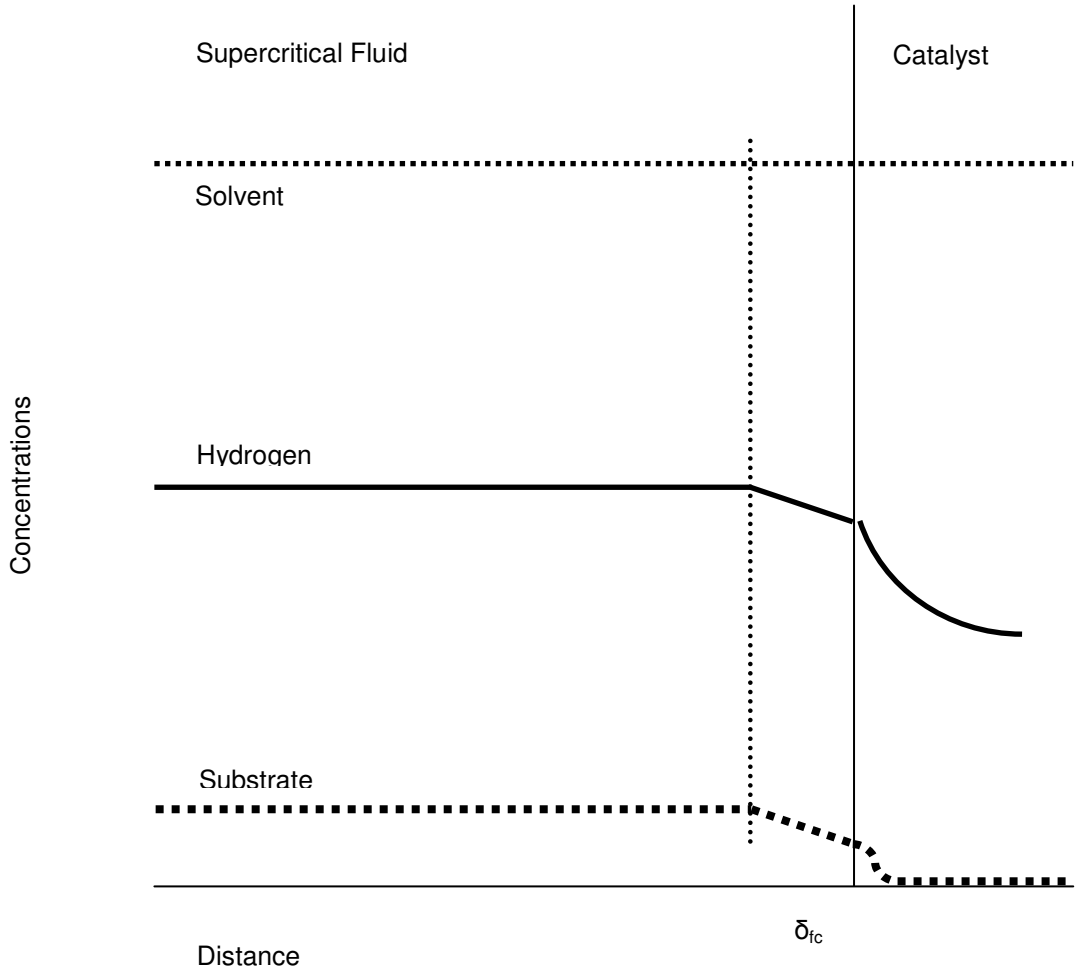

Figure 2.17. General concentration profiles in supercritical conditions (taken from Härröd *et al.*, 2001).

Macher *et al.* (1999) studied the partial hydrogenation of fatty-acid methyl ester using supercritical propane and a palladium catalyst in a fixed bed reactor. The authors reported about 500 times increase in reaction rate in supercritical

conditions compared to subcritical batch processes (Härröd *et al.*, 2001). They attributed this to the elimination of gas-liquid mass transfer and the homogenous one phase under supercritical conditions leading to a greater concentration of hydrogen at the catalyst surface. The authors also stated that higher hydrogen concentrations at the catalyst surface favour the formation of cis-fatty acids. Thus operating in supercritical conditions resulted in a reduction in trans-fatty acids formation compared to subcritical conditions.

Hitzler *et al.* (1998) studied continuous hydrogenation using SCFs such as CO_2 and propane as solvents on various noble metal catalysts. The authors demonstrated that hydrogenation in supercritical solvents can be used in a variety of organic compounds such as alkenes, alkynes, aliphatic and aromatic keytones, aldehydes, phenoles, nitrobenzenes and nitriles (Baiker, 1999).

2.7.2. Hydrogenation of aromatics

The hydrogenation of aromatics is an important process in oil refining. It is important to reduce the aromatic content in liquid fuels as a high aromatic content is associated with poor fuel quality (Monteiro-Gezork *et al.*, 2007). The efficient ring hydrogenation of aromatics is also useful for the production of high performance diesel fuel (Hiyoshi *et al.*, 2007). Moreover deca-hydro-naphthalene or decalin is proposed as the new mobile hydrogen storage medium for proton exchange membrane fuel cells (Hiyoshi *et al.*, 2007). Therefore, the efficient hydrogenation of naphthalene is an important reaction for the production of decalin as a potential hydrogen storage material.

Several supported catalysts such as noble metal or other group VIII supported on alumina, silico-alumina or acidic zeolite have been used in the hydrogenation of naphthalene (Lin and Song, 1996). It has been shown that noble metals such as platinum, palladium, rhodium, iridium and ruthenium have high activity and selectivity for naphthalene hydrogenation (Song and Schmitz, 1996; Weitkamp, 1968). Bimetallic platinum-palladium catalysts have been reported to be more active than the monometallic platinum and palladium catalysts (Pawelec *et al*., 2006) and zeolite-supported platinum catalysts have been reported to be more active than the Al_2O_3 supported platinum catalyst (Schmitz *et al*., 1996). Gold catalyst has also been found active in partial and selective hydrogenation reactions (Pawelec *et al*., 2006), however gold catalysts have a very limited capacity to dissociate H_2 molecules (Pawelec *et al*., 2006). The high activity of platinum and palladium based catalysts has been attributed to their relatively higher ability to dissociate hydrogen (Schmitz *et al*., 1996). However these noble metal catalysts have the disadvantage of higher cost and susceptibility to poisoning by sulphur containing compounds (Schmitz *et al*., 1996).

Transition metal sulphide catalysts are widely used in the petroleum and chemical industry (Chianelli *et al*., 1994). Sulphur containing compounds poison metallic and oxide catalysts however the addition of transition metals such as molybdenum or tungsten result in the catalyst retaining much of its ability and becoming very resistant to poisoning (Chianelli *et al*., 1994). The catalyst was originally used in an unsupported form but soon after alumina was used as a support. Sulfided transition metal catalysts such as nickel molybdate or cobalt molybdate supported on alumina are now very widely used in many major

reactions such as hydrogenation of olefins, ketones, aromatics as well as hydrodesulfurisation, hydrodenitrogenation, hydrometallation, dealkylation, ring opening of aromatics, isomerisation of paraffins, dehydrogenation of alcohols, Fischer Tropsch and alcohol synthesis, hydration of olefins, amination and many other reactions (Chianelli *et al.*, 1994).

2.7.3. Hydrogenation of naphthalene and reaction kinetics

Figure 2.18 shows that naphthalene is hydrogenated to tetralin through sequential cis-addition steps of two dissociatively adsorbed hydrogen atoms (Rautanen *at el.*, 2002). Tetralin forms surface complexes with the adsorbed hydrogen and active sites, and these complexes react to 9,10-octalin, which is either hydrogenated to cis-decalin or isomerised to 1,9-octalin. 1,9-Octalin is, in turn, hydrogenated to cis- and trans decalin (Rautanen *at el.*, 2002). Figure 2.18 was taken from Rautanen *et al.* (2002).

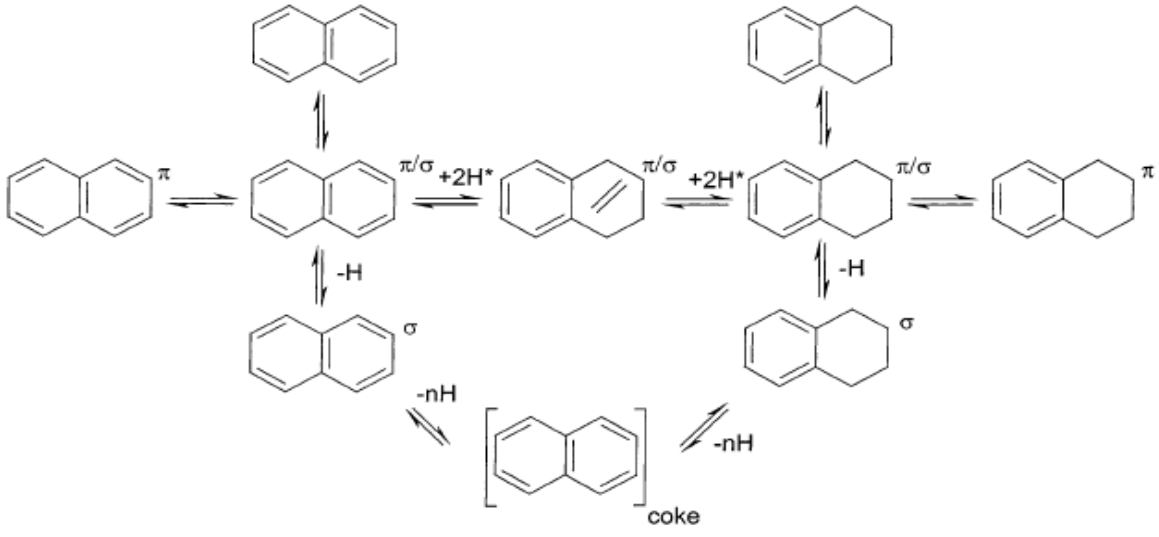

Figure 2.18. Naphthalene hydrogenation reaction network (Rautanen *et al.*, 2002).

The hydrogenation of poly and bi aromatics to monoaromatics is achieved under mild conditions (Weitkamp, 1968). It is reported that the hydrogenation rate of the first ring of naphthalene is 20 – 40 times faster than the hydrogenation of the last ring (Weitkamp, 1968; Rautanen *et al.*, 2002). The difference in hydrogenation rates of the first and last naphthalene ring is explained by the difference in aromaticity; the π-electron density of the aromatic ring of tetralin is higher than that of naphthalene which results in greater resonance energy of the aromatic ring in tetralin compared to naphthalene (Rautanen *et al.*, 2002).

Various researchers have investigated liquid and vapour phase hydrogenation of naphthalene over supported metal catalysts. Weitkamp (1968) conducted detailed research of naphthalene hydrogenation mechanism in a stirred batch reactor on noble metal catalysts such as ruthenium, rhodium, palladium, iridium and platinum over a range of temperatures (25 – 200 ℃) and pressure of 69 bar. Weitkamp (1968) reported the formation of tetralin, cis and trans-decalin as the main reaction products. He found that different catalysts showed different product selectivities. Palladium catalyst on a charcoal support showed a selectivity of 52% towards trans-decalin at 100 ℃; rhodium supported on alumina showed 15% selectivity towards trans-decalin at 25 ℃; platinum on alumina showed 10% selectivity towards trans-decalin at 200 ℃ and iridium on charcoal showed 5% selectivity towards trans-decalin at 25℃. No cis to trans-decalin isomerisation was observed.

The author described the reaction mechanism as a stepwise process of two by two additions of hydrogen and stated that the reaction was first order towards

naphthalene. The author concludes that hydrogen is added to olefins and aromatics by a mechanism that is predominantly cis addition. Trans isomers are not formed by direct addition of hydrogen but rather by a mechanism that involves intermediates that have desorbed and turned over on the catalyst. The distribution of cis and trans isomers in the products depends on the catalyst as a results of differences in the relative rates of successive steps in the reaction path (Weitkamp, 1968).

Sapre and Gates (1981) studied naphthalene hydrogenation in a batch reactor at 325 ℃, 75 bar and 0.85 mol% naphthalene feed concentration over a sulfided cobalt molybdate ($CoMo/Al_2O_3$) catalyst. The authors reported trans-decalin as the predominant isomer under their studied conditions with the ratio of trans to cis isomer being close to 2:1. Sapre and Gates found pseudo first order reaction kinetics in the hydrocarbon reactant (i.e naphthalene) with a pseudo first order rate constant k of $5.89*10^{-5} \pm 3.6$ L/gcat.s.

Huang and Kang (1995) conducted naphthalene hydrogenation in a trickle bed reactor at 200 ℃ – 260 ℃ and 17 – 87 bar over a platinum on alumina (Pt/Al_2O_3) catalyst. They assumed a piston-flow reactor operated nearly isothermally with negligible intra-particle and inter-particle transport resistances. The authors reported three main reaction products; tetralin, cis and trans-decalin. The activation energy for tetralin hydrogenation to cis and trans-decalin were 9.88 and 7.25 kcal/mol respectively. The activation energy to cis decalin is higher than trans-decalin because the tetralin cis type partial hydrogenated intermediate complex is less stable than the trans type. The authors observed cis to trans-decalin isomerisation at their studied conditions and reported the

activation energy for the isomerisation of cis to trans-decalin to be 14.75 kcal/mol. The reaction order of hydrogen for the hydrogenation of tetralin to cis and trans-decalin was 1.88 and 1.06 respectively.

Zhan and Guin (1994) studied naphthalene hydrogenation over a $NiMo/Al_2O_3$ catalyst in a trickle flow reactor at 69 bar, 160 ℃ – 300 ℃ and 0.2 mol% naphthalene feed concentration. They eliminated transport limitations by using mesh catalyst extrudates size of 40 -50. Zhan and Guin (1994) derived a pseudo first order reaction mechanism where they assumed that a) hydrogen molecules chemisorb dissociatively on the catalyst surface, b) naphthalene and hydrogen chemisorb competitively on the same type of active sites, c) adsorbed hydrogen atoms are the dominant species on the surface and that d) addition of H atom to naphthalene occurs sequentially. The following reaction mechanism was proposed (Zhan and Guin, 1994).

$$H_2 + 2^* \overset{K_H}{\Leftrightarrow} 2H^* \quad (2.16)$$

$$C_{10}H_8 + * \overset{K_N}{\Leftrightarrow} C_{10}H_8^* \quad (2.17)$$

$$C_{10}H_8^* + H^* \overset{K_{E1}}{\Longleftrightarrow} C_{10}H_9^* + * \quad (2.18)$$

$$C_{10}H_9^* + H^* \overset{K_{E2}}{\Longleftrightarrow} C_{10}H_{10}^* + * \quad (2.19)$$

$$C_{10}H_{10}^* + H^* \overset{K_{E3}}{\Longleftrightarrow} C_{10}H_{11}^* + * \quad (2.20)$$

$$C_{10}H_{11}^* + H^* \overset{k}{\Leftrightarrow} C_{10}H_{12}^* + * \quad (2.21)$$

$$C_{10}H_{12}^* \overset{1/K_T}{\Longleftrightarrow} C_{10}H_{12} + * \quad (2.22)$$

Where * represents a surface active site. It can be further assumed that the adsorbed naphthalene and desorbed hydrogen are in equilibrium with the gas-phase species and that the rate controlling step is the irreversible addition of the last H atom to $C_{10}H_{11}^{*}$ surface species (Zhan and Guin, 1994). The following Langmuir-Hinshelwood rate expressing can then be derived from the above.

$$r = \frac{kK_H^2 K_N K_E C_N C_H^2}{((1+ K_H^{0.5} C_H^{0.5} + K_N C_N + K_H^{\frac{3}{2}} K_N K_E C_N C_H^{\frac{3}{2}} + K_T C_T)^2)} \quad (2.23)$$

$$((1 + K_H^{0.5} C_H^{0.5} + K_N C_N + K_H^{\frac{3}{2}} K_N K_E C_N C_H^{\frac{3}{2}} + K_T C_T)^2) = 1 + \frac{C_{H*}}{C*}\left(1 + \frac{C_{C_{10}H_{11}^*}}{C_{H*}}\right) + \frac{C_{C_{10}H_8^*} + C_{C_{10}H_{12}^*}}{C*} \quad (2.24)$$

Where K_E is the product of K_{E1}, K_{E2} and K_{E3}. The second equation shows the denominator expressed in terms of concentrations of adsorbed species and unoccupied surface active sites.

In both Zhan and Guin's (1994) study and the work presented in this thesis, the H_2 concentration was in large excess. The H_2 concentration was between 3 – 15 times the required stoichiometric ratio, and the reactor was operated at high pressures hence it can be assumed that most of the surface active sites are occupied by adsorbed hydrogen atoms (Zhan and Guin, 1994). This means that $C_{H^*} >> C_i$, where i is the unoccupied active site or the other adsorbed species other than hydrogen. This leads to the denominator of Equation 2.23 being simplified to

$$\frac{C_{H*}}{C*} = (K_H^{\frac{1}{2}} C_H^{\frac{1}{2}})^2 \quad (2.25)$$

$$r = kK_H K_N K_E C_N C_H = kC_N C_H \quad (2.26)$$

This predicts a first order dependence on both naphthalene and hydrogen. Finally, Zhan and Guin (1994) calculated the apparent activation energy of naphthalene hydrogenation at 40.2 kJ/mol.

2.7.4. Coking during the hydrogenation of aromatics

The main causes of catalyst deactivation in hydro-processing are coking and sulphur poisoning (Absi-Halabi *et al.*,1991). The high temperature and acidic nature of the catalyst support forms high molecular weight by products that cause catalyst deactivation (Hiyoshi *et al.*, 1984). In hydro-processing, the activity of the catalyst decreases rapidly in the first few hours of operation (Thakur and Thomas, 1984). This is then followed by a slower decrease in activity. It is reported that the initial rapid deactivation is associated with significant loss in surface area as large amounts of coke deposit (Absi-Halabi *et al.*,1991). Much of the coke depositing in this initial period deposits in small pores leading to a loss in micro-porosity and surface area (Thakur and M.G. Thomas, 1984). After this coking slows down and activity and surface area decrease relatively slower (Absi-Halabi *et al.*,1991). In industry, the catalyst activity is allowed to decline to a certain value after which the operating temperature is raised to increase conversion (Absi-Halabi *et al.*,1991). However deactivation is also faster at higher temperatures.

Several coking mechanisms have been suggested in literature and those have been discussed in section 2.3.1 of this Chapter. It was reported that polymerisation or polycondensation are the main reactions leading to coke

formation and that the coke precursors are present in the original feed or can be formed during the operation if sufficient active hydrogen is not supplied (Mochida *et al.*, 1989). The H/C ratio of coke changes with time on stream. The aromaticity of coke increases and the solubility as well as reactivity decrease with time on stream (Mochida *et al.*, 1989). Figure 2.19 illustrates the formation of coke via condensation reactions and has been taken from Absi-Halabi *et al.* (1991).

Absi-Halabi *et al.* (1991) suggest that controlling of catalyst acidity would have a great impact on the initial rapid deactivation during the hydrogenation of aromatics. The acidity of the catalyst can be reduced by using carbon supported metal sulphides or other supports which show lower acidity and greater strength compared to alumina support (Absi-Halabi *et al.*, 1991).

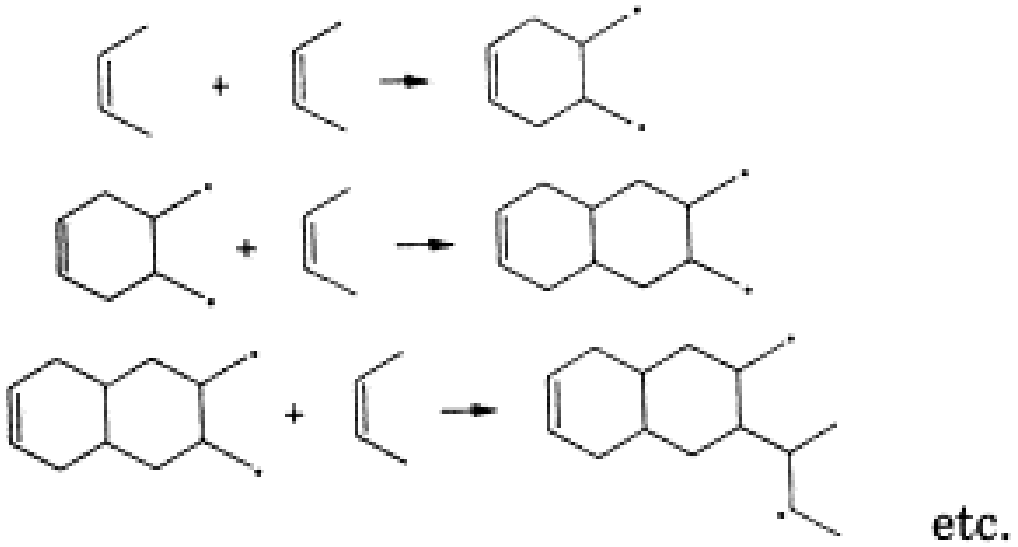

Figure 2.19. Mechanism of coke formation by condensation reactions (Absi-Halabi *et al.*,1991).

2.8. Catalyst pore structure characterisation

To understand the chemistry occurring in catalysis, knowledge of the catalyst structure is essential, hence catalyst structure characterisation is important throughout the life cycle of the catalyst (Lowell and Shields, 2004). In heterogeneous catalysis the active sites are frequently located on the solid surface however the bulk structure also plays an important role because many of the catalyst characteristics depend on it (Lowell and Shields, 2004). There are many methods to characterize the physical properties, bulk chemical properties and surface chemical properties of catalysts. The catalyst characterisation techniques used in this thesis have been briefly described in this section.

2.8.1. Nitrogen adsorption isotherms

Gas adsorption methods are often used to characterise catalysts because it allows assessment of a wide range of pore sizes, including the complete range of micro, meso and macro-pores (Chianelli *et al.*, 1994). The isotherms obtained from the adsorption measurements provide information on the surface area, pore volume and pore size distribution. N_2 adsorption at 77 K and at sub-atmospheric pressures is the most popular technique providing information on size distributions in the micro-, meso- and macro-porosity range (Paàl and Menon, 1988).

The BET theory provides a theoretical foundation of the various adsorption-desorption isotherm shapes. Figure 2.20 shows the five main adsorption

isotherms (taken from Lowell and Shields, 2004). Type I adsorption isotherm occurs in micro-porous material with pore sizes below 20 Å, where micro-pores filling and high uptakes are observed at relatively low pressures. In reality many materials contain pores over a wide range of pore sizes including micro and meso-pores hence such materials would show adsorption isotherms with features of both type I and type IV (Lowell and Shields, 2004).

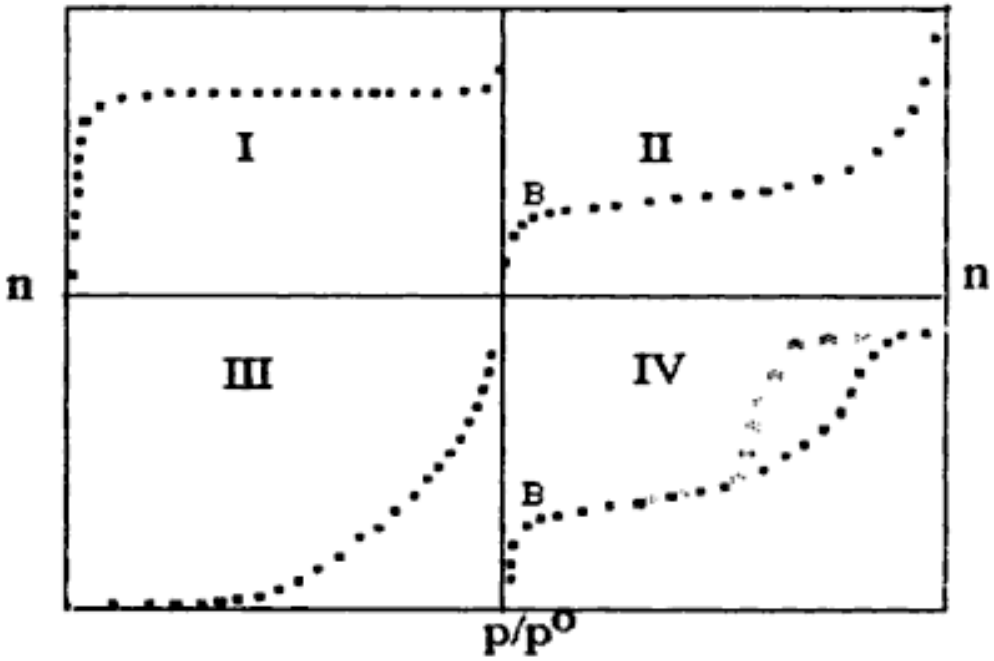

Figure 2.20. Types of adsorption isotherms (Lowell and Shields, 2004).

Figure 2.21 shows an example where the adsorption isotherm has features of type I and type IV adsorption isotherms. Figure 2.21 illustrates the semi-logarithmic isotherm plot of argon at 87 K on a zeolite Y catalyst where the micro-pores filling is in the low relative pressure range and the steep increase close to the saturation pressure represents the pore filling of the large meso-pores. Figure 2.21 was taken from Lowell and Shields (2004).

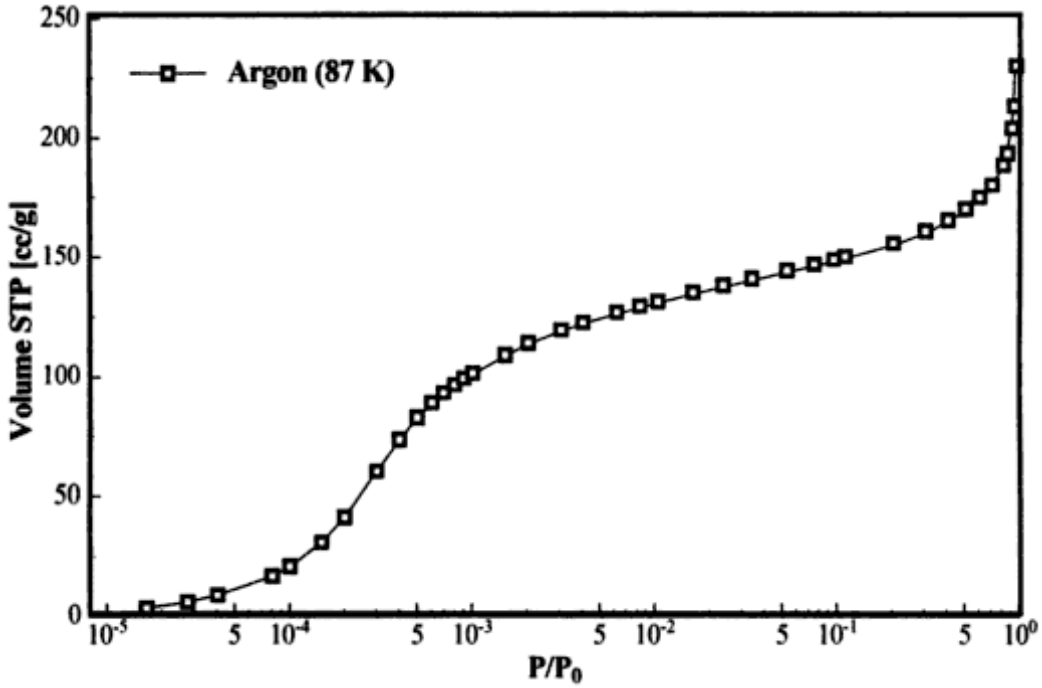

Figure 2.21. Semi-logarithmic isotherm plot of argon at 87 K on a zeolite Y catalyst.

Type II isotherms are obtained in non-porous or macro-porous adsorbents where unrestricted monolayer-multilayer adsorption can occur (Lowell and Shields, 2004). The ankle of type II isotherm indicates the stage at which monolayer coverage is complete and multilayer adsorption begins (Lowell and Shields, 1991).

Type III isotherms are not common and are characterised by heats of adsorption which are less than the adsorbate heat of liquefaction (Broekhoff and Linsen, 1970; Lowell and Shields, 1991). Type IV occurs on porous adsorbents possessing pores in the radius range of approximately 2 – 50 nm (Brunauer *et al.*, 1940; Lowell and Shields, 1991). In this adsorption isotherm the slope increases at higher elevated pressures indicating an increased uptake of adsorbate as the pores are being filled. The region of relative pressure of 0.05 ≤

P/Po ≤ 0.35 is the monolayer filling region. The ankle of this type of isotherm generally occurs near the completing of the first monolayer. The upward deviation, which occurs in the multilayer region, is the direct result of capillary condensation within the meso-pore structure. The isotherm reaches the plateau when the meso-pore filling is complete.

There are several types of hysteresis loops and de Boer (1958) described the characteristics on the types of these loops and proposed the kind of pores that can generate these adsorption-desorption loops. De Boer (1958) stated that hysteresis is neither observed in macro-pores nor in micro-pores but nearly exclusively in meso-pores and that experimental hysteresis loops may be the result of the combination of two or more types of pores.

At relative pressures above 0.3 de Boer distinguished five different types of hysteresis loops. According to de Boer's (1958) classification; type A hysteresis is due principally to cylindrical pores open at both ends. Pores of approximately cylindrical geometry are expected that pores of a given radius will fill at a higher relative pressure than they will empty. Type B hysteresis is associated with slit-shaped pores or the space between parallel plates. Type C hysteresis is a result of a mixture of tapered or wedge-shaped pores with open ends. Type D hysteresis is also produced by tapered or wedge-shaped pores but with narrow necks at one or both ends. Type E hysteresis is produced by bottle-neck pores.

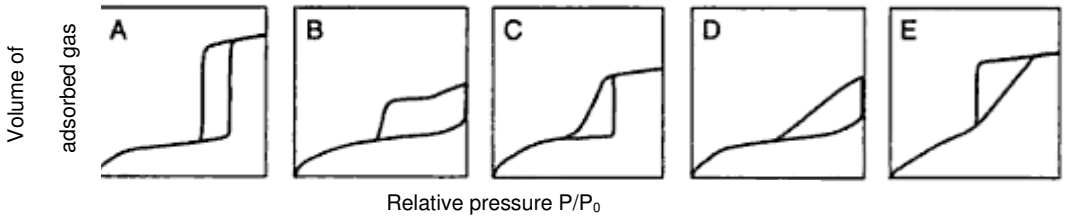

Figure 2.22. Hysteris loops according to de Boer's classification (1958).

As seen from the above discussion nitrogen adsorption is considered to be the standard procedure in the analysis of gas adsorption/desorption isotherms, however other studies also show that using additional probe molecules such as argon, butane, CO_2, water,hydrogen and hydrocarbons allows to check the consistency of the results and leads to a more comprehensive and accurate micro/mesopore size analysis of many adsorbents (Evbuomwan, 2009).

Other methods used to determine the porous properties of solids include mercury porosimetry. Mercury is a non-wetting fluid for most materials and the basic mercury porosimetry experiment consists of increasing the pressure in small increments and measuring the volume of mercury entering the sample during each pressure increment (Rigby, 2002).

Other methods based on gas sorption and/or mercury porosimetry have been developed to characterise the structure of the pore space using parameters such as the overall voidage fraction, specific surface area and pore volume, pore diameter distribution and pore connectivity (Rigby *et al.*, 2005). Rigby *et al.* (2004) also developed a method to determine the distribution of the average pore length with pore diameter using percolation theory to analyse the data arising from integrated gas sorption and mercury porosimetry experiments.

2.8.2. TGA, XRD and DRIFTS analysis

TGA can be used to determine the amount of coke deposited on the catalysts where the weight change in the catalysts during oxidation is measured whereas XRD can be used to provide an insight into the chemical nature of the active phase and crystallinity of the catalyst. DRIFTS were used to investigate the nature of the active species and nature of coke deposits on the catalyst and TPD analysis was carried out to determine the acidity of the zeolite catalysts.

2.9. Research aims

This literature review shows the research carried out in catalyst deactivation issues such as coking and different coking mechanisms proposed in literature. This review has also shown that many reactions have been successfully carried out in supercritical fluid conditions and that previous studies have shown the possibility of extracting coke deposits from the catalyst surface, thus prolonging the catalyst life time.

The work reported in this thesis will examine whether the lifetime of heterogeneous catalysts can be prolonged by operating the catalyst under supercritical conditions. The work in this thesis highlights the possible role of supercritical fluids in delaying catalyst deactivation behaviour. Detailed analysis of coke deposition and pore structural changes lead to an understanding of the effect of supercritical fluids on coking behaviour in the catalysts and reactions studied. Particular attention is paid to the effect of using supercritical fluids to extend the life of acidic catalysts such as zeolites and the potentials of using

supercritical fluids in a multi component system are explored. Overall, a conclusion is drawn and conditions to maximise the catalyst lifetime are suggested.

CHAPTER 3

MATERIALS AND METHODS

This chapter describes the apparatus, methods and the experimental conditions used in this work for carrying out reactions under sub and supercritical conditions. In addition the analytical techniques which were used to analyse the liquid product samples and the solid catalyst are presented and discussed.

The catalysts used in this work and the preparation methods are described in section 3.1. The apparatus, operating procedure and GC-FID methods are described in section 3.2. The reactions studied and phase behaviour are described in section 3.3. The catalyst characterisation techniques used in this work are described in section 3.4.

3.1. Preparation of catalyst

Three main catalysts were used in this work; ZSM5 and zeolite Y were used during the isomerisation of 1-hexene while NiMo/γ-Al_2O_3 was used during the hydrogenation of naphthalene.

3.1.1. ZSM5 and zeolite Y catalyst

The powdered forms of ZSM5 and zeolite Y were manufactured into pellets to facilitate studies in the fixed bed reactor. A sample of ZSM5 (Si/Al atomic ratio = 40, Na% = 0.05 wt %, BET surface area = 425 m^2/g, Zeolyst International) or

Zeolite Y (Si/Al mole ratio = 30, Na =0.03 wt. %, BET surface area = 780 m^2/g, Zeolyst International) was mixed with boehmite (aluminium oxide hydroxide) and appropriate quantities of methylcellulose, acetic acid, and distilled water (NH_4-ZSM5 or Zeolite Y /γ-AlO(OH)/acetic acid/water in the ratios 80/20/2/60 in weight). The mixture was then kneaded to make a paste and extruded into rods of 3.0 mm in diameter. Boehmite and acetic acid were used as binders to improve the rheology of the paste such that it could be extruded through a die to produce robust pellets. The extrudates were dried at 100 ℃ in an oven for 24 hours. The dried extrudates were then converted to the proton form by calcining at 500 ℃ in the presence of air for 6 hours. Due to the addition of boehmite, the final pellets consisted of (~80 % by mass) zeolite crystallites bound within an (~20 % by mass) alumina matrix. Figure 3.1 shows zeolite Y pellets.

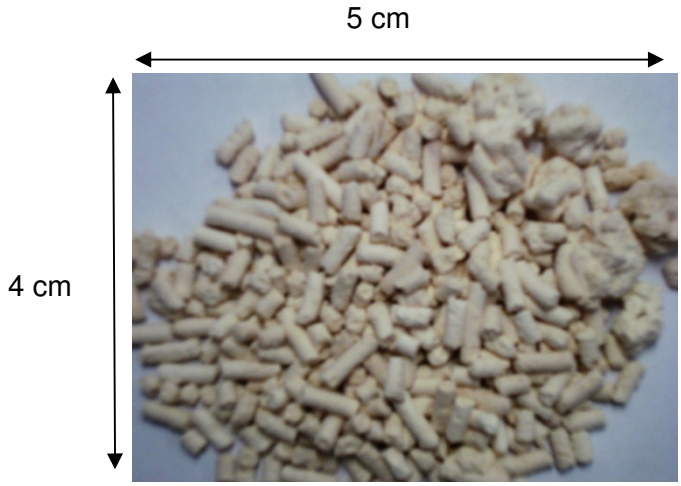

Figure 3.1. Zeolite Y pellets.

3.1.2. NiMo catalyst

A commercial porous alumina support carrying molybdenum oxide (active component) and nickel oxide (promoter), cylindrical shaped catalyst (19.5 wt.% MoO_3, 4 wt.% NiO, 0.07wt. % Na_2O, 0.03 wt.% Fe, 1.1 wt. % SO_4, Azko

Chemical Division) was used in the hydrogenation of naphthalene. The catalyst was pre-sulfided with a meso-porous pore structure (surface area of 396.2m^2/g). The catalyst was reduced at 300 ℃ with a H_2 flow rate of 10 mL/min for 2 hours prior to the reactions. Figure 3.2 shows the NiMo catalyst pellets.

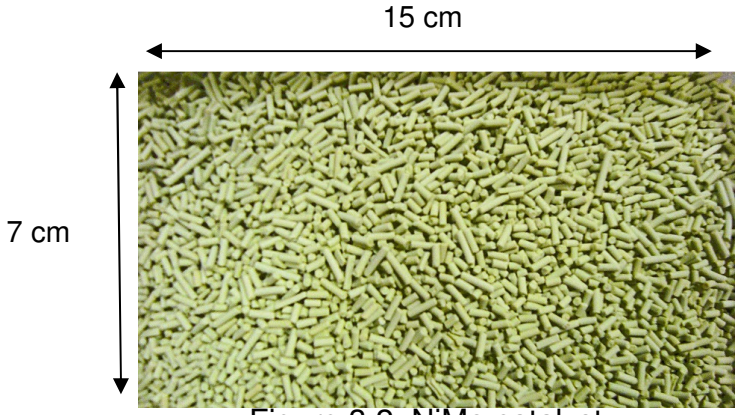

Figure 3.2. NiMo catalyst.

3.2. Apparatus and procedure

3.2.1. The rig

The supercritical reaction rig shown in Figures 3.3 and 3.4 is a fixed bed reactor system (i.d. 13 mm, length 550 mm) designed for heterogeneous reactions under supercritical conditions. The reactor is made of 3/4'' OD 316SS tube, held inside a single zone furnace by a phosphor bronze liner. The catalyst bed temperature is measured using a 1/8'' thermocouple pocket inside the reactor (T3) and separate thermocouples inside the reactor wall control the reactor wall temperature and furnace oven temperature. The reactor pressure is monitored by two pressure gauges connected before (P1) and after (P2) the reactor and the unit is protected from over pressure by a relief valve set at 270 bar (RV1).

The reactor temperature and pressure are maintained by a furnace and a back pressure regulator (V6), respectively.

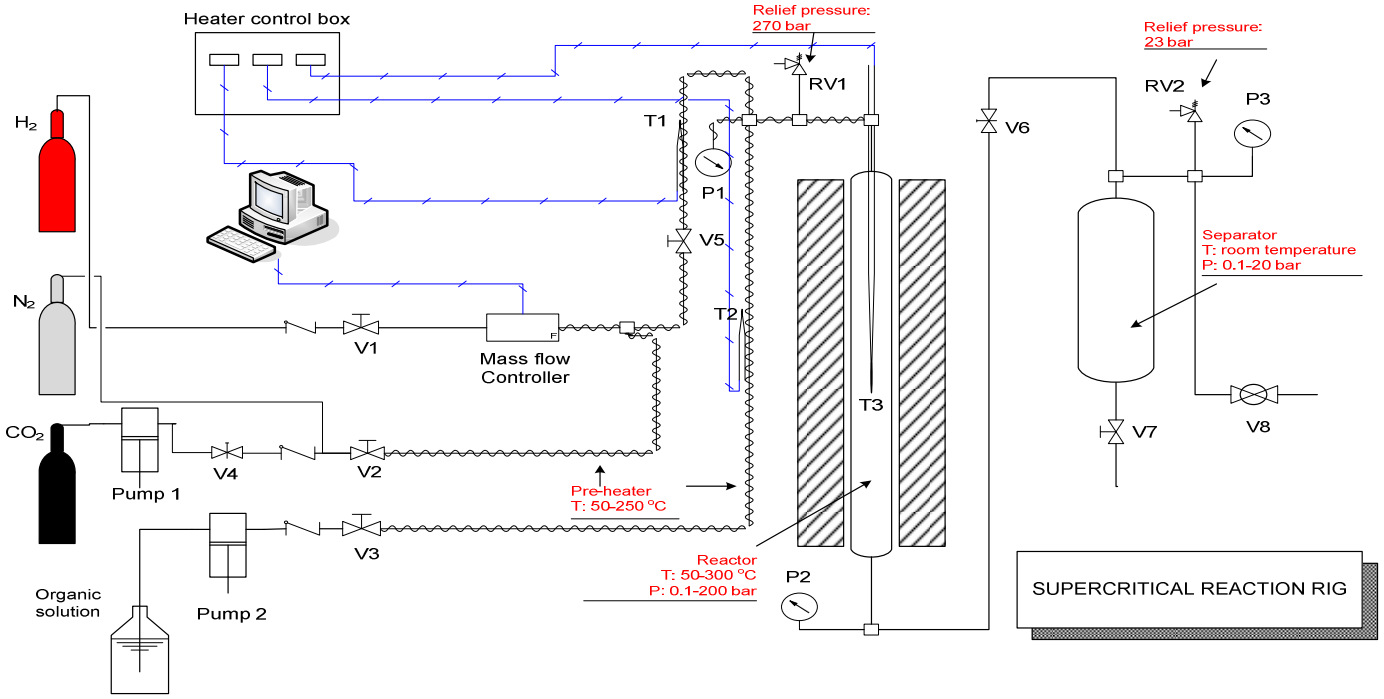

Figure 3.3. The supercritical reaction rig.

V1, V2, V3, V5, V7	V6, V4	RV1, RV2	Pump 1	Pump 2	T1, T2, T3	P1, P2, P3	Mass flow controller
Non return valves	Back pressure regulator (Tescom, 26-1700 series)	Pressure relief valve	Sc CO_2 pump (PU-1580-CO_2, Jasco)	HPLC pump (Kontron 320; Speck Analytical)	Thermocouples (1/8'')	Pressure gauges	Model 5850S, Brooks Smart Mass Flow)

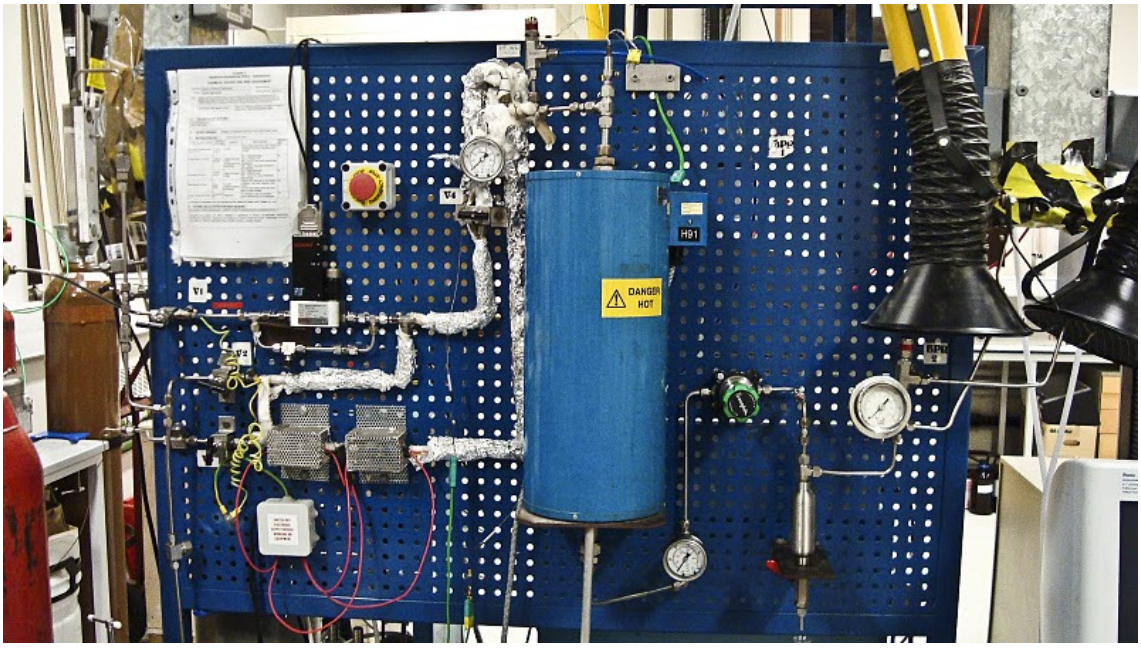

Figure 3.4. The supercritical reaction rig used in this work.

3.2.2. Start up, operating and shut down procedure

Figures 3.5a and b show the fixed bed tube image and fixed bed tube diagram respectively. The catalyst was loaded into the tube and glass beads were used to fill the empty space while glass fibre was used to separate the beads and catalyst. The system was purged with N_2, the main heater was switched on and the temperature set to the operating values. The system was pressurised with N_2 during the isomerisation reactions. The critical point of nitrogen is T_c -146.9 °C, P_c 33.9 bar, whilst the critical point of 1-hexene is T_c 231 °C and P_c 31.6 bar. Since the critical pressures for nitrogen and 1-hexene are quite similar, the reactor was started up using supercritical or subcritical nitrogen, according to the same phase required to be used in the isomerisation experiment. This approach avoided the possible coking problems which might occur if the reactor was started up under subcritical conditions then brought in to supercritical

operation at a later stage. Similarly H_2 was used to pressurise the system during the hydrogenation reactions which also ensured the reactor was started up according to the same phase required in the hydrogenation reaction.

Once the temperature stabilised and reached the required value, it was maintained at the required value by a furnace with an accuracy of ± 2-3 ℃. Once the pressure stabilised and reached the required value, it was maintained by a back pressure regulator with an accuracy of ± 1 – 2 bar.

Once the temperature and pressure reached the required values and were stable, the liquid feed pump was turned on. The feed was pre heated to reaction temperature prior to entering the reactor and a 2 mL liquid sample product collected every 30 minute for the first 2 hours and then once every hour for the remaining time on stream. The main gases used in this work have been summarised in Table 3.1.

In terms of shutdown procedure, the liquid feed pump and main heater were switched off. The system was then de-pressurised and purged with N_2.

a)

b)

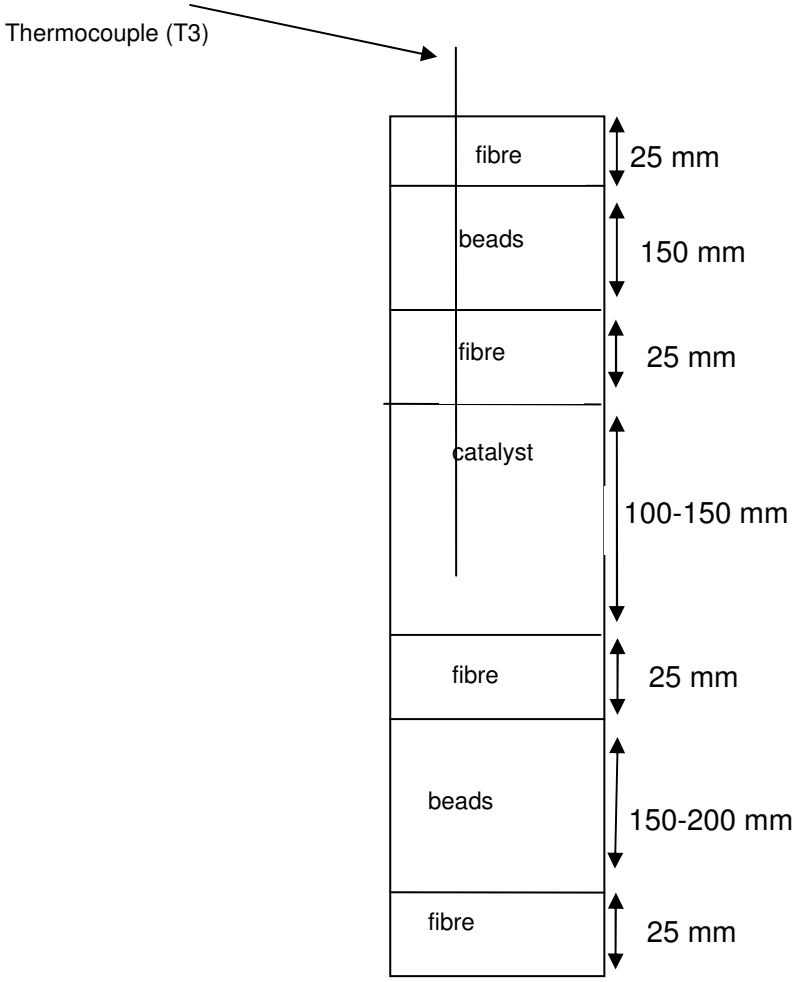

Figure 3.5. a) Fixed bed tube image; b) Fixed bed tube diagram.

Table 3.1. Gases used in this work.

Material	Use
N_2 gas (Oxygen Free, 99.9989% BOC gases)	• Used to purge the rig before and after the reactions. • Used to pressurise the system during 1-hexene isomerisation.
H_2 gas (99.995%, BOC gases)	• Used during naphthalene hydrogenation reaction. • Used to pressurise the system during naphthalene hydrogenation.
CO_2 (Liquid withdrawal, 99.99% BOC gases)	• Used to reactivate NiMo catalyst.
He gas (99.999%, BOC gases)	• GC-FID and TPD analysis carrier gas.

3.2.3. Sample analysis (GC-FID)

An Agilent 6850 GC equipped with FID detector and a 30m DB-5 capillary column was used to examine the liquid products from the reaction. The stream split ratio was 1:75; the injection volume was 0.2 μL and the carrier gas was helium.

Figure 3.6 shows the analysis method of 1-hexene, its isomers and oligomers. The temperature of the oven was held at 30 ℃ for 12 minutes, followed by a raise from 30 to 250 ℃ at a rate of 20 ℃/min. The temperature was then held at 250 ℃ for 7 minutes. The concentrations of 1-hexene and its isomers were assumed to be proportional to their peak areas. The chromatogram and calibration of the peak area are shown in Appendix 8.3.

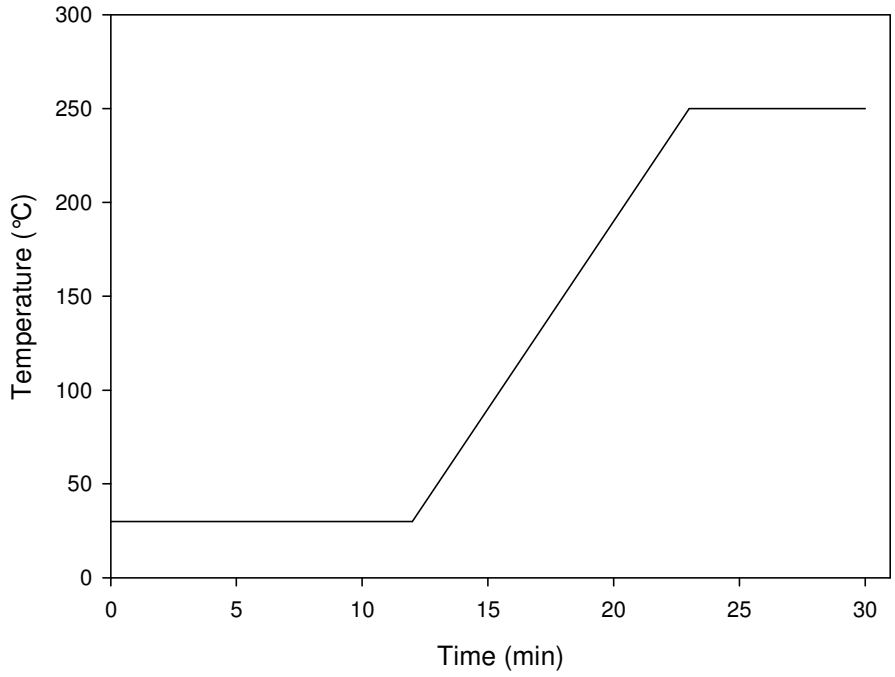

Figure 3.6. GC method for 1-hexene, its isomers and oligomors analysis.

Figure 3.7 shows the analysis method for naphthalene, tetralin and decalin. The temperature of the oven was increased from 100 ℃ to 280 ℃ at 10 ℃/min and then held at 280 ℃ for 7 minutes.

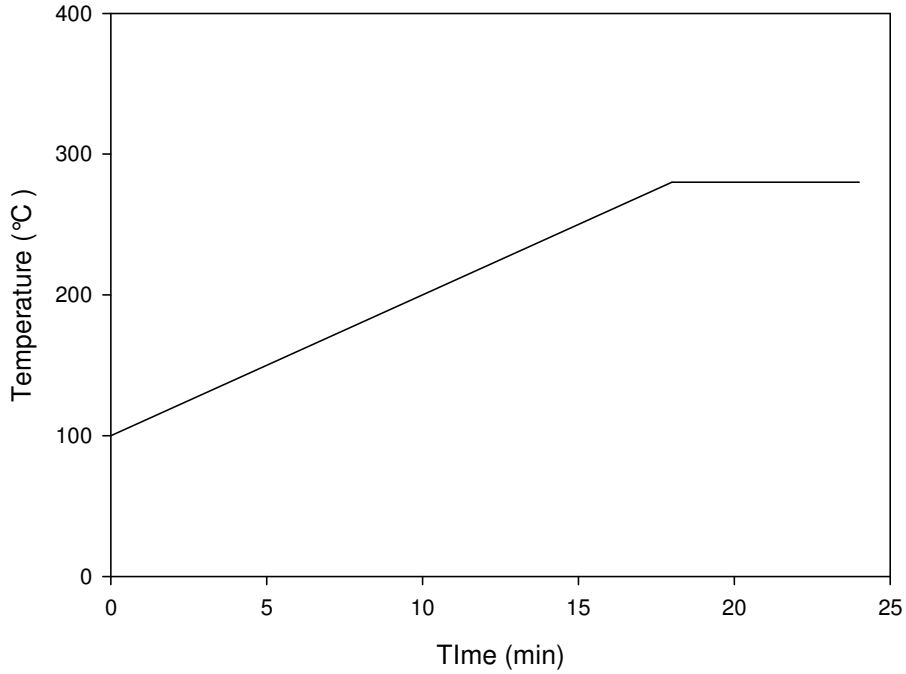

Figure 3.7. GC method for naphthalene, tetralin and decalin analysis.

3.3. Reactions studied

3.3.1. Isomerisation of 1-hexene

The isomerisation of 1-hexene was carried out using ZSM5 and zeolite Y catalysts. 1-Hexene (Aldrich, 97%) was always obtained from the same supplier to ensure a consistent feed material. Small amounts of impurities, such as peroxides, carbonyls, and water may be formed during transport or long-term storage. Alumina or molecular sieves are effective in removing these impurities (Chevron Phillips, 2008).

A blank run was carried out on alumina pellets without the zeolite and this showed that no reaction occurred over the alumina pellets. The conversion results were all reproducible within 2 – 4% accuracy.

The conversion of 1-hexene, yield of isomers, dimers and trimers at a certain time on stream were defined as follows.

The conversion of 1-hexene:

$$Conv = \frac{C^0_{1-hexene} - C_{1-hexene}}{C^0_{1-hexene}} * 100\% \quad (3.1)$$

The yields (Y_i) of isomers, dimers, and trimers:

$$Y_i = \frac{C_i}{C^0_{1-hexene}} * 100\% \quad (3.2)$$

The selectivity (S_i) of isomers, dimers, and trimers:

$$S_i = \frac{Y_i}{\sum Y_i} * 100\% \quad (3.3)$$

Where C_i^0 and C_i are the initial and the final weight concentrations for compound *i*, which could be isomers, dimers, and trimers of 1-hexene.

The activity of catalyst is described in terms of the reaction rate calculated according to the following equation:

$$r = \frac{ConvF}{m_{cat}} \quad (3.4)$$

Where *r* is the reaction rate (mol/(g_{cat}h)), *conv* is the conversion of reactant 1-hexene, *F* is the molar flow rate of the reactant (mol/s) and m_{cat} is the catalyst weight (g).

The liquid products collected from the gas–liquid separator were analysed for 1-hexene, its isomers and oligomers using the method outlined in section 3.2.3.

3.3.2. Critical properties of 1-hexene

To determine the experimental conditions for the reaction, it is important to have a thorough understanding of the boundary between regions of single and binary phases for the reaction mixture and how it moves during the reaction. The composition of the fix bed changes from pure 1-hexene to a mixture containing isomers and oligomers as the reaction progresses. The reaction mixture was simplified and 1-hexene, 1-dodecene and 1-octadecene were selected to represent isomers, dimers and trimers in the reaction mixture. The system was treated as a ternary system with particular concentrations of 1-hexene, 1-dodecene and 1-octadecene. The Peng–Robinson equation of state, Equation 3.5, was selected as the chosen physical property package. Mixing rules for a binary system are given below. The T_c, P_c, ω (the acentric factor), and binary interaction parameters, which are required to calculate parameters *a* and *b*, were taken from HYSYS library. For mixtures, the van der Waals mixing rule was used as defined by Equation 3.6 and 3.7. The values of the parameters input to the equations are listed in Tables 3.2 and 3.3.

$$P = \frac{RT}{v-b} - \frac{a}{v(v+b)+ b(v-b)} \tag{3.5}$$

$$a = \sum_i \sum_j x_i x_j \, (a_i a_j)^{0.5}(1 - \, k_{ij}) \tag{3.6}$$

$$b = \sum_i x_i b_i \tag{3.7}$$

Where x_i is the mole fraction of the *i*th component; a_i and b_i are the pure substance parameters in Peng-Robinson equation of state; and k_{ij} is the binary interaction parameter for the (*i*,*j*) pair.

Table 3.2. Pure component parameters for the Peng–Robinson equation of state.

Component	**T_c (°C)**	**P_c (bar)**	**Ω**
1-hexene	230.8	31.7	0.285
1-dodecene	383.9	18.5	0.584
1-octadecene	469.8	12.5	0.855

Table 3.3. Binary interaction parameters for the Peng–Robinson equation of state.

Component i	**Component j**	**K_{ij}**
1-hexene	1-dodecene	0.00417
1-hexene	1-octadecene	0.0133
1-dodecene	1-octadecene	0.00287

To calculate the concentration of hexenes, dimers, and trimers in the liquid and gas-phases when the reaction mixture is in a two phase region, a HYSYS case was built with one gas-liquid separator, one inlet, and two outlets. This simple flowsheet is illustrated in Figure 3.8 and it allowed a “flash” calculation to be performed for the mixture. An example HYSYS flash calculation is given in Appendix 8.4.

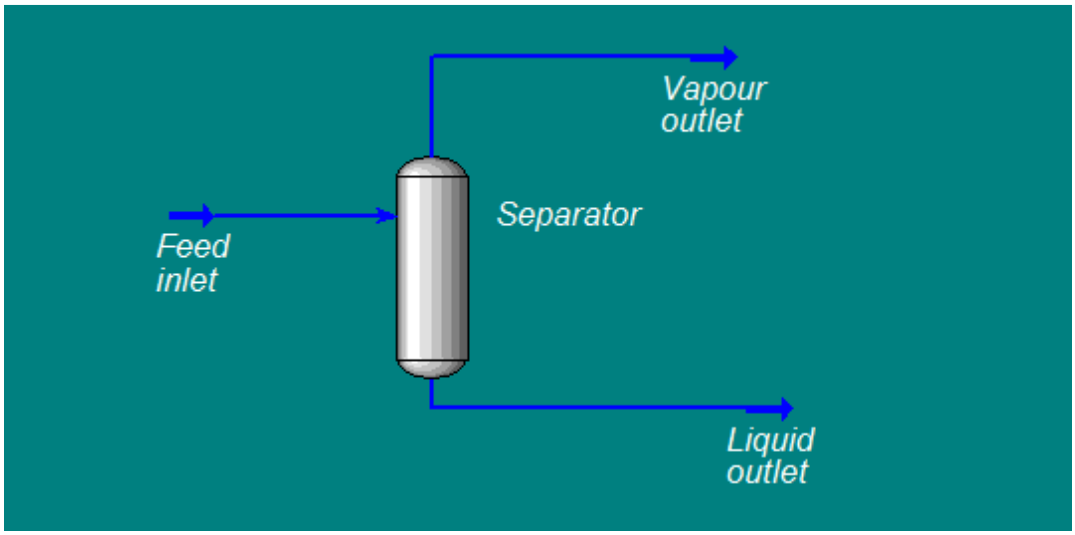

Figure 3.8. Flash calculation using a separator with one inlet and two outlets in HYSYS.

The critical properties of the system are T_c: 231 ℃ and P_c: 31.6 bar. The phase diagram is shown in Figure 3.9 and the experimental points are marked on the diagram. The experimental conditions were chosen close to the intersection between the sub and supercritical phases since this region is of most interest as the properties are very sensitive to slight changes in pressure.

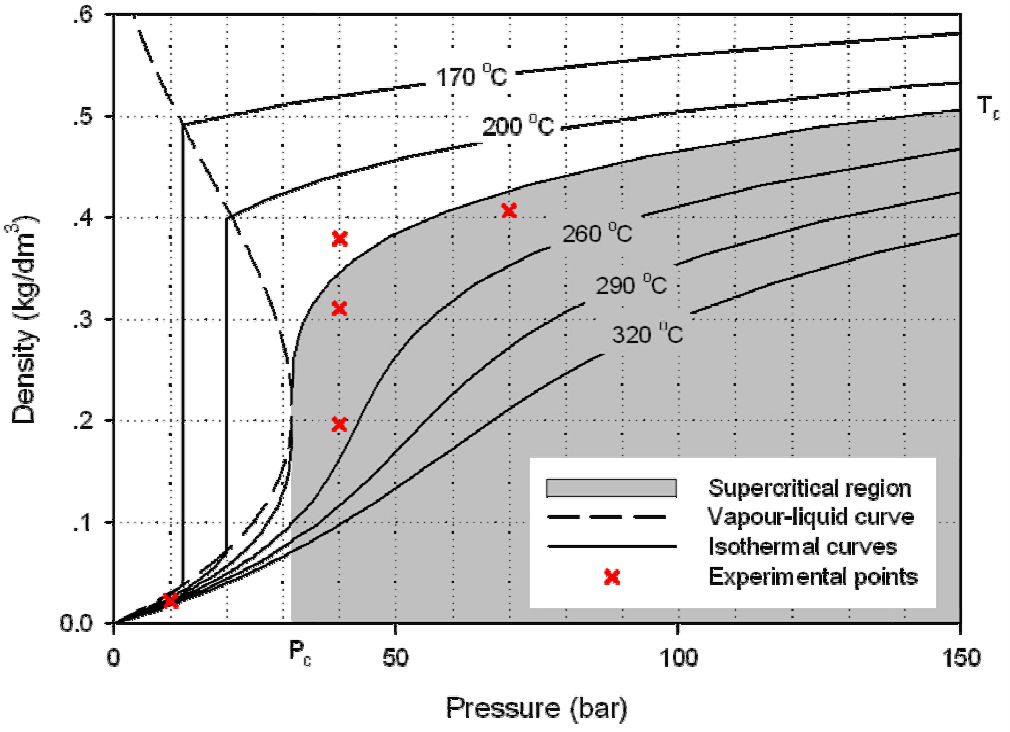

Figure 3.9. Phase diagram of 1-hexene.

3.3.3. Isomerisation of 1-hexene over ZSM5 catalyst

The isomerisation of 1-hexene was carried with 10 gramme of ZSM5 catalyst and a constant liquid 1-hexene flow rate at 0.5 mL/min for 96 hours. The experimental runs are summarised in Table 3.4. The operating temperature and pressure were varied between 220 - 250 ℃ and 10 - 70 bar, respectively, to cover a range of sub and supercritical conditions.

To further investigate the initial coke formation in the catalyst bed, experiments with a smaller amount of catalyst (0.5 gramme) and shorter time on stream were carried out at 235 ℃, 10 bar (subcritical) and 235 ℃, 40 bar (supercritical) with a constant feed flow rate of 1 mL/min for 8 hours on stream.

Table 3.4. ZSM5 catalyst experimental runs summary.

Experiment	T (℃)	P (bar)	ρ (g/mL)	Feed flow rate (ml/min)	Catalyst loading (g)	TOS (h)	Phase
1	235	10	0.02	0.5	10	96	Sub
2	235	40	0.3	0.5	10	96	Super
3	235	70	0.4	0.5	10	96	Super
4	220	40	0.4	0.5	10	96	Sub
5	250	40	0.2	0.5	10	96	Super
6	235	10	0.02	1	0.5	8	Sub
7	235	40	0.3	1	0.5	8	Super

3.3.4. Isomerisation of 1-hexene over zeolite Y

The isomerisation of 1-hexene was carried out with 0.5 gramme of zeolite Y catalyst and a constant liquid 1-hexene flow rate at 1.5 mL/min for 2 or 6 hours. The experimental runs are summarised in Table 3.5. The operating temperature was varied between 220 to 250 ℃ and the pressure was varied between 10 to 70 bar to cover a range between sub and supercritical conditions. Further experiments were carried out to investigate the effect of pore size and acidity upon the deactivation behaviour. Further experiments were carried out with ZSM5 and the results from zeolite Y were compared with those of ZSM5.

In contrast with the previous isomerisation of 1-hexene over ZSM5 experiments (section 3.3.3); nitrogen was bubbled through the 1-hexene in the feed tank for 45 minutes at a flow of 500 mL/min prior to commencing the experiments to reduce the concentration of dissolved oxygen, and the same flow of nitrogen through the feed tank was continued throughout the duration of the experiment. Appendix 8.5 shows that bubbeling N_2 for 2 hours and 45 minutes gives similar results in terms of conversion.

Table 3.5. Reaction conditions for 1-hexene isomerisation over zeolite Y and ZSM5 catalyst.

Experiment	**T (℃)**	**P (bar)**	**ρ (g/ml)**	**Feed flow rate (ml/min)**	**Catalyst Loading (g)**	**TOS (h)**	**Phase**
1	235	10	0.02	1.5	0.5 (Zeolite Y)	6	Sub
2	235	40	0.3	1.5	0.5 (Zeolite Y)	6	Super
3	235	70	0.4	1.5	0.5 (Zeolite Y)	6	Super
4	220	40	0.4	1.5	0.5 (Zeolite Y)	6	Sub
5	250	40	0.2	1.5	0.5 (Zeolite Y)	6	Super
6	235	10	0.02	1.5	0.5 (ZSM5)	6	Sub
7	235	40	0.3	1.5	0.5 (ZSM5)	6	Super
8	235	10	0.023	1.5	0.5 (Zeolite Y)	2	Sub
9	235	40	0.311	1.5	0.5 (Zeolite Y)	2	Super

3.3.5. Hydrogenation of naphthalene over NiMo catalyst

The hydrogenation of naphthalene was carried out with 2 gramme of pre-sulfided NiMo catalyst. Naphthalene (99%, Aldrich) was dissolved in cyclohexane (99.5%, Aldrich) to the required concentration (between 10 – 100 g/L) and pumped to the reactor. The liquid feed flow rate varied between 0.5 – 2.5 mL/min. The catalyst was reduced prior to the reaction as is discussed in catalyst preparation section 3.1.2.

A total of six cases were studied and are summarised in Table 3.6. In case 1, the temperature and pressure were varied between 100 ℃ – 300 ℃ and 20 – 80 bar, respectively. All reactions in the first case were conducted in supercritical fluid conditions. The reaction conditions were changed in the second case to enable the study of the effect of operating in subcritical versus supercritical conditions. The temperature and pressure were varied between 260 – 300 ℃ and 60 – 90 bar, respectively, in the second case. In the third case, the effect of cis to trans-decalin isomerisation on the product distribution was studied where pure cis-decalin was used as the feed. In the fourth case, the temperature and pressure were fixed at 300 ℃ and 80 bar to study the effect of varying naphthalene feed concentration between 10 – 100 g/L. In the fifth case, the long term deactivation behaviour was studied and conditions that would speed up the deactivation process were chosen. Finally in case six, catalyst reactivation and coke removal by supercritical CO_2 were studied.

Table 3.6. Reaction conditions for naphthalene hydrogenation over NiMo.

Case	T (℃)	P (bar)	Naphthalene feed concentration (g/L)	Hydrogen feed flow rate (mL/min)	Phase	Catalyst (g)
Case 1	300	20	10	10	Super	2
	300	50	10	10	Super	2
	300	60	10	10	Super	2
	300	80	10	10	Super	2
	280	80	10	10	Super	2
	270	80	10	10	Super	2
	250	80	10	10	Super	2
Case 2	300	60	10	2	Sub	2
	300	90	10	2	Super	2
	260	90	10	2	Sub	2
Case 3	300	80	0	10	Super	2
Case 4	300	80	10	10	Super	2
	300	80	20	10	Super	2
	300	80	40	10	Super	2
	300	80	60	10	Super	2
	300	80	80	10	Super	2
	300	80	100	10	Super	2
Case 5	300	80	100	10	Super	2
Case 6	300	80	100	10	Super	2

The critical point of the mixture was obtained from the Aspen HYSYS software. The Peng-Robinson equation of state, Equation 3.5, was used for the physical

property package (section 3.3.2). The T_c, P_c, ω and binary interaction parameters, which are required to calculate parameters *a* and *b*, were taken from HYSYS library. The van der Waals mixing rule was used and is given in Equations 3.6 and 3.7. The values used for the parameters input into the equations are listed in Tables 3.7 and 3.8.

Table 3.7. Binary interaction parameters for the Peng–Robinson equation of state during naphthalene hydrogenation.

	Naphthalene	**Cyclohexane**	**Hydrogen**	**Tetralin**
Naphthalene				
Cyclohexane	0.00114			
Hydrogen	0.292	0.285		
Tetralin	0.00007	0.00179	0.292	
Decalin	0.00032	0.00266	0.292	0.00009

Table 3.8. Pure component parameters for the Peng–Robinson equation of state for naphthalene, cyclohexane, H_2, tetralin, cis and trans-decalin.

	T_c (°C)	**P_c (bar)**	**Ω**
Naphthalene	475.2	40.51	0.302
Cyclohexane	280.1	40.53	0.213
H_2	-230.4	19.71	-0.120
Tetralin	447.0	36.20	0.328
Cis-decalin	429.1	32.0	0.286
Trans-decalin	413.9	32.0	0.270

As each reaction progressed, the composition in the fixed bed reactor changed as hydrogenated products were formed. The system then also included tetralin, decalin, hydrogen, cyclohexane and some naphthalene. This change was taken into account when calculating the critical point for each reaction mixture.

A HYSYS case was built with a gas-liquid separator, which has one inlet and two outlet streams (shown in Figure 3.8), to calculate the concentration of naphthalene, tetralin, decalin and hydrogen in the liquid and gas-phases when the reaction mixture is in a two phase region. This simple case allowed a 'flash' calculation to be performed for the reaction mixture.

Each sub section in Chapter 6 contains a summary of the reaction mixture composition and a binary HYSYS plot from the ternary system to illustrate the phase behaviour of the system under each set of conditions.

3.4. Characterisation techniques

Several characterisation techniques were used to analyse the fresh and coked catalyst samples. TGA was used to determine the amount of coke deposited on the catalyst where the weight change in the catalyst during oxidation was measured. DRIFTS were used to investigate the nature of the active species and nature of coke deposits on the catalyst. Nitrogen adsorption-desorption analysis was used to measure the specific surface area, pore size distribution and pore volume of the fresh and used catalyst. TPD was used to analyse the acidity of the zeolite catalysts. XRD was used to study the crystalline phase of the catalyst and how that was influenced by coke deposits. This section summarises the method used in each characterisation technique.

3.4.1. TGA analysis

The weight percentage of coke content was calculated as follows:

$$\%coke = \frac{w_{200} - w_{1000}}{W_{1000}} * 100\% \quad (3.8)$$

Where w_{200} is the weight of the sample at 200 ºC and w_{1000} is the weight of the sample at 1000 ºC. All samples were repeated three times and the percentage error calculated.

3.4.1.1. ZSM5 TGA method

Figure 3.10 shows the TGA method for ZSM5 catalyst. The fresh and coked catalyst samples were analysed for the removal of coke by raising the sample to a final temperature of 1000 ℃ at a rate of 10 ℃/min in air. The sample was kept at 1000 ℃ for 2 hours after which it was cooled down to room temperature at a rate of 10 ℃/min. The weight loss between 200 and 1000 ℃ was attributed to coke. The resolution of successive TGA weight losses is important in obtaining accurate weight change values; therefore, the TGA ramp rate of 10 ℃/min was selected as it gave clear distinguishable TGA curves.

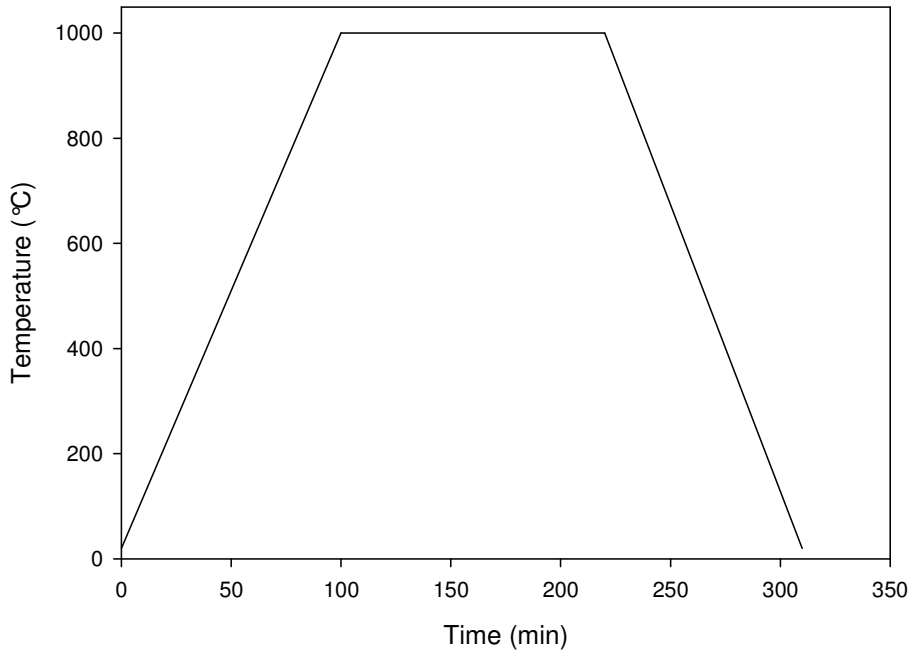

Figure 3.10. TGA method for ZSM5 catalyst.

3.4.1.2. Zeolite Y TGA method

The sample of used zeolite Y catalyst was heated to 200 ℃ at a rate of 10 ℃/min and maintained there for 60 minutes under nitrogen flow to remove any adsorbed water. The temperature was then raised to 1000 ℃ at a rate of 10 ℃/min and kept there for 30 minutes under nitrogen flow. After 30 minutes the flow was switched from nitrogen to air at 1000 ℃ and kept for two hours (Wang and Manos, 2007). The sample was then cooled to room temperature at a rate of 10 ℃/min (Figure 3.11). The weight loss between 200 ℃ and 1000 ℃ was attributed to coke.

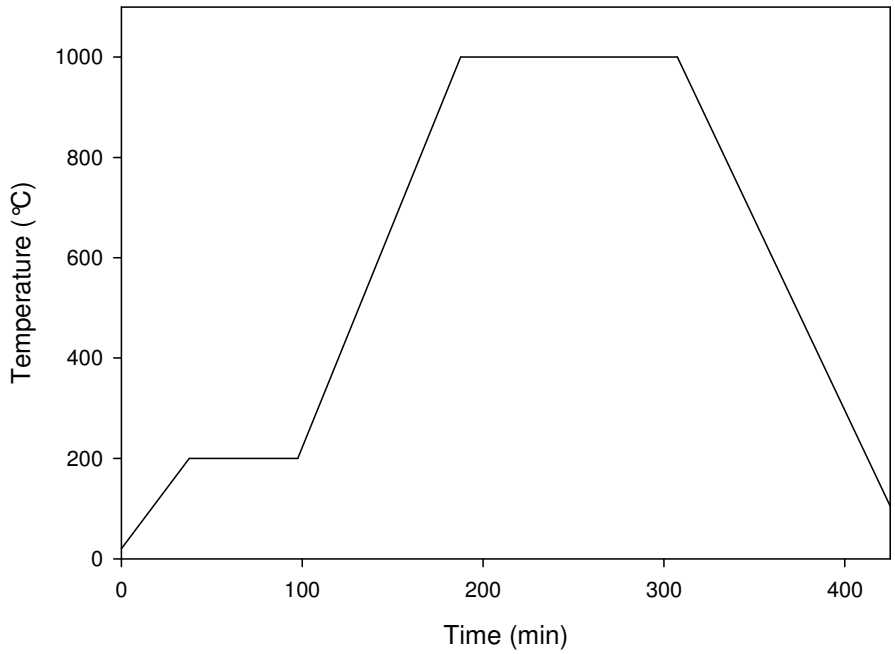

Figure 3.7. TGA method for zeolite Y analysis.

3.4.1.3. NiMo TGA method

The coked catalyst sample was heated to 200 ℃ at a rate of 10 ℃/min in air to remove any adsorbed water. It was held there for 15 minutes after which the temperature was raised to 1000 ℃ at a rate of 10 ℃/min. The temperature was constant at 1000 ℃ for one hour after which it was cooled down to room temperature at a rate of 10 ℃/min (Figure 3.12).

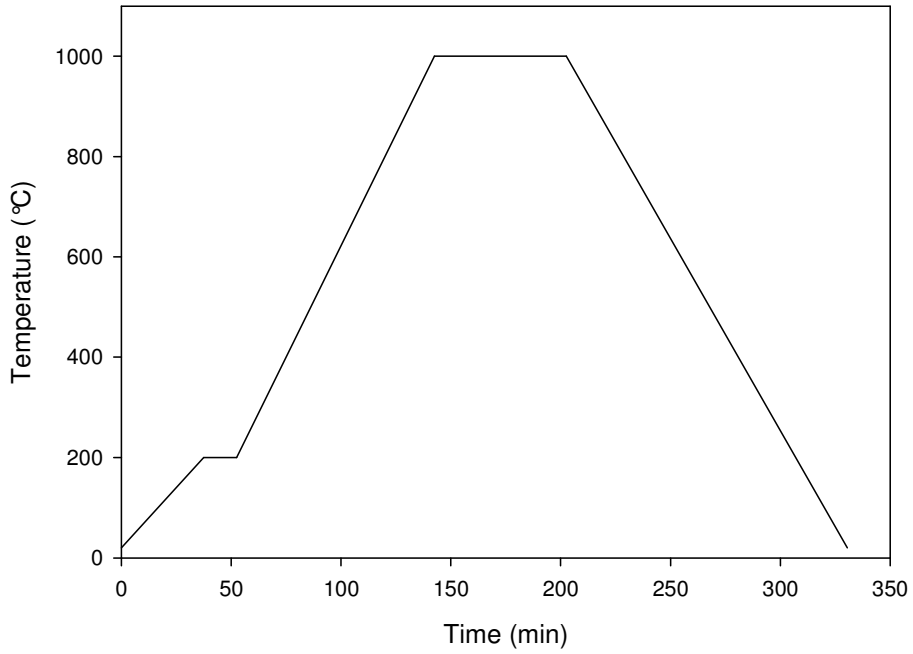

Figure 3.12. TGA method for NiMo catalyst analysis.

3.4.2. DRIFTS

Diffuse Reflectance Infrared Fourier Transform Spectra (DRIFTS) of the crushed catalysts were obtained with a Bruker Tensor 37 spectrometer. A background spectrum was recorded with KBr powder in air. The catalyst was crushed in a pestle and mortar, sieved and loaded in to the sample cup of a

thermo collector diffuse reflectance accessory. Room temperature spectra were recorded in the mid-IR range (550 - 4000 cm^{-1}). For each spectrum, 64 scans were accumulated with a nominal 2 cm^{-1} resolution.

3.4.3. Nitrogen adsorption – desorption analysis

The surface area, pore size distribution, and pore volume of the fresh and coked catalysts were determined from N_2 isotherms measured at –196 ℃ by using a micro-pore analyzer (Micromeritics ASAP 2020). Prior to the nitrogen sorption experiment, the samples were degassed at a temperature of 200 ℃. The temperature was selected to avoid the removal of coke deposition during the degassing.

3.4.4. TPD analysis

The fresh and coked samples of the catalyst were analysed with a Temperature Programmed Desorption (TPD) apparatus, a Micromeritics AutoChem 2920. TPD was carried out initially without tertbutylamine adsorption, followed by a second TPD run with tertbutylamine adsorption according to a procedure of Wang and Manos (2007). Around 50 mg of coked catalyst sample was placed in a U-shaped quartz cell which was then pre heated at 10 ℃/min to 200 ℃ (Figure 3.13). It remained at this temperature for 60 minutes to remove any adsorbed species on the surface including water. The sample was then cooled down to 50 ℃ at a rate of 10 ℃/min. Adsorption of tertbutylamine was carried out in a He stream until the catalyst surface became saturated. The sample was

then heated to 150 ℃ and kept for 30 minutes so that physisorbed tertbutylamine could be desorbed. The temperature was then heated further to 800 ℃ at a heating rate of 10 ℃/min and kept constant for 30 minutes. The desorbed tertbutylamine and coke precursors were monitored with a thermal conductivity detector.

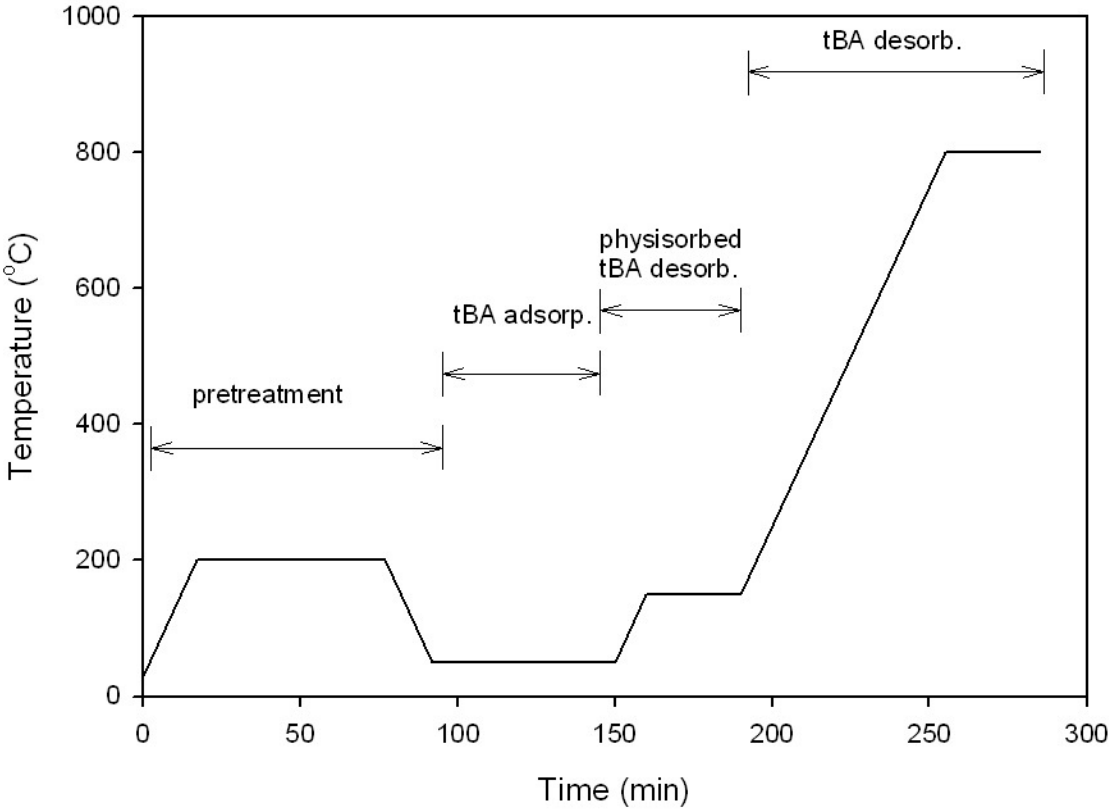

Figure 3.13. TPD method for characterising the zeolite catalysts.

A typical TPD trace without tertbutylamine shows only peaks related to desorption of coke precursors. Comparing the TPD signal with and without tertbutylamine, it is usually observed that they overlap in the high temperature zone for any coking system due to removal of coke precursors. By subtracting the signal of TPD of the coked catalyst from the one in which tertbutylamine is

adsorbed, the free acid sites of the coked sample inhabited by both coke precursors and hard coke can be calculated (Wang and Manos, 2007). The coked and fresh zeolites were analysed by this method to measure the total free acid sites. The total free mean acidity was calculated as follows in Equation 3.9.

$$N_{as} = 0.137 * \left(\frac{A_1}{(1-c)*w_1} - \frac{A_2}{(1-c)* w_2}\right) \quad (3.9)$$

Where A_1, A_2 are the peak area of desorption with and without tBA adsorption. w_1, w_2 are the sample weight for desorption with and without tBA adsorption, c is the percentage coke. Each sample was analysed at least four times and the mean acidity values, as well as the percentage error, are reported in Chapters 4 and 5.

3.4.5. XRD analysis

The crystalline phases of the fresh and coked catalyst samples were analysed using powder XRD on a Siemens D5000 powder X-ray diffractometer. The detector was PSD-Lynx Eye and the scan type was unlocked coupled. The scanning angle was in the range of 5 – 90 θ and the step size was 0.02. The peaks were assigned according to the XRD data base JCPDS; which is the standard database for X-ray powder diffraction data for natural and synthetic materials.

CHAPTER 4

1-HEXENE ISOMERISATION OVER H-ZSM5 CATALYST UNDER SUPERCRITICAL CONDITIONS

The literature review in Chapter 2 showed that many reactions have been successfully carried out in supercritical conditions and that previous studies have shown the possibility of extracting coke deposits from the catalyst surface, thus prolonging the catalyst life time. In this Chapter, the effects of changing the solvating and transportation properties of the fluid when moving from the sub to supercritical regions are compared with the amount of coke deposited in each case. The phase behaviour of the system is presented in section 4.1 and the effect of pressure and temperature on catalytic activity and product distribution are reported in section 4.2. The effect of using a smaller catalyst bed is reported in section 4.3 and catalyst characterisation is presented in section 4.4. The change in catalyst acidity due to coking is reported in section 4.5. Finally, a conclusion is drawn in section 4.6.

As previously stated, the aim of this work was to study the use of supercritical conditions for delaying coking and extending catalyst life time, however it should be noted that within pores of few Angstroms dimension, such as those that occur in zeolites, the concept of SCFs is not meaningful because the pores only contain a few molecules of the fluid, which therefore do not follow bulk behaviour. Nonetheless, at the catalyst surface and within larger pores, supercritical conditions are relevant. The enhanced solubility of coke precursors

that are formed on the catalyst surface in the supercritical solvent could therefore lead to their extraction from the catalyst.

This chapter is based on the paper: Jiawei Wang, Faiza Hassan, Peter I. Chigada, Sean P. Rigby, Bushra Al-Duri and Joseph Wood. Ind. Eng. Chem. Res. 2009, 48, 7899–7909. A copy of the paper can be found in Appendix 8.1.

4.1. Phase behaviour

Table 3.5 in Chapter 3 gives a summary of all reactions studied over ZSM5 catalyst. The isomerisation and oligomerisation of 1-hexene was carried out at a temperature range of 220 - 250 ℃ and a pressure range of 10 - 70 bar. The temperatures and pressures were chosen to cover the subcritical and supercritical region of 1-hexene. The critical temperature and pressure were 230.8 ℃ and 31.7 bar. The residence time of 1-hexene in the reactor operating at 235 ℃ was based on inlet conditions and varied from 24.5 to 433.6 seconds at 10 bar and 70 bar, respectively. The reaction products obtained were 1-hexene isomers (iC_6), dimers (C_{12}), and trimers (C_{18}). The main isomer products were trans-2hexene, cis-2-hexene, and cis/trans-3-hexene.

The Peng-Robinson equation of state was used to predict the evolving phase boundries. The evolving phase boundaries as a function of reactor time on stream are presented in Figure 4.1. As the reaction proceeds, the molar concentration of dimers and trimers increases and this causes the phase boundaries to move toward higher temperature.

The Peng-Robinson equation of state, like all cubic equations of state, can predict close to the critical point of binary and multicomponent systems [Baiker,

1999]. However, the predictions of this equation are limited to the estimation of vapour pressures and the calculated saturated liquid volumes are higher than experimental measurements [Wei and Sadus, 2000]. The application of equations of state is also limited to primarily non-polar or slightly polar components. Highly non-ideal systems are not realiably modelled by equations of state such as Peng-Robinson. Furthermore, the success of the Peng-Robinson equation of state depends greatly on the use of proper mixing rules and assignment of interaction parameters [Baiker, 1999].

For the experiment at 235 ℃ and 10 bar (subcritical), shown in Figure 4.1a, the experimental point is initially outside the two-phase envelope, indicating that the reaction occurs under gas-phase conditions. However, after 7 hours on stream it falls inside the phase boundary, indicating that a two phase mixture forms within the bulk phase. Although a two-phase mixture cannot exist within the channels of ZSM5, it is possible that in the meso-porous alumina surrounding the zeolite crystals, pockets of liquid could form within the pore structure. As the reaction mixture within the alumina pores separates it could form a hexenes-rich gas-phase and a liquid-phase, which has a high concentration of dimers and trimers.

Taking the reaction mixture at 20 hours as an example, the molar concentration of hexenes, dimers, and trimers are 81.1%, 16.4%, and 2.5%, respectively. As calculated by HYSYS, upon flashing the mixture would separate into two phases, the gas-phase having composition 88.2% of hexenes, 11.4% of dimers, and 0.5% of trimers in mole concentration and the liquid-phase having composition 37.1% of hexenes, 47.6% of dimers, and 15.3% of trimers in mole

concentration (example calculation in Appendix 8.4). The mole concentrations of dimers and trimers in liquid-phase are, respectively, more than 4 and 30 times higher than the ones in the gas-phase. Therefore, it is more likely that dimers and trimers would condense within the alumina meso-pores and around the surface and pore entrances of the ZSM5 zeolite and thus could be considered as coke precursors. For the other four experiments, as shown in Figures 4.1b-e, the experimental points are in the one phase region during the reaction. The calculated phase behaviour suggests that all isomers, dimers, and trimers form a homogeneous mixture, which could facilitate the removal of heavy hydrocarbon.

a)

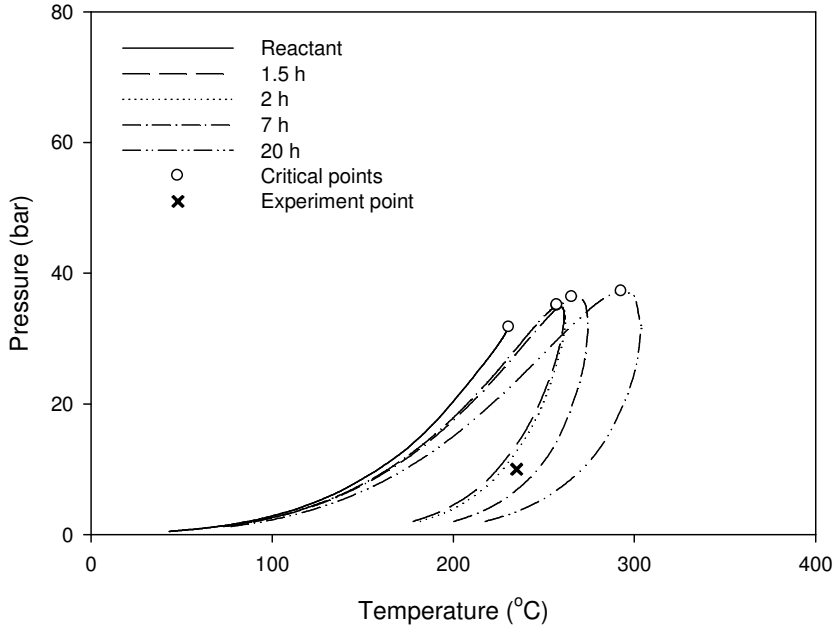

b)

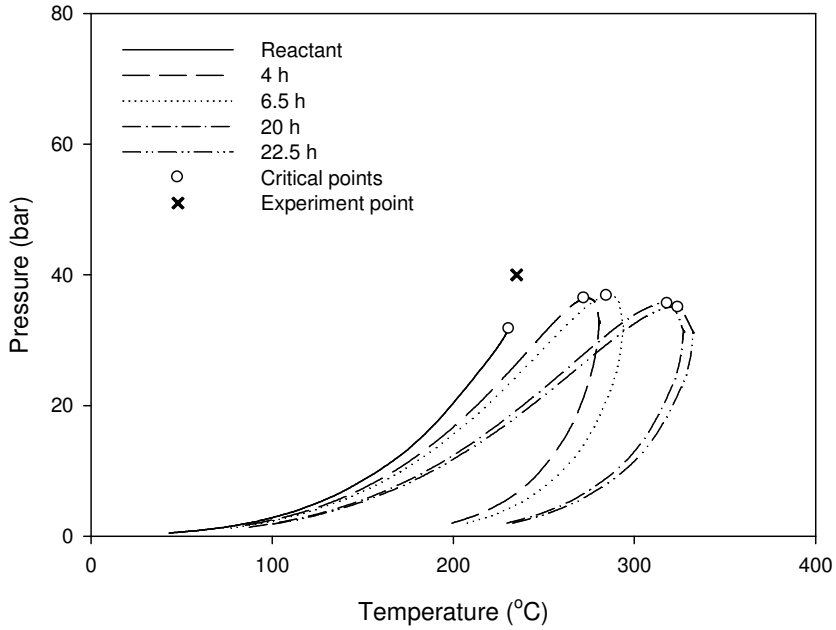

Figure 4.1. Calculated phase boundary for the isomerisation and oligomerisation reaction mixture in the first 24 hours; a) 235 ºC 10 bar; b) 235 ºC 40 bar. Symbols o represents the calculated critical points. Symbols x represent the reaction conditions.

c)

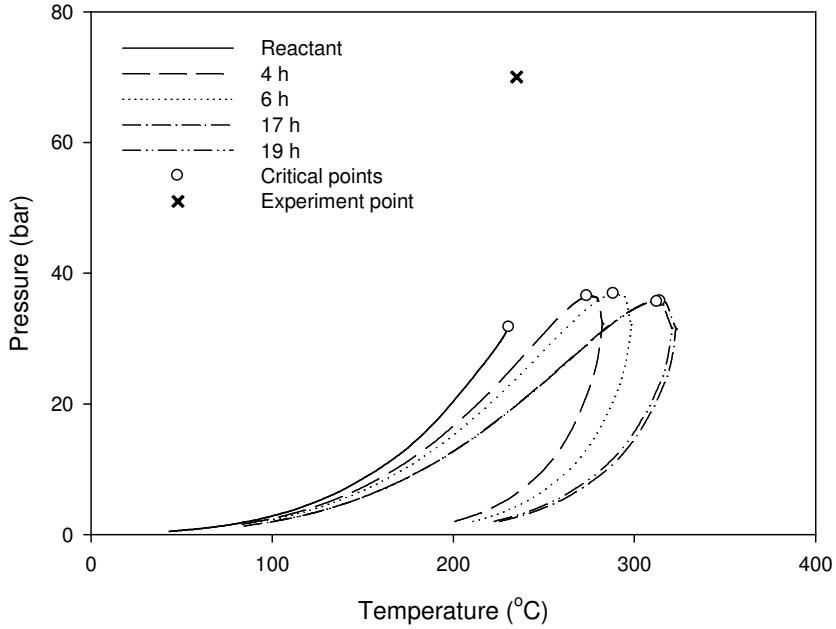

d)

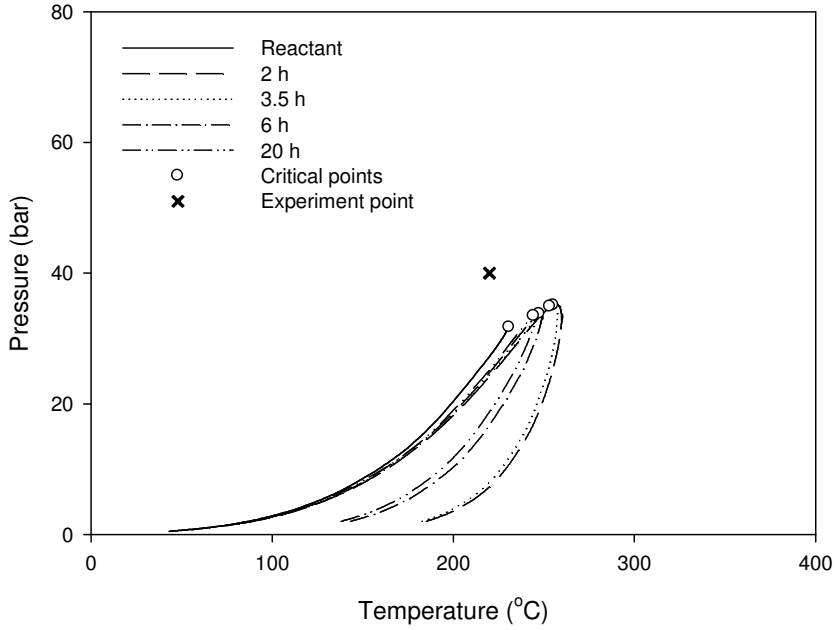

Figure 4.1. Calculated phase boundary for the isomerisation and oligomerisation reaction mixture in the first 24 hours; c) 235 ºC 70 bar; d) 220 ºC 40 bar. Symbols o represents the calculated critical points. Symbols x represent the reaction conditions.

e)

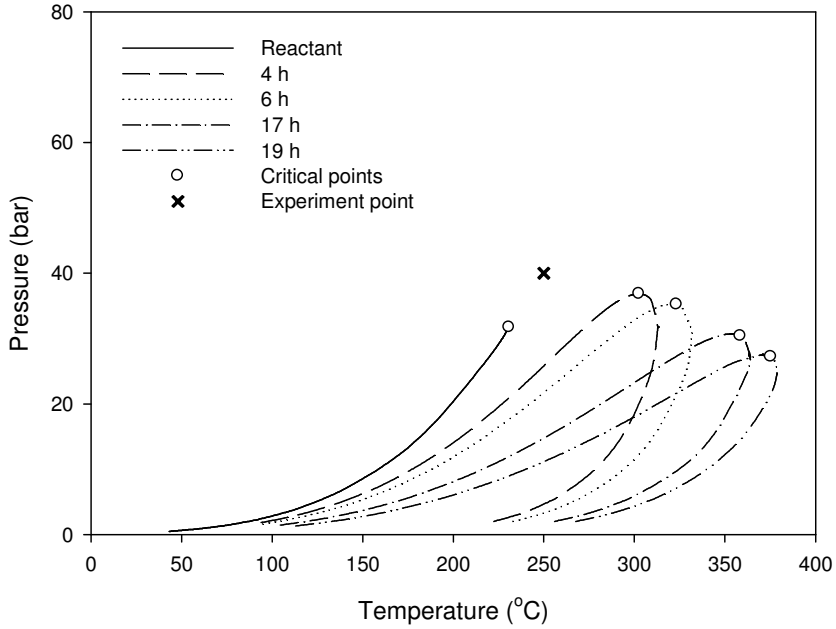

Figure 4.1. Calculated phase boundary for the isomerisation and oligomerisation reaction mixture in the first 24 hours; e) 250 ºC 40 bar. Symbols o represents the calculated critical points. Symbols x represent the reaction conditions.

4.2. Temperature and pressure effect on catalytic activity and product selectivity

Figure 4.2 shows 1-hexene conversion against time at different pressures of 10, 40 and 70 bar at a set temperature of 235 ºC for 96 hours on stream. The experiments show a catalyst start up effect, where an increase in conversion is observed in the initial hours of operation. This is thought be due to the time required for thorough wetting of the catalyst surface with reactants, diffusion of reactants to the catalyst active sites and formation of adsorbed intermediates upon the catalyst surface which participate in the isomerisation reaction.

Figure 4.2 shows that at 40 and 70 bar (supercritical), the conversions of 1-

hexene ranged from 94 - 98% whereas at 10 bar (subcritical) the conversion was between 94 – 95% with a slight deactivation observed after 80 hours. Overall the activity of the catalyst was stable for 96 hours on stream. Similarly, Li *et al.* (2003) found that ZSM5 catalyst with a Si/Al ratio of 90 has remarkable stability for isomerisation of light FCC naphtha.

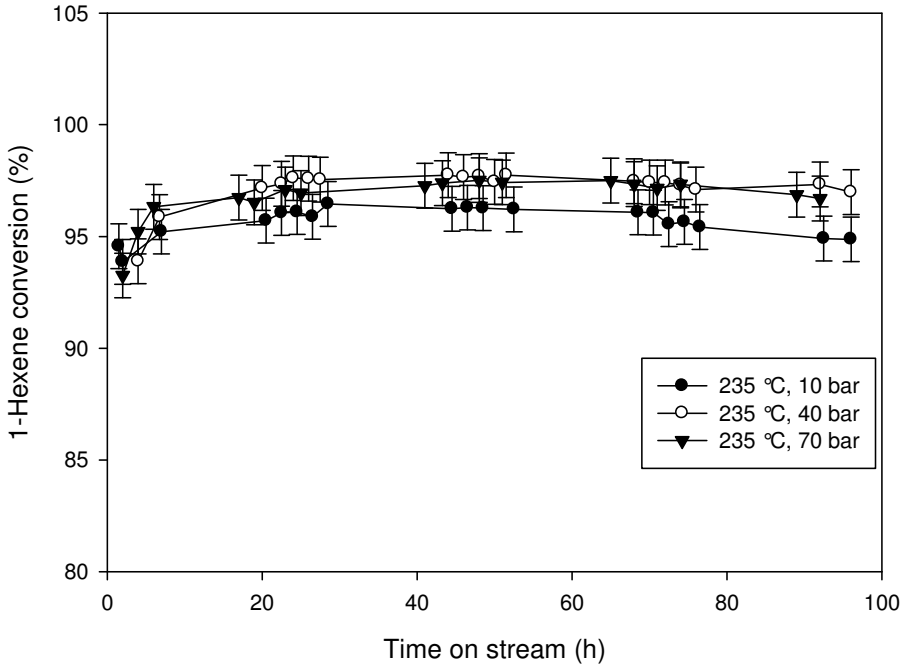

Figure 4.2. 1-hexene conversion against time at 235 ºC and 10, 40 and 70 bar for 96 hours on stream.

Figures 4.3a-c show the yield of isomers, dimers and trimers against time on stream at different pressures of 10, 40 and 70 bar at set temperature of 235 ℃ for 96 hours on stream. Figure 4.3a shows that the yield of isomers decreases with time on stream and stabilises after 30 hours on stream. At 10 bar; the yield of isomers drops from 77% to 39% after 30 hours on stream and remains stable increasing slightly to 41% after 96 hours on stream. Similarly at 40 bar, the yield

drops from 65% to 36% after 30 hours on stream and remains stable. At 70 bar, the yield of isomers decreases from 67% to 37% after 30 hours on stream and decreases slightly to 34% after 96 hours on stream.

a)

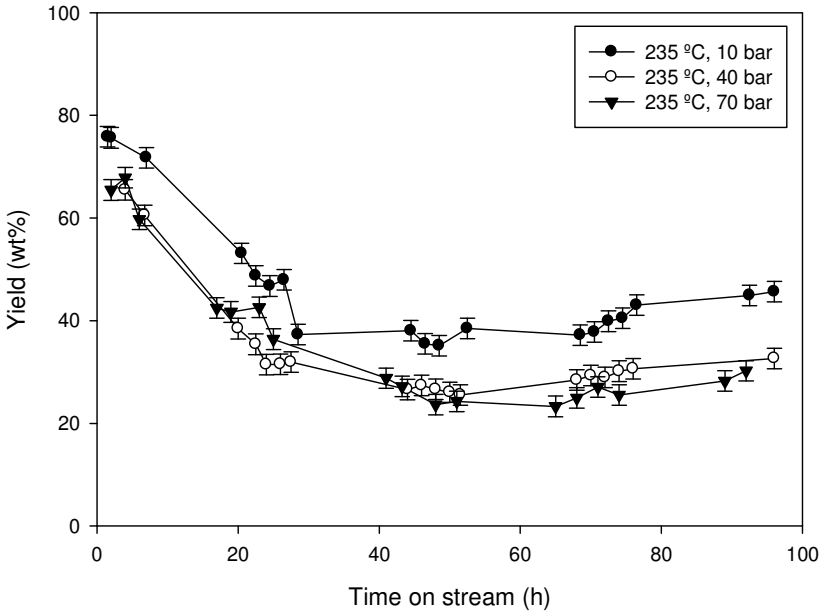

Figure 4.3. a) Yield of isomers at 235 ºC and 10, 40 and 70 bar.

b)

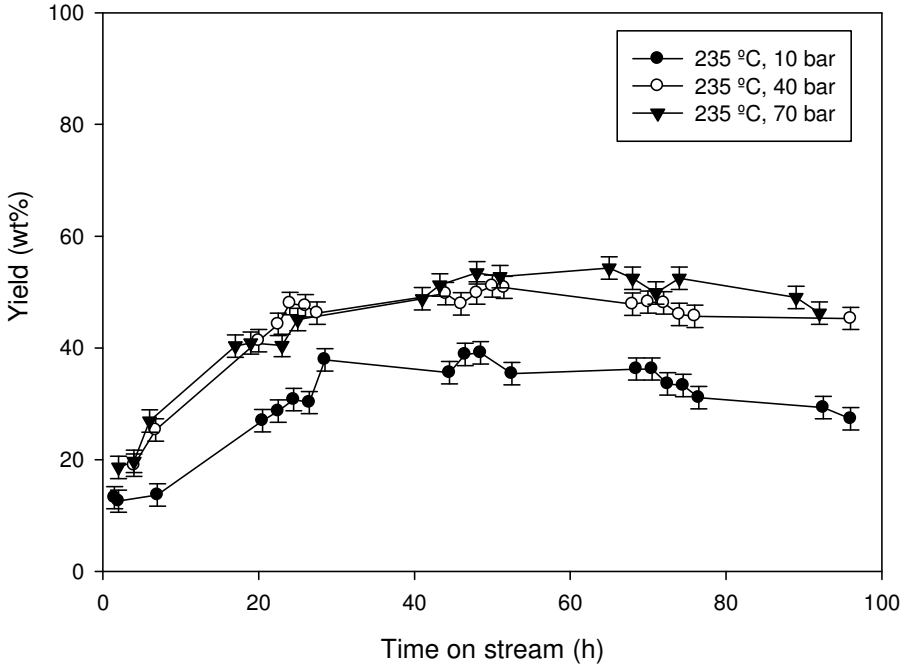

c)

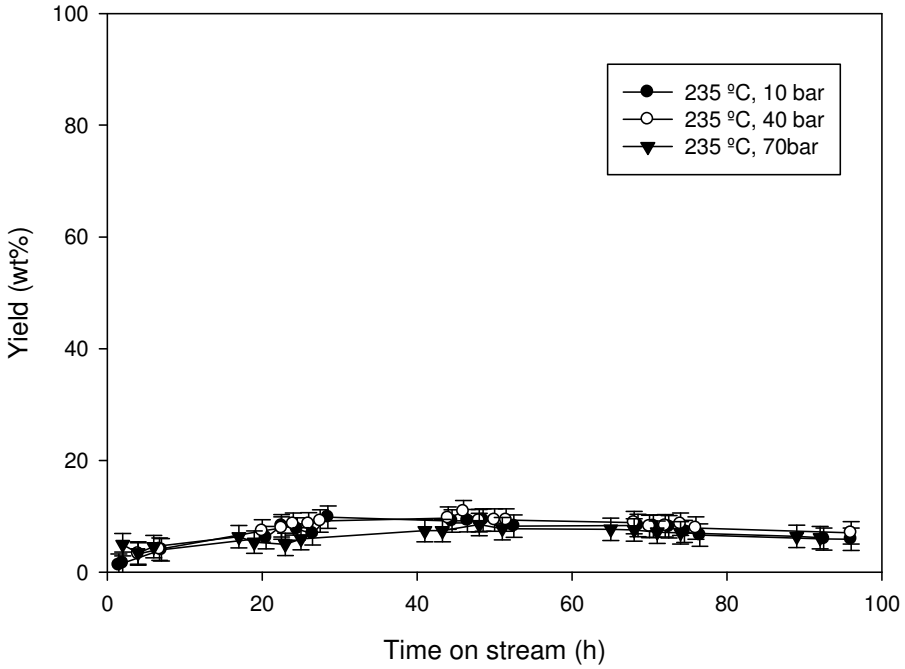

Figure 4.3. b) Yield of dimers at 235 ºC and 10, 40 and 70 bar; c) Yield of trimers at 235 ºC and 10, 40 and 70 bar.

Overall, there was a shift from the formation of isomers to the formation of dimers with increasing operating time. The yield of dimers increased from 18% at 0.5 hours on stream to 38% after 30 hours on stream at 10 bar, whereas at 40 and 70 bar this increases from 20% to about 45% after 30 hours on stream (Figure 4.3b). The yield of trimers is stable throughout between 3 - 5% (Figure 4.3c).

There are several possible explanations for the shift towards dimers with increasing operating time. Firstly, the diffusivity of dimers and trimers is lower than that of 1-hexene. During the reaction, 1-hexene was rapidly converted to its isomers, followed by diffusion controlled oligomerisation. The ratio of cis-2-hexene to trans-2-hexene reached the thermodynamic equilibrium ratio 0.42 at 235 ℃ (Sundaramurthy and Lingappan, 2000).

As a comparison of the relative rates of diffusion of the different compounds involved in the reaction, calculation of the bulk phase self-diffusivity of 1-hexene, 1-dodecene, and 1-octadecene at the critical point gave values of 6.19 $\times 10^{-8}$, 5.97 $\times 10^{-8}$, and 3.99 $\times 10^{-8}$ m^2/s, respectively, from a correlation of Lee and Thodos (1983) (an example calculation is given in Appendix 8.6). This demonstrates that in the bulk phase, the diffusivity of a C_{18} compound is 36% lower than that of a C_6 compound. However, it must be noted that inside the catalyst pores, the diffusivities will be several orders of magnitude slower than in the bulk phase. For example, using a cylindrical internal reflectance infrared spectroscopy technique, Süer *et al.* (1997) showed that the counter diffusion coefficients of *n*-hexane through 1-hexene were 7.6 $\times 10^{-17}$ and 2.8 $\times 10^{-16}$ m^2/s, respectively. Similar diffusion measurements of components adsorbed

upon porous solids have been performed using pulsed field gradient nuclear magnetic resonance (Karger and Pfeifer, 1987). As a layer of coke precursors forms upon the catalyst the rates of diffusion of dimers and trimers within this layer are slower than that of the reactant 1-hexene and therefore the process may become more limited by mass transfer of reactants to the catalyst.

Secondly, the distribution of acid sites of the zeolite may change during the reaction and therefore affect the relative rates of the isomerisation and dimerisation reactions. For example Mihindou-Koumba *et al.* (2008) observed a similar effect, in which the deliberate addition of a poison, collidine, to H-EU-1-type zeolite led to complete deactivation of the zeolite. This was not only due to poisoning of the acid sites on the outside surface of the pellets, but also due to the poisoning of acid sites at the pore mouths and blockage of the catalyst pores. The change in catalyst acidity due to coking will be explored further in the catalyst acidity characterisation section 4.5.

Thirdly, the formation of dimers and trimers changes the critical point of the mixture at 10 bar, such that at the same operating conditions a two-phase mixture forms. Finally, once a layer of coke builds up on the catalyst surface, there is a possibility that the coke itself may catalyse or take part in the reactions. Similar effects are known to occur in reactions such as the hydrogenation of acetylene, where a particular type of polymer species formed during the initial period of deactivation can be responsible for promotion of catalyst activity on a Pd/SiO_2 catalyst (Ahn *et al.*, 2007). In this work, evidence of coke deposition, but lack of deactivation in terms of 1-hexene conversion, strongly suggest that the latter effect does occur.

Table 4.1 shows the reaction pressure had a positive effect on the conversion of 1-hexene as it increased from 96% at 10 bar to 97% at 70 bar. The yield of isomers decreased with reaction pressure from 49% to 31% at 10 and 70 bar respectively. On the other hand, the yield of dimers increased with the reaction pressure from 42% to 61% at 10 and 70 bar respectively. In terms of the thermodynamics, high pressure favours light olefin oligomerisation to high molecular weights (Quann *et al.*, 1988). However, the pressure has less effect on the yield of trimers as it remains between 8 – 10%. This could be due to both the diffusional limitations within the pore system and the lower probability of coincident reaction centres of the molecules for a bimolecular reaction (Quann *et al.*, 1988).

Table 4.1. Average conversion and product selectivity with 10 gramme catalyst after 96 hours on stream.

Reaction conditions	**Conversion (%)**	**Product selectivity (iC_6)**	**Product selectivity (C_{12})**	**Product selectivity (C_{18})**
235 ℃, 10 bar	96	48	42	10
235 ℃, 40 bar	98	34	56	10
235 ℃, 70 bar	97	31	61	8
220 ℃, 40 bar	96	90	10	0
235 ℃, 40 bar	98	34	56	10
250 ℃, 40 bar	99	7	72	21

Figure 4.4 shows 1-hexene conversion against time on stream at different temperatures of 220, 235 and 250 ºC at a set pressure of 40 bar for 96 hours on stream. All reactions show a catalyst start up effect similar to the one observed in Figure 4.2.

Figure 4.4 shows that at 220 ºC (subcritical) the conversion increases to 94% and remains stable throughout 96 hours on stream. At 235 and 250 ºC (supercritical) the conversion increases to 96 and 98% respectively and remains stable.

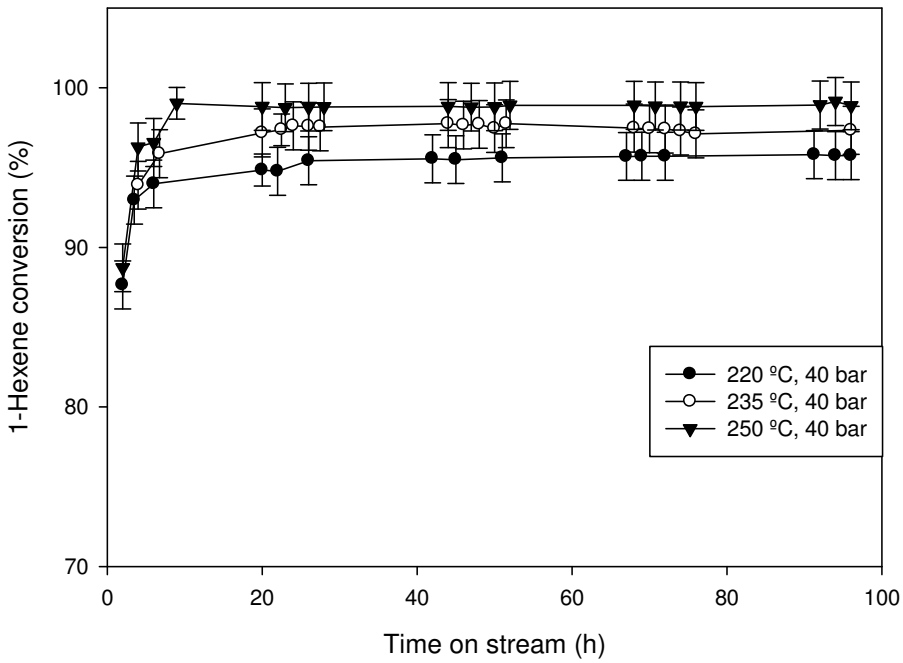

Figure 4.4. 1-Hexene conversion against time at 40 bar and 220, 235 and 250 ºC.

Figures 4.5a-c and Table 4.1 show that the reaction temperature has a significant effect on the product distribution. The selectivity toward the isomers of 1-hexene decreases from 90% to 7% at 220 and 250 ºC respectively, while the selectivity to dimers increased from 10% at 220 ºC to 72% at 250 ºC. The

selectivity to trimers also increased from 0% at 220 ℃ to 21% at 250 ℃. These results indicate that lower temperatures favour isomerisation whereas higher temperatures favour dimerisation. This is because at higher temperatures the necessary activation energy is provided to make carbon-carbon bonds between different molecules and thus form dimers and trimers, while at lower temperatures the activation energy is only sufficient to cause rearrangements within the molecule. The same effect was observed on oligomerisation of propylene over ZSM5 in the temperature range of 200 - 300 ℃ (Tabak *et al.*, 1986). It was also explained by Quann *et al.* (1988) that reaction rates may not be sufficiently fast to give a high degree of chain growth even though high molecular weight is favoured at low temperature. Hence the best operating conditions for maximising isomers selectivity is 220 ℃ and 40 bar.

a)

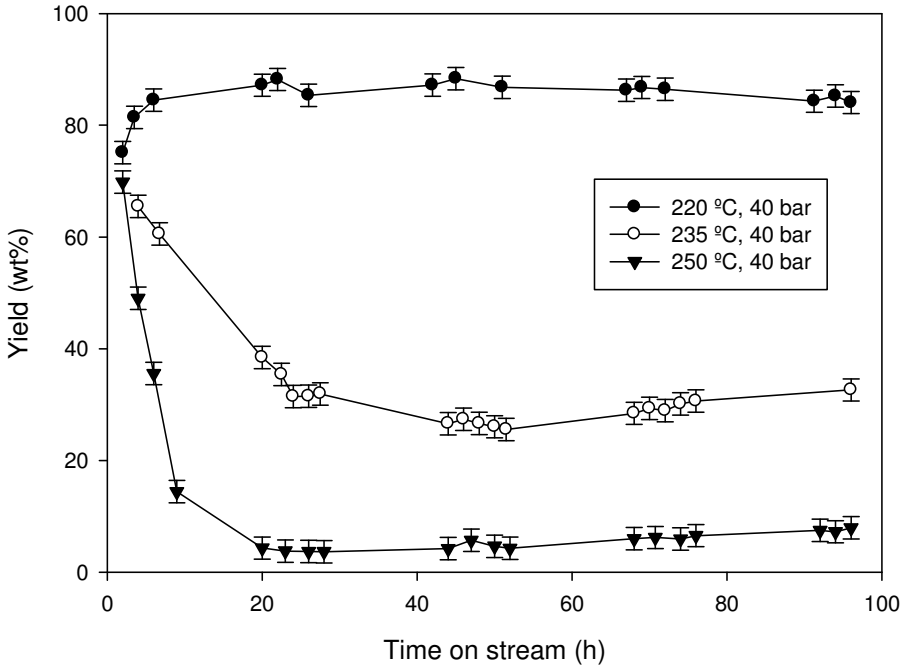

Figure 4.5. a) Yield of isomers against time at 40 bar and 220, 235 and 250 ºC.

b)

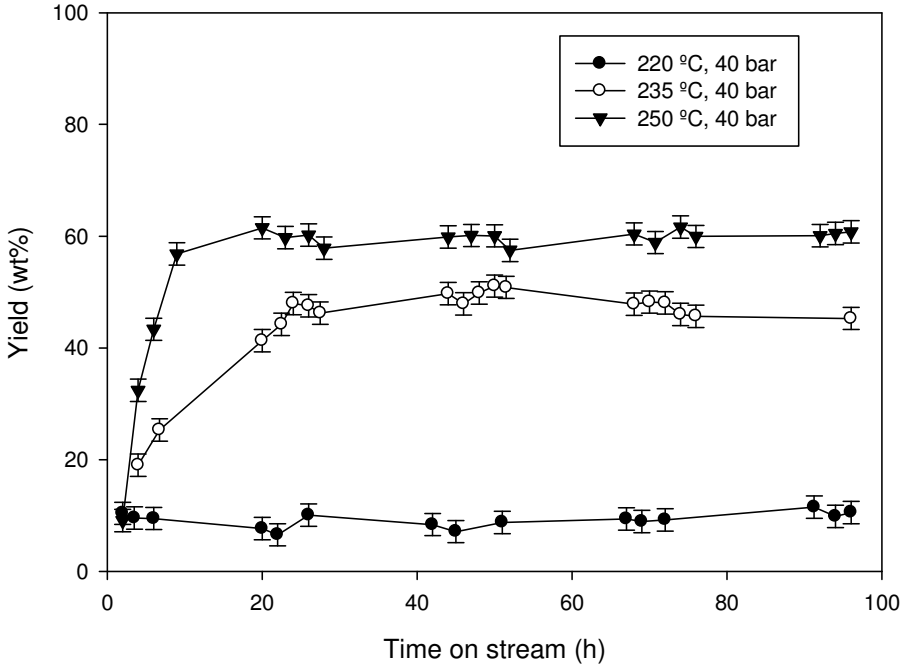

c)

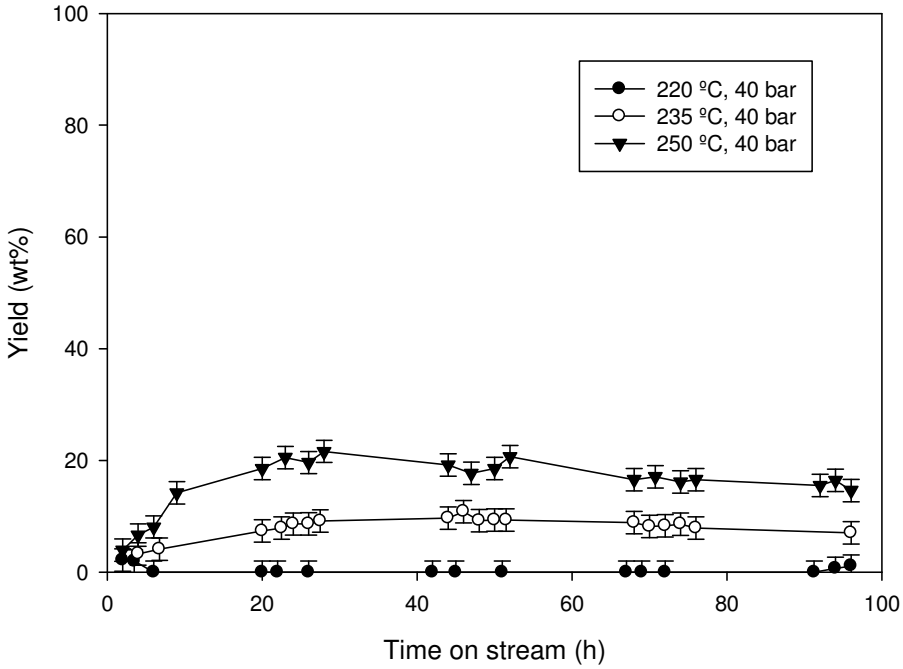

Figure 4.5. b) Yield of dimers at 40 bar and 220, 235 and 250 ºC; c) Yield trimers at 40 bar and 220, 235 and 250 ºC.

4.3. Smaller catalyst bed (0.5 gramme)

Two experiments with lower catalyst loading and shorter time on stream were carried out at 235 ℃, 10 bar (subcritical) and 235 ℃, 40 bar (supercritical) to study the initial coke in the catalyst bed. The catalyst loading was 0.5 gramme and the feed flow rate was 1 mL/min. The reaction was carried out for 8 hours on stream and the results are shown in Figure 4.6, which shows the conversion of 1-hexene dropped from 13% to 8% after 8 hours at 10 bar (subcritical), while it increased from 17% to 22% after the same period at 40 bar (supercritical). The conversion profile indicates that ZSM5 had a fast initial deactivation in the first 3 hours and reached a stable state in the subcritical region. In the supercritical region, the catalyst was stable and no deactivation was observed in the period of 8 hours on stream. There were no dimers and trimers detected in the liquid products, suggesting isomerisation is much faster than oligomerisation. The formed dimers and trimers could penetrate the pore structure and eventually transform into coke.

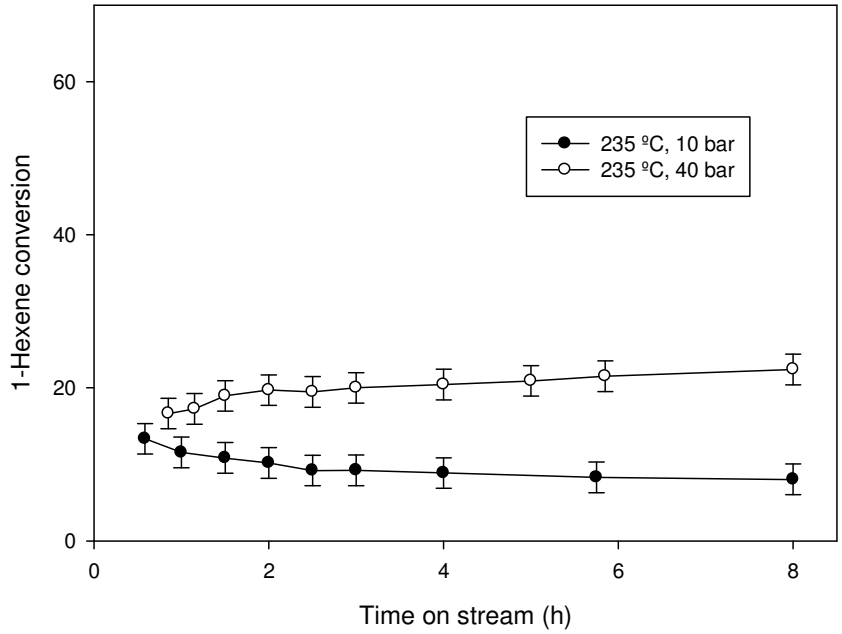

Figure 4.6. 1-Hexene conversion against time at 235 ºC, 10 bar and 40 bar.

4.4. Catalyst characterisation

The amount of coke deposited on the catalysts was measured by TGA equipment while the surface area, pore size distribution, and pore volume of the fresh and coked catalysts were determined from N_2 isotherms. DRIFTS of the crushed catalysts were obtained and TPD was used to determine the acidity of the fresh and coked catalyst.

4.4.1. Amount of coke

TGA of the coked catalysts was carried out in air, the weight loss between 200 and 1000 ºC being considered due to the removal of the coke deposits and used to calculate the amount of coke formed on every sample. Figure 4.7 shows a typical TGA and derivative thermogravimetry (DTG) curves of coked

catalyst after 96 hours on stream. There are three evident exothermic peaks in the DTG curve, corresponding to three steps in the TGA curve. The peak around 100 ℃ originates from the loss of water (step a), while the other two peaks (steps b and c) above 200 ℃ are from the removal of coke on the surface of the used catalyst. DTG curves of coked catalysts at different conditions show similar peaks except their heights and position differ slightly.

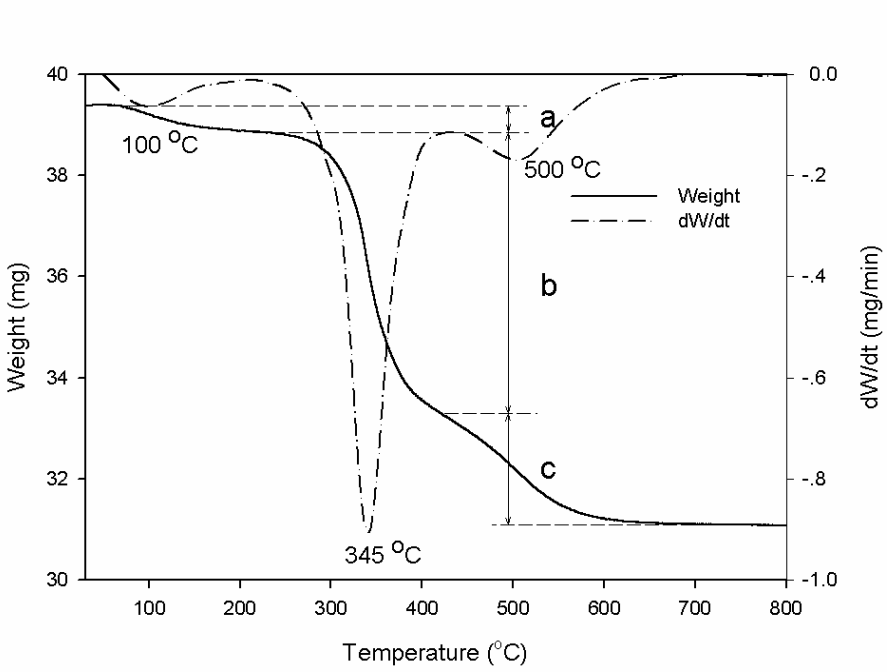

Figure 4.7. Typical TGA and DTG profile of coked catalyst. The weight loss was divided into three stages based on DTG profile; a) Room temperature – 200 ºC; b) 200 – 410 ºC; c) 410 – 1000 ºC.

One TGA measurement was also carried out in N_2 atmosphere with the temperature ramp from room temperature to 700 ℃ at 10 ℃/min and the gas flow was switched from N_2 to air when the furnace temperature reached 700 ℃. No weight loss was observed after the gas switch. Abbot *et al.* (1985) observed that coke deposition upon their ZSM5 catalyst in 1-hexene isomerisation in the temperature range 200 - 350 ℃ contained mainly olefinic compounds. Their

results were in agreement with Guisnet and Magnoux's (2001) conclusion that cokes formed at low reaction temperatures (below 200 ℃) are not polyaromatic being mainly from condensation and rearrangement steps, while coke formation at high temperature (above 350 ℃) involves hydrogen transfer steps in addition to condensation and rearrangement steps. In a study of Anderson *et al.* (1989) it was shown that naphthalenes and polycyclic aromatics were only seen in the catalyst residue at 320 ℃ and above.

The amount of coke deposited on the used catalyst is summarised in Table 4.2 As the reaction pressure increased to 40 bar and reached the supercritical state, the coke deposition dropped sharply from 18.8% at 10 bar to 10.4% at 40 bar. The pressure change from 40 to 70 bar had little effect on coke deposition. These results suggest that the transition from subcritical to supercritical state has significant effect on coke formation and deposition, but once in the supercritical region the overall amount of coke deposited is quite similar.

Increasing the temperature from 220 to 235 ℃ at a constant pressure of 40 bar, resulted in no remarkable change in the amount of coke deposited. The amount deposited was between 10.5 – 10.1%. Lower amounts of catalyst (0.5 gramme) had similar percentage coke deposit as the larger amount of catalyst (10 gramme) used in the reaction.

Table 4.2. Coke deposition on used catalysts at different conditions.

Reaction conditions	**Catalyst weight (g)**	**Feed flow rate (mL/min)**	**Total coke (wt%)**
235 °C, 10 bar	10	0.5	18.8 ± 0.05
235 °C, 40 bar	10	0.5	10.4 ± 0.05
235 °C, 70 bar	10	0.5	9.8 ± 0.05
220 °C, 40 bar	10	0.5	10.5 ± 0.05
235 °C, 40 bar	10	0.5	10.4 ± 0.05
250 °C, 40 bar	10	0.5	10.1 ± 0.05
235 °C, 10 bar	0.5	0.5	20.2 ± 0.05
235 °C, 40 bar	0.5	0.5	12.1 ± 0.05
235 °C, 10 bar	0.5	1	18.3 ± 0.05
235 °C, 40 bar	0.5	1	12.9 ± 0.05

4.4.2. Nature of coke

DRIFTS spectra of fresh and coked catalysts are shown in Figure 4.8. Figure 4.8a shows the whole spectra with the wave number from 600 to 4000 cm^{-1}, while Figure 4.8b-e give more detail of the spectra in four predominant regions, namely 3800 - 3300, 3800 - 3700, 3000 - 2800, and 1600 - 1000 cm^{-1}.

In the V(O-H) region (Figure 4.8b,c), the fresh catalyst shows four characteristic

bands of H-ZSM5. The band at 3740 cm^{-1} represents isolated Si-OH groups which have no significant interaction with other species (Bjorgen *et al.*, 2008; Pu and Inui, 1997). The band at 3664 cm^{-1} can be assigned to terminal and bridging OH groups in dimeric $(Al(OH)_3)_2$ species (Brand *et al.*, 1997). The 3610 cm^{-1} band represents Brønsted acid sites, which are responsible for the catalytic activity. The very broad band with a maximum at 3460 cm^{-1} was also observed in the spectrum of fresh catalyst. The band can be assigned to a variety of internally located Si-OH sites involved in relatively strong hydrogen bonds (Bjorgen *et al.*, 2008).

In the spectrum of coked catalyst, the intensity of the broad band between 3800 and 3000 cm^{-1} decreased, which is caused by coke deposition, thus the SiOH sites were covered with coke and the bands relevant to SiOH disappeared (Gil, 2007). The Si-OH groups on the external surface at 3740 cm^{-1} and strongly acid sites at 3610 cm^{-1} were also affected by coke.

New bands that appeared in the C-H stretching (Figure 4.8d) and C-H deformation regions (Figure 4.8e) in the spectrum of the coked catalyst are the evidence that hydrocarbon species are deposited on or inside the catalyst. In the region of 3000-2800 cm^{-1}, new bands were observed at 2959, 2925, 2870, and 2856 cm^{-1}, which are assigned to saturated C-H stretching (Trombetta *et al.*, 1997). The bands at 1464 and 1378 cm^{-1} are typical positions of symmetric vibration of $–C-H_2$ and $C-H_3$ -C groups (Bautista and Delmon, 1995). No bands corresponding to =C-H stretching (3100 - 3000 cm^{-1}) and C=C stretching (1630 - 1580 cm^{-1}) were detected (Andy *et al.*, 1998), suggesting that the cokes

formed during the reaction are most likely to be saturated hydrocarbon species.

It is also observed that the band at 1211 cm^{-1}, corresponding to asymmetric stretching of the external Si-O-Si groups (Fanning and Vannice, 2002) in the fresh catalyst was red-shifted to 1194 cm^{-1} in the coked catalyst, as shown in Figure 4.8e. This indicates that the environment which surrounds the external Si-O-Si groups changed. The red-shift was found in every coked sample and it appeared that the amount of coke deposited on the catalyst had an effect on the shift. The red-shift was about 17 cm^{-1} when the coke deposition was 18.8 wt%, while it was about 12 cm^{-1} with a coke deposition of 9.8 wt%, suggesting that the environment surrounding the Si-O-Si groups is affected by the quantity of coke deposited.

The artifact band attributed to specular reflectance (Fanning and Vannice, 2002) also red-shifted from 1335 cm^{-1} in the fresh sample to 1250 cm^{-1} in the sample with 18.8 wt% coke and to 1284 cm^{-1} in the sample with 9.8 wt % coke. The shift could also be the result of coke deposition, as a smaller shift was observed with less coke deposition.

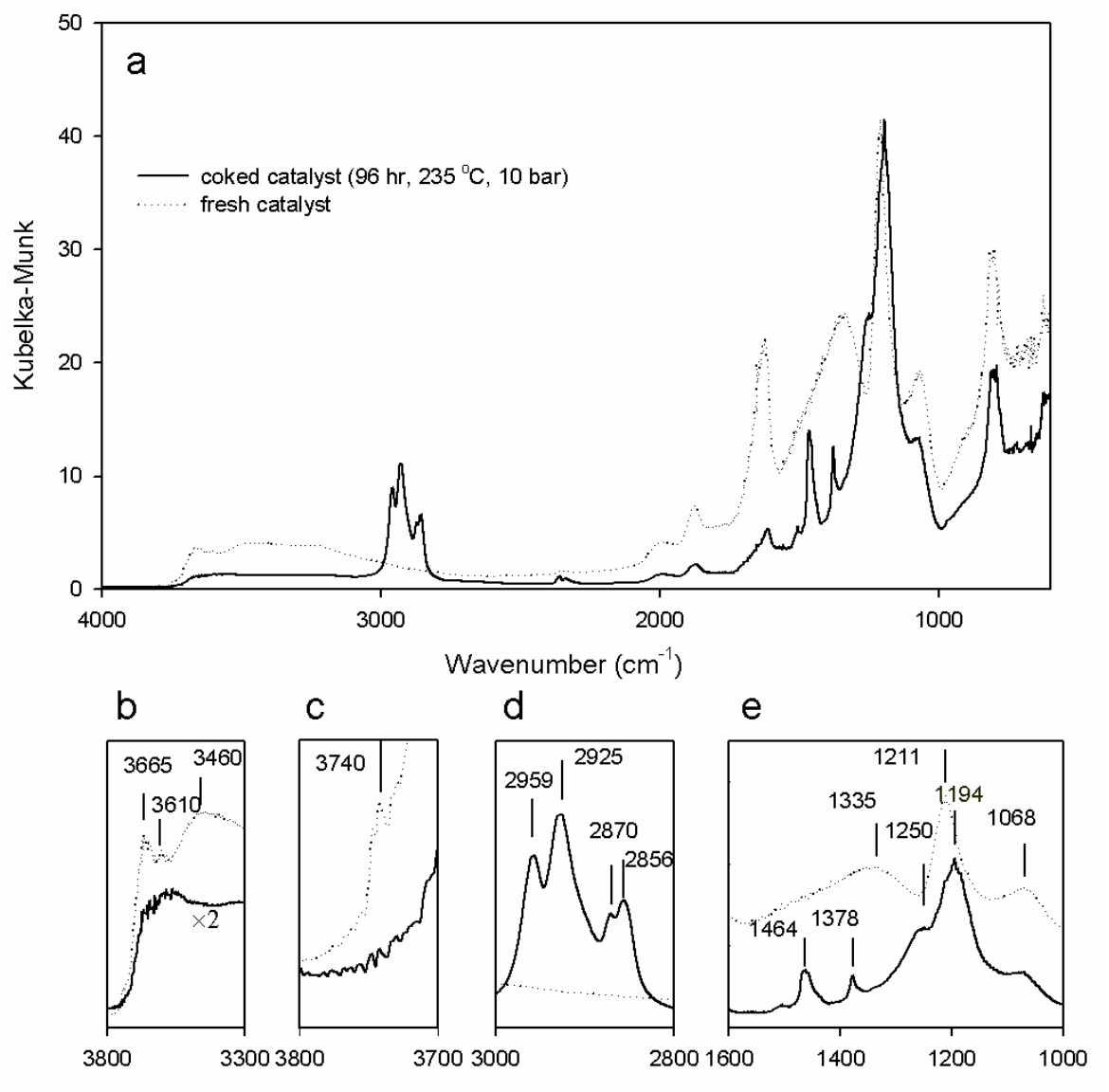

Figure 4.8. DRIFTS spectra of the fresh catalyst and coked catalyst. a) 4000 – 600; b) 3800 – 3300; c) 3800 – 3700; d) 3000 – 2800; e) 1600 – 1000 cm^{-1}. The dotted lines are for the fresh catalyst and the solid lines are for the coked catalyst.

4.4.3 Pore structure evolution

Following reaction, the discharged catalyst samples were examined using nitrogen adsorption and XRD techniques. Figure 4.9 shows the XRD patterns obtained for the series of runs carried out, with a catalyst loading of 10 gramme

and time on stream of 96 hours, at a fixed temperature of 235 ºC but varying pressure over the range 10 - 70 bar. From Figure 4.9, it can be seen that the main peak, located at 22.5 2θ 23.5, is a doublet for the fresh catalyst, and remains so for the coked samples. Previous work (Lin *et al.*, 2007) suggested that if substantial amounts of coke are forming within the zeolite pores, then it may be expected that the doublet peak would change into a singlet.

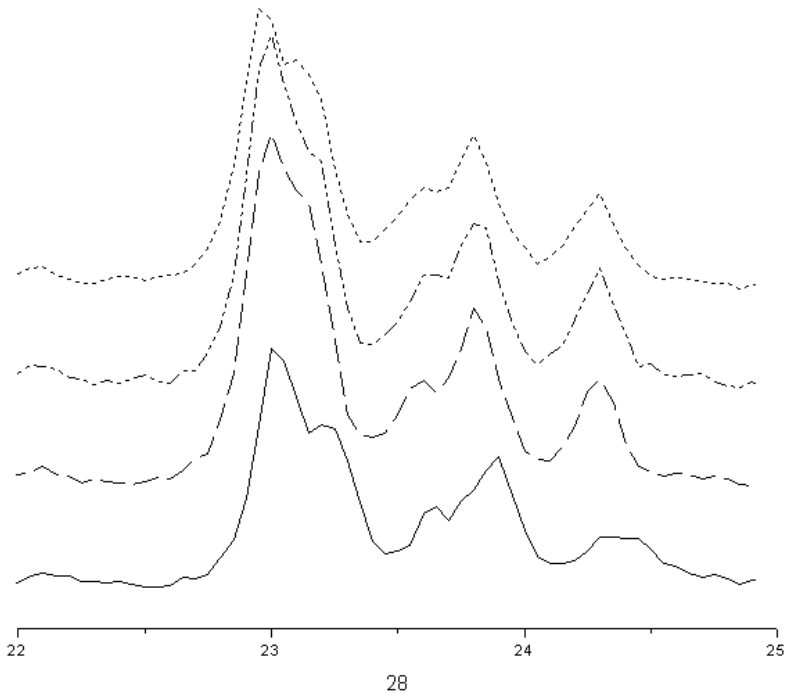

Figure 4.9. XRD data for fresh (solid line) and coked samples run at 235 ºC and 10 bar (dashed line), 40 bar (dot-dash line) and 70 bar (dotted line) for 96 hours (Figure by P.I Chigada and S.P. Rigby, 2009).

Figures 4.10 and 4.11 show the nitrogen adsorption isotherms. All nitrogen uptake values for isotherms for coked samples have been re-normalized to the amount of nitrogen adsorbed per unit mass of catalyst, rather than per unit mass of sample, using the TGA data.

Figure 4.10 shows the adsorption isotherms for the fresh catalyst and the coked

catalyst obtained for the series of runs carried out, with a catalyst loading of 0.5 gramme and time on stream of 8 hours, at a fixed temperature of 235 ℃ but varying pressure over the range 10 - 40 bar.

In the low relative pressure region ($P/P_0 < 0.2$) adsorption is dominated by pore-filling of micro-pores, and monolayer-multilayer build-up in any meso-pores and macro-pores (Rouquerol *et al.*, 1999).

a)

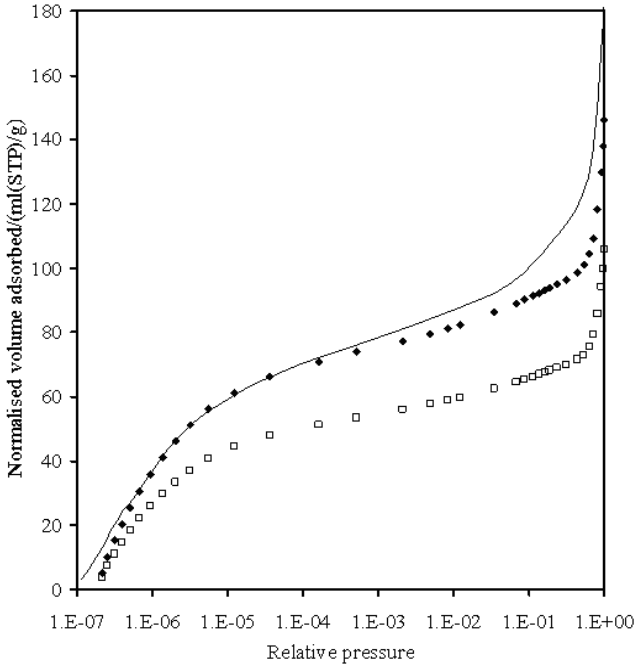

b)

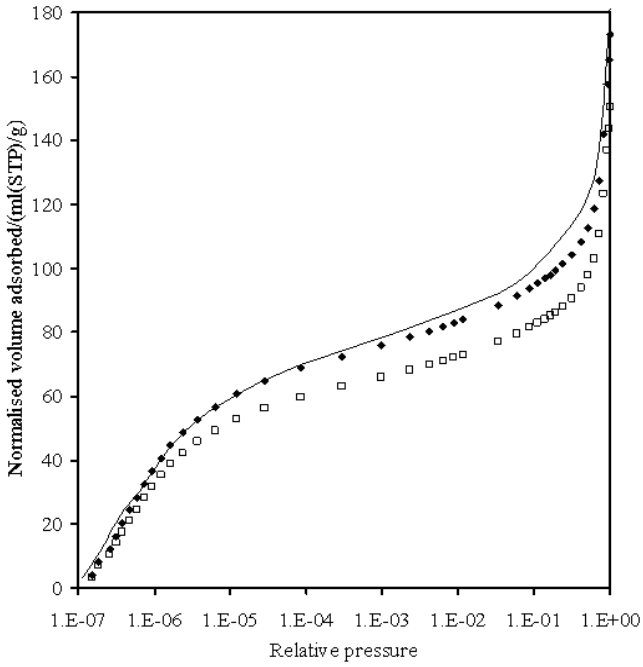

Figure 4.10. Nitrogen adsorption isotherms for fresh (solid line) and coked samples (□) run at 235 ºC and a) 10 or b) 40 bar for 8 hours,0.5g catalyst bed. Also shown are isotherms for coked samples (♦) where each point has been multiplied by a constant factor of a)1.38 and b)1.15 (Figure by P.I Chigada and S.P. Rigby, 2009).

From Figure 4.10 it is clear that, for the studies with lower catalyst loading and shorter time on stream, even if the amount adsorbed on the coked catalyst is multiplied by a constant factor, the adsorption isotherms for the coked catalysts are not able to be superposed on the isotherm for the fresh sample. The loss of accessible pore volume, in conjunction with a change in shape of the adsorption isotherm, suggests that the internal catalyst pore structure and/or surface chemistry have been modified. Since the TGA results indicate that coke has been formed on the catalyst, this modification of the isotherms is probably due to coke deposits. These findings suggest that at the top of the catalyst bed and for short times reactants do penetrate into the pores and form coke deposits therein.

Figure 4.11 shows the corresponding set of isotherms obtained under the same conditions except that the catalyst loading was 10 gramme and the time on stream was 96 hours. From Figure 4.11 it can be seen that, as the operating pressure is increased, the amount adsorbing in the micro-porous region ($P/P_0 < 0.2$) is decreasing. However, it can also be seen that, if the amount adsorbed on the coked catalyst is multiplied by a constant factor, then the isotherms for the coked catalyst can be superposed fairly well over the isotherm for the fresh sample over almost all of the micro-porous region ($\sim 10^{-6} < P/P_0 < \sim 10^{-1}$). This finding is consistent with the suggestion that the coke is generally formed surrounding, and not within, some of the zeolite crystallites, since the shape of the isotherms is retained while the total uptake is reduced. The changes in the shapes of the isotherms for coked samples at very low relative pressure may be due to the lower experimental sensitivity in this region, but the systematic

variation observed suggests that the change is probably real.

The initial part of the adsorption isotherm is shifted to higher relative pressure indicating a loss of the highest energy adsorption sites and thus lower surface affinity for the adsorbate, probably due to some surface chemistry effects from the coke present.

a)

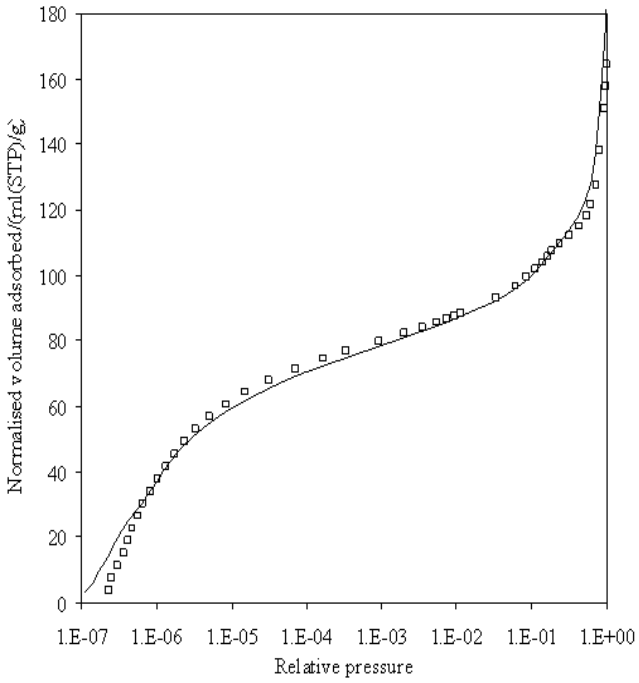

b)

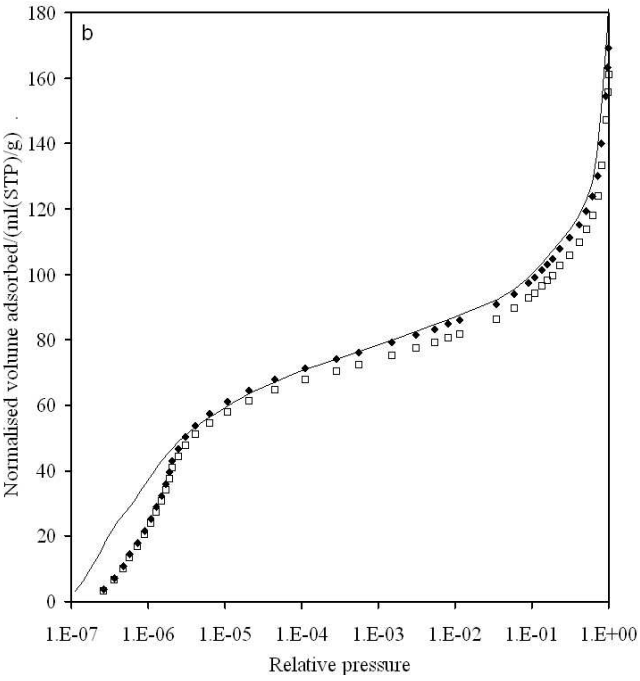

Figure 4.11. Nitrogen adsorption isotherms for fresh (solid line) and coked samples (□) run at 235 ºC and a) 10; b) 40 for 96 hours, 10g catalyst bed. Also shown are isotherms for coked samples (♦) where each point has been multiplied by a constant factor of a)1.05 and b)1.3 (Figure by P.I. Chigada and S.P. Rigby, 2009).

c)

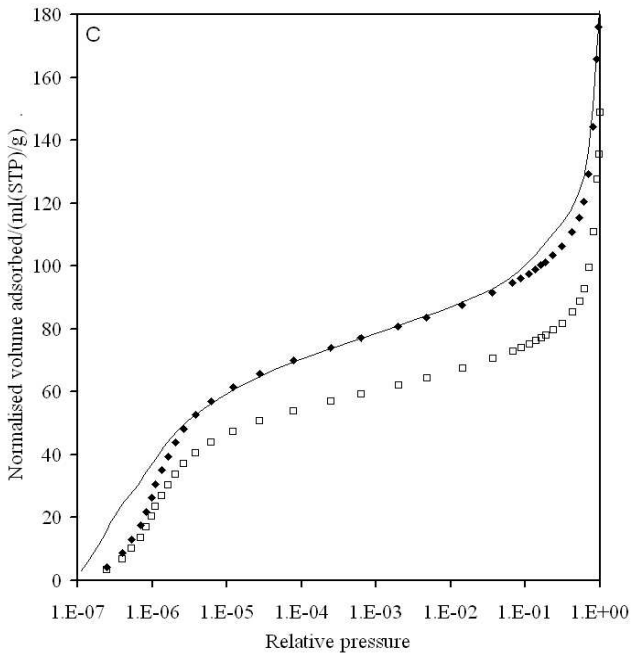

Figure 4.11. Nitrogen adsorption isotherms for fresh (solid line) and coked samples (□) run at 235 ºC and a) 10; b) 40; c) 70 bar for 96 hours, 10g catalyst bed. Also shown are isotherms for coked samples (♦) where each point has been multiplied by a constant factor of a)1.05 and b)1.3 (Figure by P.I. Chigada and S.P. Rigby, 2009).

In addition, the experimental adsorption isotherms were each fitted to a two-component composite model comprising Langmuir-type and BET-type components. Since the zeolite is micro-porous, adsorption within zeolite crystallites is expected to be of type I (or Langmuir) character, while the initial adsorption on the surface of the meso-pores surrounding the zeolite crystallites is likely to be of type II (or BET) character. Hence, the two-component model is able to separate the contributions to adsorption from within and without the zeolite micro-porosity. Table 4.3 shows the ratios of the statistical monolayer capacities of each of the two components, fitted to a given isotherm for a coked sample, to the corresponding values for the fresh catalyst. The BET constant energy parameters for the various model fits were in the range 80 - 260, while

the corresponding energy parameters for the Langmuir component fits were always significantly higher, as would be expected if the Langmuir component reflected adsorption in the highly confined micro-porosity, while the BET component reflected adsorption on the "external" meso-porous surface.

From Table 4.3, it can be seen that, while there is little or no decline in the Langmuir component surface area, there is a much more significant drop in the BET component surface area in each case. Hence, from the above findings, it is suggested that following initial shallow pore filling over shorter contact times, the pore mouth subsequently becomes blocked and coke mainly forms on the outside of the zeolite crystallites.

Table 4.3. Results of two-component, Langmuir and BET, composite model fit to adsorption isotherms for coked samples.

Reaction conditions	**V/V_0 (BET)**	**V/V_0 (Langmuir)**
235 °C, 10 bar, 96 hours	0.87	1.0
235 °C, 40 bar, 96 hours	0.79	1.0
235 °C, 70 bar, 96 hours	0.57	0.82
235 °C, 10 bar, 8 hours	0.43	0.75
235 °C, 40 bar, 8 hours	0.70	0.87

Notes: V/V_0 is the ratio of the statistical monolayer capacity of the relevant component, V, for the coked sample, to the corresponding value, V_0, for the fresh catalyst.

It is noted that the shorter time on stream corresponds to the time period before the conversion of 1-hexene and the yields of the isomers become stable, while the longer time on-stream corresponds to the period when the conversion and yields have stabilised. Hence, the transient period before stabilisation may correspond to the loss of the regions of the catalyst having high heats of adsorption for nitrogen.

Nitrogen has a quadrupole moment and might be expected to adsorb strongly to highly confined or polar sites, such as silanol groups and Brønsted acid sites (Rouquerol *et al.*, 1999). The higher values of $P/P_0 > 0.2$ correspond to the region of capillary condensation in the meso-pores and macro-pores, which are probing the pore size of the alumina surrounding the zeolite crystals. In contrast with the zeolite pores, which will become blocked by small quantities of coke, the meso-pores of alumina may become narrower without actually blocking. El-Nafaty and Mann (1999) have presented a stochastic pore network model of the micro-pore/macro-pore clusters in zeolitic FCC catalyst particles, which together with coke burn off experiments was able to reveal the extent coke deposition in micro-and macro-pores. However in this work, it was discussed that the coke molecules are likely too large to penetrate into the zeolite structure and therefore most of the deposited coke is likely to be within the extra-zeolite porosity. This would be consistent with a reduction in access to the internal zeolite porosity as the reaction proceeds.

4.5. Catalyst acidity and TPD measurements

It was shown in the literature review in Chapter 2, section 2.5.3, that the strength and density of the catalyst acid sites affect the rate of coking and the selectivity to coke. It was discussed that ZSM5 has acid sites that are identical in acid strength which means that the greater the coke content, the greater the deactivating effect of the coke molecule (Guisnet *et al.*, 1997). This is different in other zeolite catalysts such as Y type where the acid sites are of different strengths hence low coke content can cause a great deactivating effect (Guisnet *et al.*, 1997).

TPD was used to measure the acidity of the fresh catalyst compared to coked samples. TPD spectra assigns a single population of acid sites with the same strength to a broad TPD peak and the position of the desorption peak may greatly be affected by experimental conditions (Mori *et al.*, 1991). Each TPD experimental run was repeated a minimum of four times to ensure the reliability of these measurements. All variations were taken into consideration and mean free acidity was calculated as well as the percentage error.

Figure 4.12 shows the TPD spectra for the catalyst coked at 235 ℃, 10 bar. The signal with tertbutylamine was subtracted from the signal without tertbutylamine and the free acidity is shown in Figure 4.12. The acidity values are reported in Table 4.4 and are in the similar range of values reported in literature (Salguero *et al.*, 1997; Karge and Weitkamp, 1989). Both Figure 4.12 and Table 4.4 show a loss in acid sites in the coked samples compared to the fresh sample. At 10 bar the acidity is lost by 82% while at 40 bar the acidity is lost by 77%. This is consistent with TGA results which show more percentage

coke deposit at 10 bar compared to 40 bar. This is also consistent with nitrogen adsorption isotherms which show a greater loss of pore volume at the subcritical conditions of 10 bar.

Coke is not thought to deposit within the micro-pores of the ZSM5 catalyst. It is mainly thought to deposit on the outside surface of the ZSM5 crystallites and within the meso-porous alumina binder of the pellets. Alumina shows a strong acidity with values of 0.11 mmol/g. Overall, the loss of acidity in the ZSM5 catalyst is mainly due to the loss acid sites on the outside surfaces and acid sites on the alumina binder rather than the sites within the micro-pores of the zeolite crystallites.

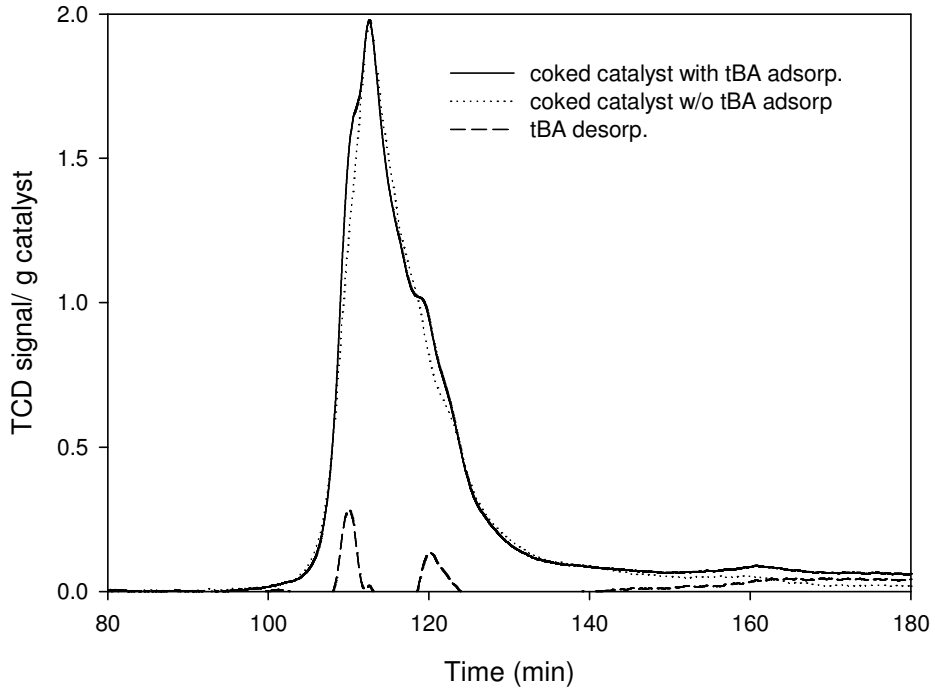

Figure 4.12 TPD spectra for catalyst coked at 235 ℃, 10 bar.

Table 4.4. Total mean free acidity at different reaction conditions.

Reaction conditions	**Total mean free acidity (mmol/g)**
Fresh ZSM5	0.56 ±0.02
Alumina binder	0.11 ± 0.02
Coked ZSM5, 235 ℃, 40 bar, 6 hours	0.13 ± 0.02
Coked ZSM5, 235 ℃, 10 bar, 6 hours	0.10 ± 0.02

4.6. Conclusions

During isomerisation and oligomerisation of 1-hexene over ZSM5, the catalyst was stable for 96 hours. Only slight deactivation was observed after 80 hours in the subcritical region (235 ℃ and 10 bar). The product selectivity changed to form more oligomers in the first 20 - 30 hours and became stable afterwards. The operating temperature had a significant effect on product selectivity. Oligomerisation was preferred at high temperature as well as higher pressure. However, the effect of the operating pressure upon product distribution was less than the effect of temperature within the ranges studied.

Characterisation of samples coked at different condition by TGA in air and DRIFTS measurements shows that deposited coke is mainly polyolefinic. The amount of coke decreased considerably from 18.8 wt% in the subcritical region to 10 wt% in the supercritical region. The decrease was due to the *in situ*

removal of coke by supercritical hexene.

The location of coke was also studied by N_2 sorption. Nitrogen sorption suggests that following initial shallow pore filling over shorter contact times, the pore mouth subsequently becomes blocked and coke mainly forms on the outside of the zeolite crystallites. The catalyst acidity is lost due to coking. This loss in acidity is mainly due to the loss acid sites on the outside surfaces and acid sites on the alumina binder rather than the sites within the micro-pores of the zeolite crystallites.

CHAPTER 5

DEACTIVATION DURING 1-HEXENE ISOMERISATION OVER ZEOLITE Y AND ZSM5 CATALYSTS UNDER SUPERCRITICAL CONDITIONS

In this chapter the isomerisation of 1-hexene on zeolite Y is reported and comparisons are drawn between the different coking behaviour and acidity of zeolite Y and the results for ZSM5, which were presented in Chapter 4.

In previous studies, Niu *et al.* (1995a) demonstrated the significant power of supercritical fluids for the *in-situ* regeneration of zeolite Y catalyst coked during the disproportionation of ethylbenzene. Niu *et al.* (1995b) further derived deactivation and coke removal kinetics and demonstrated that coke deposition profiles were dependent on the physio-chemical properties of the catalysts used (Niu and Hofmann, 1996).

In this Chapter, the effects of operating temperature and pressure on catalyst activity and selectivity are reported in section 5.1. Catalyst characterisation is reported in section 5.2 and a comparison is drawn between zeolite Y and ZSM5 in section 5.3. Conclusions are reported in section 5.4.

As discussed previously in Chapter 4, the aim of this work was to study the use of supercritical conditions for delaying coking and extending catalyst life time, however it should be noted that within pores of few Angstroms dimension, such as those that occur in zeolites, the concept of SCFs is not meaningful because the pores only contain a few molecules of the fluid, which therefore do not follow bulk behaviour. Nonetheless, at the catalyst surface and within larger pores, SC conditions are relevant. The enhanced solubility of coke precursors that are

formed on the catalyst surface in the SC solvent could therefore lead to their extraction from the catalyst.

This chapter is based on the paper: Faiza Hassan, Jiawei Wang, Peter I. Chigada, Sean P. Rigby, Bushra Al-Duri and Joseph Wood. Accepted April 2011. Ind. Eng. Chem. Res.

5.1. Effects of temperature and pressure upon 1-hexene conversion and selectivity

The isomerisation of 1-hexene was carried out with 0.5 gramme of zeolite Y or ZSM5 catalyst and a constant liquid 1-hexene flow rate at 1.5 mL/min for 2 or 6 hours on stream. The liquid products collected were analysed for 1-hexene, its isomers and oligomers.

The conversion of 1-hexene and product isomer composition with process time was measured. The experimental temperature was varied between 220 to 250 ℃ and pressure was varied between 10 bar to 70 bar to cover a range between sub and supercritical conditions. The critical condition for the reaction mixture is T_c: 231 ℃ and P_c: 31.6 bar.

For zeolite Y the conversion (Figure 5.1a) started in the range of 47 – 56 %, depending upon the temperature, and decayed gradually from these higher values throughout the reaction, indicating that deactivation occurs. Detailed comparison with the results for ZSM5 is made in section 5.3, but, in summary, conversion for ZSM5 lay in the range 22 - 35 % at 235 ℃, 40 bar, which was lower than the conversion for zeolite Y at the same conditions.

The results for zeolite Y in Figure 5.1a show a larger percentage loss in catalytic activity at subcritical conditions compared to supercritical conditions. For example, in Figure 5.1a the conversion value declined by 17 % at the end of the reaction from the value recorded after 1 hour at 220°C, 40 bar, but only by 10 % and 11 % at respectively 235 °C and 250 °C, 40 bar.

As more molecules penetrate the pores of the zeolite Y coke can form and deposit in those pores and possibly lead to mass transfer resistances in the catalyst pellet. In order to estimate whether this phenomenon occurred, reaction rates were calculated at the temperatures of 235 °C and 250 °C from the 1-hexene conversions using the integrated fixed bed reactor design equation given by Clark and Subramaniam (1999). It was assumed that both of these temperatures lie within the supercritical phase and from the calculated reaction rates the activation energies at different times during the reaction were estimated using the Arrhenius equation.

For example at 1.43 hours on stream, where the conversions are almost the same at 235°C and 250 °C, the apparent activation energy is ~6.0 kJ/mol, whilst at 3 hours on-stream a larger difference in conversion occurs and the apparent activation energy is ~26.3 kJ/mol, thereafter decreasing again at 4 - 5 hours on stream. These low values of the activation energy (<50 kJ/mol) suggest that the reaction may be limited by mass transfer of 1-hexene through the catalyst pores, whilst it would be expected that higher activation energies (>100 kJ/mol) correspond to the reaction limited regime (Satterfield, 1991). The variations in apparent activation energy with times on-stream result from differences in the rate of coking in each of the experimental runs.

As the channels in zeolite Y are large enough to accommodate carbonaceous residues, it is thought that coke deposition leads to both loss of active sites and increased mass transfer resistance, resulting in a drastic loss of catalytic activity. Detailed modelling studies of pore structure evolution due to coke deposition and mass transport within catalyst pellets (Pd/Al_2O_3) have been carried out as part of the same project reported in this thesis by Chigada *et al.* (2010).

a)

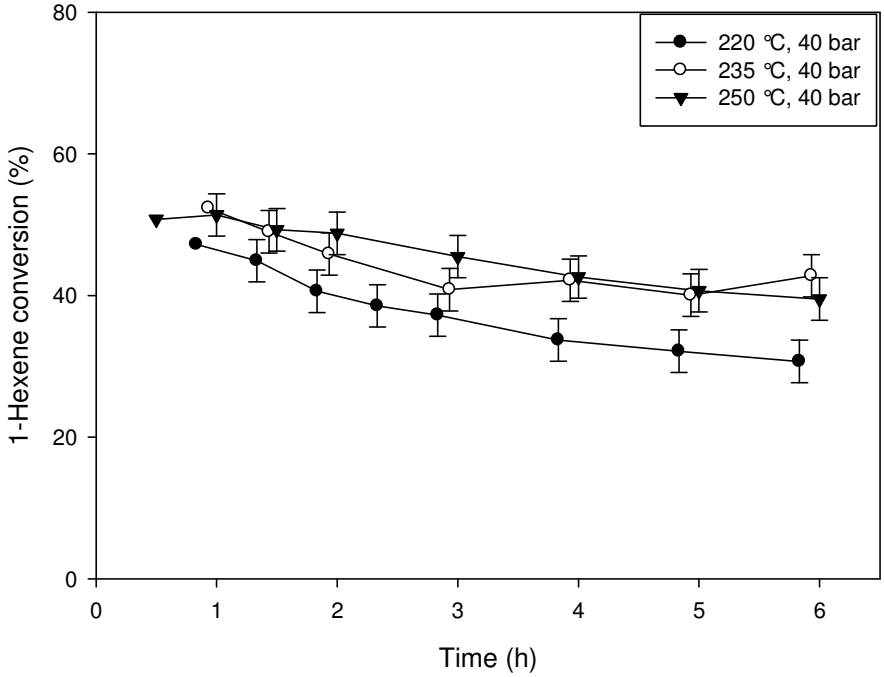

b)

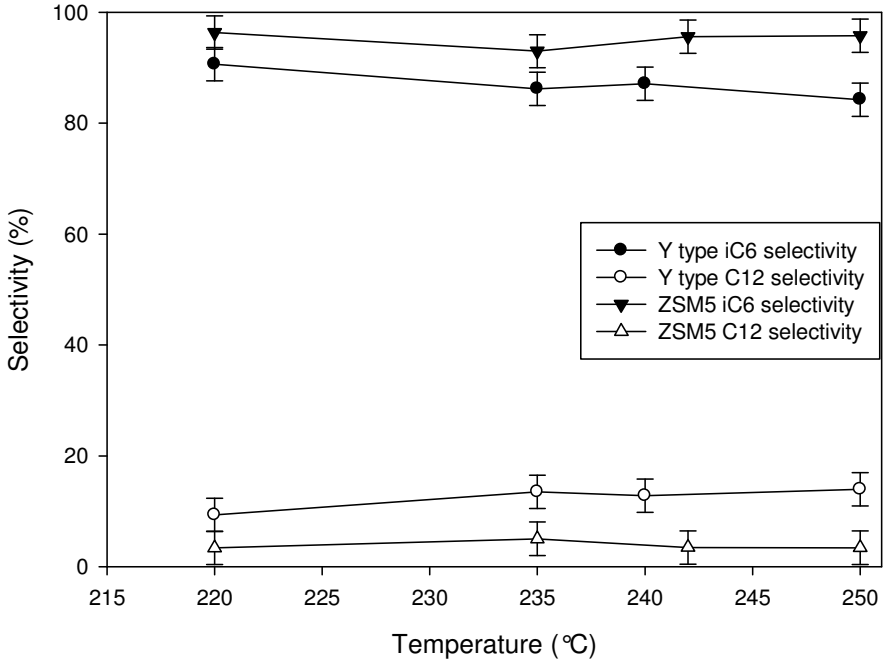

Figure 5.1 a) 1-Hexene conversion, on zeolite Y, versus time on stream at 40 bar and 220 ℃, 235 ℃, 250 ℃ after 6 hours on stream; b) Selectivity towards iC_6 and C_{12} on zeolite Y and ZSM5 at 220 ℃, 235 ℃, 250 ℃ after 6 hour on stream.

The reaction products, shown in Figure 5.1b, were mainly 1-hexene isomers (iC_6) and dimers (C_{12}). No trimers (C_{18}) were detected. The main isomer products were trans-2-hexene, cis-2-hexene and cis/trans-3-hexene. The product distribution changed very little over the temperature range studied. The selectivity towards C_{12} dimers was slightly lower at 220 °C than 250 °C, since dimer formation is more thermodynamically favourable at higher temperatures (Abbot *et al.*, 1985). Comparing the product distributions of zeolite Y and ZSM5 in Figure 5.1b, it was observed that the production of C_6 isomers was slightly higher for ZSM5, whilst the production of dimers was slightly higher in zeolite Y. Changing the temperature also had relatively little effect upon the product distribution over ZSM5 catalyst.

Figure 5.2 shows the effect of pressure upon conversion at constant temperature, where an exponential decay coking behaviour was observed. At subcritical conditions (10 bar) the initial deactivation was particularly pronounced during the early part of the run from 1 – 1.5 hours, where conversion decreased from 47% to 31% yielding a conversion loss rate of 32% per hour. Between 1 and 6 hours the conversion decreased from 31% to 21% yielding an average conversion loss rate of 2% per hour. Therefore, under subcritical conditions, a substantial part of the deactivation was caused by the initial coke deposition. Under supercritical conditions, at 40 bar, the rate of deactivation was notably lower compared with the subcritical run at 10 bar, with the conversion declining gradually during the first 3 hours of operation, thereafter levelling off at around 42%. At the higher pressure of 70 bar, the conversion showed a slight increase between 1 and 1.5 hours, followed by

deactivation between 1.5 hours to 6 hours on stream during which conversion decreased from 49% to 38%.

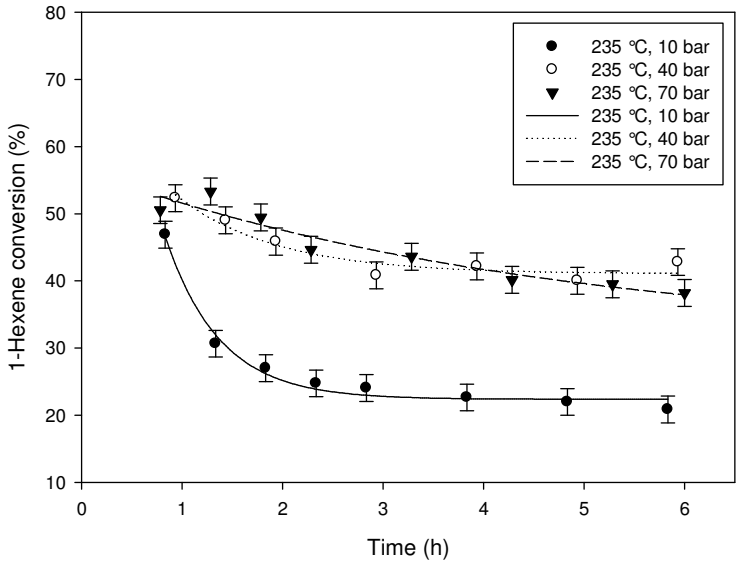

Figure 5.2. 1-Hexene conversion, on zeolite Y, versus time at 235 °C and 10, 40 and 70 bar at 6 hour on stream. The data were fitted by Equation 5.1.

The steepest stage of exponential deactivation is attributed to initial coke deposition inside the catalyst pores which causes direct suppression of the most active catalytic active sites, while the more gradual deactivation that occurs later in the reaction is attributed to the growth of coke deposits by polymerisation (Wolf and Alfani, 1982). The slower deactivation under supercritical conditions possibly indicate enhanced solubilisation of coke precursors by the SCF, which is able to remove some of the deposited coke from the catalyst.

In comparison, Saim and Subramaniam (1990) observed two deactivation stages during the isomerisation of 1-hexene on platinum on alumina catalyst in subcritical conditions. During the initial stage the conversion decreased linearly

with time on stream at a conversion loss rate of 1.2% per hour. The second deactivation stage yielded a conversion loss rate of 0.2% per hour. Similarly, Saim and Subramaniam (1990) attributed the initial deactivation stage to coke deposition inside the catalyst pores and the second stage was due to the growth of coke deposits by polymerisation which tends to induce a slower deactivation rate. The authors also reported that during supercritical conditions the different deactivation stages were absent and became apparent only after 8 hours on stream. They attributed this delay to the enhanced solubilisation of the coke precursors in supercritical conditions.

The coking reaction was assumed to be first order in terms of the current activity, with the resulting deactivation leading to exponential decay of 1-hexene conversion (Fogler, 2006). The deactivation was fitted by equation 5.1 (Wang *et al.*, 2009), which is the same as equation 2.4 given in Chapter 2, section 2.4:

$$X = C + X_0 e^{-kt} \tag{5.1}$$

Where X is the conversion, C and X_0 are constants, k is the deactivation rate constant and t is time in hours. The fitted parameters are shown in Table 5.1 and the lines fitted to the data are shown in Figure 5.2. The fastest deactivation was at 10 bar with an initial deactivation rate constant k of 1.85, which also showed the best fit of Equation 5.1 to the data, as indicated by the high R^2 value. The value of k decreased to 1.01 and 0.22 at 40 bar and 70 bar respectively, which also showed a poorer fit to the exponential decay equation.

Table 5.1. Deactivation parameters. Fitted constants of Equation 5.1 to the data plotted in Figure 5.2a.

	10 bar	**40 bar**	**70 bar**
C	22.37	41.08	31.08
X_0	113.03	30.09	25.54
k	1.85	1.01	0.22
R^2	0.98	0.93	0.92

In Figure 5.3a, the C_6 isomer selectivity shows a slight decrease with increasing pressure, whilst the C_{12} selectivity shows a slight increase for zeolite Y. Thus at increasing pressure more dimers were formed and detected in the liquid product. This is because high pressure favours light olefin oligomerisation to high molecular weights (Quann, 1998). Pressure had relatively little influence upon the production of isomers and dimers on ZSM5. Only a small decrease in isomer production, together with increase in dimer formation was observed with increasing pressure for this catalyst.

Figure 5.3b shows 1-hexene conversion at different pressures after only 2 hours on stream in order to examine the effect of operating under supercritical conditions upon the coke deposition early in the reaction run. The lowest conversion was recorded at 10 bar. Both the density of the reaction mixture and the number of moles of reactants per unit volume increased as the pressure was increased from 10 bar to 25 bar, and the corresponding conversion also substantially increased over this range of pressures. Around the critical point large changes in the density of the mixture occur with small changes in

pressure. The density increased from 0.02 g/mL to 0.3 g/mL at 10 bar and 40 bar respectively. The increase from 10 to 40 bar had a greater effect on conversion compared to the increase from 40 to 70 bar. This suggests that in SCFs increasing the conditions further into the supercritical region does not necessarily show much improvement in activity, possibly because higher pressures in the supercritical region will produce liquid-like reaction mixtures that would exacerbate pore diffusion limitations.

a)

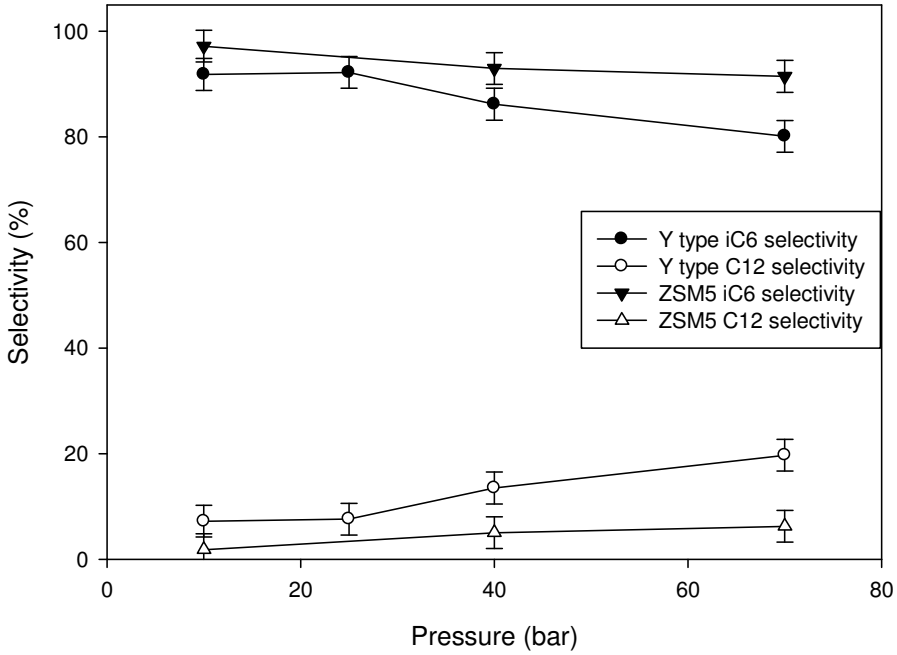

b)

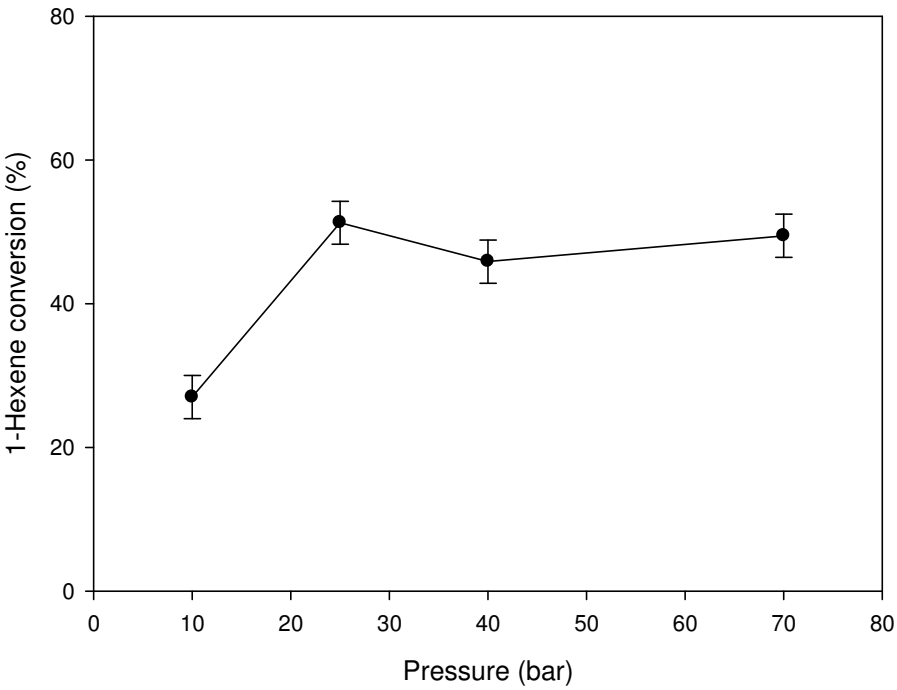

Figure 5.3. a) Selectivity towards iC_6 and C_{12}, on zeolite Y and ZSM5 at 235 ℃ and 10, 40 and 70 bar at 6 hour on stream; b) Effect of pressure on conversion of 1-hexene at 2 hours on stream on zeolite Y at 235 ℃.

5.2. Catalyst characterisation

5.2.1. Percentage coke deposition

TGA was used to determine the amount of coke deposited on the catalyst via the weight change in the catalyst during oxidation. Figure 5.4 shows the TGA data for zeolite Y coked at 10 and 40 bar. The initial loss of sample weight below 200 °C is due to removal of adsorbed water and volatile species, and subsequent losses between 200 - 1000 °C are due to coke which are progressively harder to remove as desorption temperature increases. From the magnitude of the second step, the weight percentage coke in the sample was determined.

The largest amount of coke (23.0 wt%) was deposited at 235 ºC, 10 bar. As the reaction pressure increased above the critical pressure to 40 bar, the percentage mass of coke decreased to 19.9 wt%. However with increased pressure to 70 bar (Table 5.2) the amount of coke went slightly up again to 20.2%. Comparing the amount of coke deposited (Table 5.2) with Figures. 5.2 and 5.3b, it is noted that the higher coke deposition at 10 bar led to lower conversion compared with 40 and 70 bar. Considering that the error in the measurement of approximately ± 0.05 % coke, the difference in coke deposition between 10 bar and 40 bar may be considered to be small but statistically significant, whilst the coke depositions at 40 and 70 bar are almost the same. The decreased percentage coke deposit at supercritical conditions further indicates enhanced solubilisation and removal of coke precursors under those conditions.

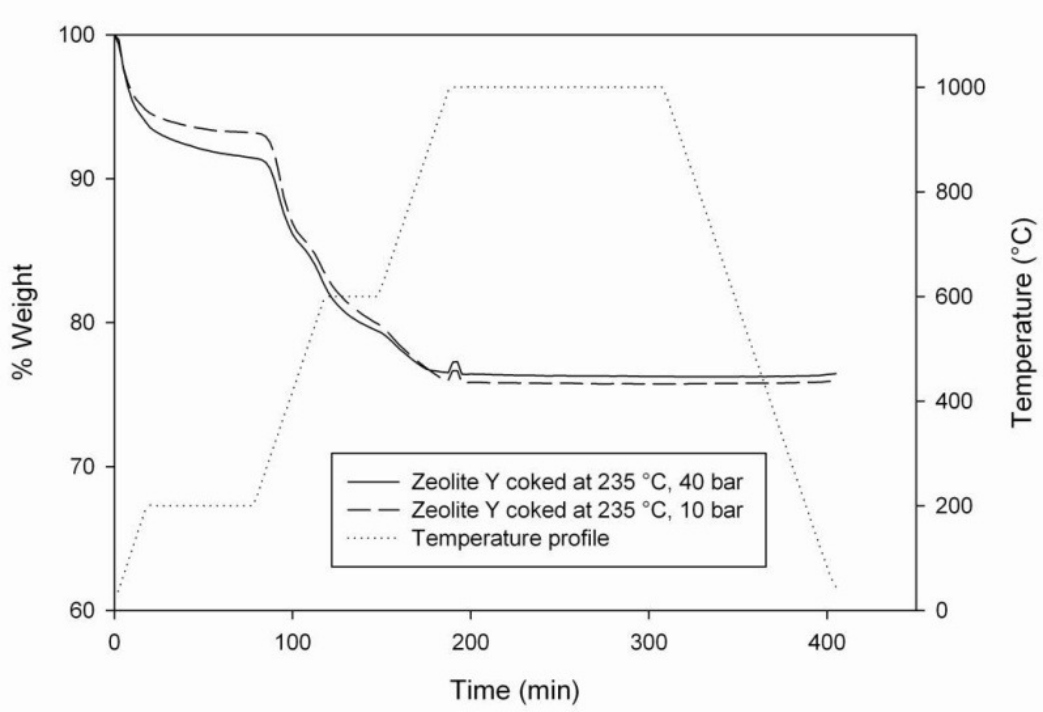

Figure 5.4. TGA data for zeolite Y coked at 10 and 40 bar after 6 hour on stream.

Table 5.2. Summary of percentage weight change in TGA for zeolite Y.

Reaction conditions	**Coke (wt%)**	**Time on stream (hr)**
235 ºC, 10bar	23.0 ± 0.05	6
235 ºC, 25bar	20.5 ± 0.05	6
235 ºC, 40bar	19.9 ± 0.05	6
235 ºC, 70bar	20.2 ± 0.05	6
220 ºC, 40bar	17.6 ± 0.05	6
235 ºC, 40bar	19.9 ± 0.05	6
240 ºC, 40bar	19.1 ± 0.05	6
235 ºC, 10bar	22.2 ± 0.05	2
235 ºC, 40bar	20.9 ± 0.05	2

As shown in Table 5.2, the amount of coke deposited in the catalyst increased slightly from 17.6 wt% to 19.9 wt% as the reaction temperature was increased from 220 – 235 °C. This is because the temperature plays a large part in determining the rate of coking and the nature of coke composition due to its effect on the thermodynamics of the reaction and coke retention (Guisnet and Magnoux, 1994). At low temperatures (100 °C) condensation reactions are thermodynamically favoured and coke molecules are retained due to the low volatility of oligomers. Coke formation at higher temperatures (350 °C) involves hydrogen transfer steps, some condensation and rearrangement steps. Coke molecules formed at higher temperatures are retained due to their size which results in steric blockage in the cavities or at channel intersections (Guisnet and Magnoux, 1994).

To evaluate the change in coke deposition with time on stream a series of shorter experiments at two hours on stream were conducted (Table 5.2). These results clearly show that nearly all coke deposits on the catalyst before two hours on stream. Since after only 2 hours the catalyst samples contain 20.9 - 22.2 wt% coke and after 6 hours they contain 17.6 – 23.0 wt% coke. This suggests that after the first two hours of operation the amount of coke does not substantially increase and may decrease in certain conditions. An interesting finding is that at 40 bar (supercritical), the percentage of coke on the catalyst seemed to decrease slightly from 20.9 wt% at two hours to 19.9 wt% at six hours suggesting that a small amount of the coke had been solubilised and removed from the catalyst surface.

5.2.2. DRIFTS

Figure 5.5 shows the DRIFTS spectra of fresh and coked catalyst samples at sub and supercritical conditions in zeolite Y and ZSM5. Figure 5.5a shows the whole spectrum from 500 to 4000 cm^{-1}. Figures 5.5b to 5.5d show more detail of the spectra with wavenumbers from 3800 – 3300, 3000 – 2800 and 1750 – 1000 cm^{-1}. DRIFTS spectra for the fresh and coked ZSM5 catalyst have been previously discussed in Chapter 4.

In the spectra displayed in Figure 5.5b, a very broad peak was observed around 3500 cm^{-1} which could be assigned to hydroxyl groups of the internal zeolite surface (Petkovic *et al.*, 2005) or could result from adsorbed water on the catalyst surface. The OH groups in zeolite Y are associated with Brønsted acids and therefore of importance to the catalytic activity (Schoonheydt and Uytterhoeven, 1970). In all coked catalyst samples the intensity of the OH band at 3500 cm^{-1} decreased dramatically, compared with spectra of the fresh catalyst, indicating that the hydroxyl groups on the surface of the catalyst were covered by coke or that less water was adsorbed upon the coke surface compared with the fresh catalyst surface.

Similarly, TGA data shows that sample weight is lost in both fresh and coked catalysts below 200 °C, which was due to adsorbed water. For the fresh catalyst, the band at 1650 cm^{-1}, assigned to water, confirms that greater water adsorption occurs upon the fresh catalyst. In Figure 5.5c, new bands appeared on all coked catalyst samples between 3000 – 2800 cm^{-1}. These bands were assigned to aliphatic C-H stretching (Trombetta *et al.*, 1997). However bands at 1650 cm^{-1} and 3100 – 3000 cm^{-1} which would be assigned to C=C stretching

and =C-H stretching (Andy *et al.*, 1998) were not detected for the coked sample spectra, indicating that the coke formed is most likely saturated hydrocarbon species.

In Figure 5.5d, the coked samples developed bands in the region of 1580 – 1610 cm^{-1} which were assigned to complex mixtures of hydrogen deficient carbonaceous deposits (Petkovic *et al.*, 2005). The band observed around 1490 cm^{-1} was assigned to C-H deformation of $-CH_3$ groups (Petkovic *et al.*, 2005). For the fresh catalyst peaks below 1500 cm^{-1} were assigned to skeletal vibrations of the zeolite structure (Petkovic *et al.*, 2005).

As reported in Chapter 4, the DRIFTS spectra indicate that new bands appear in the region of 3000 – 2800 cm^{-1} for the coked samples which can be assigned to saturated C-H stretching. Similar to the DRIFTS results in zeolite Y, the coke formed in ZSM5 is most likely to be saturated hydrocarbon species.

a)

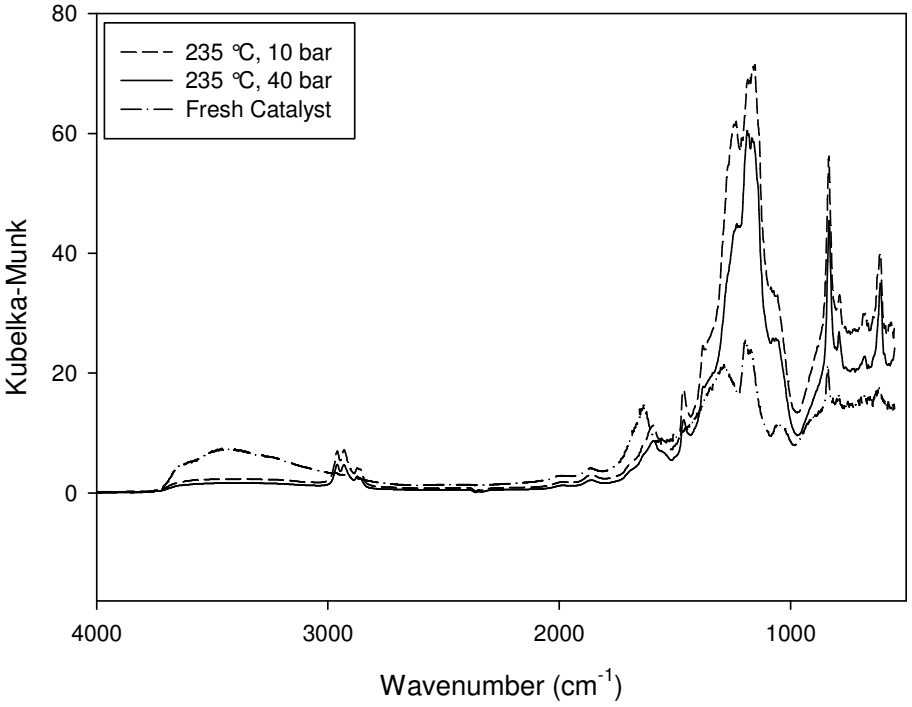

b)

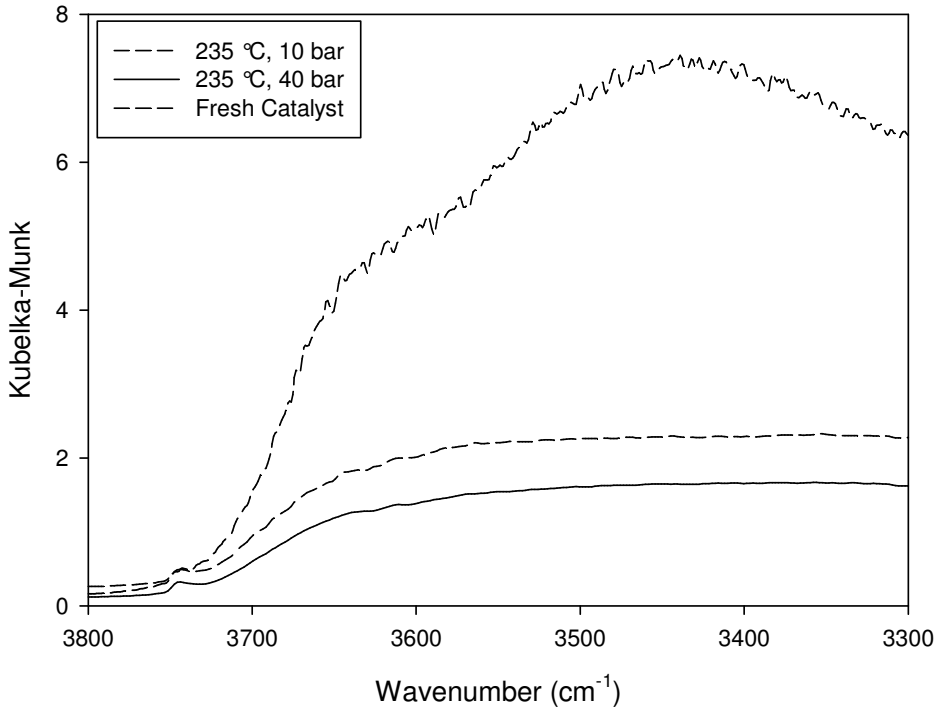

Figure 5.5. DRIFTS spectra of fresh and coked zeolite Y catalyst after 6 hours on stream at 235 ℃ and either 10 bar or 40 bar; a) 4000-500 cm^{-1}; b) 3800-3300 cm^{-1}

c)

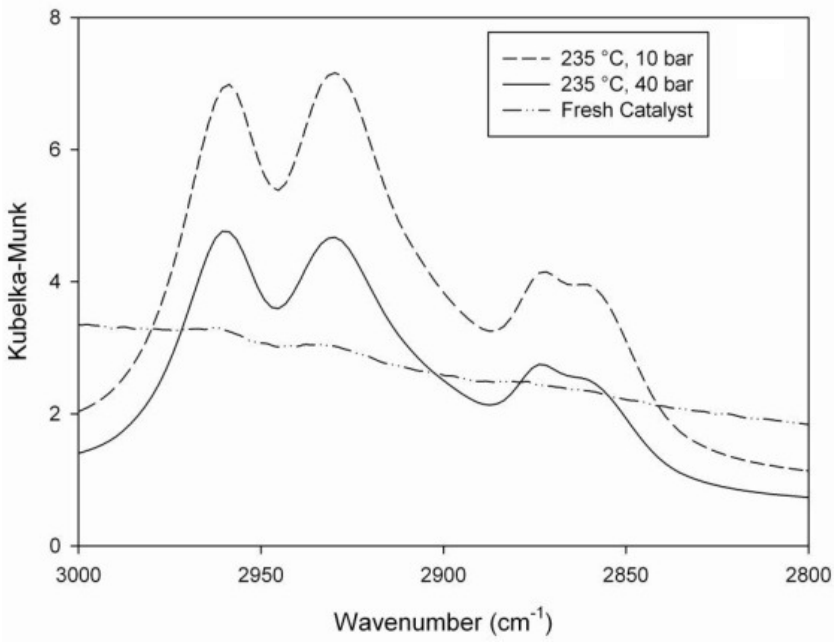

d)

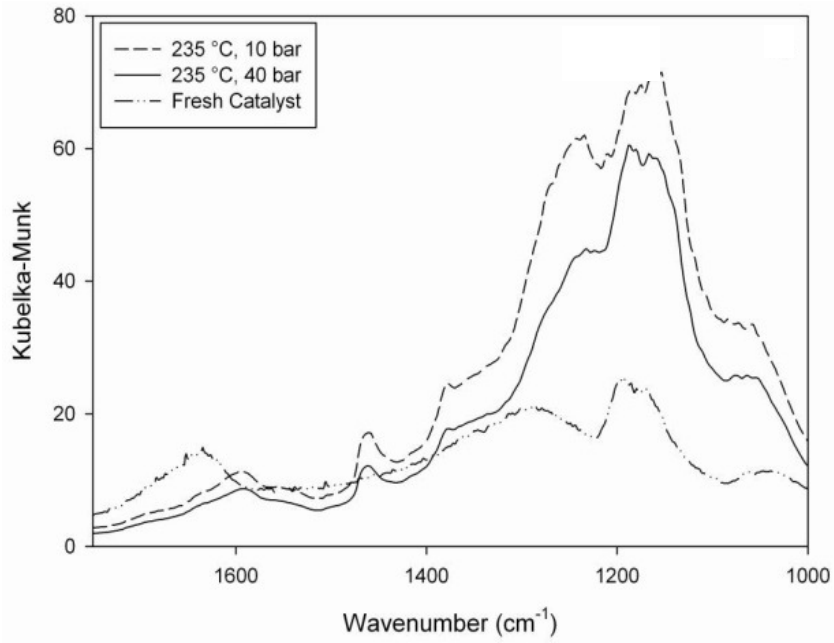

Figure 5.5. DRIFTS spectra of fresh and coked zeolite Y catalyst after 6 hours on stream at 235 ℃ and either 10 bar or 40 bar; c) 3000-2800 cm^{-1}; d) 1750-1000 cm^{-1}.

5.2.3. Gas adsorption

Figure 5.6 shows nitrogen adsorption isotherms for fresh catalysts and discharged catalysts following 6 hours on stream under reaction conditions of 235 ℃ and, either 10 bar or 40 bar. It can be seen that coking led to the loss of the marked, main step up in adsorption at a relative pressure of ~0.00015 for the fresh catalyst. Also shown in Figure 5.6 are fits of the reversible parts of the isotherms ($P/P_0<0.4$) to a two-component, composite isotherm model consisting of Langmuir and BET components, as described in previous work (Wang *et al.*, 2009) and Chapter 4. The Langmuir component can account for adsorption in the micro-pores, within the zeolite crystallites, while the BET component accounts for adsorption in the surrounding meso-porosity.

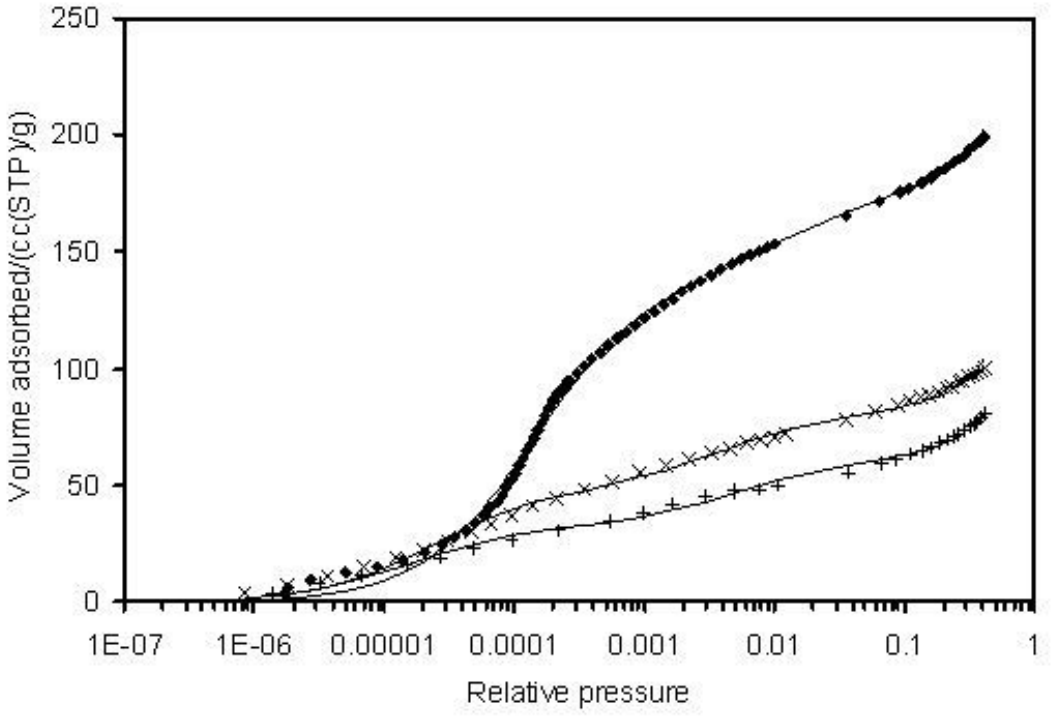

Figure 5.6. Reversible regions of nitrogen adsorption isotherms for fresh (■) catalyst, and for spent catalysts (zeolite Y) after 6 hour on stream at 235 ℃ and, either 10 bar (+) or 40 bar (×). The solid lines are fits of the experimental data to two-component Langmuir and BET composite isotherm models as described in the text.

Table 5.3 shows the ratios of the fitted adsorption capacity parameters (for each model component), V, for the spent catalysts to the corresponding values for the fresh catalyst, V_0. It can be seen that the Langmuir component decreases more significantly than the BET component under both sets of reaction conditions considered. This suggests that coke lay-down was predominantly affecting access to the micro-pore network.

The amount of coke laid down in the meso-porosity was estimated from the resultant decrease in adsorbed amount outside the micro-porosity (up to P/P_0=0.99), assuming the adsorbed phase had the same properties as bulk liquid nitrogen at 77 K. Hence, from the total amount of coke laid down on the sample, as determined by TGA, the amount of coke specifically laid down within the micro-porosity could be obtained. Assuming a coke density of 1.2-1.3 g cm^{-3} (Sotelo *et al.*, 1994), the volume of coke within the micro-porosity was determined. The pore size distribution for the micro-porosity was obtained using the Saito-Foley method (Saito and Foley, 1991), and used to determine the remaining accessible micro-porosity (diameters < 1.8 nm) for spent catalysts.

The values of the ratio of the volume of coke left in the micro-pores, V_C, to the inaccessible micro-pore volume, V_{SF}, for the spent catalysts are shown in Table 5.3. Given the uncertainty in the coke density, it can be seen that this ratio is quite close to 1 for the spent catalysts, despite the loss of 2/3-3/4 of the accessible micro-porosity. This suggests that there is relative little remaining open porosity being rendered inaccessible by being completely surrounded by coke, as might be otherwise expected for high coking levels. Hence, it seems likely that the lay-down of coke occurs is in a correlated way, with later layers of

coke being laid down on existing coke, thereby leaving the remaining pore network generally accessible. Therefore the change in porosity is different from ZSM5, in which coke was concluded to deposit onto the outside surfaces of the zeolite and within the meso-porous alumina binder, but not to deposit within the pores of the zeolite (Wang *et al.*, 2009).

Table 5.3. Sample parameters determined from adsorption data for zeolite Y.

Reaction conditions	**TOS/h**	**Langmuir** V/V_0	**BET** V/V_0	V_c/V_{SF}
Fresh catalyst	0	1.0	1.0	0.0
235 ℃, 10 bar	6	0.23±0.01	0.75±0.02	0.95±0.02
235 ℃, 40 bar	6	0.35±0.01	0.86±0.02	0.88±0.02

5.2.4. TPD acid sites

Guisnet and Magnoux (1994) have shown that the rate of coking and the selectivity to coke depends greatly on the strength and density of the acid sites and pore structure. As discussed in Chapter 2, sections 2.5.3 and 2.5.4, coking occurs rapidly from alkenes and polyaromatics on acid catalysts. The authors also reported that the stronger the acid sites the faster the reactions and the slower the diffusion of basic intermediates hence the faster the coke formation.

Figure 5.7 shows the TPD spectra for the fresh sample and a coked sample of zeolite Y with and without tertbutyl amine adsorption. Comparing the signals of

the coked sample with and without tertbutylamine, it can be observed that they overlap between 380 ℃ – 800 ℃ for the removal of coke. The signal with tertbutylamine was subtracted from the signal for the sample without tertbutylamine to calculate the free acidity, which is also plotted on Figure 5.7. Similarly, the acidity of the fresh catalyst was determined by subtraction of the signals with and without tertbutylamine adsorption and the acidities of all samples are reported in Table 5.4. TPD with amines is an excellent tool for determination of the total acidity of the catalyst and effect of coke upon acidity, but its limitations must also be considered. TPD spectra can only be used to roughly distinguish the various acid sites strength. It often assigns a single population of acid sites with the same strength to a broad TPD peak. Furthermore, the position of desorption peaks may be greatly affected by experimental conditions (De Lucas *et al.*, 1997). To allow for the possible experimental errors, each TPD run was repeated a minimum of four times to ensure the reliability of these measurements. All variations were taken into consideration and mean free acidity was calculated as well as the percentage error. Further example calculations of the acidity are within Appendix 8.7.

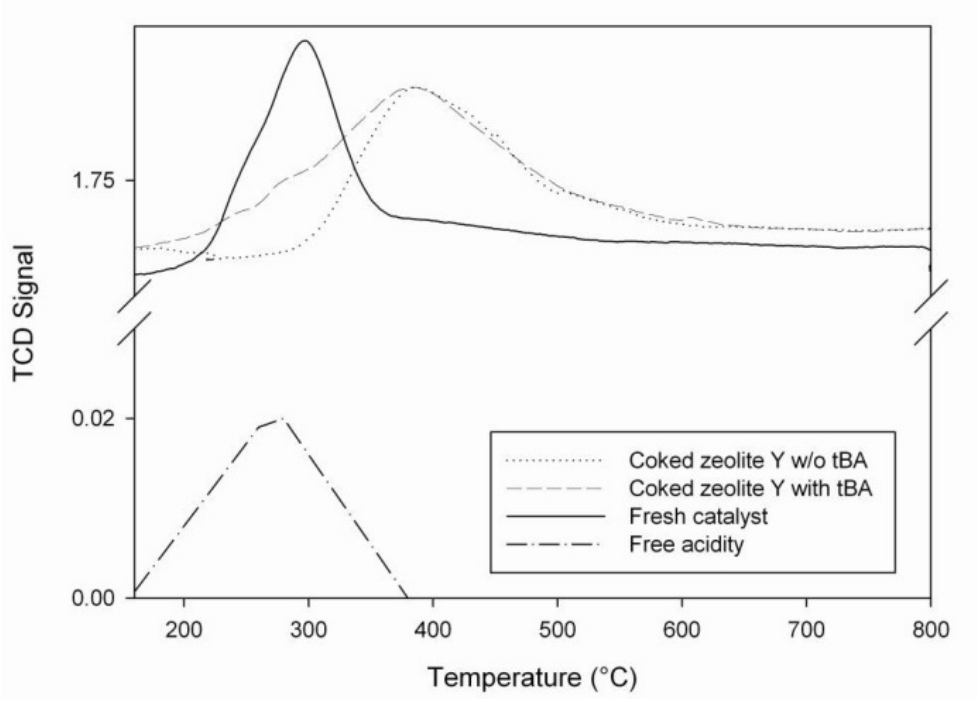

Figure 5.7. TPD spectra of fresh zeolite Y and coked zeolite Y at 235 ℃, 10 bar, 6 hour on stream with and without tertbutylamine and total free acidity.

The acidity values reported in Table 5.4 represent total acidity and are in a similar range to values in the literature. The acidity of H-ZSM5 catalyst has been reported to be between 0.48 – 0.66 mmol/g whereas the acidity of zeolite Y was reported to be between 0.62 – 0.96 mmol/g (Salguero *et al.*, 1997; Karge and Weitkamp, 1989). The results, in Table 5.4, show a significant loss of acidity in the coked samples compared to the fresh sample. Although the total mean acidity for the sample coked at 40 bar is slightly higher than at 10 bar, considering the error in the measurement, the two acidity values are almost the same. Comparing with the TGA data in Table 5.2, the sample coked at 10 bar contained 3.1 wt% more coke than the sample coked at 40 bar in Y zeolite. However, if the acid sites are lost during the initial stages of coke deposition, the total acidity (Table 5.4) may not correlate directly with the weight percentage

of coke at the end of the reaction. This is because some coke may deposit in multi-layers over acid sites which are already deactivated, leading to differences in coke deposit for similar values of acidity.

Table 5.4. Zeolite Y and ZSM5 total mean free acidity TPD results in fresh and coked samples at 235 ℃ and either 10 bar or 40 bar at 6 hour on stream.

Reaction conditions	**Total mean free acidity (mmol/g)**
Fresh Zeolite Y	0.65 ± 0.06
Fresh ZSM5	0.56 ±0.02
Alumina pellets	0.11 ±0.02
Coked Zeolite Y, 235 ℃ 40 bar, 6h	0.25 ± 0.05
Coked Zeolite Y, 235 ℃ 10 bar, 6h	0.23 ± 0.04
Coked ZSM5, 235 ℃, 10 bar, 6h	0.10 ± 0.02

As shown in Table 5.5, the amount of coke deposited upon zeolite Y after coking at 10 bar was 23.0 wt%, but upon ZSM5 was 20.2 wt%. However, after coking at 235 °C and 10 bar zeolite Y lost 62% of its acid sites, whilst ZSM5 lost 82% of its acid sites. As discussed in Chapter 4, coke is mainly thought to deposit on the outside surfaces of ZSM5 crystallites and within the meso-porous alumina binder of the pellets, but to a less extent within the micro-pores of the zeolite itself. However the strengths of the acid sites in these two zeolites also

have to be taken into account. ZSM5 has acid sites of identical strength, which deactivate uniformly with increasing coke coverage. In zeolite Y the situation is more complex, as the strongest acid sites, which are the most active, deactivate first (Guisnet and Magnoux, 1994). This results in a large deactivating effect of coke in zeolite Y, as observed in this work.

5.3. Comparison of 1-hexene isomerisation over zeolite Y with ZSM5

The results from zeolite Y were compared with those of ZSM5, to investigate the effect of pore size and acidity upon the deactivation behaviour. As already noted in the literature review, in section 2.5.1, ZSM5 has smaller pores compared with zeolite Y (Abbot *et al*., 1985) as well as lower initial acidity.

Figure 5.8 shows the percentage 1-hexene conversion against time for both zeolite Y and ZSM5. With zeolite Y, the exponential deactivation pattern, mentioned in section 5.1, was observed where conversion declined with time on stream in both the sub and supercritical experimental conditions. For ZSM5 catalyst at 40 bar, during the initial 2 hours of operation an increase, from 22% to 30%, in conversion was observed. This effect was also observed by Wang *et al.* (2009) and is thought to be due to a catalyst start up effect, whereby the reactor takes some time to reach a stable state of operation. This could be due to the time required for thorough wetting of the catalyst surface with reactants, diffusion of reactants to the catalyst active sites and formation of adsorbed intermediates upon the catalyst surface which participate in the isomerisation reaction. However this effect was not observed for zeolite Y, possibly because any increase in conversion that would occur due to the reactor reaching stable

operation could be masked by the strong deactivation which predominates from the first sample onwards. Also, the smaller pores in ZSM5 may have led to a greater mass transfer resistance, thus requiring additional time for diffusion of reactants in to the catalyst pellets.

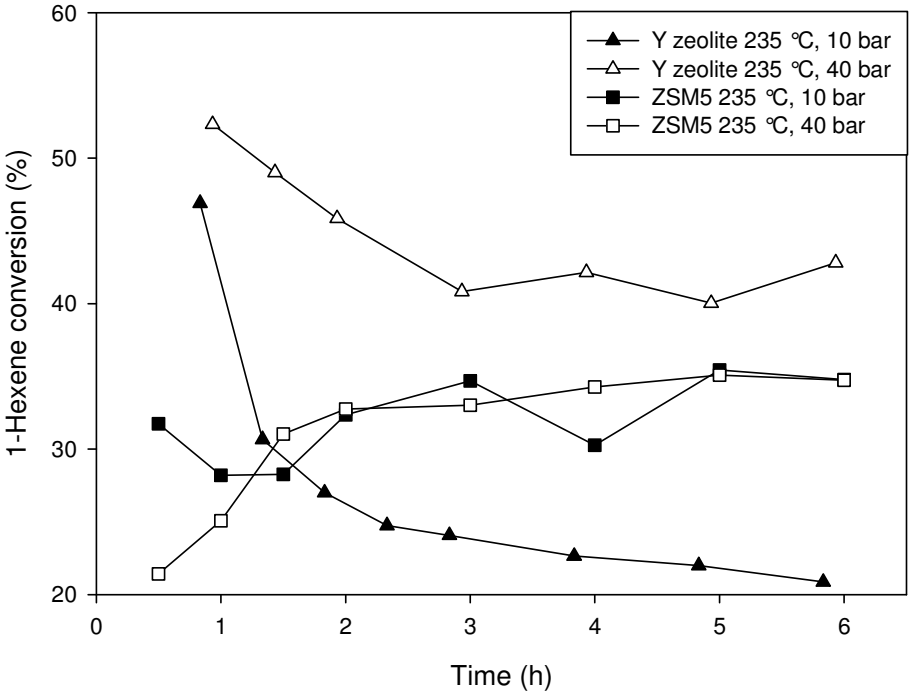

Figure 5.8. 1-Hexene conversion versus time at 235 °C, 10 bar or 40 bar, 6 hours on stream in zeolite Y and ZSM5.

Referring again to Figure 5.8, with ZSM5 no clear deactivation was observed after 6 hours on stream. The conversion at 10 bar, 235 °C was relatively stable within the 1-hexene conversion range 27 – 35 % and did not show a consistent decline. By contrast, over ZSM5 catalyst Wang *et al.* (2009) observed 1-hexene conversion commencing at 14 % after 30 minutes and decreasing to 9 % over 8 hours of operation at the same temperature and pressure. The increased conversion in the study reported here and lack of deactivation was attributed to

the pre-treatment of the feed by bubbling with nitrogen, which was not carried out by Wang *et al.* (2009). This pre-treatment was thought to reduce the formation of oxygenates which may otherwise lead to lower catalyst activity and deactivation.

In Figure 5.8 conversion at 40 bar in ZSM5 showed a small increase up to two hours on stream after which it became relatively stable at a 1-hexene conversion of ~34 % with no decline after 6 hours on stream. This conversion was also higher than the value of 22% recorded by Wang *et al.* (2009), which again may be attributed to the differences in feed pre-treatment. As observed from Figure 5.8 there was a distinct effect of operating in the sub or supercritical region on the conversion over zeolite Y, however with ZSM5 no such difference was observed and the conversion was similar for the sub and supercritical experimental runs.

As shown in Table 5.5, less coke was deposited on ZSM5 at both sub and supercritical conditions compared with zeolite Y. A comparative study (Abbot Wojciechowski, 1984) of coke formation in H-ZSM5, H-Y and mordenite, also showed that significantly less coke was formed in ZSM5. It was concluded that the difference must lie in the size and structure of the pores. Differences in coke formation were attributed to spatial constraints, where larger hydrocarbons were being prevented from reacting further to produce coke in the smaller ZSM5 pores. ZSM5 also shows very high shape selectivity in catalysis. This geometrical shape selectivity imposes a constraint on the formation of large polynuclear hydrocarbons which are responsible for coking.

Table 5.5. Summary of percentage weight change in TGA analysis, in zeolite Y and ZSM5 at 235 ℃ and either 10 bar or 40 bar at 6 hours on stream.

Reaction conditions	**Coke (wt%)**
ZSM5, 235 ℃, 10 bar, 6h	20.2 ± 0.05
ZSM5, 235 ℃, 40 bar, 6h	12.1 ± 0.05
Y-type, 235 ℃, 10 bar, 6h	23.0 ± 0.05
Y-type, 235 ℃, 40 bar, 6h	19.9 ± 0.05

Referring again to Table 5.5, for zeolite Y, increasing the pressure from 10 bar to 40 bar led to a reduction of coke deposition by just 3.1 wt. %. Despite this relatively small decrease in coke deposit, a large effect upon the final conversion in the reaction was observed, since in Figure 5.8, the conversion after 6 hours under supercritical conditions at 40 bar is ~42%, whilst under subcritical conditions at 10 bar it is ~21%. Consequently, the small change in coke deposit upon zeolite Y caused by moving in to the supercritical region leads to around double the final conversion compared to that observed at subcritical conditions. The same effect is not observed in ZSM5. In ZSM5 the change in coke deposit upon increasing the pressure from 10 bar to 40 was much larger than in zeolite Y, being a reduction of 8.1 wt% (Table 5.5). However this relatively large reduction in coke deposit did not show any appreciable effect on catalytic activity, with final conversions of ~34 % being observed at reaction pressures of both 10 and 40 bar (Figure 5.8).

The contrasting behaviours of these two zeolites as a function of operating pressure suggests that the use of supercritical conditions can improve the viability of zeolite Y as choice of catalyst by leading to improved conversion compared with ZSM5. The reasons for these differences in behaviour can be rationalized by considering the changes in pore structure and acidity that occur due to coking.

Other studies found that coke deposits were primarily formed on the outer surfaces of the ZSM5 catalyst which explains the resistance of this catalyst to aging (Abbot *et al.*, 1985). The larger percentage coke removal from ZSM5 is thought to result from coke being solubilised from the outer surfaces of the ZSM5 crystallites by the SCF. In contrast to ZSM5, for H-Y and mordenite, the channels are large enough to accommodate carbonaceous residues which lead to loss of catalytic activity and fast aging.

Similar deactivation behaviour was observed by Mori *et al.* (1991) in a different reaction of n-hexane cracking over zeolites H-Y and H-ZSM5 in a pulse reactor. They found that H-Y was deactivated by the proton coverage, which is considered to be an active site, with coke whilst H-ZSM5 was not deactivated under the conditions studied. A decrease in acidity was observed for the H-Y but not H-ZSM5 (Mori *et al.*, 1991).

In the present study, the higher initial conversion in zeolite Y may be explained by the higher initial acidity compared with ZSM5 (Table 5.4), the strong acid sites leading to increased isomerisation. The significant deactivation of zeolite Y is thought to occur because the pores become blocked by coke, thus preventing 1-hexene from penetrating in to the zeolite Y network and accessing the acid

sites. By contrast, in ZSM5 it is thought that the micro-pores do not block with coke to the same extent, and the activity of ZSM5 shows little decline, or even increases during the course of the reaction at the pressure of 40 bar. Although a substantial loss of acidity over both catalysts was observed in the present study, it is thought that the early loss of stronger acid sites in zeolite Y helps to explain the large deactivation effect observed early in the reaction.

Referring again to Figures 5.1 and 5.3a, the higher proportion of dimers over zeolite Y compared with ZSM5 is consistent with the higher coke production over zeolite Y (Table 5.5), since the higher production of dimers is likely to lead to further polymerisation to form coke precursors and eventually coke. The larger pores in zeolite Y allow the formation of dimers more easily than the smaller, constrained pores of ZSM5.

Figures 5.9a and b compare the cis/trans-2-hexene ratio and 3/2-hexene ratios respectively in zeolite Y and ZSM5. Zeolite Y showed substantially higher cis/trans and lower 3/2-hexene ratio compared with ZSM5. The ratios of cis-2-hexene to trans-2-hexene for reactions over zeolite Y lie in the range 0.6 – 0.85, which are above the equilibrium value of 0.39 (Abbot and Wojciechowski, 1984). This is an indication that the reaction is kinetically controlled and this ratio shows a higher relative rate of production of the cis isomer compared with the equilibrium. The excess of the cis isomer with respect to the cis/trans equilibrium ratio is attributed to steric effects leading to its preference (Abbot and Wojciechowski, 1984). The cis isomer is often the desirable component of the reaction, analogously to the hydrogenation of fats, in which trans products are undesirable because of health considerations. Therefore zeolite Y is

superior in terms of production of the cis- isomer. The highest cis/trans ratios occur at low conversion of 1-hexene, which corresponds to the fresh catalyst. The fresh catalyst had a high acidity as shown in Table 5.4, as well as accessible pore structure, which appears to be favourable for high production of cis-2-hexene. Figure 5.9a shows that the cis/trans ratio decreased with conversion of 1-hexene. Higher 1-hexene conversion corresponds to the catalyst decreasing in acidity and further deposits of coke forming on its surface, which may adversely influence the cis/trans ratio of the products. Additionally at high conversion of 1-hexene, the product mixture contains an increased concentration of 2-hexenes compared with the start of the reaction, and these products may undergo further isomerisation to form trans-2-hexene rather than cis-2-hexene.

a)

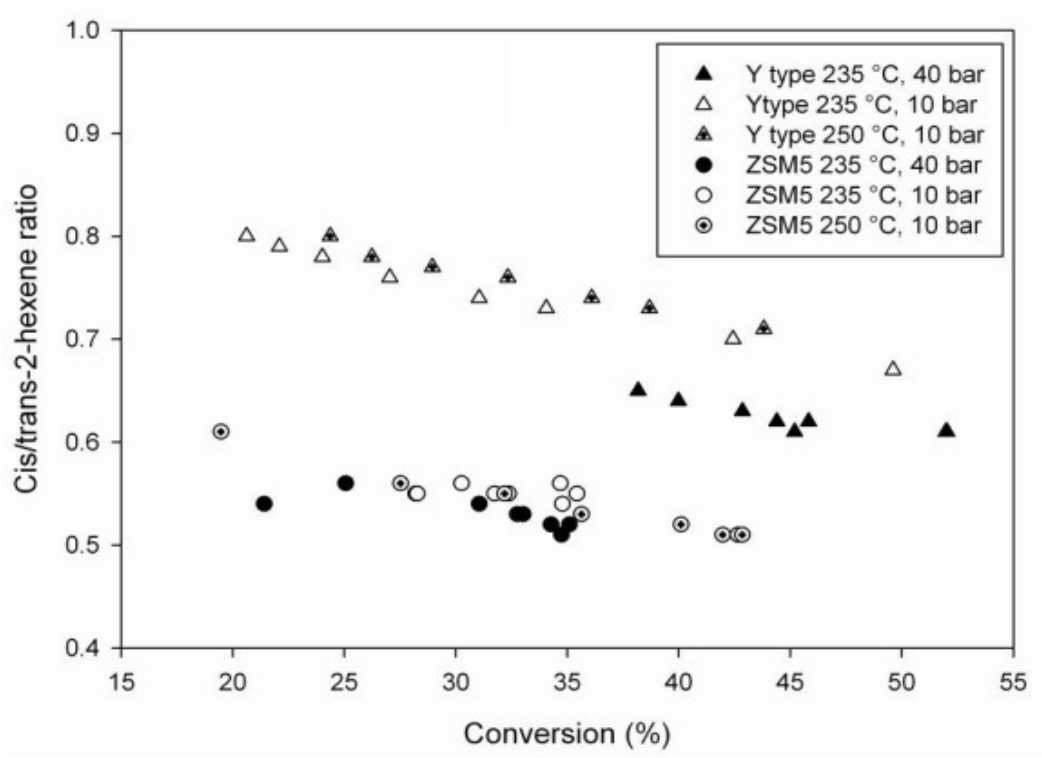

b)

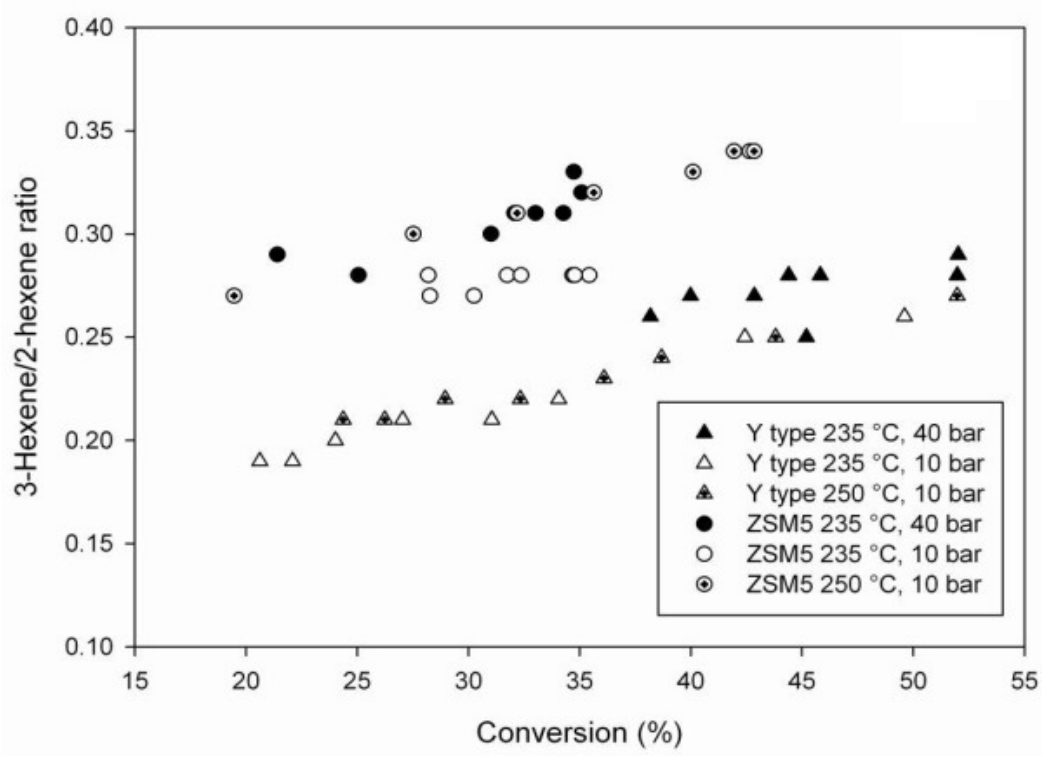

Figure 5.9. a) Cis/trans-2-hexene ratio over zeolite Y and ZSM5 versus conversion of 1-hexene; b) 3-Hexene/2-hexene ratio over zeolite Y and ZSM5 versus conversion.

5.4. Conclusions

In zeolite Y a clear deactivation pattern was observed with the rate of deactivation being slower in supercritical conditions compared to subcritical conditions. In supercritical runs at higher pressure, the deactivation rate was reduced to a more gradual level, such that catalyst activity was sustained for longer periods. Consequently, the final conversion after 6 hours reaction time for zeolite Y operating under supercritical conditions could be maintained at a higher value than ZSM5. In both catalysts higher temperatures and pressures favoured dimer formation with greater concentration being detected in the liquid products.

TGA results showed that coke deposition in zeolite Y decreased by 3.1 wt% upon increasing the pressure from 10 bar to 40 bar, and thus moving in to the supercritical region. However in ZSM5 the equivalent decrease in coke deposition was measured as 8.1 wt%, showing a much larger change above the critical pressure.

Nitrogen adsorption showed that there was a significant loss in surface area in the coked samples. ZSM5 was resistant to aging due to the very small pore size (5.3 – 5.6 Å) which prevents coke molecules from penetrating and depositing inside the pores.

The relatively large change in coke deposit in moving from sub to supercritical conditions was thought to result from extraction of coke from the outside surfaces of zeolite crystals within the alumina binder matrix. Zeolite Y showed faster aging compared to ZSM5 due to the larger pore size (7.4 Å) which can accommodate coke deposits, thus making coke more difficult to remove by the

SCF and leading to lower changes in coke deposit upon moving in to the supercritical region when compared with ZSM5. Most coke forms on the catalyst before two hours on stream and was shown to comprise mainly saturated hydrocarbon species. Its deposition upon the catalyst surface affects the hydroxyl groups on the zeolite, leading to reduction of the acidity of the catalyst.

In zeolite Y the strongest acid sites are deactivated first, leading to the large observed decrease in catalyst activity whilst in ZSM5 the acid site coverage is thought to occur in a more uniform way, which does not cause such a large decrease in activity.

The novel finding of this study was that SCFs are useful for improving the performance of zeolite Y through extraction of coke and coke precursors from the catalyst surface. This helps to keep the pores open to a sufficient extent for reaction conversion to be substantially improved to around double the value observed under subcritical conditions, and greatly improves the viability of using zeolite Y for 1-hexene isomerisation. By contrast, ZSM5 does not show a strong deactivation under subcritical conditions and therefore operating under supercritical conditions has relatively little effect upon the overall conversion.

CHAPTER 6

HYDROGENATION OF NAPHTHALENE

Hydrogenation is an important process in industry and the efficient ring hydrogenation of aromatics is useful for the production of high performance diesel fuel (Hiyoshi *et al.*, 2007). The hydrogenation of naphthalene is an example of this type of reaction. Several researchers have investigated the liquid and vapour phase hydrogenation of naphthalene over supported metal catalysts (Weitkamp, 1968; Huang and Kang, 1995; Hiyoshi *et al.*, 2007). The reaction mechanism, kinetics and deactivation issues in the hydrogenation of aromatics using naphthalene hydrogenation as a model reaction have been studied (Sapre and Gates, 1981; Zhan and Guin, 1994; Rautanen *et al.,* 2002). However catalyst deactivation remains a problem when hydrogenating aromatic molecules. Härröd *et al.* (2001), Trabelsi *et al.* (2000) and Hiyoshi *et al.* (2007) studied the use of SCFs to overcome mass transport issues in gas-liquid phase hydrogenation reactions as well as the use of SC solvents such as CO_2 to extract coke deposit and thus prolong the catalyst life time. Further understanding is required of how the operating conditions and phase behaviour influence the catalyst deactivation, hence the motivation for this study.

In this Chapter the effects of operating at supercritical versus subcritical conditions upon catalyst life time during the hydrogenation of naphthalene are reported. CO_2 is not used as the SC solvent but rather the system temperature and pressure are increased above the critical point such that naphthalene, cyclohexane solvent and hydrogen are reactants in the SC phase.

In section 6.1 the phase behaviour is presented and in section 6.2 the effect of operating temperature and pressure on catalytic activity and selectivity data are reported. A comparison between operating in subcritical and supercritical conditions in terms of catalyst activity and coke deposition is drawn in section 6.3. The hydrogenation of naphthalene is accompanied by other reactions, including the isomerisation of reaction products such as decalin. In order to study the extent of isomerisation compared with hydrogenation, some separate isomerisation experiments were carried out using cis-decalin in the absence of hydrogen. The results of cis-decalin isomerisation is reported in section 6.4 and the effects of change in naphthalene feed concentration and its influence on catalytic activity and coke deposition are reported in section 6.5. Studies of the long term deactivation behaviour are reported in section 6.6. A kinetic model for the reaction was determined and the activation energy calculated, as reported in section 6.7. Catalyst characterisation is discussed in section 6.8 and post reaction coke extraction using SC CO_2 is presented in section 6.9. Finally, conclusions are drawn in section 6.10.

6.1. Phase composition and critical properties

In order to feed naphthalene to the reactor it was dissolved in a cyclohexane solvent, which is passed through trace-heated lines to vaporise it then mixed with hydrogen gas just before entering the reactor. In order to understand the prevailing conditions within the reactor, it was necessary to carry out some phase behaviour calculation for the feed. The feed components are

naphthalene dissolved in cyclohexane and hydrogen. As the reaction proceeds, the system composition within the fixed bed reactor changes as hydrogenated products are formed. The system then also includes tetralin and decalin together with unreacted hydrogen, cyclohexane and naphthalene. The system composition changed with the varying reaction conditions and therefore it was necessary to calculate the phase diagram of the reacting mixture under each set of conditions. The following sub sections contain a table and phase diagrams to summarise the phase composition of the mixtures.

Table 3.7 in Chapter 3 provides a detailed summary of all reaction conditions studied during naphthalene hydrogenation, however a brief summary has also been given in Table 6.1. A set of six different cases were investigated, as detailed below:

- In case one, the feed composition was fixed to investigate the effect of operating temperature and pressure. The temperature and pressure were varied between 100 – 300 ℃ and 10 – 80 bar, respectively, and all the reactions in case one were conducted in the SC phase.
- The reaction conditions were changed in the second case to enable the study of subcritical versus supercritical reaction conditions. Supercritical reaction conditions of 300 ℃, 90 bar were studied and compared to subcritical conditions of 260 ℃, 90 bar and 300 ℃, 60 bar.
- In the third case, the effect of cis to trans-decalin isomerisation on the product distribution was studied, using pure cis-decalin as the feed.
- In the fourth case, the temperature and pressure were fixed at 300 ℃ and 80 bar and the naphthalene feed concentration was varied between

10 – 100 g/L to study its influence on coke deposition and catalyst deactivation.

- In case five, the long term deactivation behaviour was studied and conditions that would speed up the deactivation process were chosen.
- Finally in case six, catalyst reactivation and coke extraction by SC CO_2 were studied.

Table 6.1. Summary of reaction systems studied during naphthalene hydrogenation.

Case	**T (°C)**	**P (bar)**	**Naphthalene feed concentration (g/L)**	**Feed flow rate (mL/min)**	**H_2 feed flow rate (mL/min)**	**Phase**	**Catalyst (g)**
C1	100-300	10–80	10	0.5	10	Super	2
C2	260-300	60-90	10	2.5	2	Super versus sub	2
C3	300	80	0	1.5	10	Super	2
C4	300	80	10-100	0.5	10	Super	2
C5	300	80	100	1.5	10	Super	2
C6	300	80	100	1.5	10	super	2

6.2. Effect of temperature and pressure on catalytic activity and product distribution

6.2.1. Temperature effect on catalytic activity and product distribution

The conversion of naphthalene produced three hydrogenated products for all of the studied reactions, tetralin, cis and trans-decalin. The reaction is sequential where naphthalene is hydrogenated to tetralin, followed by subsequent hydrogenation to cis or trans-decalin. The conversion and the product selectivity depended on the reaction conditions. The composition of the reactant feed in this section is summarised in Table 6.2

Table 6.2. Composition of the reaction feed for case 1.

Naphthalene in cyclohexane feed Flow rate (mL/min)	**H_2 feed flow rate (mL/min)**	**Naphthalene in feed (g/L)**	**Naphthalene in mixture (mol%)**	**Hydrogen in mixture (mol%)**	**Cyclohexane in mixture (mol%)**
0.5	10	10	0.2	86.1	13.7

The temperatures studied were 100, 250, 270, 280 and 300 ℃ while the pressure was kept constant at 80 bar. All of these reaction conditions were located within the single SC phase as is shown in the HYSYS ternary phase diagrams in Figures 6.1a-c. The blue lines in the diagrams in Figures 6.1a-c

show the phase envelope and the red lines show the tie lines. The white circle with a cross indicates the reactor operating conditions. As the reaction progresses, tetralin and decalins are formed but the reaction mixture remains in the SC phase since the composition does not change sufficiently to enter the two phase region. The phase diagrams at 280 and 270 ℃ are very similar therefore only the phase diagram at 280 ℃ is shown here (phase diagram for 270 ℃ is shown in Appendix 8.8).

a)

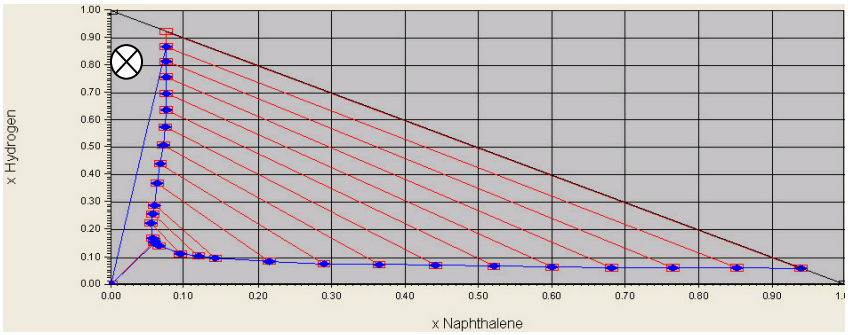

b)

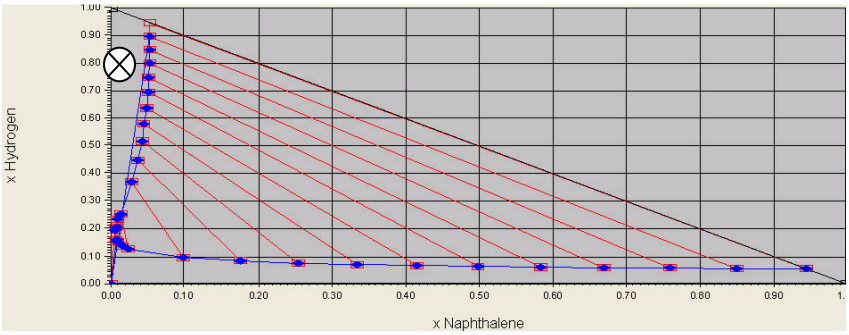

c)

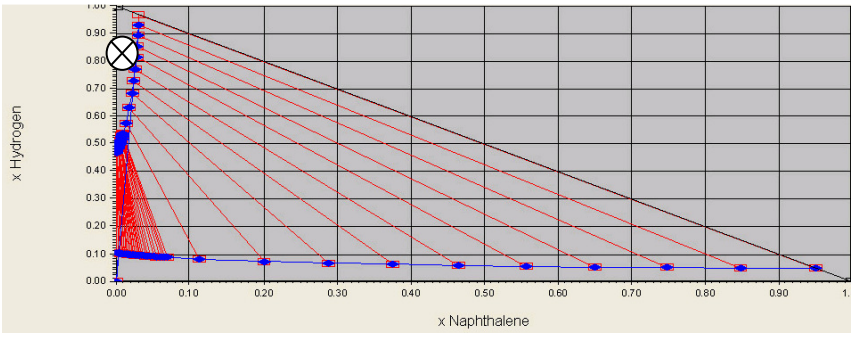

Figure 6.1. HYSYS binary plot from ternary system. a) At 300 ℃ and 80 bar; b) At 280 ℃ and 80 bar; c) At 250 ℃ and 80 bar.

Figure 6.2 shows naphthalene conversion against time on stream at 300 ℃, 280 ℃, 250 ℃ and 100 ℃ at a set pressure of 80 bar. The experimental run at 270 ℃ was excluded from the graph as too many lines make the patterns unclear; however it is shown in a separate Figure in Appendix 8.8 and included in the discussion in this section for comparison purposes.

All the experimental results show a catalyst start up effects with some time required for the diffusion of reactants into the catalyst pores. This leads to the conversion increasing slightly from the value at the initial sample after 1 hour to the value after 2 hours on stream. This was previously observed in other works (Wang *et al*., 2009). The liquid samples were collected as soon as liquid product was available at the reactor outlet which usually was between 1 – 1.5 hour from the starting point, depending on the feed flow rate.

Figure 6.2 shows that at 300 ℃, the conversion starts at 89% and goes up to 97% after 6 hours on stream. There is no evidence of deactivation after 6 hours on stream. At 280 ℃, the conversion starts at 92% and increases up to 100% after which it is stable and shows no deactivation after 6 hours on stream. At 270℃, the conversion starts at 90% and increases to 98% at 2 hours after which it stabilises and remains at 98% after 6 hours on stream. At 250 ℃, the conversion starts at 97% and gradually drops to 86% over 6 hours on stream. At 1.5 hours on stream the highest conversion of 98% occurs at reaction temperature 250℃. Figure 6.2 shows that the conversions at temperatures of 250 ℃, 280 ℃ and 300 ℃ cross over each other after 2.5 hours on stream, around 95% conversion. This could be due to the different amounts of coke deposited on the catalyst at 2 hours on stream at the various temperatures

investigated, which is later explored in the catalyst characterisation in section 6.8. The reaction run at 100 ℃ shows conversions between 2 – 15%. This low conversion is due to the fact that the catalyst used, NiMo, only becomes active at higher temperatures (Shao and Song, 2001). Therefore, the results at 100 ℃ have not been used for further analysis.

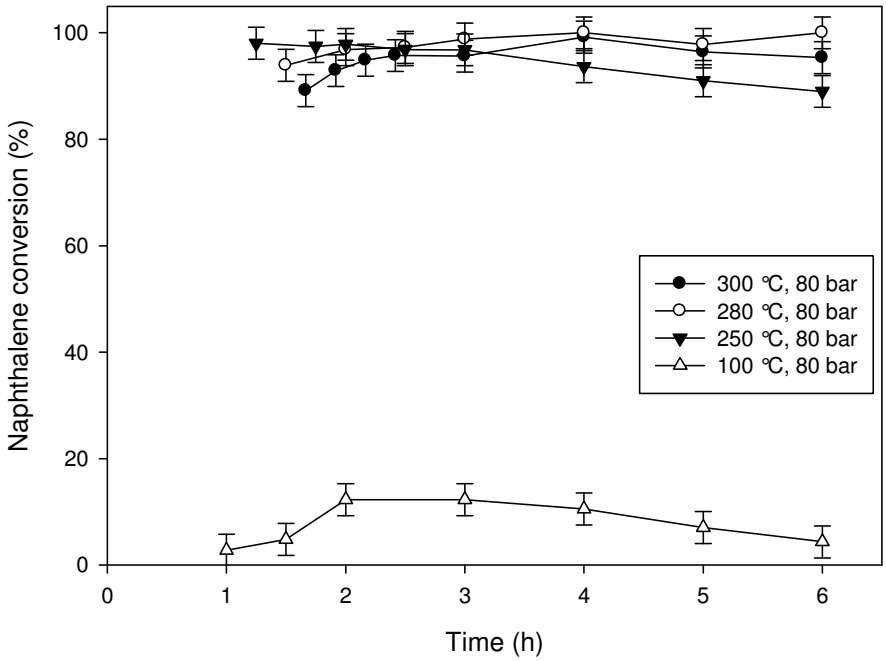

Figure 6.2. Naphthalene conversion against time at 300 ℃, 280 ℃, 250 ℃, 100 ℃ at 80 bar.

The hydrogenation of aromatics is an exothermic process which is thermodynamically favoured at lower temperatures (Weitkamp, 1968). The equilibrium conversion of naphthalene at 300 ℃ and 69 bar is 99.7% according to Frye's equilibrium correlation (Frye and Weitkamp, 1969). Since the experimental conversions of naphthalene, 99% at 80 bar and 100% at 60 bar,

reached close to to equilibrium conditions, this suggests that they were not affected by thermodynamic considerations.

From Figure 6.2 it was observed that increasing the temperature from 250 ℃ to 280 ℃ led to an increase in conversion at 6 hours reaction time. However, the conversions at 270, 280 and 300 ℃ lay within a narrow range of 96 – 100 %, within the value of the error bars. Therefore, it was concluded that the optimum temperature is in the range of 270 ℃ – 300 ℃. Other researchers (Zhan and Guin, 1994; Rautanen *et al.*, 2002) have shown that an increase in temperature, from 80 to 300 ℃, resulted in an increase in reaction rate constants and thus the overall reaction conversion. A further increase in the reaction temperature above 450 ℃ results in thermodynamic limitations and although the reaction rate constant increases with temperature the overall conversion decreases (Weikamp, 1968).

Figure 6.3 shows the product selectivity at different temperatures of 250, 270, 280 and 300 ℃ at a set pressure of 80 bar, illustrating that for all temperature runs, trans-decalin was the main reaction product with selectivity above 60%. As temperature was increased from 250 ℃ to 280 ℃, the selectivity to trans-decalin increased to above 80%, before decreasing as the temperature was raised to 300 ℃. Figure 6.3 further shows that tetralin, which is an intermediate product, had a selectivity of 20% at 250 ℃. However tetralin selectivity decreased to ~0.4% at 280 ℃ which means that nearly all naphthalene became fully hydrogenated to either cis or trans decalin. As the temperature increased to 300 ℃ tetralin was produced again with a selectivity of 14%. The selectivity to cis-decalin dropped from 20% at 250 ℃ to 9% at 300 ℃. No partially

hydrogenated products such as octahydronaphthalene or hexahydronaphthalene were detected. The increase in tetralin formation at the higher temperature of 300 ℃ could be due to the effect of coke formation at higher temperatures on product distribution. With higher surface concentration of tetralin molecules on the catalyst surface this would lead tetralin to form multi-layers of tetralin molecules, which would then make the filipping of 1,9-octalin intermediate more difficult. This then results in a decrease in the formation of trans-decalin (Rautanen *et al.*, 2002).

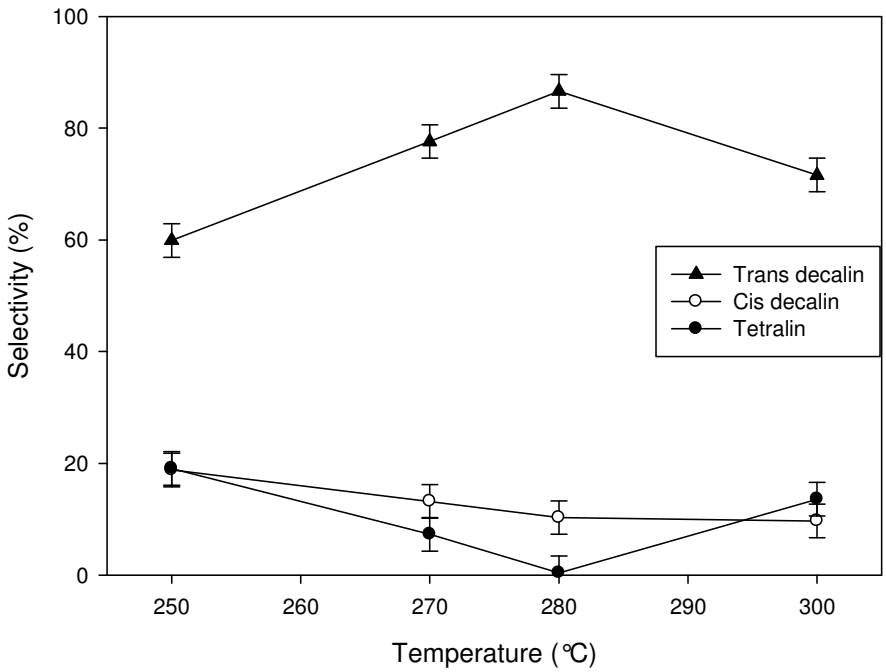

Figure 6.3. Temperature effect on product selectivity at 250 ℃, 270 ℃, 280 ℃, 300 ℃ at 80 bar at 2 hours on stream.

Miyazawa and Pitzer (1958) reported standard heats of formation for cis-decalin and trans-decalin of -169 and -182 kJ/mol, respectively. Huang and Kang (1995) reported apparent activation energies for tetralin hydrogenation to cis

and trans-decalin of 41.4 and 30.4 kJ/mol, respectively. The activation energy for tetralin hydrogenation to cis-decalin is larger than that to trans-decalin as the cis type partial hydrogenated intermediate complex of tetralin is less stable than the trans type (Huang and Kang, 1995). Furthermore, Weitkamp (1968) has studied the detailed reaction mechanism of naphthalene hydrogenation and reported that tetralin reacts to 9,10-octalin which is further hydrogenated to cis-decalin or isomerised to 1,9-octalin. 1,9-Octalin is in turn hydrogenated to cis or trans-decalin. Rautanen *et al.* (2002) reported that the isomerisation rate of 9,10-octalin to 1,9-octalin was 1-3 orders of magnitude higher than the hydrogenation rate of 9,10-octalin on a Ni/Al_2O_3 catalyst, which could explain trans-decalin as the predominant isomer as is shown in Figure 6.3.

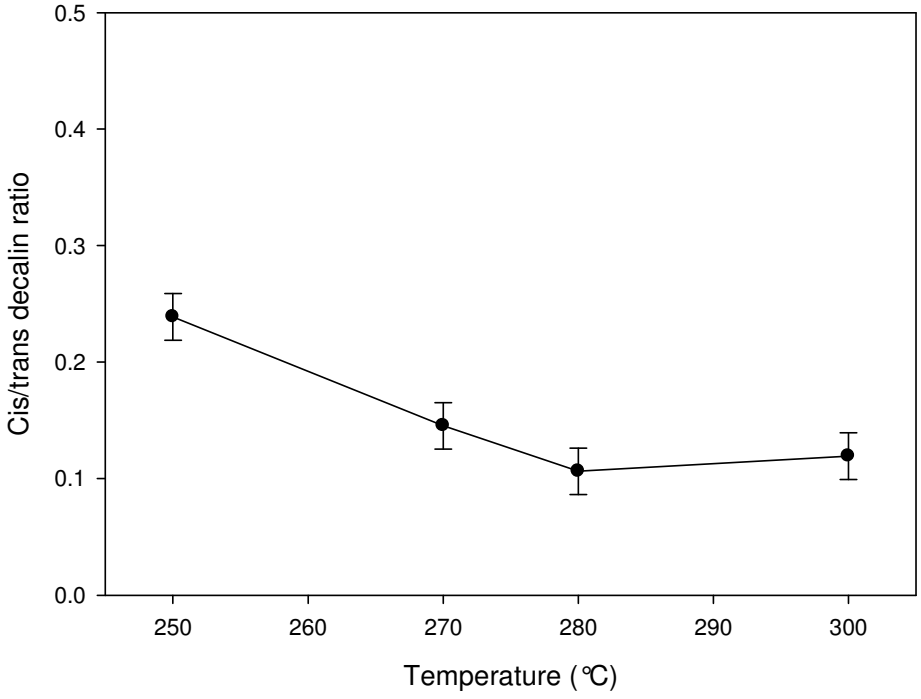

Figure 6.4. Cis/trans-decalin ratio at 250 ℃, 270 ℃, 280 ℃, 300 ℃ at 80 bar, at 2 hours on stream.

Figure 6.4 shows the cis to trans-decalin ratio at different temperatures of 250, 270, 280 and 300 ℃ at a set pressure of 80 bar, indicating that the trans-decalin ratio decreased from 0.2 at 250 ℃ to 0.1 at 300 ℃. This further confirms that trans-decalin is the favoured product in these reaction sets and that an increase in temperature results in a decrease in cis to trans-decalin ratio by almost a half. Sapre and Gates (1981) reported trans-decalin as the predominant isomer in naphthalene hydrogenation over CoMo catalyst at 325 ℃ and 75 bar, while Weitkamp (1968) reported cis-decalin as the predominant isomer over Pt/Al_2O_3 catalyst. Overall, the distribution of cis and trans isomers in the products depends on the catalyst as a result of differences in the relative rates of successive steps in the reaction path (Weitkamp, 1968).

6.2.2. Pressure effect on catalytic activity and product distribution

The pressure experiments were carried out at 20, 50, 60 and 80 bar at a constant temperature of 300 ℃. The feed composition was the same for all pressure experimental runs and is summarised in Table 6.2. Again all these experimental runs were conducted in the SC phase as is shown in the ternary phase diagrams in Figures 6.5a–d, for each representative pressure studied.

a)

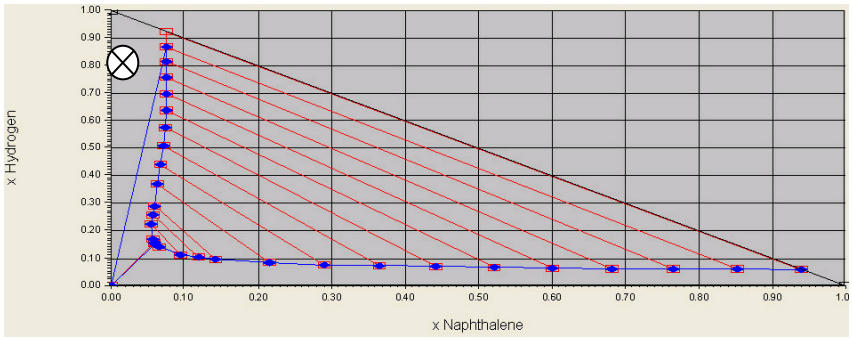

b)

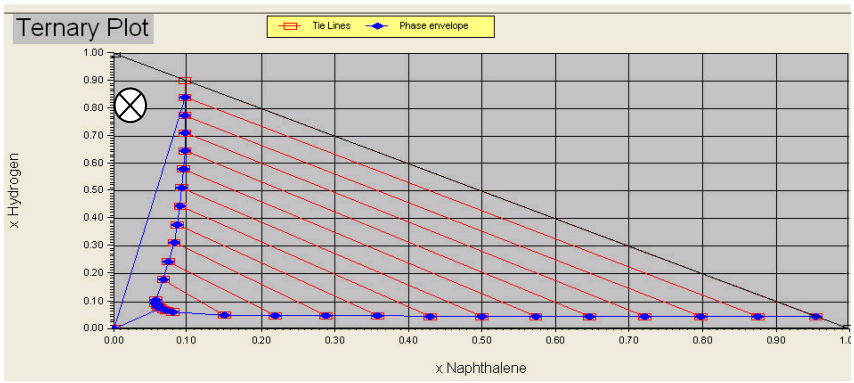

Figure 6.5. HYSYS binary plot from ternary system at a) 300 ℃ and 80 bar; b) 300 ℃ and 60 bar.

c)

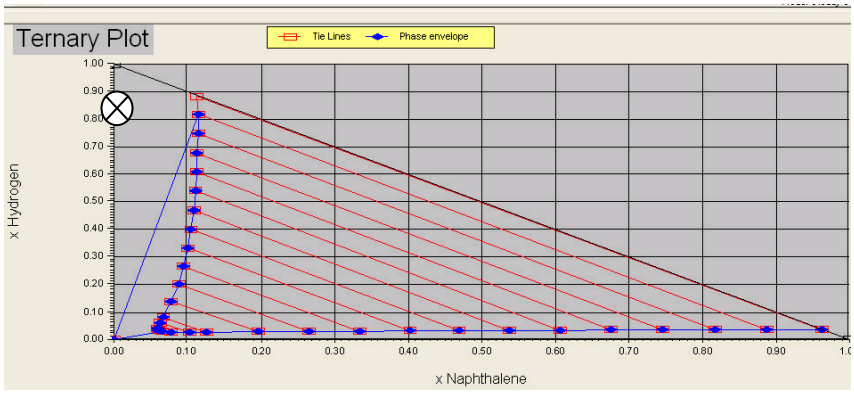

d)

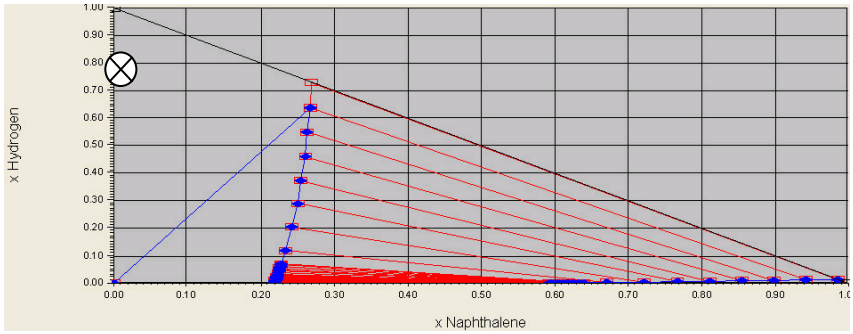

Figure 6.5. HYSYS binary plot from ternary system at c) 300 ℃ and 50 bar; d) 300 ℃ and 20 bar.

Figure 6.6 shows the conversion against time on stream at pressures of 20, 50, 60 and 80 bar at a set temperature of 300 ℃. Between 1 – 2 hours on stream, all the reaction runs showed a catalyst start up effect, similar to Figure 6.2, where time is required for diffusion of reactants into the catalyst pores and this results in the conversion being lower for the initial points at 1 hour on stream compared to 1.5 hour on stream. Figure 6.6 shows that as the pressure is increased from 20 to 50 bar there was an increase in conversion. At 20 bar, the conversion was only 40 – 60% whilst at 50 bar the conversion was 75 – 80%.

As the pressure was increased further to 60 bar the conversion reached 100% and was steady between 2 – 6 hours on stream. A further increase in pressure to 80 bar, results in a slight decrease in conversion to within the range 88 – 97% and a slight increase in coke deposit of 5.4 wt% as evaluated by TGA. This is to be expected as higher pressures favour side reactions and oligomerisation (Quann, 1988).

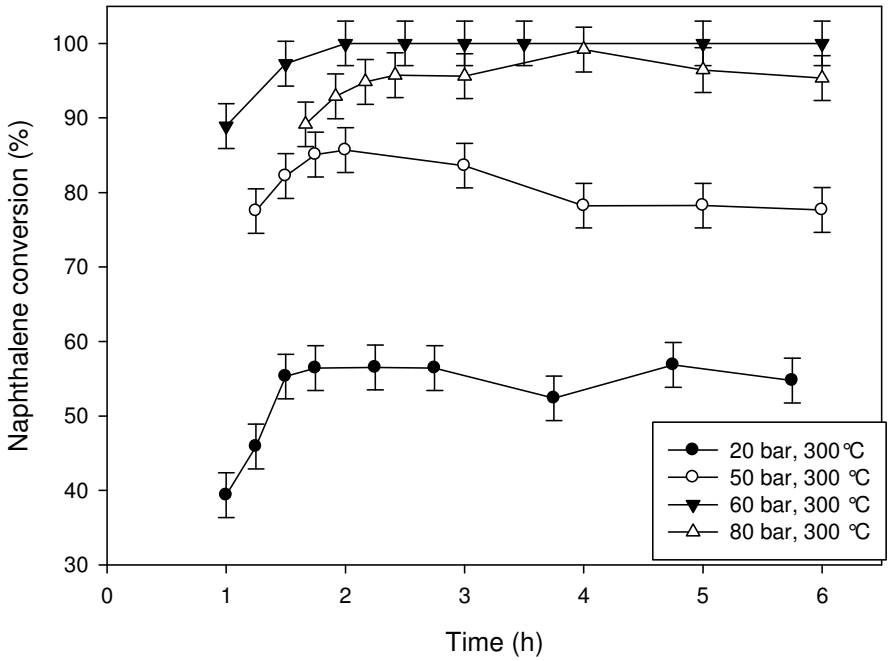

Figure 6.6. Pressure effect on conversion at 300 ℃ and 20 bar, 50 bar, 60 bar and 80 bar.

Various effects can lead to the results observed in Figure 6.6. Firstly, as the pressure was increased, the reacting mixture density increased from 5.7 kg/m^3 at 20 bar to 16.9 kg/m^3 at 60 bar and 22.4 kg/m^3 at 80 bar. This means that the mixture density increased by 3 and 4 times at 60 and 80 bar, respectively, compared to the value at 20 bar.

Secondly, high pressures generally lead to faster reaction rates and higher conversions due to increased adsorption on the catalyst surface. At 60 bar of hydrogen pressure, the hydrogen coverage of the catalyst surface is thought to have increased which caused the conversion to reach 100%. This also corresponds to the lowest coke deposit on the catalyst surface of 5.3 wt%, as evaluated by TGA. It shows that at this pressure hydrogen also acts to remove some of the coke. Increasing the pressure further to 80 bar causes a slight decrease in conversion, although the conversion values are within the error bar region for 60 and 80 bar after 2 hours on stream. The results reported lead to conclude that the optimum operating pressure is around 60 bar.

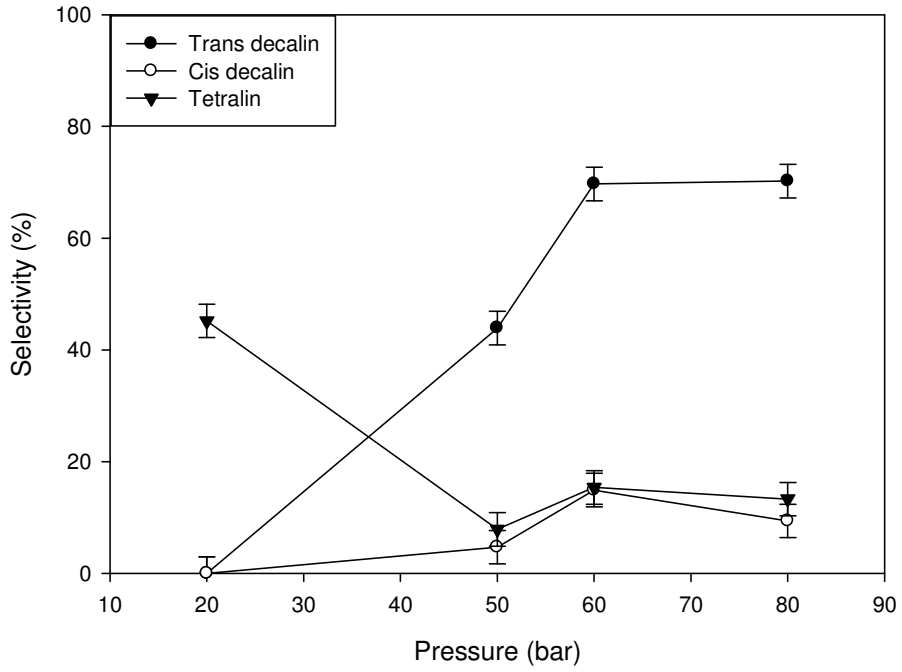

Figure 6.7. Product selectivity at 20, 50, 60 and 80 bar at 300 ℃, at 2 hours on stream.

Figure 6.7 shows the pressure effect on product selectivity at 20, 50, 60 and 80 bar at a constant temperature of 300 ℃, illustrating that pressure has a positive effect on the selectivity towards trans-decalin which increases from 0% at 20 bar to 70% at 60 and 80 bar. Pressure also has a positive effect on cis-decalin formation as it increases from 0% at 20 bar to 15% at 60 bar, however this decreases to 9% at 80 bar. Higher pressures favour full hydrogenation of naphthalene as opposed to partial hydrogenation. As a result of increasing pressure, tetralin selectivity decreases from 45% at 20 bar to 13% at 60 and 80 bar (Figure 6.7). Weitkamp (1968) suggested that the influence of hydrogen partial pressure had less of an effect on the formation of trans-decalin compared to cis-decalin because tetralin can react directly to form cis-decalin at high pressure, whereas it could not hydrogenate directly to form trans-decalin and has to go through the intermediate octalin. In comparison, the experimental results reported here show that at higher pressures above 60 bar, trans-decalin formation is affected less than cis-decalin formation as the selectivity towards trans-decalin is constant and does not increase or decrease further as a result of pressure.

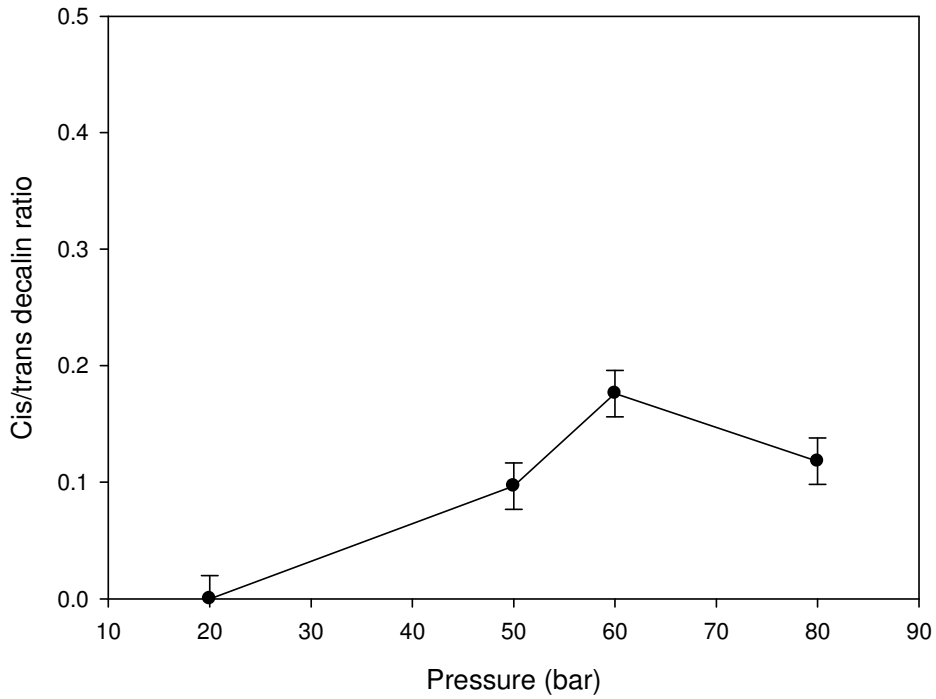

Figure 6.8. Cis/trans-decalin ratio at 20, 50, 60 and 80 bar at 300 ℃, at 2 hours on stream.

Figure 6.8 shows the effect of pressure on cis/trans-decalin ratio at 20, 50, 60 and 80 bar at a constant temperature of 300 ℃. In Figure 6.8, the cis to trans-decalin ratio increases from 0.1 at 50 bar to ~0.2 at 60 bar and then decreases to 0.1 at 80 bar.

As cis-decalin forms from the direct hydrogenation of tetralin, an increase in cis to trans-decalin ratio with increasing pressure suggests a rapid direct hydrogenation of tetralin molecules adsorbed on the catalyst active sites. Another possibility is a lower desorption rate of 1,9-octalin; as trans-decalin is formed via the flipping rotation of octalin, a lower desorption rate of 1,9-octalin would favour the formation of cis-decalin (Rautanen *et al.*, 2002).

In studies reported in the literature, different catalysts show varying selectivities towards the products. Rhodium catalyst showed a very high selectivity of 98% towards cis-decalin, while palladium catalyst was 50% selective towards trans-decalin (Weitkamp, 1968). Rautanen *et al.* (2002) reported selectivities of up to 60% towards trans-decalin on Ni/Al_2O_3 catalyst and Sapre and Gates (1981) reported trans-decalin as the major product on CoMo catalyst. The catalyst used in this investigation, NiMo, shows very high selectivities of above 50% towards trans-decalin as the more stable product, as is shown in Figures 6.3 and 6.7. This could be due to the way reaction intermediate products adsorb onto the catalyst surface. Trans-decalin is formed via intermediates that have desorbed and turned over on the catalyst (flipping rotation of 1,9-octalin) which means that the higher selectivity of the NiMo catalyst used could be due to a faster flipping rate of the 1,9-octalin intermediate compared to the direct hydrogenation of tetralin to form cis-decalin.

Cis and trans-decalin have different applications and the favoured product depends on the intended product application. For example the cis isomer can be used to produce sebacic acid or in the manufacture of nylon and plasticizers (Hiyoshi *et al.*, 2007). Decalin can be used as a hydrogen storage material and the cis isomer is more favoured because its dehydrogenation rate is faster than the trans isomer (Hiyoshi, 2007).

6.3 Effect of operating at subcritical versus supercritical conditions

To investigate the effect of operating in sub or supercritical conditions the mixture composition given in Table 6.3 was chosen.

Table 6.3. System composition during sub versus SC reactions.

Naphthalene in cyclohexane feed Flow rate (mL/min)	**H_2 feed flow rate (mL/min)**	**Naphthalene in feed (g/L)**	**Naphthalene in mixture (mol%)**	**H_2 in mixture (mol%)**	**Cyclohexane in mixture (mol%)**
2.5	2	10	1.2	19.8	79.0

The critical point for this system is T_c = 282 °C and P_c = 86.6 bar. As the reaction progresses and the mixture includes tetralin and decalins, the critical point changes slightly to T_c = 280 °C and P_C = 86.2 bar. The change is very small and can be neglected as the reaction phase does not change from super to subcritical or vice versa due to this change in composition. The phase diagram in Figure 6.9 shows the experimental points. All experiments have been carried out close to the boundary between sub and supercritical as this region is of most interest since in the near-critical region the properties are very sensitive to slight changes in pressure.

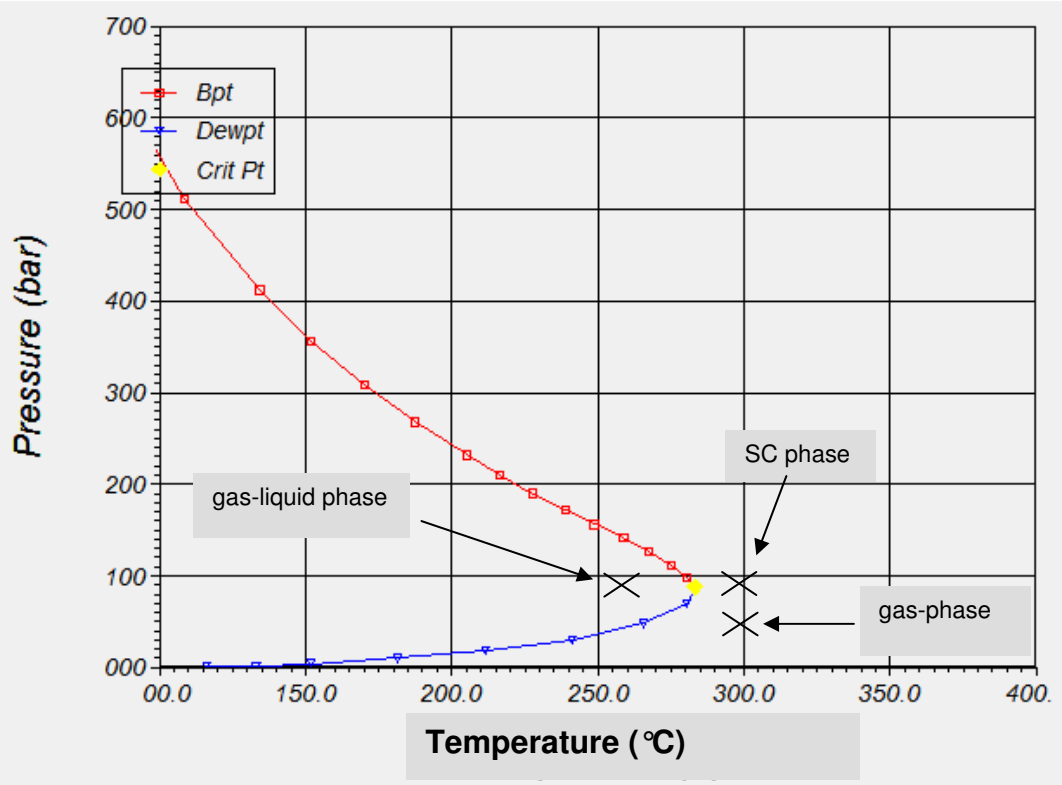

Figure 6.9. Calculated phase boundary for the hydrogenation of naphthalene. Symbol X represents the reaction conditions.

In the experiments already reported in this chapter, the catalyst did not show any deactivation after 6 hours on stream (Figures 6.2 and 6.6) and the conversion was relatively stable. Therefore, some deactivation needed to be observed to determine whether SCFs can prolong the catalyst life time and suppress catalyst deactivation. This was done by increasing the feed flow rate from 0.5 mL/min to 2.5 mL/min which in turn increased the WHSV from 0.29 h^{-1} to 13.25 h^{-1}. Furthermore the hydrogen feed flow rate was reduced from 10 mL/min to 2 mL/min which decreased the hydrogen content in the system from 86 mol% to 19.8 mol%. This still meant that hydrogen was in large excess of three times the stoichiometric ratio (i.e. H_2/naphthalene of 5:1 mol/mol). This

was done to achieve a well-defined catalyst deactivation pattern and thus be able to distinguish the effects of operating in sub and supercritical conditions.

Two experimental runs were carried out at a set temperature of 300 ℃ and pressures of 60 bar and 90 bar. The residence time was based on the inlet conditions and varied between 11 seconds at 300 ℃, 60 bar to 20 seconds at 300 ℃ and 90 bar. The results are shown in Figure 6.10. Initially for both reactions the conversion starts relatively high at 88%. The conversion is similar for both runs until two hours on stream with conversion being relatively stable and only decreasing by 2%. After two hours on stream the two runs diverge. The subcritical run at 60 bar declines rapidly to 35% after seven hours on stream whereas the supercritical run declines at a much slower rate and reaches 50% after nearly 10 hours on stream.

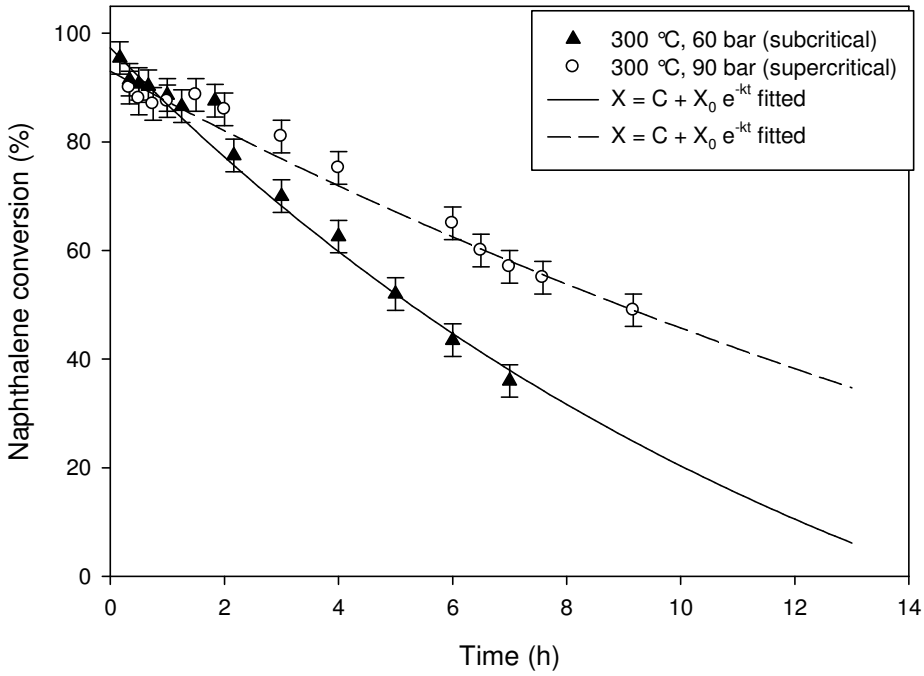

Figure 6.10. Naphthalene conversion against time at 300 ℃, 60 bar and 90 bar.

As the pressure was increased from 60 to 90 bar, the phase of the reaction changed from subcritical (gas-phase) to supercritical. The density of the mixture increased from 127 kg/m^3 to 226 kg/m^3 at 60 bar and 90 bar respectively. The reaction mixture at 90 bar was supercritical and therefore would have much greater solvating powers enabling the removal of freshly formed coke precursors which in turn resulted in the much slower deactivation shown in Figure 6.10. This is further supported by TGA results, which show a coke deposit of 15.5 wt% in subcritical conditions compared to 9.6 wt% in supercritical conditions, which is a decrease of 38% in coke deposit. The two experimental runs diverge after 2 hours on stream, which suggests that most coke deposits on the catalyst surface after 2 hours on stream in the subcritical conditions whereas in supercritical conditions coke deposition seems to be more gradual. Another factor causing the difference in the two reactions was that the solubility of hydrogen is much higher in SCFs which would result in much better contact between the substrates and the solid catalyst (Baiker, 1999).

Previously, Figure 6.6 showed that once the operating conditions are in the supercritical region an increase in the pressure from 60 bar to 80 bar had little effect on conversion with both runs being within the error margin of each other. Figure 6.10 on the other hand shows a large difference between operating at 60 and 90 bar which suggests that the main difference lies in the reaction phase. It is apparent that changing the reaction conditions from the gas-phase to dense supercritical phase does prolong the catalyst life time by decreasing the coke

deposits by 38%. Once the reaction conditions are in the SC phase the optimum pressure is around 60 bar as previously discussed in section 6.2.2.

Experimental runs were also conducted at temperatures of 260 and 300 ℃ at a set pressure of 90 bar to study the effect of temperature upon operating in the subcritical (gas-liquid) and supercritical conditions.

Figure 6.11 shows that at 300 ℃ (supercritical) the conversion starts relatively high at 88% and declines to 49% after nearly 10 hours on stream. At 260 ℃ (subcritical) the conversion starts at 85% and declines to 30% after 6 hours on stream.

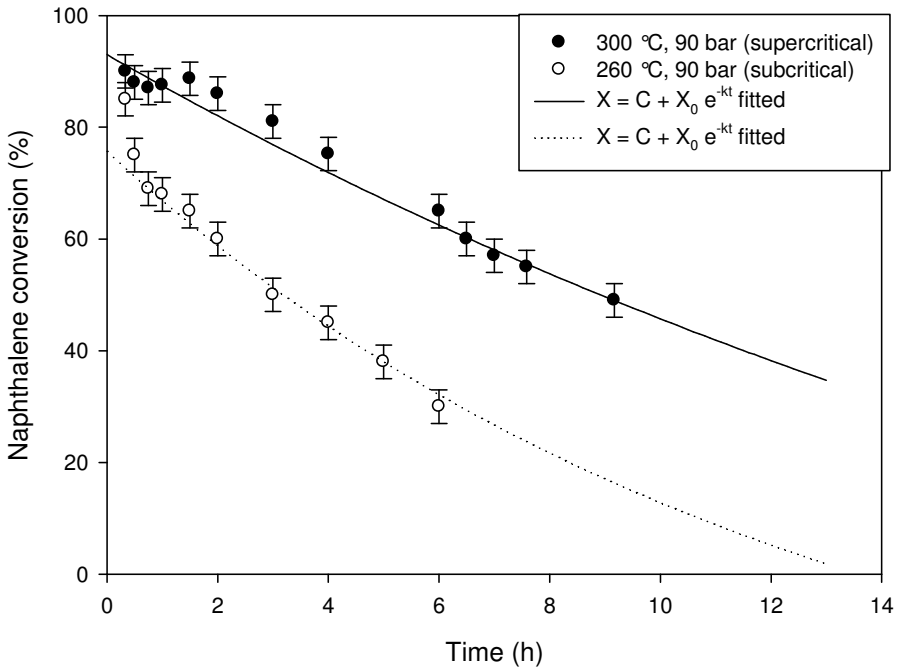

Figure 6.11. Naphthalene conversion against time at 260 ℃, 300 ℃ and 90 bar.

At operating conditions of 260 ℃ and 90 bar, the molar concentrations of naphthalene, cyclohexane and hydrogen are 1.2%, 79.0% and 19.8%

respectively. The liquid feed flow rate was 2.5 mL/min while the gas flow rate was 2 mL/min. As calculated by HYSYS, upon flashing the mixture would separate into two phases, the gas-phase having composition of 0.3% of naphthalene, 54.8% of cyclohexane and 44.9% of hydrogen in mole concentration and the liquid-phase having a composition of 1.4% of naphthalene, 86.0% of cyclohexane and 12.6% of hydrogen. The concentration of naphthalene in the liquid-phase is 4.6 times higher than the one in the gas-phase. Therefore, it is more likely that naphthalene would condense within the catalyst pores and pore entrances to form coke (Appleby *et al.*, 1962).

As the temperature is increased from 260 ℃ to 300 ℃; the phase changes from gas-liquid phase to dense supercritical. This results in a significantly slower deactivation rate in the supercritical conditions compared to subcritical. When operating in dense supercritical phase, the reaction mixture is in one homogeneous phase, which reduces any mass and heat transfer issues as well as having higher solvating powers and diffusivities enabling the extraction of coke deposits from the catalyst surface area (Baiker, 1999). TGA further confirm this as the percentage coke deposition decreases by 43% from 16.9 to 9.6 wt% as the reaction phase is changed from subcritical (gas-liquid phase) to supercritical. Note that Figure 6.3 previously showed that when the reaction conditions were in the supercritical phase changing the temperature from 250 – 300 ℃ did not result in a significant difference in conversion such as the one observed in Figure 6.11. Hence, this suggests that the difference observed in Figures 6.10 and 6.11 are due to the phase change, from gas and gas-liquid to supercritical, rather than the change in temperature or pressure.

Similar to the findings reported in this study, Tiltscher *et al.* (1981) reported the ability of SCFs to maintain catalyst activity, while Clark and Subramaniam (1998) showed that when operating in the SC region the catalyst activity was stable and did not show much decay with time. Furthermore, Saim and Subramaniam (1991) showed that by operating in SC conditions the percentage coke deposit decreased by 33%. Wang *et al.* (2009) showed that operating in the SC phase did prolong the catalyst life time compared to operating in subcritical conditions.

The deactivation was fitted by Equation 6.1 (previously equations 2.4 and 5.1). The coking reaction was assumed to be first order.

$$X = C + X_0 e^{-kt} \tag{6.1}$$

Where X is the conversion, C and X_0 are constants, k is the deactivation rate constant and t is the time in hours. The lines fitted are shown in Figure 6.10 and 6.11 and the fitted parameters in Table 6.4.

The deactivation was fastest in the subcritical conditions with a deactivation rate constant of 0.072 h^{-1} and 0.080 h^{-1} at 300 ℃, 60 bar and 260 ℃, 90 respectively. This is compared to a deactivation rate constant of 0.038 h^{-1} in supercritical conditions at 300℃, 90 bar. The fitted equation shows a better fit at the supercritical conditions with R^2 value of 0.99 compared to R^2 values of 0.98 in both subcritical conditions.

Table 6.4. Deactivation parameters. Fitted constants of Equation 6.1 to the data plotted in Figures 6.11 and 6.12.

	300 ℃, 60 bar (subcritical)	**300 ℃, 90 bar (SC)**	**260 ℃, 90 bar (subcritical)**
C	-0.53	-0.56	-0.38
X_0	1.50	1.46	1.14
k (h^{-1})	0.072	0.038	0.080
R^2	0.98	0.99	0.98

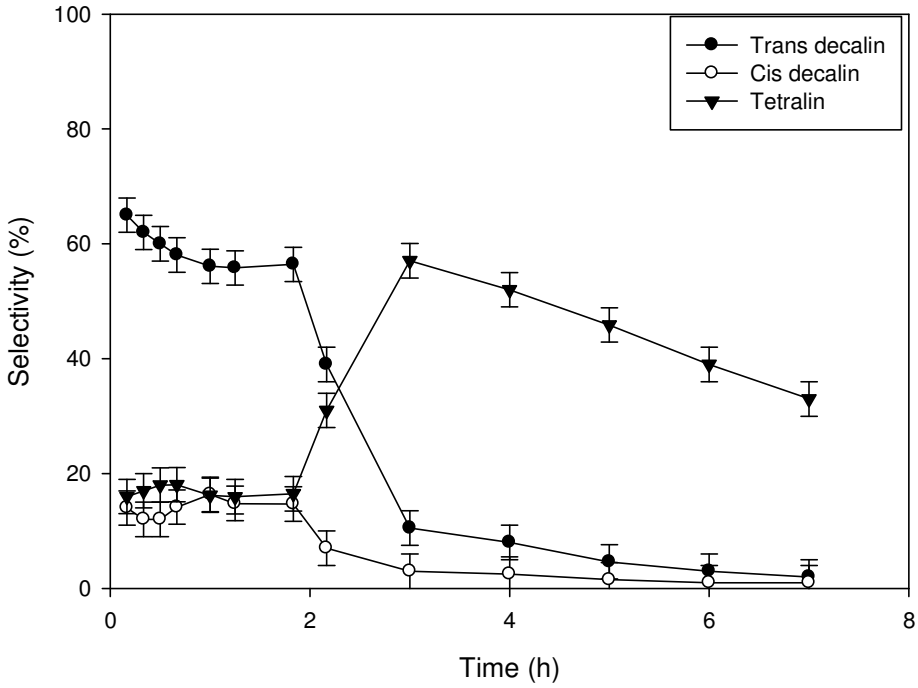

Figure 6.12. Product distribution at 300 ℃, 60 bar (subcritical).

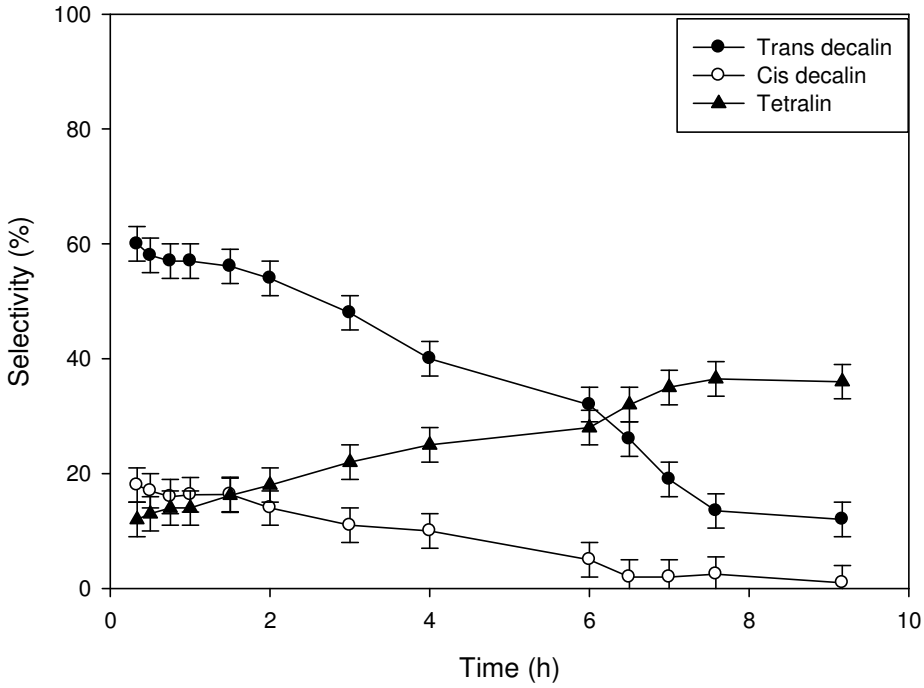

Figure 6.13. Product distribution at 300 ℃ and 90 bar (SC).

Figures 6.12 and 6.13 compare the effect of operating in the sub and SC region on the product distribution. Figure 6.12 shows the product distribution at 300 ℃ and 60 bar (subcritical conditions), indicating that initially trans-decalin was the main product with selectivities up to 1.8 hours on stream between 63% - 57%. This decreased dramatically to 10% at 3 hours on stream. The selectivity to trans-decalin declined further to 1% after 7 hours on stream. Tetralin selectivity was initially 18% after which it increased to 57% at 3 hours on stream, taking over from trans-decalin as the major product. In comparison, Figure 6.13 shows that when operating in SC conditions at 300 ℃ and 90 bar, trans-decalin was the major reaction product at 60% at 0.5 hours on stream. This dropped gradually to 32% at 6 hours on stream. Tetralin selectivity increased gradually from 12% to 36% between 0.5 to 9 hours on stream.

Comparing both Figures 6.12 and 6.13, it is observed that the change in major product distribution is more gradual in Figure 6.13. In Figure 6.12 tetralin is the major reaction product after 2 hours on stream whereas in Figure 6.13 the shift from trans-decalin to tetralin takes more than 6 hours.

The dramatic step change observed in the data in Figure 6.12 can be due to many factors. Although the reaction is in the gas phase, it is possible that a phase transition occurs where the gas and liquid phase separate. This would then result in mass transfer problems. Another possibility is the effect of the rate of coking and catalyst deactivation on product selectivity. Rautanen *et al.* (2002) reported that the hydrogenation rate of tetralin to decalins is much more affected by coking and deactivation compared to the hydrogenation rate from naphthalene to tetralin on Ni/Al_2O_3 catalyst. They stated that as the reaction proceeds, the active sites become blocked with coke as aromatics adsorb onto and bond with the catalyst active sites. This causes an effect on the formation of the intermediate 1,9-octalin which in turn affects the formation of cis or trans-decalin.

The gradual shift in the product distribution observed in Figure 6.13 is probably due to a slower rate of coke deposit in SC conditions. TGA results show that the production of trans-decalin as major product under SC conditions is consistent with lower coke deposit of 9.6 wt% at 300 °C 90 bar whereas the shift to tetralin as major product upon moving into the subcritical conditions at 300 °C and 60 bar corresponds to higher coke deposit of 15.5 wt%.

Comparing these results with previous Figures 6.3 and 6.7, which were conducted in the SC phase, it is observed that trans-decalin was the major reaction product up to 6 hours on stream in SC conditions. This shows that operating in the SC phase favours the formation of the fully hydrogenated trans-decalin over the partially hydrogenated tetralin product. This also means that in the SC phase the reaction proceeds to the fully hydrogenated products for a longer period of time whereas in the subcritical conditions this is not the case. Hiyoshi *et al.* (2007) also observed that using SC CO_2 solvent changes the product distribution in favour of the fully hydrogenated decalin product.

Overall, a further study into the dramatic step change observed in product selectivity in Figure 6.22 would be useful as it would help to explain the factors affecting this change.

6.4. Cis-decalin isomerisation

The isomerisation of cis-decalin was carried out to study the effect of isomerisation rate on product distribution in the absence of simultaneous hydrogenation reactions. Pure cis-decalin dissolved in cyclohexane was used as the feed. Table 6.5 shows the system composition and Figure 6.14 shows the results.

Table 6.5. Cis-decalin isomerisation reactions feed composition.

Reaction conditions	**Naphthalene in cyclohexane feed flow rate (mL/min)**	**H_2 feed flow rate (mL/min)**	**Cis-decalin in feed (g/L)**	**Cis-decalin in mixture (mol%)**	**H_2 in mixture (mol%)**	**Cyclohexane in mixture (mol%)**
300 ℃, 80 bar	1.5	10	10	0.5	67.3	32.2

Figure 6.14 shows that of the pure cis-decalin injected, approximately 40% isomerises to trans-decalin. The conversion of cis-decalin to trans-decalin started at 46% at 0.5 hours on stream. This decreased to 40% at 2 hours on stream and remained constant up to 5 hours on stream after which it decreased slightly to 39% after 6 hours on stream. After 2 hours on steam a stable ratio of 60% cis-decalin and 40% trans-decalin occurred, which corresponds to a cis/trans ratio of 3:2. It is apparent that the isomerisation of cis-decalin occurs easily in the chosen range of reaction conditions and that it seems to contribute to the formation of the more stable trans-decalin product.

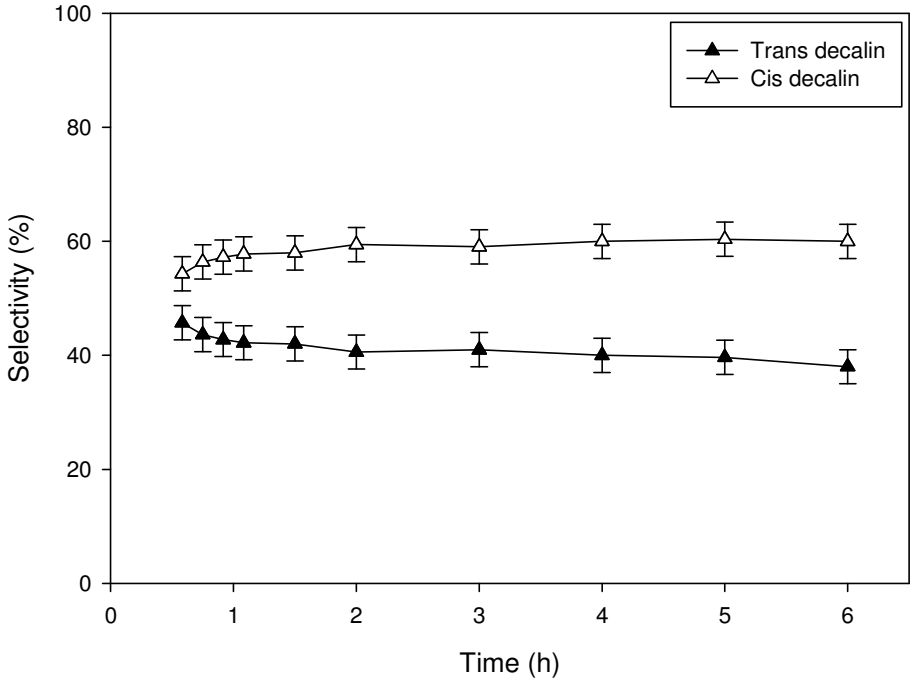

Figure 6.14. Cis-decalin isomerisation to trans-decalin at 300 ℃ and 80 bar.

The isomerisation of cis to trans-decalin occurs at certain conditions. Researchers such as Rautanen *et al.* (2002) and Romero *et al.* (2008) did not detect any cis to trans isomerisation under their studied reaction conditions of 80 – 160 ℃ and 20 – 40 bar on Ni/Al_2O_3 and $NiMo/\gamma Al_2O_3$ catalysts. Other researchers such as Weitkamp (1968) and Huang and Kang (1995) did observe cis to trans isomerisation under their studied reaction conditions of 200 – 260 ℃ and 17 – 87 bar on varying noble metal catalysts. Hooper *et al.* (1979) reported that the isomerisation of hydroaromatics is significant at higher temperatures. Thus at lower reaction temperatures (below 200 ℃) cis-decalin does not isomerise to trans-decalin. Higher reaction temperatures (above 200 ℃) are needed to isomerise cis to trans-decalin and this is in agreement with the

experimental results reported in this section where the temperature range studied was between 250 °C – 300 °C, hence isomerisation is observed.

Huang and Kang (1995) determined the isomerisation rate constants at 5.4 and 11.77 h^{-1} at 220 °C and 240 °C respectively. The authors calculated the apparent activation energy of cis-decalin isomerisation to trans-decalin at 61.8 kJ/mol. The authors further determined that naphthalene and tetralin act as poison to the isomerisation of cis to trans-decalin because they adsorb more easily on the catalyst surface. Therefore, pure cis-decalin has an isomerisation rate constant that is higher by an order of magnitude compared to the isomerisation rate constant in a system with naphthalene and tetralin. Consequently, even though Figure 6.14 shows 40% of pure cis-decalin isomerises easily to trans-decalin; in the hydrogenated system with naphthalene and tetralin, cis-decalin does not isomerise as easily to trans-decalin. Therefore the higher product selectivities towards trans-decalin observed in the reactions reported in this Chapter are thought to be mainly due to the selectivity of the catalyst and reaction conditions leading to the direct hydrogenation of naphthalene to trans-decalin, rather than cis-decalin isomerising to trans-decalin.

6.5. Naphthalene concentration change effect

The concentration of naphthalene in the feed was changed from 10 to 100g/L to investigate the effect it had on conversion, product distribution, coke deposition

and catalyst deactivation. Table 6.6 shows the system composition for different naphthalene concentrations in the feed.

Table 6.6. System composition with change in Naphthalene feed concentration.

Naphthalene in cyclohexane feed flow rate (mL/min)	**H_2 feed flow rate (mL/min)**	**Naphthalene in feed (g/L)**	**Naphthalene in mixture (mol%)**	**H_2 in mixture (mol%)**	**Cyclohexane in mixture (mol%)**
0.5	10	10	0.2	86.1	13.7
0.5	10	20	0.4	85.9	13.7
0.5	10	40	0.8	85.6	13.6
0.5	10	60	1.2	85.2	13.6
0.5	10	80	1.6	84.9	13.5
0.5	10	100	2.0	84.5	13.5

The naphthalene in cyclohexane feed flow rate was constant at 0.5 mL/min and the hydrogen feed flow rate was constant at 10 mL/min. All reactions were carried out at a temperature of 300 ℃ and pressure of 80 bar and were performed in the SC phase.

As the concentration of naphthalene in the feed was increased, from 10 to 100g/L, the percentage mole of naphthalene in the system increased from 0.2 mol% to 2 mol%. However, the change in the concentration of naphthalene was not sufficiently large to cause a substantial change to the critical point and the reaction mixture remains in the SC phase. The HYSYS ternary phase diagram in Figure 6.15 shows the phase envelope for the system, illustrating that the reaction mixture is in the single phase region. The blue lines show the phase envelope and the red lines show the tie lines. The white circles show where the system is on this ternary diagram. Due to space limitations on the plot only 3 points are shown. These points are 10g/L, 60g/L and 100g/L respectively.

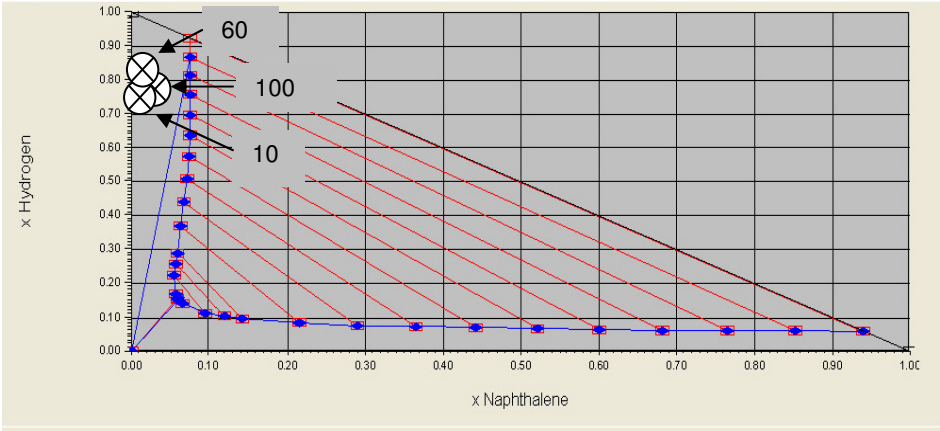

Figure 6.15. HYSYS binary plot from ternary system at different naphthalene concentrations.

Figure 6.16 shows conversion against time on stream for naphthalene feed concentrations of 10, 40, 80 and 100 g/L. For the purposes of clarity in observing the trends in data, the reactions at 20 and 60 g/L have not been included in Figure 6.16 as they are very similar to the reaction run at 40 g/L.

However, they have been included in the discussion and shown separately in Appendix 8.8.

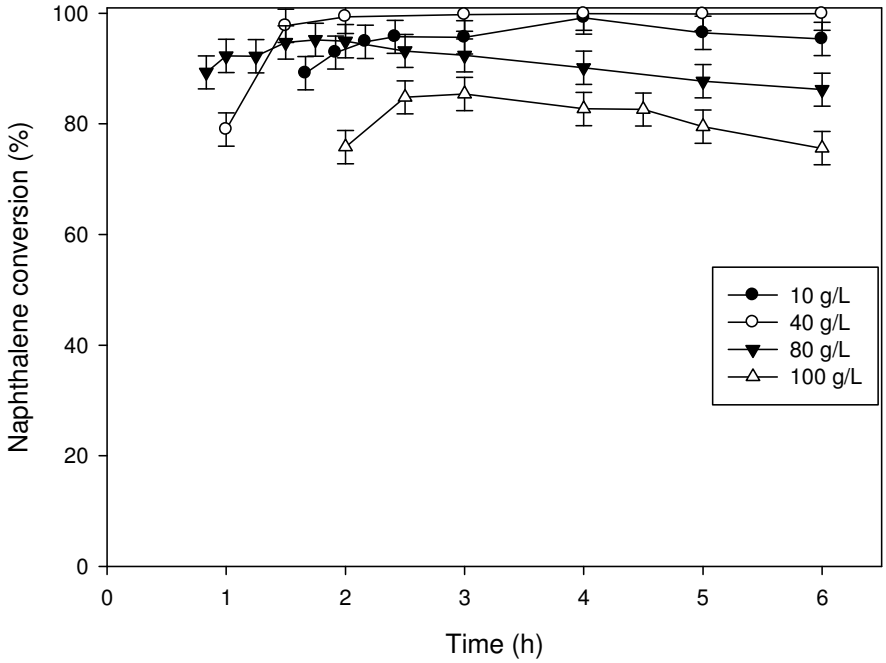

Figure 6.16. Naphthalene conversion against time on stream at 10, 40, 80 and 100 g/L naphthalene feed concentration.

Figure 6.16 shows that all reaction runs show a catalyst start up effect where the conversion at 1 hour on stream is lower than the conversion at 2 hour on stream due to the time required for the diffusion of reactants into the catalyst pores. Figure 6.16 shows that the reaction at 10 g/L of naphthalene feed concentration stabilised after 2 hours on stream and the conversion was constant at 95%. At the conditions of 20, 40 and 60 g/L the conversion stabilised after 2 hours on stream and was constant at 98% up to 6 hours on stream. The reaction at 80 g/L started at 95% and decreased to 87% at 6 hours on stream. The reaction at 100 g/L took longer to stabilise, 2.5 hour on stream, after which the conversion dropped from 85% to 75% between 2.5 and 6 hours

on stream. Overall, only the reactions at the higher naphthalene feed concentrations of 80 and 100 g/L show a slight deactivation after 6 hours on stream.

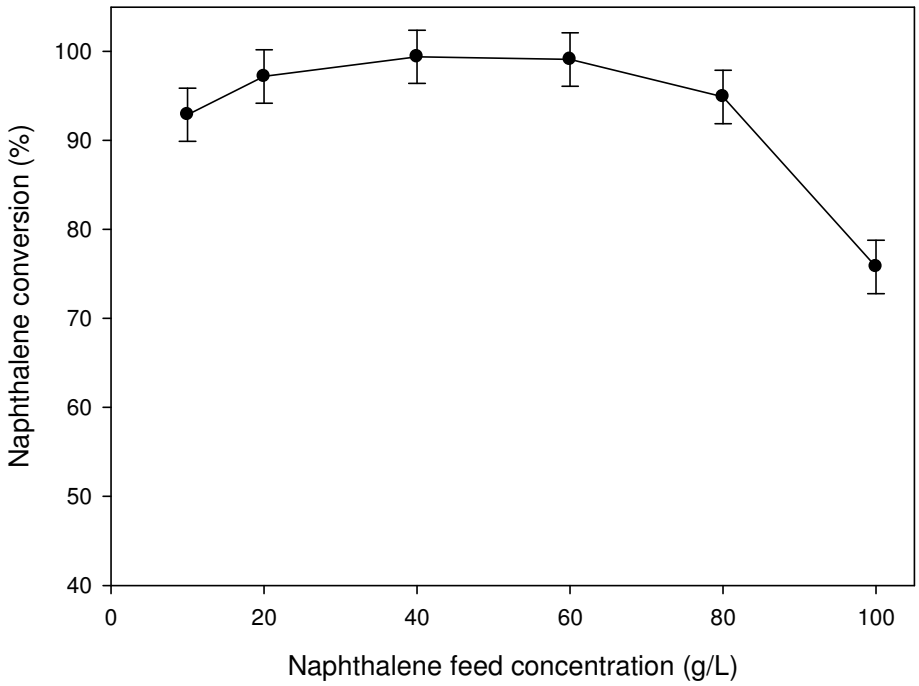

Figure 6.17. Naphthalene conversion against concentration at 10, 20, 40, 60, 80 and 100 g/L feed concentration at 2 hours on stream.

Figure 6.17 shows conversion against naphthalene feed concentrations of 10, 20, 40, 60, 80 and 100 g/L. As the concentration of naphthalene in the feed increases from 10 g/L (0.2 mol%) to 60 g/L (1.2 mol%), the conversion increases slightly and reaches nearly 100% at 40 g/L (0.8 mol%). At concentrations above 60 g/L the conversion drops with further increase in naphthalene feed concentration. Thus, increasing the naphthalene concentration in the feed causes an increase in conversion up to an optimum point in the range of 40 – 60 g/L; after this the increase in naphthalene

concentration in the feed results in a decrease in conversion. In comparison, Appleby *et al.* (1962) reported that naphthalene adsorbs strongly on the catalyst surface and reacts further to form coke. Thus the higher the concentration of naphthalene in the feed the more coke deposits on the catalyst and hence the higher the deactivation effect. This is supported by TGA results, which show a 54% increase in coke deposit from 5.4 to 11.5 wt% at 10 and 100 g/L, respectively. Hence there is a trade off between faster hydrogenation kinetics at higher naphthalene feed concentration versus increased coking that also occurs at high concentration. The optimum point is between 40 – 60 g/L naphthalene feed concentration as is shown in Figure 6.17.

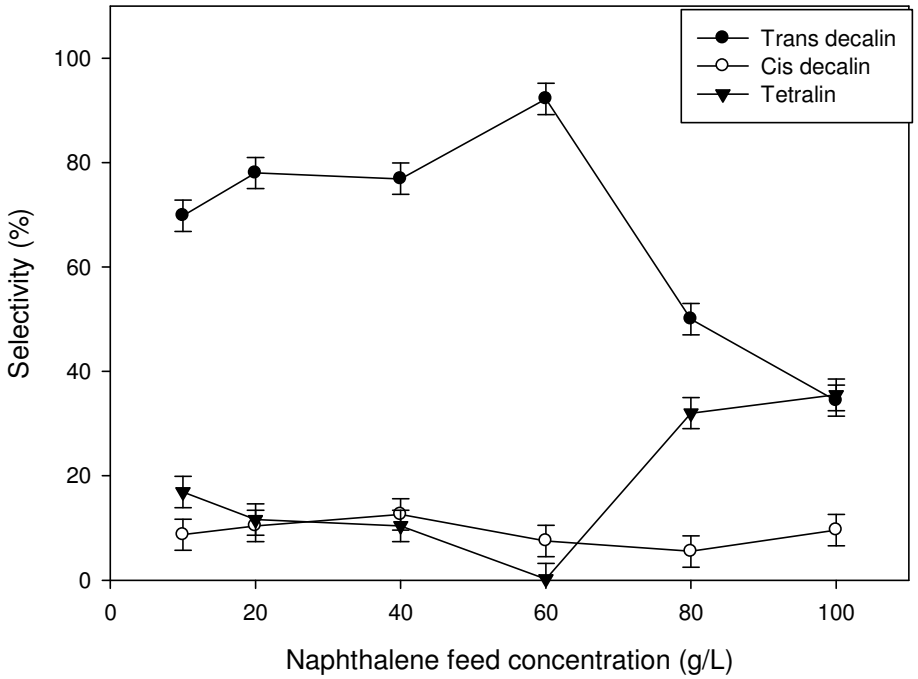

Figure 6.18. Product selectivity against naphthalene feed concentration at 6 hours on stream.

Figure 6.18 shows the product selectivity at 6 hours on stream for naphthalene feed concentrations of 10, 20, 40, 60, 80 and 100 g/L at 300 ℃ and 80 bar, indicating that the main product with 10 g/L to 80 g/L of naphthalene feed concentration is trans-decalin. The product selectivity for trans-decalin increases from 70% at 10 g/L to 90% at 60 g/L of naphthalene feed concentration. The selectivity to tetralin decreases to nearly 0% at 60 g/L naphthalene feed concentration where most products are trans and cis-decalin. After 60 g/L and as the concentration of naphthalene in the feed increases, the product selectivity starts to shift from trans-decalin to tetralin. At 80 g/L naphthalene feed concentration, trans-decalin decreases to 50% and tetralin selectivity increases to 32%. Trans-decalin selectivity drops further to 34% at higher naphthalene feed concentrations of 100 g/L whereas tetralin selectivity increases slightly to 35%. The selectivity to cis-decalin remains in the narrow range of 9 - 13% at the different naphthalene feed concentrations.

The shift of the product selectivity towards tetralin at the higher naphthalene feed concentration can be due to the effect of coking. As explained earlier coking affects the product distribution and results in an increase in tetralin formation compared to decalins. Weitkamp (1968) reported that the formation of cis-decalin does not depend greatly on reaction conditions but rather on the type of catalyst selected. Figure 6.18 shows that changing the naphthalene feed concentration does not affect the amount of cis-decalin formed greatly.

6.6. Catalyst deactivation (long term behaviour)

Experiments with longer time on stream were conducted to see the deactivation trend of the NiMo catalyst over longer periods of time. The feed composition is summarised in Table 6.7. Figures 6.2 and 6.6 showed that the catalyst is very resistant to deactivation by coking. To achieve a deactivation trend within reasonable time the feed flow rate was increased from 0.5 to 1.5 mL/min which increased the WHSV from 0.29 to 2.6 h^{-1}. The naphthalene concentration was increased to 100 g/L. Hydrogen was still in large excess of nearly three times the stoichiometric ratio (i.e. H_2/naphthalene of 5:1 mol/mol). The reaction was conducted in the SC region as is shown in the ternary phase diagram in Figure 6.19.

Table 6.7. Reaction mixture feed concentration for long term deactivation behaviour during naphthalene hydrogenation.

Naphthalene in cyclohexane feed flow rate (mL/min)	**H_2 feed flow rate (mL/min)**	**Naphthalene in feed (g/L)**	**Naphthalene in mixture (mol%)**	**H_2 in mixture (mol%)**	**Cyclohexane in mixture (mol%)**
1.5	10	100	4.6	64.5	30.9

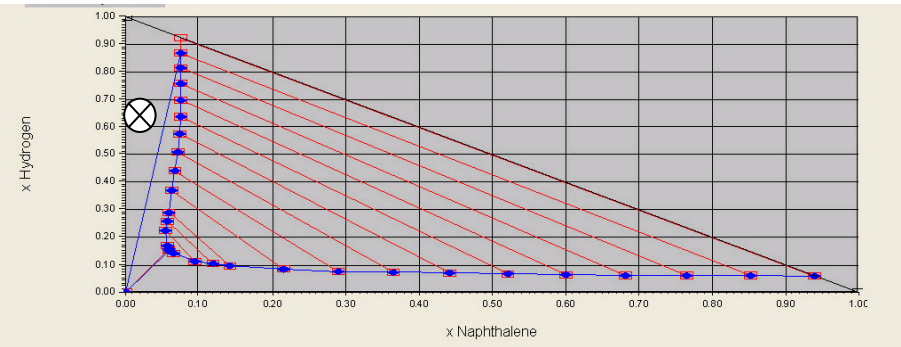

Figure 6.19. HYSYS binary plot from ternary system for longer times on stream reaction.

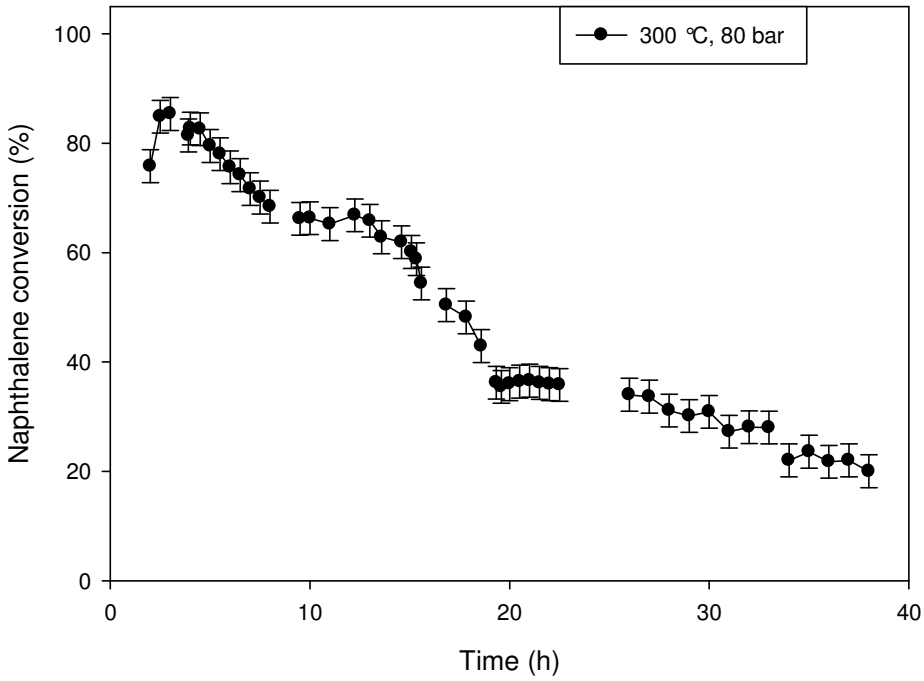

Figure 6.20. Naphthalene conversion against time at 300 ℃ and 80 bar for 38 hours on stream.

Figure 6.20 shows the conversion against time at 300 ℃ and 80 bar for 38 hours on stream. Figure 6.20 shows that in the first 8 hours the conversion decreased by ~17% from 84% to 70%. Subsequently between 10 and 19 hours the conversion decreased from 70% to 35%. After 19 hours on stream the conversion decreased gradually to 21% at 38 hours on stream.

In hydro-processing the activity of the catalyst decreases rapidly in the first few hours of operation which is then followed by a slower decrease in activity (Absi-Halabi and Stanislaus, 1991). It is reported that the initial rapid deactivation is associated with significant loss in surface area as large amounts of coke deposits (Thakur and Thomas, 1984). Much of the coke depositing in this initial period is located in small pores leading to a loss in micro-porosity and surface area, after this coking slows down and the activity and surface area decrease relatively slower (Absi-Halabi and Stanislaus, 1991). This is in agreement with the experimental results observed in the present study. Figure 6.20 shows that the conversion decreases rapidly in the initial few hours and becomes stable after 18 hours on stream.

Some of the coked catalyst was removed after 8 hours on stream for analysis on TGA. The WHSV was kept constant throughout the experiment. The TGA results show a coke deposit of 9.7 wt% and 22.7 wt% at 8 and 38 hours on stream, respectively. This indicates that the rate of coke deposition is higher during the first 8 hours of operation compared with the subsequent 30 hours, similar to the findings reported by Thakur and Thomas (1984).

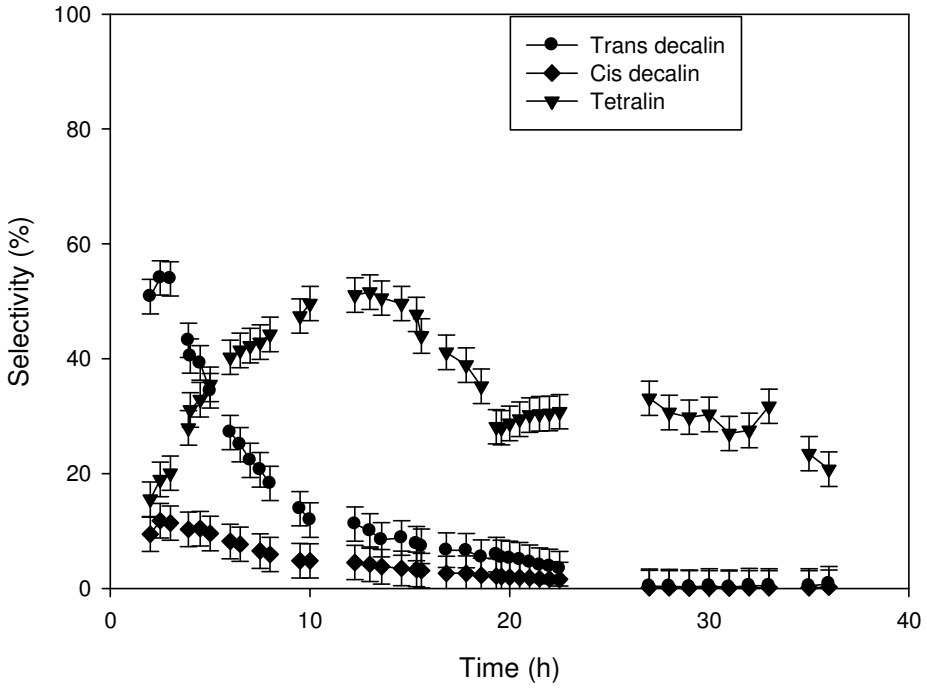

Figure 6.21. Product distribution at 300 ℃, 80 bar for 38 hours on stream.

Figure 6.21 shows the product distribution at 300 ℃ and 80 bar for 38 hours on stream, which changes from the fully hydrogenated product, trans-decalin, to the partially hydrogenated product, tetralin, over time on stream. In the initial 2 hours on stream, trans-decalin is the major product with selectivities between 50 – 55%. Over the same period of operation, the selectivity to tetralin and cis-decalin are between 15 – 20% and 9 – 11% respectively. After 5 hours on stream, tetralin becomes the main reaction product. At 10 hours on stream trans-decalin selectivity decreased to 12% and tetralin selectivity is 50%. The selectivity to tetralin starts to decrease after 12 hours on stream and the decalin selectivity decreases slightly further down. At 38 hours on stream the product

selectivity is ~0.8%, ~0.2% and ~20% for trans-decalin, cis-decalin and tetralin, respectively.

As reported earlier in section 6.3, the hydrogenation from tetralin to cis and trans decalins is much more affected by coking and deactivation compared to the hydrogenation from naphthalene to tetralin. This explains the shift from trans-decalin to tetralin as the major product with time on stream as more coke deposits on the catalyst surface in the longer run experiments, thus suppressing the further hydrogenation of tetralin to decalin.

6.7. Reaction kinetics

As discussed in Chapter 2 (section 2.7.3), researchers in literature described the reaction as a sequential one via tetralin to cis and trans-decalin. Several researchers have published materials on the reaction mechanism of naphthalene hydrogenation. In this thesis a pseudo first order model, which is a simplification of the Zhan and Guin (1994) model, is assumed.

In the present work, the power-law rate model in Equation 6.2 is used. This is the same as Equation 2.25 in Chapter 2 (section 2.7.3).

$$r = kC_N C_H \tag{6.2}$$

Where r is rate of reaction, k is rate constant, C_N is the concentration of naphthalene and C_H is the concentration of H_2.

The kinetic data was fitted to the experimental data by a numerical integration of the following Equation 6.3.

$$V_{bed} = F_{A0} \int_0^{X_A} \frac{dX_A}{-r_{Abed}} \quad (6.3)$$

Where F_{A0} is the molar flow rate at the entry and X_A is the conversion.

$$-r_{Abed} = \left(-r_{ref}\right)(1 - \varepsilon_b) \quad (6.4)$$

Where ε_b is the bed voidage.

The rate equation was integrated according to Equation 6.3 to calculate the bed volume, using Simpson's rule with 10 strips. The solver feature of MS Excel was then used to adjust the rate constant to the required value to make the calculated bed volume match the actual bed volume. The value of r_{ref} was determined from Equation 6.2 with upper and lower limits of conversion taken from the experimental results. The fitted values of the kinetic constants are in Table 6.8. As the temperature is increased the rate constant *k* increases from 10.2 to 23.1 s^{-1}, which is to be expected from the Arrhenius law dependence.

Table 6.8. Reaction rate constants, *k*, at 250, 270, 280 and 300 ℃.

Reaction conditions	**Rate constants, k (s^{-1})**
250 ℃, 80 bar	10.2
270 ℃, 80 bar	14.4
280 ℃, 80 bar	15.9
300 ℃, 80 bar	23.1

The rate constants were evaluated for the four different temperatures and from these values an Arrhenius plot was constructed in Figure 6.22, in order to determine the activation energy of the reaction. The apparent activation energy calculated from Figure 6.22 is 40.0 kJ/mol. In comparison, Zhan and Guin (1994) reported an activation energy of 40.2 kJ/mol for naphthalene hydrogenation on NiMo/Al_2O_3 catalyst. Sekine *et al.* (2008) reported activation energies of 56 and 45 KJ/mol for Pd/Al_2O_3 and Ni/SiO_2-Al_2O_3 catalysts, respectively. Sekine *et al.* (2008) also reported values between 46 – 65 kJ/mol for platinum supported on H-Y zeolite and values between 95 – 115 kJ/mol for naphthalene hydrogenation on platinum supported on $SiO_2Al_2O_3$ catalysts (Romero *et al.*, 2008). These values are much higher than the activation energy calculated in this work. It has been suggested that an activation energy larger than 25 kJ/mol may imply that the operation is in a reaction controlled region (Romero *et al.*, 2008).

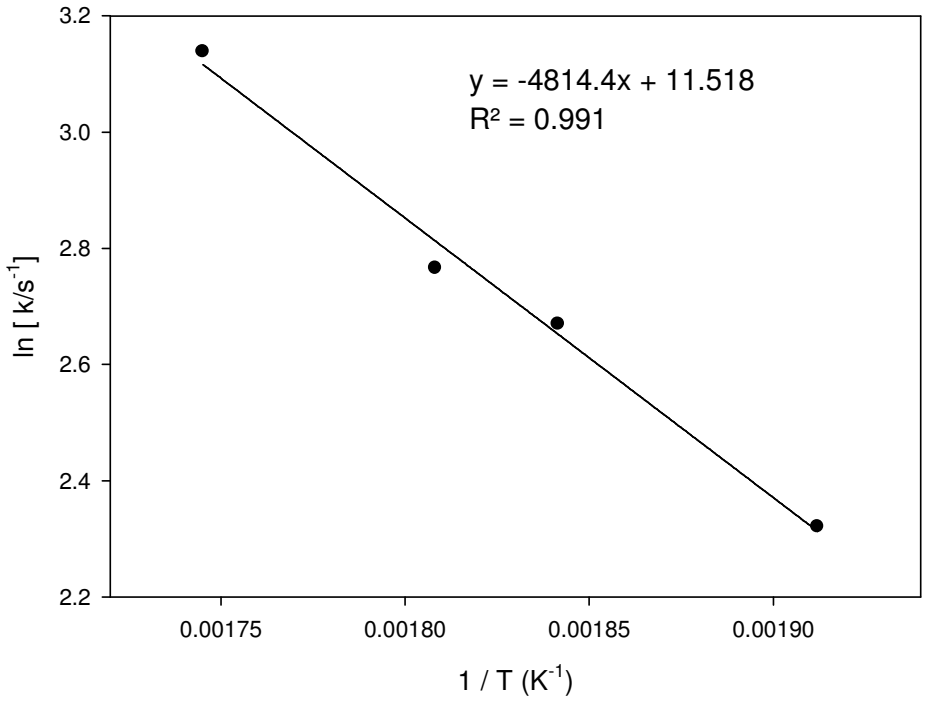

Figure 6.22. Arrhenius plot.

6.8. Catalyst characterisation

The fresh and used catalysts were analysed and characterised using techniques similar to previous characterisation of catalyst in Chapters 4 and 5. TGA analysis was used to determine the amount of coke deposited on the catalyst surface where the weight change in the catalyst during oxidation was measured. The nitrogen adsorption-desorption analysis was used to measure the specific surface area, pore size distribution and pore volume of the fresh and used catalyst.

For the nitrogen adsorption experiments, the calculated BET surface area's are mean values of different samples taken from the same batch of pellets and of repetitions carried out under the same reaction conditions.

DRIFTS were used to investigate the nature of the active species and nature of coke deposits on the catalyst. XRD was used to study the crystalline phase of the catalyst and how that was influenced by coke deposits. The findings of the catalyst characterisations are discussed in this section.

6.8.1. Effect of temperature and pressure on coke deposition

TGA was used to determine the amount of coke deposited on the catalyst. It was carried out in air and the weight loss between 200 – 1000 ℃ was considered to be due to the removal of coke deposits and used to calculate the amount of coke formed on every sample. Figure 6.23 shows typical TGA and DTG curves. There are three exothermic peaks in the DTG curve corresponding to three steps in the TGA curve. The peak around 100 ℃ corresponds to the loss of water, while the two other peaks at 630 and 800 ℃ correspond to the removal of coke from the used catalyst. Peaks above 330 ℃ correspond to the deposit of hard coke on the catalyst surface (Sahoo *et al.*, 2004). All DTG and TGA curves of coked catalysts show similar peaks with different heights.

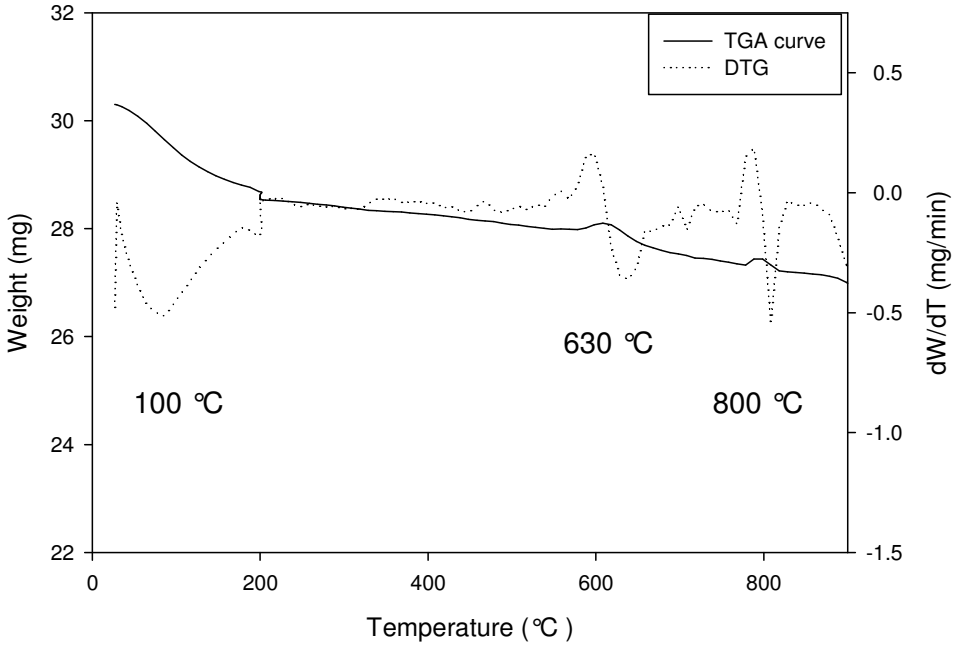

Figure 6.23. Typical TGA and DTG profile of coked catalysts. The weight loss is in three stages based on the DTG profile; a) Room temperature – 200 ℃; b) 200 – 650 ℃; c) 650 – 800 ℃.

Sahoo *et al*. (2004) studied coke deposition during hydrocracking of crude oil on H-Y, CoMo/γAl_2O_3 and NiMo/γAl_2O_3 catalyst at a temperature of 370 ℃, and pressure ranging between 70 and 170 bar for 150 hours on stream. The authors reported a coke deposit of 10 wt% on H-Y catalyst at conditions of 370 ℃ and 170 bar, 5.5 wt% deposit on CoMo/γAl_2O_3 and 5 wt% deposit on NiMo/γAl_2O_3 at conditions of 370 ℃ and 70 bar. The catalyst coke deposits were characterised using TGA and the coked samples showed three distinct temperature regions; region 1 at temperature below 180 ℃, region 2 at temperatures between 180 – 330 ℃ and region 3 at temperatures between 330 – 750 ℃. The authors ascribed region 1 to the loss of water and volatile species, regions 2 and 3 to desorption of coke. The coke desorbed in region 2 is more mobile

carbonaceous deposits (soft coke) whereas in region 3 the coke is more bulky and highly condensed (hard coke). Soft coke is made up of oxygenated polyaromatic hydrocarbons which form below operating temperatures of 250 ℃ and accumulate in the pores of the catalyst and on the external surface (Sahoo *et al,*. 2001). Hard coke is made up of less oxygenated polyaromatic compounds which form at temperature ranges between 350 ℃ – 500 ℃ (Antunes *et al.*, 2001). Figure 6.23 shows the two distinct coke temperature regions are at 630 and 800 ℃ which suggest that all coke formed in this study is hard coke.

The amount of coke deposited on the used catalyst is summarised in Table 6.9. Table 6.9 shows that as the reaction pressure is increased there is a decrease in amount of coke depositing from 7.5 wt% to 5.4 wt% at 20 and 80 bar, respectively. This is mainly due to the increased density of the mixture, from 5.7 to 22.4 kg/m^3 at 20 and 80 bar respectively, and extraction of coke precursors at higher density and pressure.

Table 6.9 also shows that as the reaction temperature was increased, the amount of coke depositing increased slightly from 4.8 wt% to 5.4 wt% at 250 and 300 ℃ respectively. This is to be expected as higher temperatures favour side reactions that lead to coke formation (Abbot *et al.*, 1985). Guisnet *et al.* (1997) have also reported that an increase in operating temperature results in an increase in coke deposition due to the formation of side products via side reactions.

Table 6.9. Catalyst wt% coke deposition at different conditions during naphthalene hydrogenation for 6 hours on stream.

Reaction conditions	**Coke content (wt%)**
Fresh	0
20 bar, 300 ℃	7.5 ± 0.05
50 bar, 300 ℃	7.1 ± 0.05
60 bar, 300 ℃	5.3 ± 0.05
80 bar, 300 ℃	5.4 ± 0.05
80 bar, 280 ℃	4.6 ± 0.05
80 bar, 250 ℃	4.8 ± 0.05

In both temperature and pressure runs the range of variation in coke deposition is relatively small and between 1 - 2 wt% difference between samples. This is due to the fact that NiMo/γAl_2O_3 catalyst is very resistant to coking and all reaction sets were conducted in the SC phase.

6.8.2. Effect of naphthalene hydrogenation reaction temperature and pressure upon on nitrogen adsorption-desorption isotherms for used catalysts

The different types of adsorption isotherms and hysteresis loops have been discussed in the literature review in section 2.8.1 of Chapter 2 of this thesis. The

experimental results of this system fit closely with adsorption isotherm IV which occurs on porous adsorbents possessing pores in the radius range of approximately 2 – 50 nm (Lowell and Shields, 2004). However due to the low number of data on the desorption isotherm, the shape of the hysteresis is inconclusive. Figure 6.24 shows the nitrogen adsorption isotherms for coked samples at 300 ℃ and 20, 50, 60 and 80 bar. The monolayer filling region is between $0.05 \leq P/P_o \leq 0.35$, the ankle of the isotherm occurs between $0.54 \leq P/P_o \leq 0.55$ and the isotherms reach a plateau at $P/P_o \geq 0.95$. As the pressure was increased from 20 to 80 bar the amount adsorbing in the monolayer increased, which indicates less loss of catalyst surface area.

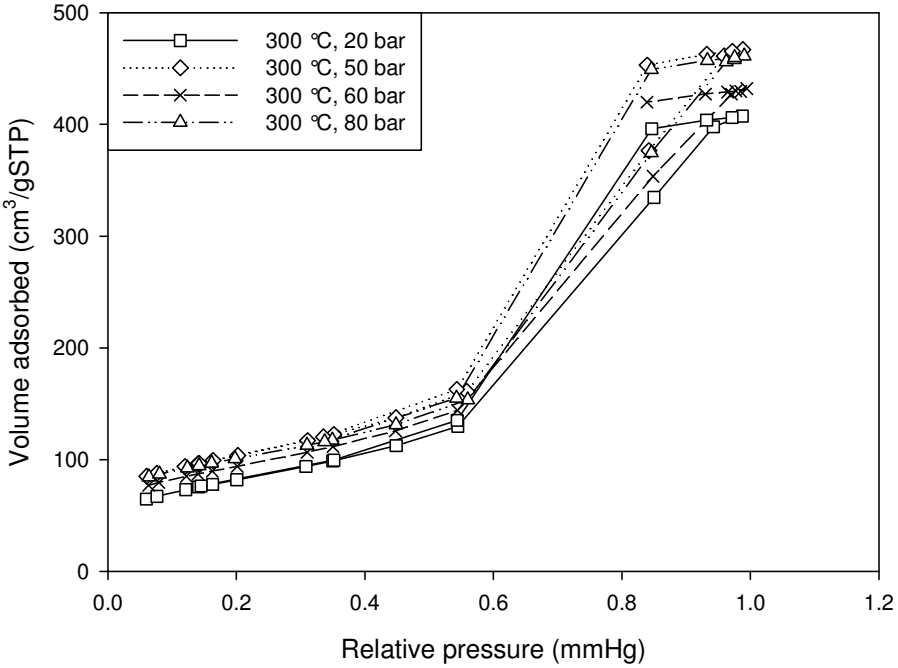

Figure 6.24. Nitrogen adsorption isotherms for catalyst coked at 20, 50, 60 and 80 bar.

All BET plots show a linear relation in the relative pressure range of 0.05 – 0.35. In some of the plots this linear relationship extends to relative pressures of 0.56. An example of a typical BET fit has been included in Appendix 8.9.

Table 6.10 shows the BET surface area, fitted relative pressure range for the BET plot, the BET coefficient and r^2 values. Table 6.10 shows that the coked samples show a loss in surface area compared to the fresh catalyst.

The surface area decreased from 396 m^2/g in the fresh catalyst to 294, 365 and 355 m^2/g in samples coked at 20, 50 and 80 bar respectively. These losses in catalyst surface area correspond to the formation of coke as is shown in the TGA results in Table 6.9, where 7.5 wt%, 7.1 wt% and 5.4 wt% coke deposits at 20, 50 and 80 bar respectively. Peña *et al.* (1996) reports the initial drop in catalyst activity during naphthalene hydrogenation is due to uniform coking and after this initial drop, coking at whiskers (filamentary carbon with a corkscrew structure) takes place, leading to a slower deactivation of the catalyst.

Table 6.10 also shows that as the temperature increases, the catalyst surface area decreases from 360, 360, 355 m^2/g at 250, 280 and 300 °C respectively. This loss of surface area is due to coke deposition and corresponds to coke deposits of 4.8 wt%, 4.6 wt% and 5.4 wt% at 250, 280 and 300 °C respectively.

Table 6.10. BET analysis on fresh and coked catalysts at varying conditions.

Reaction conditions	**BET surface area (m^2/g)**	**Fitted relative pressure range for BET plot**	**C (BET)**	**r^2**
Fresh	396 ± 0.5 m^2/g	0.06-0.2	127	0.9999
20 bar, 300 ℃	294 ± 0.6 m^2/g	0.06-0.2	144	0.9999
50 bar, 300 ℃	365 ± 1.8 m^2/g	0.06-0.2	359	0.9999
60 bar, 300 ℃	333 ± 1.3 m^2/g	0.06-0.2	276	0.9999
80 bar, 300 ℃	355 ± 1.1 m^2/g	0.06-0.2	250	0.9999
80 bar, 280 ℃	360 ± 1.9 m^2/g	0.05-0.2	505	0.9999
80 bar, 250 ℃	360 ± 1.0 m^2/g	0.05-0.2	212	0.9999

The experimental hysteresis loops, in Figure 6.24, resemble type A (see Chapter 2, section 2.8.1). However, due to the low number of data-points on the desorption isotherm this is inconclusive.

6.8.3. Effect of sub versus supercritical reaction conditions upon coke deposition

Table 6.11 shows the coke deposits at super and subcritical conditions. The results show that the coke deposit decreased by 38% from 15.5 wt% at subcritical (gas-phase) conditions of 300 ℃ and 60 bar to 9.6 wt% at supercritical conditions of 300 ℃ and 90 bar. Table 6.11 also shows that coke deposition decreased by 43% from 16.9 wt% at subcritical (gas-liquid phase) conditions of 260 ℃ and 90 bar to 9.6 wt% at supercritical conditions of 300 ℃ and 90 bar. This suggests that coke precursors have been solubilised and removed by operating in supercritical conditions. In comparison, Saim and Subramaniam (1991) reported a decrease by 33% in coke deposits as the reaction conditions were changed from sub to supercritical. This was attributed to the higher solvating powers in SCFs which helped solubilise and remove coke deposits.

Table 6.11 also shows the surface area for the fresh catalyst and samples coked at temperatures of 260 and 300 ℃ and pressure of 60 and 90 bar. The results in Table 6.11 show that the catalyst coked at subcritical conditions has lost more surface area compared to the catalyst sample coked at supercritical conditions. The catalyst surface area decreased by 13% from 364 m^2/g at supercritical conditions (300 ℃ and 90 bar) to 319 m^2/g at subcritical conditions (300 ℃ and 60 bar). The surface area was lowest at 315 m^2/g at conditions of 260 ℃ and 90 bar which corresponds to the highest weight percent of coke deposits at 16.9%.

Table 6.11. TGA results and BET surface area at sub and supercritical conditions.

Reaction conditions	**wt% coke deposit**	**Surface area (m^2/g)**	**Fitted relative range for BET plot**	**C (BET)**	**r^2**
Fresh	0	396 ± 0.5 m^2/g	0.06-0.2	127	0.9999
300 ℃, 60 bar (Gas-phase)	15.5 ± 0.05	319 ± 1.3 m^2/g	0.06-0.2	262	0.9999
300 ℃, 90 bar (supercritical)	9.6 ± 0.05	364 ± 2.2 m^2/g	0.05-0.2	240	0.9999
260 ℃, 90 bar (Gas-liquid phase)	16.9 ± 0.05	315 ± 1.7 m^2/g	0.06-0.2	290	0.9999

6.8.4. Coke deposition and nitrogen adsorption-desorption isotherms at different naphthalene feed concentrations

Table 6.12 shows that as the naphthalene concentration in the feed increased, the wt% coke deposit also increased. The coke deposit increased from 5.4 wt% at 10 g/L naphthalene feed concentration to 11.5 wt% at 100 g/L naphthalene feed concentration.

Table 6.12. BET surface area and coke content on catalysts coked at different naphthalene feed concentration.

Reaction conditions	**Surface area (m^2/g)**	**Fitted relative pressure range for BET plot**	**C (BET)**	**r^2**	**Coke content (wt%)**
Fresh	396.± 0.5 m^2/g	0.06-0.2	127	0.9999	0
10 g/L (0.2 mol%)	355 ± 1.1 m^2/g	0.06-0.2	250	0.9999	5.4 ± 0.05
20 g/L (0.4 mol%)	311 ± 1.4 m^2/g	0.06-0.2	350	0.9999	4.7 ± 0.05
40 g/L (0.8 mol%)	310 ± 1.2 m^2/g	0.06-0.2	270	0.9999	6.3 ± 0.05
60 g/L (1.2 mol%)	309 ± 1.4 m^2/g	0.06-0.2	330	0.9999	6.9 ± 0.05
80 g/L (1.6 mol%)	296 ± 2.0 m^2/g	0.06-0.2	340	0.999	10.7 ± 0.05
100 g/L (2 mol%)	302 ± 1.6 m^2/g	0.06-0.2	320	0.9999	11.5 ± 0.05

Figure 6.25 shows the nitrogen adsorption isotherms for coked samples at different naphthalene feed concentrations ranging from 10 to 80 g/L. The adsorption isotherms are similar in shape to the ones in the previous Figure 6.24. The least amount of nitrogen is adsorbed at 80 g/L naphthalene concentration which corresponds to 10.7 wt% of coke deposit. The nitrogen adsorption isotherms at 20, 40 and 60 g/L naphthalene concentrations are nearly identical. This corresponds to similar amounts of coke being deposited at those conditions varying from 4.7 – 6.9 wt%. As the naphthalene concentration

in the feed increases to 100 g/L, the coke deposit increases to 11.5 wt%. These results indicate that at higher concentrations of naphthalene more coke deposits and hence more of the catalyst surface area is lost. Similarly, Appleby *et al.* (1961) reported that the coke deposit is expected to increase with increasing naphthalene concentration in the feed as naphthalene adsorbs onto the catalyst surface and readily undergoes a protonation to form positive ionic species which continue the coking reaction. The authors also reported that two naphthalene molecules couple (dimerise) and further polymerise to form coke which deposits onto the catalyst surface.

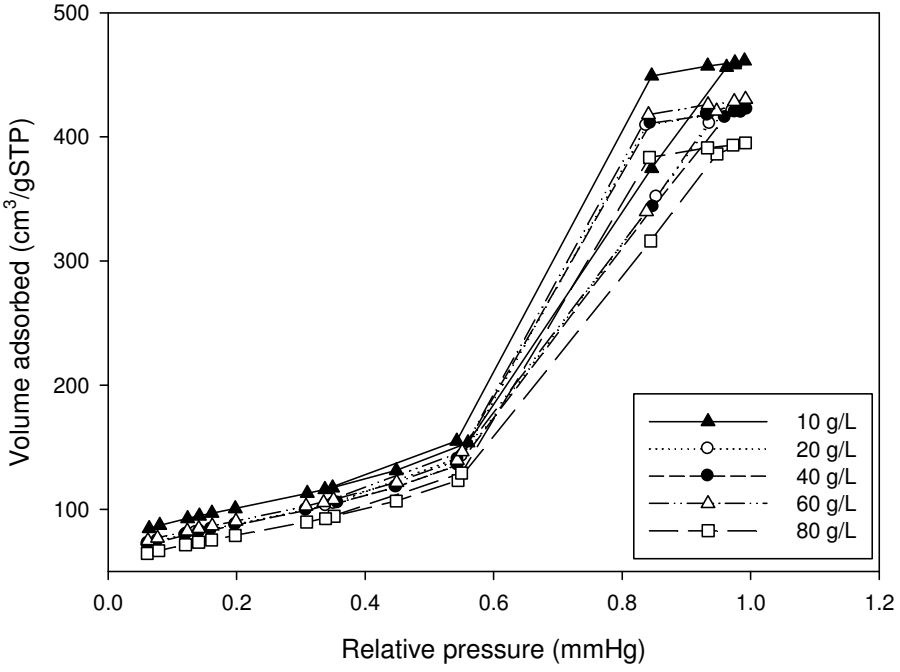

Figure 6.25. Nitrogen adsorption-desorption cycle at 10, 20, 40, 60 and 80 g/L naphthalene feed concentration.

6.8.5. DRIFTS

Figure 6.26 shows the DRIFTS spectra for the fresh catalyst and two coked samples, at 300 ℃; 60 and 80 bar. Figure 6.26a shows the whole spectrum from 500 to 4000 cm^{-1}, while Figure 6.26b shows more detail of the spectra between 2900 and 3000 cm^{-1}. All DRIFTS spectra for the catalysts coked at different reaction conditions show peaks at similar wave numbers hence only one spectrum is illustrated to represent all the other spectra for the purposes of clarity.

Figure 6.26a shows a broad band between 3500 – 3100 cm^{-1}, a very small band appears in the coked samples between 3000 – 2900 cm^{-1}. Other bands are also observed at 1750 – 1560 cm^{-1} and various bands are observed below 1200 cm^{-1}.

a)

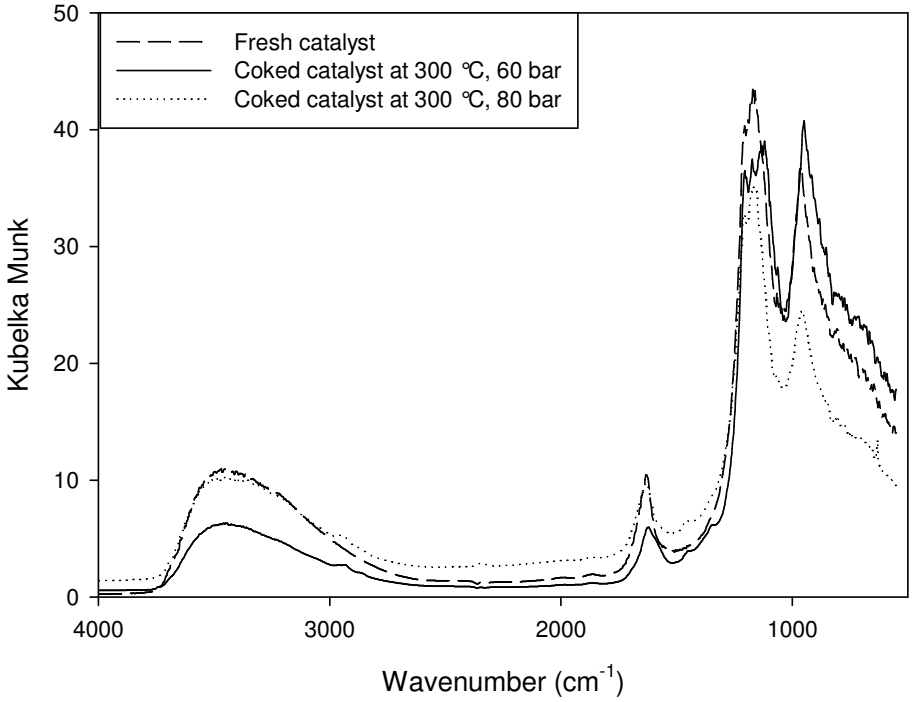

b)

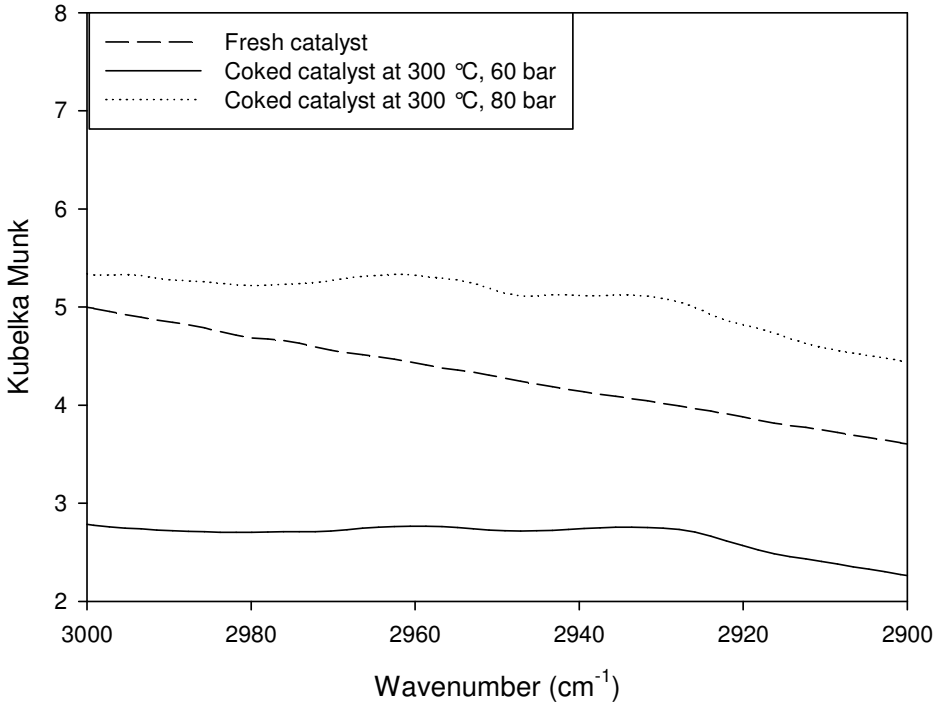

Figure 6.26 DRIFTS spectra for fresh catalyst and two coke samples at 300 ℃, 80 bar and 60 bar. a) Whole spectrum from 4000 – 500 cm^{-1}; b) Spectrum between 3000 – 2900 cm^{-1}.

The broad peak observed between 3500 to 3100 cm^{-1} is consistent with the OH group of the Al_2O_3 catalyst support carrier as well as the O-H valence vibrations of absorbed moisture (Marafi *et al.*, 2007). There is a significant decrease in the intensity of the peak for the coked catalysts, which suggests that coke deposition has an effect on the hydroxyl group. Others have also reported similar observations (Matsushita *et al.*, 2004).

The sharp peak observed at 1750 – 1560 cm^{-1} can be attributed to the Ni-Mo-S phase on $NiMo/Al_2O_3$ catalyst (Koizumi *et al.*, 2010). Coke deposition seems to affect the intensity of this peak.

Figure 6.26b shows the DRIFTS between 3000 – 2900 cm^{-1} in more detail, showing two weak bands are observed at 2965 and 2925 cm^{-1} in both coked samples. These bands correspond to aliphatic C-H bands of asymmetric CH_2 and CH_3 stretching and have been reported to correspond to soft coke deposits (Trombetta, 1997). These bands, in Figure 6.26b, look fairly weak compared with bands observed in the DRIFTS Figures 4.8 and 5.4 in Chapters 4 and 5 respectively. No bands corresponding to =C-H stretching (3100 - 3000 cm^{-1}) and C=C stretching (1630 - 1580 cm^{-1}) are detected (Andy, 1998), suggesting that the cokes formed during the reaction are most likely to be saturated hydrocarbon species.

6.8.6. X-ray diffraction analysis

The crystalline phases of the fresh and coked catalyst samples were analysed using powder XRD. The JCPDS library pattern is shown in Figure 8.15 in

Appendix 8.8. Figure 6.27 shows a comparison between the XRD spectra for the fresh catalyst and coked samples. For the fresh catalyst, in Figure 6.27a, the peak at 67° can be assigned to the Al_2O_3 phase. The peak at 46° can be assigned to the formation of one or more crystalline sulphided phase. It can be related to Mo_3Ni, Mo_3Ni_1 and Mo_3NiS_4 as was found on the XRD data base (JCPDS). The small peak at 32° corresponds with $NiMoO_4$ phase. The small peaks between 10° and 20° are related to $NiMoS_4$. The peak at 6° is related to nickel aluminium silicate hydrate. The coked sample in Figure 6.27a shows that the coked sample retains all the peaks observed in the fresh catalyst without any change. This suggests that coking does not affect the crystalline phase of the catalyst in a significant way. This is further confirmed by comparing the fresh catalyst with other samples coked at 50, 60 and 80 bar (Figure 6.27b). XRD analysis was conducted on all the coked samples and the patterns show the same result. The temperature does not affect the crystalline phase, which is to be expected as Peña *et al.* (1996) observed that the XRD results for the fresh and aged catalyst were the same on Ni/NiAl2O4 catalyst during the hydrogenation of acetylene to ethylene and ethane at reaction temperatures between 150 and 220 ℃.

a)

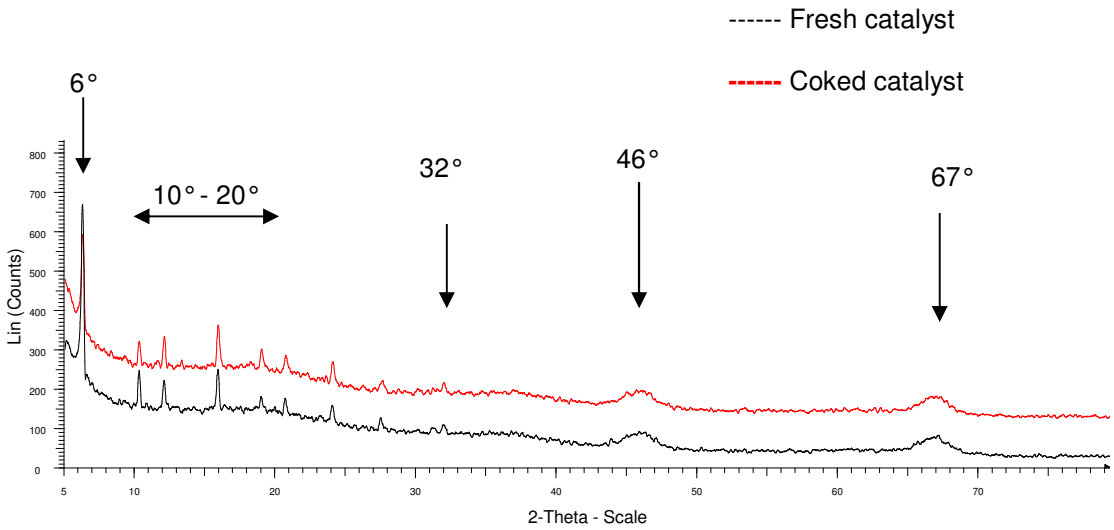

b)

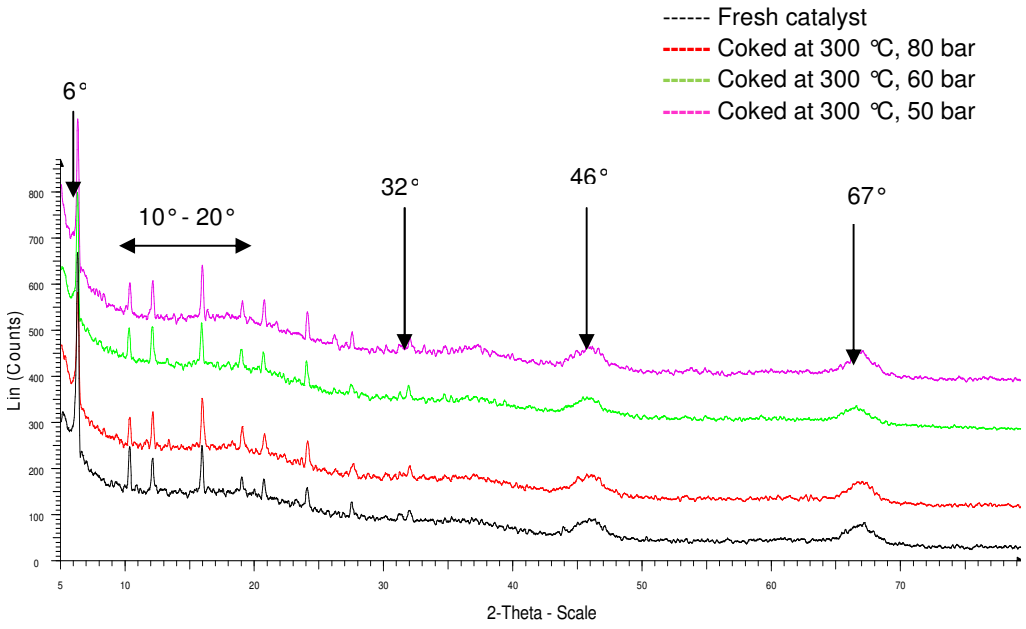

Figure 6.27. XRD analysis of fresh catalyst and coked samples. a) Fresh catalyst and coked sample at 300 ℃ and 80 bar; b) Fresh catalyst and coked samples at 300 ℃, 50, 60, and 80 bar.

6.9. Catalyst re-activation using SC CO_2

The effect of SC CO_2 solvent in re-activating the coked catalyst and ex situ removal of coke on the catalytic activity, catalyst structure and coke deposition was studied. Table 6.13 and Figure 6.28 show the feed composition and the ternary phase diagram for this reaction mixture, respectively.

Table 6.13. Reaction feed composition during the coking of the catalyst prior to re-activation with SC CO_2.

Naphthalene in cyclohexane feed flow rate (mL/min)	H_2 feed flow rate (mL/min)	Naphthalene in feed (g/L)	Naphthalene in mixture (mol%)	H_2 in mixture (mol%)	Cyclohexane in mixture (mol%)
1.5	10	100	4.6	64.5	30.9

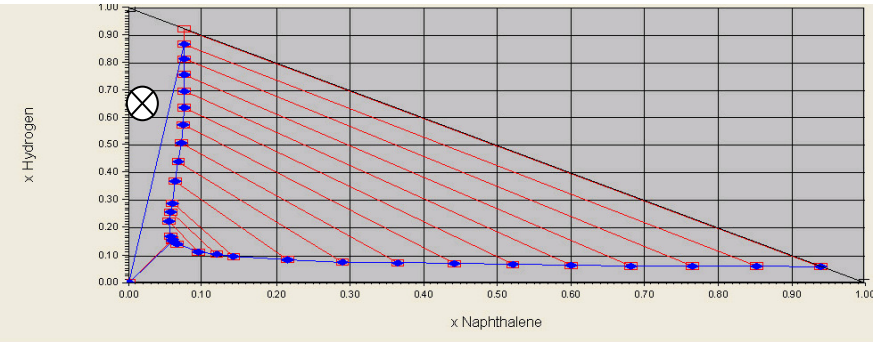

Figure 6.28. HYSYS binary plot from ternary system for the reaction mixture at 300 ℃, 80 bar.

Two gramme of $NiMo/Al_2O_3$ catalyst was coked during naphthalene hydrogenation, at a reaction temperature of 300 ℃ and pressure of 80 bar for 38 hours on stream. Subsequently, 0.67 gramme of the catalyst was removed to analyse by TGA and BET, whilst 1.33 gramme of the catalyst remained in the rig. SC CO_2 was pumped through the rig at a flow rate of 10 mL/min,

temperature of 60 ℃ and pressure of 80 bar for 6 hours on stream. Following that, 0.67 gramme of the catalyst was removed to analyse by TGA and nitrogen adsorption experiments, whilst 0.67 gramme of the catalyst remained in the rig. Naphthalene hydrogenation at 300 ℃ and 80 bar was carried out with the last remaining 0.67 gramme of catalyst in the rig to study whether some of the catalytic activity was restored.

Initially, SC CO_2 (T_c = 31.04 ℃ and P_c = 73.8 bar) was used as a solvent during naphthalene hydrogenation reaction to compare the effect of *in situ* coke removal to post reaction coke removal. The composition of the reactions chosen to study are summarised in Table 6.14. Naphthalene hydrogenation was carried out in three different CO_2 concentrations; 83 mol%, 34 mol% and 5 mol%. However, no liquid samples were available for the systems with 83 mol% and 34 mol% CO_2, indicating that CO_2 could have been acting as an anti-solvent (Chattopadhyay and Gupta, 2001). For the reaction system with 5 mol% CO_2, the liquid samples collected crystallised immediately after collection, as illustrated in Figure 6.29, which made it impossible to analyse any samples on the GC. The aim was to study the post reaction coke removal of SC CO_2 and a comparison with *in situ* SC CO_2 coke removal would have been ideal. However, it was decided to proceed with SC CO_2 post reaction coke removal only.

Table 6.14. Cases studied with SC CO_2.

	Case 1 (mol%)	**Case 2 (mol%)**	**Case 3 (mol%)**
Naphthalene	0.1	0.4	0.6
Cyclohexane	7.1	29.0	41.9
Hydrogen	8.9	36.3	52.5
Carbon dioxide	83.9	34.3	5.0

Figure 6.29. Crystallised sample for reaction condition of 300 ℃ and 80 bar; in case 3.

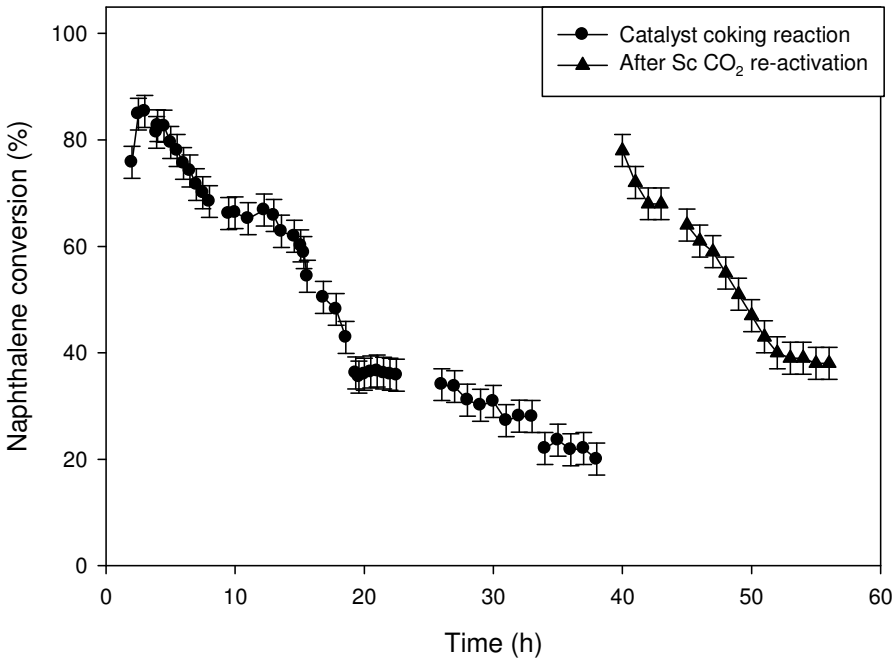

Figure 6.30. Naphthalene conversion against time at 300 ℃, 80 bar before and after re-activation with SC CO_2.

Figure 6.30 shows the conversion profile of naphthalene during hydrogenation over the fresh catalyst, followed by the used catalyst after regeneration in SC CO_2. There is an initial start up period similar to previous observations. The conversion dropped from 84% at 1.5 hours to 35% at 19 hours on stream. The conversion stabilised at 35% from 19 hours to 22.5 hours on stream. After this the activity decayed further to 21% at 38 hours on stream. The long term deactivation behaviour of the catalyst was discussed in section 6.6.

SC CO_2 was pumped through the system, at a temperature of 60 ℃ and pressure of 80 bar, to remove and extract the coke deposited on the catalyst surface. After 6 hours on stream, the CO_2 line was closed and the reaction was

repeated with the used catalyst at the same initial reaction conditions of 300 ℃ and 80 bar.

The results in Figure 6.30 show that 93% of the activity was restored after CO_2 reactivation. The conversion is increased to 78% after reactivation, which is only 6% lower than for the fresh catalyst. This is then followed by a slow decline to 38% after 16 hours on stream (56 hours from the original reaction start up time). The recovery of the catalytic activity after the post reaction SC CO_2 treatment can be attributed to effective cleaning of some of the catalyst active sites previously covered or blocked by coking.

Trabelsi *et al.* (2000) carried out the hydrogenation of 1,5,9-cyclododecatrience in a batch reactor at 160 ℃, 12 bar on a Pd/Al_2O_3 catalyst. They reported that after SC CO_2 coke extraction, the used catalyst showed similar activity as the fresh catalyst after which it loses this to reach the values of the used catalyst prior to re-activation. They attributed this to the effective cleaning of a number of palladium active sites and the modification of some of the remaining hard coke caused by the solvent nature of SCFs. This is in agreement with the experimental results reported here which show a very high recovery of catalytic activity after SC CO_2 extraction (Figure 6.30), after which this drops back to reach similar conversions as pre-activation.

Figure 6.39 shows that the product selectivity shifts from trans-decalin after 5 hours on stream to tetralin. The reasons for this have been discussed in section 6.6. Following the catalyst reactivation using SC CO_2, the product selectivity shifts back to trans-decalin at 42% after 42 hours on stream. Trans-decalin

formation declines to 2% after 56 hours on stream. Tetralin formation is at 28% at 40 hours on stream (after the re-activation) and this increases slowly to 35% after 56 hours on stream, which makes tetralin the main reaction product. The selectivity towards cis-decalin also increases after the re-activation back to 8% after which it decreases slowly to 1% after 56 hours on stream.

Overall, during the SC CO_2 extraction, coke is removed from the catalyst surface which results in the product selectivity shifting to trans-decalin. As the reaction progresses and coke deposits on the catalyst again, the product selectivity shifts back to tetralin. This supports the suggestion that coking affects tetralin hydrogenation to decalin more than naphthalene hydrogenation to tetralin (Rautanen *et al.*, 2002).

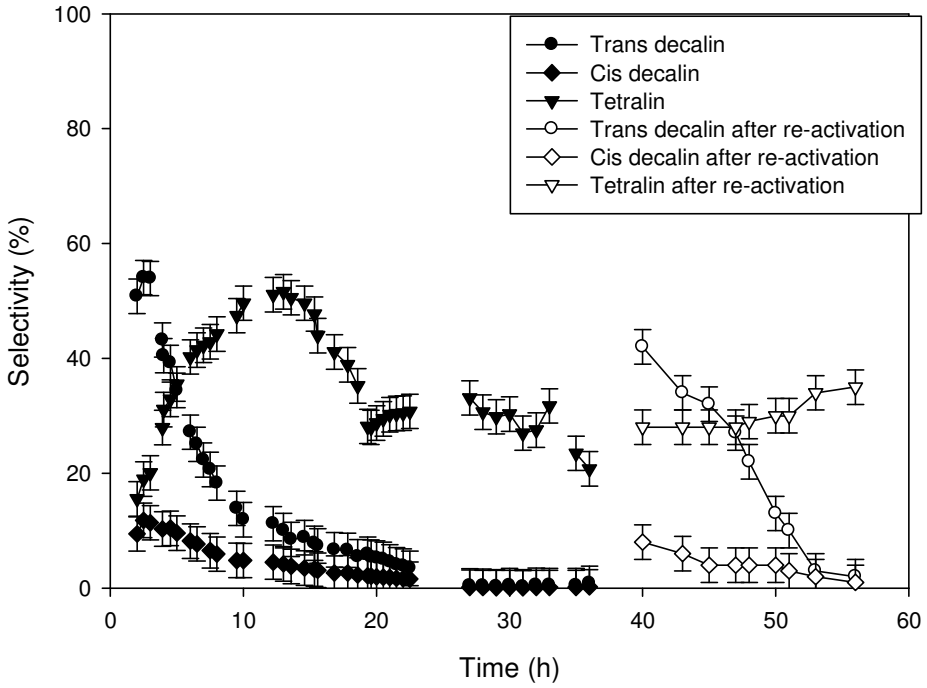

Figure 6.31. Product selectivity before and after SC CO_2 re-activation.

Table 6.15. The TGA analysis of the catalyst samples.

Wt% coke deposit after 38 hours on stream	**wt% coke deposit after SC CO_2 post reaction removal**
22.7 ± 0.05	14.3 ± 0.05

Table 6.15 shows the wt% coke deposit before and after treatment with SC CO_2. The results show that after 38 hours on stream, 22.7 wt% coke deposits on the catalyst surface. This decreases by 37% to 14.3 wt% after the post reaction coke removal by SC CO_2. This indicates that SC CO_2 does extract coke from the catalyst surface, which results in the recovery of the catalytic activity as is shown in Figure 6.30. However, some coke does still remains on the catalyst surface after the post reaction SC CO_2 treatment. This means that although SC CO_2 removes some of the coke on the catalyst, it is unable to remove hard coke, at the conditions studied. This hard coke would have had enough time to become highly oligomerised and stabilised. In comparison, Trabelsi *et al.* (2000) conducted an *ex situ* coke removal at 65 ℃ and 250 bar with pure CO_2 at a flow rate of 1 L/min for 5 hours on stream. He reported that 80 wt% of deactivating materials was removed by SC CO_2, while the remaining coke must have become highly oligomerised and stabilised.

Figure 6.40 shows the nitrogen adsorption-desorption cycle analysis which shows the fresh catalyst compared to the coked catalyst before and after re-activation by SC CO_2. A higher gas volume is adsorbed on the catalyst after re-

activation with SC CO_2 which indicates that coke was extracted from some of the pores previously blocked.

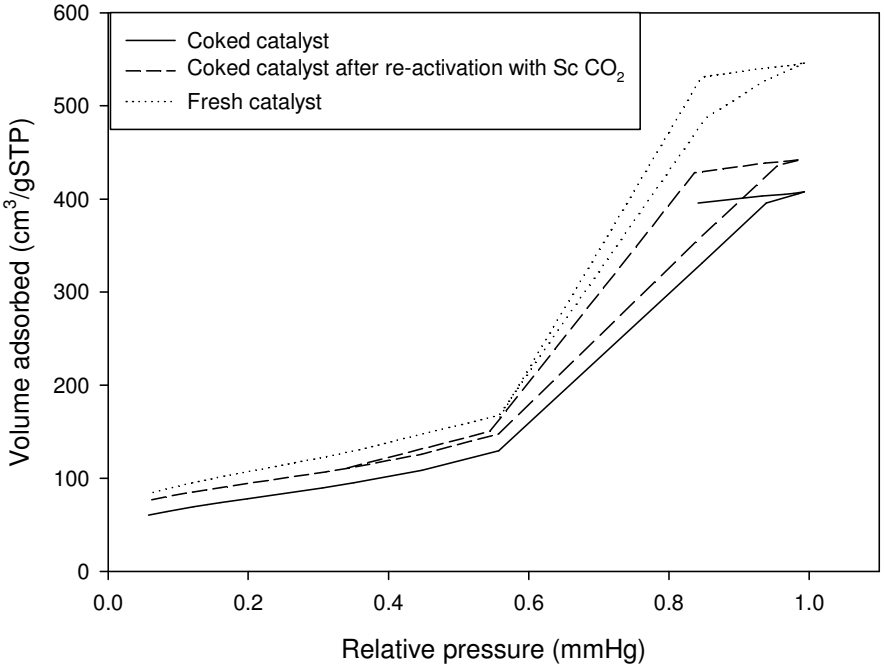

Figure 6.32. Nitrogen adsorption-desorption cycle before and after SC CO_2 removal.

6.10. Conclusions

In this Chapter, naphthalene hydrogenation on NiMo/γ-Al_2O_3 catalyst was studied. The effect of temperature, pressure, varying naphthalene feed concentration as well as operating in sub and supercritical conditions were studied.

Operating in the supercritical phase shows higher catalytic activity, slower catalyst decay (see Figures 6.10 and 6.11), 38% lower percentage coke deposits and 13% less catalyst surface area loss. Thus it can be said that SCFs

do prolong the catalyst life time by suppressing and extracting coke deposits from the catalyst surface.

In the supercritical phase the optimum temperature is in the range of 280 – 300 ℃ and the optimum pressure is around 60 bar (see Figures 6.2 and 6.6). The optimum naphthalene feed concentration is between 40 – 60 g/L and any further increase leads to faster coking.

The catalyst used is very selective towards the more stable trans-decalin product. Although cis-decalin isomerises easily in the range of temperatures chosen to study, it does not contribute very much to the formation of trans-decalin as naphthalene and tetralin adsorb more easily onto the catalyst surface and act as a poison to the isomerisation of cis-decalin.

The reaction was first order towards naphthalene and the activation energy was 40.0 kJ/mol.

NiMo/γ-Al_2O_3 is very resistant to coking with coke deposits varying from 3 – 22.7 wt%. The nitrogen adsorption desorption isotherms showed all coked catalyst lost some surface area due to coking and that coke most likely deposited into the catalyst pores. In comparison, in previous Chapters 4 and 5, ZSM5 and zeolite Y showed coke deposits between 12 – 23 wt% where most coke deposited on the external surface in ZSM5 and penetrated into the pores of zeolite Y.

SC CO_2 was used to re-activate the coked catalysts. This resulted in recovering 93% of the catalytic activity and 37% of the coke was effectively extracted by SC CO_2.

Overall, SCFs do prolong the catalyst life by suppressing coking and extracting coke from the catalyst surface.

CHAPTER 7

CONCLUSIONS AND FUTURE WORK RECOMMENDATIONS

7.1. Conclusions

During the isomerisation of 1-hexene on ZSM5, the catalyst was stable for 96 hours on stream with only a slight deactivation observed after 80 hours in the subcritical region (235 °C, 10 bar). DRIFTS results show that the coke deposited was mainly polyolefinic while TGA results show the amount of coke decreased greatly from 18.8 wt% in the subcritical region to 10 wt% in the supercritical region. This was attributed to the *in situ* removal of coke by supercritical hexane. In ZSM5, the pore mouth becomes blocked after an initial shallow pore filling over shorter contact times. Coke is mainly formed outside the zeolite crystallites and the loss in acidity is mainly due to the loss in acid sites on the alumina binder and outside surface acidity.

In zeolite Y a clear deactivation pattern was observed with the rate of deactivation being slower in supercritical conditions compared to subcritical conditions. In the subcritical run at 235 °C, 10 bar a substantial decrease in conversion during the first two hours was observed, while at supercritical conditions of 235 °C, 40 bar the deactivation rate was reduced to a more gradual level which maintains the catalyst activity for longer periods of time. TGA results showed that coke deposition in zeolite Y decreased by 3.1 wt% upon increasing the pressure from 10 bar to 40 bar, and thus moving in to the supercritical region. However in ZSM5 the equivalent decrease in coke

deposition was measured as 8.1 wt%, showing a much larger change above the critical pressure.

ZSM5 was resistant to aging due to the very small pore size (5.3 – 5.6 Å) which prevents coke molecules from penetrating and depositing inside the pores. The relatively large change in coke deposit in moving from sub to supercritical conditions was thought to result from extraction of coke from the outside surfaces of zeolite crystals within the alumina binder matrix.

Zeolite Y showed faster aging compared to ZSM5 due to the larger pore size (7.4 Å) which can accommodate coke deposits, thus making coke more difficult to remove by the SCF and leading to lower changes in coke deposit upon moving in to the supercritical region when compared with ZSM5. Most coke forms on the catalyst before two hours on stream and was shown to comprise mainly saturated hydrocarbon species. Its deposition upon the catalyst surface affects the hydroxyl groups on the zeolite, leading to reduction of the acidity of the catalyst.

In zeolite Y the strongest acid sites are deactivated first, leading to the large observed decrease in catalyst activity whilst in ZSM5 the acid site coverage is thought to occur in a more uniform way, which does not cause such a large decrease in activity.

The novel finding of this study was that SCFs are useful for improving the performance of zeolite Y through extraction of coke and coke precursors from the catalyst surface. This helps to keep the pores open to a sufficient extent for reaction conversion to be substantially improved to around double the value observed under subcritical conditions, and greatly improves the viability of using

zeolite Y for 1-hexene isomerisation. By contrast, ZSM5 does not show a strong deactivation under subcritical conditions and therefore operating under supercritical conditions has relatively little effect upon the overall conversion.

In Chapter 6, naphthalene hydrogenation on NiMo/γ-Al_2O_3 catalyst was reported. Operating in the supercritical region during naphthalene hydrogenation resulted in slower catalyst decay and 38 wt% lower coke deposits. NiMo/γ-Al_2O_3 catalyst is very selective towards trans-decalin. The product selectivity shifted towards tetralin with longer times on stream.

SC CO_2 was used to re-activate the coked catalysts and this resulted in recovering 93% of the catalytic activity and 37% of the coke was effectively extracted by SC CO_2.

7.2. Further investigations

In terms of future work recommendations, there are several aspects that need further investigations. These are listed below:

- Investigating the use of a supercritical solvent during the isomerisation of 1-hexene and its effect on conversion, coke deposition and catalyst activity. This can then be compared to the results reported in Chapters 4 and 5.
- Reactivating the zeolite catalysts with SC CO_2 and comparing with reactivation of NiMo catalyst in chapter 6.

- Using a more accurate acidity characterisation technique such that the acid sites with different strengths can be distinguished. This would allow a more accurate determination of which sites are most affected by coking.
- The effect of supercritical fluids on the reaction pathway during 1-hexene isomerisation and naphthalene hydrogenation was not studied in this work as that was beyond the scope of this research. However understanding the effect of SCFS on the reaction pathway and how it changes can greatly help in developing ways to prolong the catalyst life time by using SCFs.
- Further investigate hydrogenation reaction under supercritical fluids, in particular naphthalene hydrogenation in SC CO_2. The *in situ* coke removal by SC CO_2 was not investigated in this work and comparison between *in situ* and *ex situ* coke removal by CO_2 would be very interesting.
- The determination of solubility data over a range of conditions for SC CO_2 extraction of coke deposits for the results discussed in Chapter 6, section 6.9. This can be done by extracting coke at various conditions and comparing the results.
- A further study into the product inversion seen in Figure 6.12 to understand fully why such a dramatic step change occurs and the factors influencing this change.
- Characterising the catalyst by using SEM and TEM. It would be valuable to obtain and compare images of the coked and fresh catalyst..

REFERENCES

Abbot, J. and Wojciechowski, B.W., 1984. The nature of active sites in the isomerization of 1-hexene on cracking catalysts. *Journal of catalysis*, 90 (2), 270-278.

Abbot, J., Corma, A. and Wojciechowski, B.W., 1985. The catalytic isomerization of 1-hexene on HZSM5 zeolite: The effects of a shape-selective catalyst. *Journal of catalysis*, 92 (2), 398-408.

Absi-Halabi, M., Stanislaus, A. and Trimm, D.L., 1991. Coke formation on catalysts during the hydroprocessing of heavy oils. *Applied catalysis*, 72 (2), 193-215.

Ahn, I.Y., Lee, J.H., Kum, S.S. and Moon, S.H., 2007. Formation of C4 species in the deactivation of a Pd/SiO_2 catalyst during the selective hydrogenation of acetylene. *Catalysis today*, 123 (1-4), 151-157.

Albright, L.F. and Baker, R.T.K., eds., 1982. Coke formation on metal surfaces. *American chemical society,* 202, i-vi.

Anderson, J. R., Chang, Y. F. and Western, R.J., 1989. Retained and desorbed products from reaction of 1-hexene over H-ZSM5 zeolite: Routes to coke precursors. *Journal of catalysis*, 118 (2), 466-482.

Anderson, J.R. and Boudart, M., eds., 1984. *Catalysis, science and technology*. New York: Springer.

Andy, P., Gnep, N.S., Guisnet, M., Benazzi, E. and Travers, C., 1998. Skeletal isomerization of n-butenes, II. Composition, mode of formation, and influence of coke deposits on the reaction mechanism. *Journal of catalysis*, 173 (2), 322-332.

Antunes, A.P., Ribeiro, M.F., Silva, J.M., Ribeiro, F.R., Magnoux, P. and Guisnet, M., 2001. Catalytic oxidation of toluene over CuNaHY zeolites: Coke formation and removal. *Applied catalysis B: Environmental*, 33 (2), 149-164.

Appleby, W.G., Gibson, J.W. and Good, G.M., 1962. Coke formation in catalytic cracking. *Industrial and engineering chemistry process design and development*, 1 (2), 102-110.

Baerlocher, Ch., Meier, W.M. and Olson, D.H., 2001. *Atlas of zeolite framework types. 5th edition*. Amsterdam: Elsevier B.V.

Baiker, A., 1999. Supercritical fluids in heterogeneous catalysis. *Chemical reviews,* 99 (2), 453-473.

Baptist-Nguyen, S. and Subramaniam, B., 1992. Coking and activity of porous catalysts in supercritical reaction media. *American institute of chemical engineers journal,* 38 (7), 1027-1037.

Bartholomew, C.H., 2001. Mechanisms of catalyst deactivation. *Applied* catalysis *A*, 212 (1-2), 17-60.

Bartholomew, C.H. and Fuentes, G.A. eds., 1997. *Catalyst deactivation, proceedings of 7th international symposium on catalyst deactivation*. Amsterdam: Elsevier.

Bartholomew, C.H., 1994. Sintering kinetics of supported metals: Perspectives from a generalized power law approach. In: B. Delmon and G.F. Froment, eds., 1994. *Catalyst deactivation, proceedings of the 6th international symposium.* Ostend: Elsevier B.V. 1-18.

Bartholomew, C.H. and Butt, J.B., eds., 1991. *Catalyst deactivation*. Amsterdam: Elsevier.

Bartholomew, C.H., 1982. Carbon deposition in steam reforming and methanation. Catalysis reviews: Science and Engineering, 24 (1), 67-112.

Bartholomew, C.H., 1984. Catalyst deactivation and regeneration. *Chemical engineering journal*, 91 (23), 96**-**112.

Bautista, F.M., Delmon, B., 1995. 1-Butanol dehydration on $AlPO_4$ and modified $AlPO_4$: Catalytic behavior and deactivation. *Applied catalysis A: General*, 130 (1), 47-65.

Bellare, A., Dadyburjor, D.B., 1993. Evaluation of modes of catalyst deactivation by coking for cumene cracking over zeolites. *Journal of catalysis*, 140 (2), 510-525.

Bjorgen, M., Joensen, F., Spangsberg Holm, M., Olsbye, U., Lillerud, K.P. and Svelle, S., 2008. Methanol to gasoline over zeolite H-ZSM5: Improved catalyst performance by treatment with NaOH. *Applied catalysis A: General*, 345 (1), 43-50.

Boreskov, K.,2003. *Heterogeneous catalysis*. New York: Nova Science Publishers, Inc.

Bowker, M., 1998. *The basis and applications of heterogeneous catalysis*. Oxford: OUP Oxford.

Brand, H.V., Redondo, A. and Hay, P.J., 1997. Theoretical studies of CO adsorption on H-ZSM5 and hydrothermally treated H-ZSM5. *Journal of molecular catalysis A: Chemical*, 121 (1), 45-62.

Brennecke, J.F., Debenedetti, P.G., Eckert, C.A. and Johnston, K.P., 1990. Letters to the editors. *American institute of chemical engineers journal,* 36 (12), 1927-1928.

Broekhoff, J.C.P. and De Boer, J.H., 1968. Studies on pore systems in catalysts. *Journal of Catalysis*, 10 (4), 153-165.

Broekhoff, J.C.P. and Linsen, B.G., 1970. *Physical and chemical aspects of adsorbents and catalysts*. New York, Academic Press.

Bukur, D.B., Lang, X., Akgerman, A. and Feng, Z., 1997. Effect of process conditions on olefin selectivity during conventional and supercritical fischer–tropsch synthesis. *Industrial and engineering chemistry research*, 36 (7), 2580–2587.

Butt, J.B., Petersen E.E., 1988. *Activation, deactivation, and poisoning of catalysts*. San Diego: Academic Press.

Cerqueira, H.S., Magnoux, P., Martin, D. and Gusinet, M., 1999. Effect of contact time on the nature and location of coke during methylcyclohexane transformation over a USHY zeolite . In: B. and G.F Froment, eds., 1999.

Catalyst deactivation, proceedings of the 8th international symposium. Amsterdam: Elsevier, 105-112.

Chattopadhyay, P., Gupta, R.B., 2001. Production of antibiotic nanoparticles using supercritical CO_2 as antisolvent with enhanced mass transfer. *Industrial and engineering chemistry research*, 40 (16), 3530 – 3539.

Chevron Phillips, 2008. Safe Handling & Storage of 1-Hexene and 1-Octene Alpha Olefins. (online). Available at:http://www.cpchem.com/bl/nao/en-us/shglibrary/1-Hexene_1-Octene_2008_rev0.pdf. (Accessed 10/09/2011)

Chianelli, R.R., Daage, M. and Ledoux, M.J., 1994. Fundamental studies of transition-metal sulfide catalytic materials. In: D.D. Eley, H. Pines and W.O. Haag, eds., 1994. *Advances in catalysis.* Amsterdam: Elsevier B.V., 177-232.

Chigada, P.I., Wang, J., Al-Duri, B., Wood, J. and Rigby, S.P., 2010. Modelling of pore structure evolution during catalyst deactivation and comparison with experiment. *Chemical engineering science*, 65 (20), 5550- 5558.

Clark, M.C. and Subramaniam, B., 1999. Kinetics on a supported catalyst at supercritical, nondeactivating conditions. *American institute of chemical engineers journal,* 45 (7), 1559-1565.

Clark, M.C. and Subramaniam, B., 1998. Extended alkylate production activity during fixed-bed supercritical 1-butene/isobutane alkylation on solid acid catalysts using carbon dioxide as a diluent. *Industrial and engineering chemistry research*, 37 (4), 1243–1250.

Clark, M.C. and Subramaniam, B., 1996. 1-Hexene isomerization on a Pt/γ-Al_2O_3 catalyst: The dramatic effects of feed peroxides on catalyst activity. *Chemical engineering science*, 51 (10), 2369-2377.

Clifford, T., 1999. *Fundamentals of supercritical fluids*. New York: Oxford University Press.

Corma, A., 2003. State of the art and future challenges of zeolites as catalysts. *Journal of catalysis*, 216 (1-2), 298-312.

Dardas, Z., Süer, M.G. and Moser, W.R., 1996. High-temperature, high-pressure *in situ* reaction monitoring of heterogeneous catalytic process under supercritical conditions by CIR-FTIR. *Journal of catalysis*, 159 (1), 204-211.

deBoer, J.H., 1958. *The structure and properties of porous materials*. London, Butterworths.

deLucas, A., Canizares, P., Duran, A., Carrero, A., 1997. Coke formation, location, nature and regeneration on dealuminated H-ZSM5 type zeolites. *Applied catalysis A: General*, 156 (2), 299-317.

Denny, P.J. and Twigg, M.V., 1980. Factors determining the life of industrial heterogeneous catalysts. In: B. Delmon, and G.F. Froment, eds., 1980. *Catalyst deactivation, international symposium proceedings.* Amsterdam: Elsevier, 577-600.

Eckert, C.A. and Knutson, B.L., 1993. Molecular Charisma in Supercritical Fluids. *Fluid phase equilibria*, 83, 93-100.

Eckert, C. A. and Chandler, K., 1997. Tuning fluid solvents for chemical reactions. *The 4th International Symposium on Supercritical Fluids*, Sendai, Japan, 799-806.

Ekart, M.P., Bennett, K.L., Ekart, S.M., Gurdial, G.S., Liotta,C.L. and Eckert, C.A., 1993. Cosolvent interactions in supercritical fluid solutions. *American institute of chemical engineers journal*, 39 (2), 235-248.

El-Nafaty, U.A. and Mann, R., 1999. Support-pore architecture optimization in FCC catalyst particles using designed pore networks. *Chemical engineering science*, 54 (15-16), 3475-3484.

Evbuomwan, I., 2009. *The structural characterisation of porous media for use as model reservoir rocks, adsorbents and catalysts.* Ph.D. thesis. University of Bath.

Fan, L., Nakamura, I., Ishida, S. and Fujimoto, K., 1997. Supercritical phase alkylation reaction on solid acid catalysts: Mechanistic study and catalyst development. *Industrial and engineering chemistry research*, 36 (5), 1458-1463.

Fanning, P. E. and Vannice, M. A., 2002. A DRIFTS study of Cu-ZSM5 prior to and during its use for N_2O decomposition. *Journal of catalysis*, 207 (2), 166-182.

Farrauto, R.J. and Bartholomew, C.H., 1997. *Fundamentals of industrial catalytic processes*. London: Chapman & Hall, Kluwer Academic Publishers.

Fischer, A., Mallat, T. and Baiker, A., 1999. Continuous amination of propanediols in supercritical ammonia. *Angewandte chemie international*, 38 (3), 351-354.

Fogler, H. S., 2006. *Elements of Chemical Reaction Engineering. 4th Edition.* New York: Pearson.

Froment, G.F., 1982. A rigorous formulation of the effect of coke formation on catalyst acivitiy. In: J.L. Figueiredo, ed., 1982. *Progress in catalyst deactivation: Institute proceedings, NATO science series E.* The Hague: Martinus Nijhoff, 103-126

Frye, C.G. and Weitkamp, A.W., 1969. Equilibrium hydrogenations of multi-ring aromatics. *Journal of chemical and engineering data*, 14 (3), 372-376.

Fuller, G.G., 1976. A Modified Redlich-Kwong-Soave equation of state capable of representing the liquid state. *Industrial and engineering chemistry fundamentals*, 15 (4), 254-257.

Gao, Y., Liu, H.Z., Shi, Y.F. and Yuan, W.K., 1997. *The 4th international symposium on supercritical fluids*, Sendai, Japan, 531-534.

Gates, B.C., Katzer, J.R. and Schuit, G.C.A., 1979. *Chemistry of catalytic processes*. New York: McGraw-Hill.

Gil, B., Mierzynska, K., Szczerbinska, M. and Datka, J., 2007. In situ IR catalytic studies of the effect of coke on acid properties of steamed zeolite Y. *Microporous and mesoporous materials*, 99 (3), 328-333.

Ginosar, D.M. and Subramaniam, B., 1995. Olefinic oligomer and cosolvent effects on the coking and activity of a reforming catalyst in supercritical reaction mixtures. *Journal of catalysis*, 152 (1), 31-41.

Grotten, W.A., Wojciechowski, B.W. and Hunter, B.K., 1992. On the relationship between coke formation chemistry and catalyst deactivation. *Journal of catalysis*, 138 (1), 343-350.

Guisnet, M. and Magnoux, P., 1997. Deactivation by coking of zeolite catalysts: Prevention of deactivation, optimal conditions for regeneration. *Catalysis Today*, 36 (4), 477-483.

Guisnet, M. and Magnoux, P., 1994. Fundamental description of deactivation and regeneration of acid zeolites. In: B. Delmon and G.F. Froment, eds., 1994. *Catalyst deactivation, proceedings of the 6th international symposium*. Amsterdam: Elsevier. 53-68.

Guisnet, M. and Magnoux, P., 1989. Coking and deactivation of zeolites: Influence of the pore structure. *Applied catalysis*, 54 (1),1-27.

Guisnet, M., Magnoux, P. and Martin, D., 1997. Roles of acidity and pore structure in the deactivation of zeolites by carbonaceous deposits. In: C.H. Bartholomew and G.A Fuentes, eds., 1997. *Catalyst deactivation, proceedings of the 7th international symposium*. Amsterdam: Elsevier, 1-19.

Guisnet, M. and Magnoux, P., 2001. Organic chemistry of coke formation. *Applied catalysis A: General*, 212(1-2), 83-96.

Härröd, M., Macher, M.B., van den Hark, S. And Møller, P., 2001. Hydrogenation under supercritical single-phase conditions. In: A. Bertucco and G. Vetter, eds., 2001. *High pressure process technology: Fundamentals and applications*. Amsterdam: Elsevier B.V., 496-508.

Health and safety executive, 2011. General hazards of carbon dioxide. (online) Available at: http://www.hse.gov.uk/carboncapture/carbondioxide.htm

Hegedus, L.L. and McCabe, R.W., 1984. *Catalyst poisoning*. New York: Marcel Dekker.

Hegedus, L.L. and McCabe, R.W., 1980. Catalyst poisoning. In: B. Delmon and G.F. Froment, eds., 1980. *Catalyst deactivation, proceedings of international symposium*, 471-505.

Hitzler, M.G., Smail, F.R., Ross, S.K. and Poliakoff, M., 1998. Friedel–Crafts alkylation in supercritical fluids: continuous, selective and clean. *Chemical communications, 29 (20),* 359-360.

Hiyoshi, N., Osada, M., Rode, V., Sato, O. and Shirai, M., 2007. Hydrogenation of benzothiophene-free naphthalene over charcoal-supported metal catalysts in supercritical carbon dioxide solvent. *Applied catalysis A: General*, 331, 1-7.

Hooper, R.J., Battaerd, H.A.J. and Evans, D.G., 1979. Thermal dissociation of tetralin between 300 and 450 °C. *Fuel*, 58 (2), 132-138.

Huang, T. and Kang, B., 1995. Naphthalene Hydrogenation over Pt/Al2O3 Catalyst in a Trickle Bed Reactor. *Industrial and engineering chemistry research*, 34 (7), 2349-2357.

Hughes, R., 1984. *Deactivation of catalysts*. London: Academic Press.

Humphries, A., Harris, D.H. and O'connor, P., 1993. The nature of active sites in zeolites: Influence on catalyst performance. In J.S. Magee and M.M. Mitchell, Jr. eds., 1993. *Fluid Catalytic Cracking: Science and Technology.* Amsterdam: Elsevier B.V., 41-82.

Johnston, K.P., Peck, D.G. and Kim, S., 1989. Modeling supercritical mixtures: How predictive is it? *Industrial and engineering chemistry research*, 28 (8), 1115–1125.

Kabadi, V.N. and Danner, R.P., 1985. A modified Soave-Redlich-Kwong equation of state for water-hydrocarbon phase equilibria. *Industrial and engineering chemistry process design and development*, 24 (3), 537-541.

Karge, H.G., 1991. Coke formation on zeolites. In: H. van Bekkum, E.M. Flanigen and J.C. Jansen, eds., 1991. *Introduction to Zeolite Science and Practice*. Amsterdam: Elsevier, 531-570.

Karger, J. and Pfeifer, H., 1987. NMR self-diffusion studies in zeolite science and technology. *Zeolites*, 7 (2), 90-107.

Koizumi, N., Hamabe, Y., Jung, S., Suzuki, Y., Yoshida, S. And Yamada, M., 2010. *In situ* observation of Ni-Mo-S phase formed on $NiMo/Al_2O_3$ catalyst sulfided at high pressure by means of Ni and Mo *K*-edge EXAFS spectroscopy. *Catalysis letters*, 135 (3-4), 175-181.

Köll, P. And Metzger, J., 1978. Thermal degradation of cellulose and chitin in supercritical acetone. *Angewandte chemie international*, 17 (10), 754-755.

Law, S. and Lielmezs, J., 1984. Modified van der Waals equation of state for saturated vapour-liquid equilibrium. *Thermochimica acta*, 84, 71-81.

Lee, H. and Thodos, G., 1983. Generalized treatment of self-diffusivity for the gaseous and liquid states of fluids. *Industrial and engineering chemistry fundamentals*, 22 (1), 17-26.

Li, D., Li, M., Chu, Y., Nie, H. and Shi, Y., 2003. Skeletal isomerization of light FCC naphtha. *Catalysis today*, 81 (1), 65-73.

Li, C., Chen, Y., Yang, S. and Yen, R., 1994. In-situ FTIR investigation of coke formation on USY zeolite. *Applied surface science*, 81 (4), 465-468.

Lin, S.D. and Song, C., 1996. Noble metal catalysts for low-temperature naphthalene hydrogenation in the presence of benzothiophene. *Catalysis today*, 31 (1-2), 93-104.

Lin, X., Fan, Y., Shi, G., Liu, H. and Bao, X., 2007. Coking and deactivation behavior of HZSM5 zeolite-based FCC gasoline hydro-upgrading catalyst. *Energy and Fuels*, 21 (5), 2517-2524.

Lowell, S., Shields, J.E., Thomas, M.A.M. and Thommes, M., 2004. *Characterization of porous solids and powders: surface area, pore zide and density*. Dordrecht: Kluwer Academic Publishers.

Lowell, S. and Shields, J.E., 1991. *Powder surface area and porosity. 3rd edition*. London: Chapman & Hall.

Macher, M.B., Högberg, J., Moller, P. and Härröd, M., 1999. Partial hydrogenation of fatty acid methyl esters at supercritical conditions. *European journal of lipid science and technology*, 101 (8)**,** 301-305.

Manos, G. and Hofmann, H., 1991. Coke removal from a zeolite catalyst by supercritical fluids. *Chemical engineering and technology*, 14 (1), 73-78.

Marafi, A., Hauser, A. and Stanislaus, A., 2007. Deactivation patterns of Mo/Al_2O_3, $Ni\text{-}Mo/Al_2O_3$ and $Ni\text{-}MoP/Al_2O_3$ catalysts in atmospheric residue hydrodesulphurization. *Catalysis today*, 125 (3-4), 192-202.

Masuda, T., Tomita, P., Fujikata, Y. and Hashimoto K., 1999. Deactivation of HY-type zeolite catalyst due to coke deposition during gas-oil cracking. In: B. Delmon and G.F. Froment, eds., 1999. *Catalyst deactivation, proceedings of the 8th international symposium*. Amsterdam: Elsevier, 89-96.

Matsushita, K., Hauser, A. and Marafi, A., 2004. Initial coke deposition on hydrotreating catalysts, Part 1. Changes in coke properties as a function as a function of time on stream. *Fuel*, 83 (7-8), 1031-1038.

McCoy, B.J. and Subramaniam, B., 1995. Continuous-mixture kinetics of coke formation from olefinic oligomers. *American institute of chemical engineers journal*, 41 (2), 317-323.

Minchev, Ch., Kanazirev, V., Mavrodinova, V., Penchev, V. and Lechert, H., 1989. On the nature of the catalytic activity of SAPO-5. In H.G. Karge and J. Weitkamp, eds., 1989. *Zeolites as catalysts, sorbents, and detergent builders: Applications and innovations*. Amsterdam: Elsevier B.V., 29-38.

Minder, B., Mallat, T., Pickel, K.H., Steiner, K. and Baiker, A., 1995. Enantioselective hydrogenation of ethyl pyruvate in supercritical fluids. *Catalysis letters*, 34 (1-2), 1-9.

Mihindou-Koumba, P.C., Comparot, J.D., Laforge, S. and Magnoux, P., 2008. Methylcyclohexane transformation over H-EU-1 zeolite: Selectivity and catalytic role of the acid sites located at the pore mouths. *Journal of catalysis*, 255 (2), 324-334.

Miyazawa, T. and Pitzer, K.S., 1958. Thermodynamic functions for gaseous cis- and trans-decalins from 298 to 1000K. *Journal of American chemical society*, 80, 60-62.

Mochida, I., Zhao, X.Z., Sakanishi, K., Yamamoro, S., Takashuira, H. and Vemura, S., 1989. Structure and properties of sludges produced in the catalytic hydrocracking of vacuum residue. *Industrial and engineering chemistry research*, 28 (4), 418-421.

Monteiro-Gezork, A.C.A., Effendi, A. and Winterbottom, J.M., 2007. Hydrogenation of naphthalene on NiMo- and Ni/Al2O3 catalysts: Pre-treatment and deactivation. *Catalysis Today*, 128 (1-2), 63-73.

Mori, N., Nishiyama, S., Tsuruya, S. and Masai, M., 1991. Deactivation of zeolites in n-hexane cracking. *Applied catalysis*, 74 (1), 37-52.

Naccache, C., 1985. Deactivation of acid catalysts. In: J. Oudar and H. Wise, eds., 1985. *Deactiuation and poisoning of catalysts*. New York: Marcel Dekker, 185-203.

New world encyclopedia, 2011. Supercritical fluid. (online) Available at: http://www.newworldencyclopedia.org/entry/Supercritical_fluid.

Niu, F.H., Kolb, G. and Hofmann, H., 1995a. In-situ regeneration of the coked Y-zeolite under supercritical conditions by example of ethylbenzene disproportionation. *Chemische technik (Leipzig)*, 47 (2), 68-73.

Niu, F.H., Kolb, G. and Hofmann, H., 1995b. Deactivation kinetics and modeling of coke removal under supercritical conditions for the example of ethylbenzene disproportionation. *Chemical engineering and technology*, 18 (4), 278-283.

Niu, F.H. and Hofmann, H., 1996. Investigation of various zeolite catalysts under supercritical conditions. *Process technology proceedings*, 12, 145-150.

Niu, F.H. and Hofmann, H., 1997a. Investigation of coke extraction from zeolite-HY under supercritical and near-critical conditions. The *Canadian journal of chemical engineering*, 75 (2), 346-352.

Niu, F.H. and Hofmann, H., 1997b. Studies on deactivation kinetics of a heterogeneous catalyst using a concentration controlled recycle reactor under supercritical conditions. *Applied catalysis A: General*, 158 (1-2), 273-285.

Oudar, J. and Wise, H., 1985. *Deactivation and poisoning of catalysts*. New York: Marcel Dekker.

Paál, Z. and Menon, P.G., 1988. *Hydrogen effects in catalysis: fundamentals and practical applications*. New York: Marcel Dekker Incorporated. Pawelec, B., La Parola, V., Thomas, S. and Fierro, J.L.G., 2006. Enhancement

of naphthalene hydrogenation over $PtPd/SiO_2$-Al_2O_3 catalyst modified by gold. *Journal of molecular catalysis A: Chemical*, 253 (1-2), 30-43.

Peña, J.A., Herguido, J. and Guimon, C., 1996. Hydrogenation of acetylene over $Ni/NiAl_2O_4$ catalyst: characterization, coking, and reaction studies. *Journal of Catalysis*, 159 (2), 313-322.

Peters, C.J., 1994. Multiphase equilibria in near-critical solvents. In E. Kiran and J.M.H. Levelt Sengers, eds., 1994. *Supercritical Fluids: Fundamentals for Application*; Dordrecht: Kluwer Academic Publishers, 117-146.

Petkovic, L.M., Ginosar, D.M. and Burch, K.C., 2005. Supercritical fluid removal of hydrocarbons adsorbed on wide-pore zeolite catalysts. *Journal of catalysis*, 234 (2), 328-339.

Pham, H.N., Reardon, J. and Abhaya, K.D., 1999. Measuring the strength of slurry phase heterogeneous catalysts. *Powder technology*, 103 (2), 95-102.

Pu, S.B. and Inui, T., 1997. Diffuse reflectance IR spectroscopic study on hydroxyl groups of H-ZSM5s having different sizes and properties. *Zeolites*, 19 (5-6), 452-454.

Quann, R.J., Green, L.A., Tabak, S.A. and Krambeck, F.J., 1988. Chemistry of olefin oligomerization over ZSM5 catalyst. *Industrial and engineering chemistry research*, 27 (4), 565-570.

Ramôa Ribeiro, F., Alvarez, F., Henriques, C., Lemos, F., Lopes, J.M. and Ribeiro, M.F., 1995. Structure-activity relationship in zeolites. *Journal of molecular catalysis A: Chemical*, 96 (3), 245-270.

Rautanen, P.A., Lylykangas, M.S., Aittamaa, J.R. and Krause, A.O.I., 2002. Liquid-phase hydrogenation of naphthalene and tetralin on Ni/Al2O3: Kinetic modelling. *Industrial and engineering chemistry research*, 41 (24), 5966-5975.

Reid, R.C., Prausnitz, J.M. and Poling, B.E., 1988. *The properties of gases and liquids*. 4th edition. New York: McGraw-Hill.

Rigby, S.P., 2002. New methodologies in mercury porosimetry. In F. Rodriguez-Reinoso, B. McEnaney, J. Rouquerol and K. Unger, eds., 2002. *Characterization of Porous Solids VI, Proceedings of the 6th International Symposium on the Characterization of Porous Solids.* Amsterdam: Elsevier, 185-192.

Rigby, S.P., Watt-Smith, M.J. and Fletcher, R., 2005. Integrating gas sorption with mercury porosimetry. *Adsorption*, 11 (1), 201-206.

Rigby, S.P. and Fletcher, R.S., 2004a . Interfacing mercury porosimetry with nitrogen sorption. *Particle & particle systems characterization*, 21 (2), 138-148.

Rigby, S.P., Watt-Smith, M.J. and Fletcher, R.S., 2004b. Simultaneous determination of the pore length distribution and pore connectivity for porous catalyst supports using integrated nitrogen sorption and mercury porosimetry. *Journal of catalysis*, 227 (1), 68-76.

Rollmann, L.D. and Walsh, D.E., 1979. Shape selectivity and carbon formation in zeolites. *Journal of catalysis*, 56, 139-140.

Romero, C.M.C., Thybaut, J.W. and Martin, G.B., 2008. Naphthalene hydrogenation over a NiMo/γ-Al_2O_3 catalyst: Experimental study and kinetic modelling. *Catalysis today*, 130 (1), 231-242.

Roque-Malherbe, R., Wendelbo, R., Mifsud, A. and Corma, A., 1995. Diffusion of aromatic hydrocarbons in H-ZSM-5, H-Beta, and H-MCM-22 zeolites. *The journal of physical chemistry*, 99 (38), 14064-14071.

Rostrup-Nielsen J.R. and Trimm, D.L., 1977. Mechanisms of carbon formation on nickel-containing catalysts. *Journal of catalysis*, 48 (1-3), 155-165.

Rouquerol, F., Rouquerol, J. and Sing, K., 1999. *Adsorption by powders and porous solids: principles, methodology and applications*. London: Academic Press.

Sahoo, S.K., Ray, S.S. and Singh, I.D., 2004. Structural characterization of coke on spent hydroprocessing catalysts used for processing of vacuum gas oils. *Applied catalysis A: General*, 278 (1), 83-91.

Sahoo, S.K., Viswanadham, N., Ray, N., Gupta, J.K. and Singh, I.D., 2001. Studies on acidity, activity and coke deactivation of ZSM-5 during *n*-heptane aromatization . *Applied catalysis A: General*, 205 (1-2), 1-10.

Saim, S. and Subramaniam, B., 1990. Isomerization of 1 -hexene on Pt/y-A1203 catalyst at subcritical and supercritical reaction conditions: Pressure and temperature effects on catalyst activity. *The journal of supercritical fluids*, 3 (4), 214-221.

Saim, S. and Subramaniam, B., 1991. Isomerization of 1-hexene over Pt/gamma-Al2O3 catalyst: Reaction mixture density and temperature effects on catalyst effectiveness factor, coke laydown, and catalyst micromeritics. *Journal of catalysis*, 131 (2), 445-456.

Saito, A. and Foley, H.C., 1991. Curvature and Parametric Sensitivity in Models for Adsorption in Micropores. *American institute of chemical engineers journal*, 37 (3), 429-436.

Salguero, C.C., Lam, Y.L. and Schmal, M., 1997. Propane transformation over H-ZSM5 Zeolite Modified with Germanium. *Catalysis letters*, 47 (2), 143-154.

Sapre, A.V. and Gates, B.C., 1981. Hydrogenation of aromatic hydrocarbons catalyzed by sulfided cobalt oxide-molybdenum oxide/.alpha.-aluminum oxide. Reactivities and reaction networks. *Industrial and engineering chemistry process design and development*, 20 (1), 68-73.

Satterfield, C.N., 1991. *Heterogeneous Catalysis in Industrial Practice*. 2nd Edition. New York: McGraw Hill.

Savage, P.E., Gopalan, S., Mizan, T.I., Martino, C.J. and Brock, E.E., 1995. Reactions at supercritical conditions: Applications and fundamentals. *American institute of chemical engineers journal*, 41 (7), 1723-1778.

Schaink, H.M. and Venema, P., 2007. The van der Waals equation of state and the law of corresponding states: A spreadsheet experiment. *Journal of chemical education*, 84 (12), 2030.

Schmitz, A.D., Bowers, G. and Song, C., 1996. Shape-selective hydrogenation of naphthalene over zeolite-supported Pt and Pd catalysts. *Catalysis today*, 31 (1-2), 45-56.

Schneider, G.M., 1994. Physicochemical properties and phase equilibria of pure fluids and fluid mixtures at high pressures. In E. Kiran and J. Levelt Sengers, eds., 1994. *Supercritical fluids* f*undamentals for application:* NATO ASI Series E, Applied Sciences. Dordrecht: Kluwer academic publishers, 91–115.

Schoonheydt, R.A. and Uytterhoeven, J.B., 1970. Influence of temperature on the OH-band Intensity in the infrared spectra of decationated zeolites X and Y. *Journal of catalysis*, 19 (1), 55-63.

Sekine, H., Ohshima, M., Kurokawa, H. and Miura, H., 2008. Liquid phase hydrogenation of naphthalene in the presence of CO over supported Ni catalyst. *Reaction kinetics and catalysis letters*, 95 (1), 99-105.

Shao, J. and Song, C., 2001. Regioselective hydrogenation of 1-naphthol over supported Pt and Pd catalysts for producing high-temperature jet fuel stabilizer. *Catalysis today*, 65 (1), 59-67.

Song, C. and Schmitz, A.D., 1996. Zeolite-supported Pd and Pt catalysts for low-temperature hydrogenation of naphthalene in the absence and presence of benzothiophene. *Energy and fuels*, 11 (3), 656-661.

Sotelo, J.L., Uguina, M.A., Valverde, J.L. and Serrano, D.P., 1994. Deactivation of toluene alkylation with methanol over magnesium-modified ZSM5 shape selectivity changes induced by coke formation. *Applied catalysis A: General*, 114 (2), 273.

Subramaniam, B., 2001. Enhancing the stability of porous catalysts with supercritical reaction media. *Applied catalysis A: General*, 212 (1-2), 199-213.

Subramaniam, B. and McCoy, B.J., 1994. Catalyst activity maintenance or decay: A model for formation and desorption of coke. *Industrial and engineering chemistry research*, 33 (3), 504-508.

Subramaniam, B. and McHugh, M.A., 1986. Reactions in supercritical fluids: A reveiw. *Industrial and engineering chemistry process design and development*, 25 (1), 1-12.

Sundaramurthy, V. and Lingappan, N., 2000. Isomorphic substitution of boron in ZSM5 type zeolites by using TBP as template. *Journal of molecular catalysis A: Chemical*. 160 (2), 367-375.

Süer, M.G., Dardas, Z., Lu, Y., Moser, W.R. and Ma, Y.H., 1997. In-situ CIR-FTIR study of the diffusion of supercritical hydrocarbons in zeolite L. *American institute of chemical engineers journal*, 43 (7), 1717-1726.

Szostak, R., 2001. Secondary synthesis methods. In H. Van Bekkum, P.A. Jacobs, E.M. Flanigen and J.C. Jansen, eds., 2001. *Introduction to zeolite science and practice*. Amsterdam: Elsevier B.V., 261-298.

Tabak, S.A., Krambeck, F.J. and Garwood, W.E., 1986. Conversion of propylene and butylene over ZSM-5 catalyst. *American institute of chemical engineers journal,* 32 (9), 1526-1531.

Thakur, D.S. and Thomas, M.G., 1984. Catalyst deactivation during direct coal liquefaction: A review. *Industrial and engineering chemistry product research and development*, 23 (3), 349-360.

Tiltscher, H., Wolf, H. and Schelchshorn , J., 1981. A mild and effective method for the reactivation or maintenance of the activity of heterogeneous catalysts. *Angewandte chemie international edition*, 20 (10), 892-894.

Tiltscher, H., Wolf, H. And Schelchshorn, J., 1984. Utilization of supercritical fluid solvent-effects in heterogeneous catalysis. *Berichte der bunsengesellschaft für physikalische chemie*, 88 (9), 897-900.

Trabelsi, F., Stüber, F., Abaroudi, K., Larrayoz, M.A., Recasens, F. and Sueiras,J.E., 2000. Coking and ex situ catalyst reactivation using supercritical CO_2: A preliminary study. *Industrial and engineering chemistry research*, 39 (10), 3666-3670.

Tiltscher, H. and Hofmann, H., 1987. Trends in high pressure chemical engineering. *Chemical engineering science*, 42 (5), 959-977.

Trimm, D.L., 1977. The formation and removal of coke from nickel catalyst. *Catalysis reviews: Science and engineering*, 16 (2), 155-189.

Trimm, D.L., 1983. Catalyst design for reduced coking. *Applied catalysis*, 5 (3), 263-290.

Trombetta, M., Busca, G., Rossini, S., Piccoli, V. and Cornaro, U., 1997. FTIR studies on light olefin skeletal isomerization catalysis. II. The interaction of C4 olefins and alcohols with HZSM5 zeolite. *Journal of catalysis*, 168 (2), 349-363.

Uguina, M.A., Serrano, D.P., Grieken, R.V. and Venes, S., 1993. Adsorption, acid and catalytic changes induced in ZSM-5 by coking with different hydrocarbons. *Applied catalysis*, 99 (2), 97-113.

Wang, B. and Manos, G., 2007. A novel thermogravimetric method for coke precursor characterisation. *Journal of catalysis*, 250 (1), 121-127.

Wang, B. and Manos, G., 2007. Acid site characterisation of coked USHY zeolite using temperature programmed desorption with a component non-specific detector. *Industrial and engineering chemistry research*, 46 (24), 7977-7983.

Wang, J., Chigada, P., Rigby, S.P., Al-Duri, B. and Wood, J., 2009. Prolonging catalyst lifetime in supercritical isomerization of 1-hexene over a platinum/alumina catalyst. *Chemical engineering science*, 64 (15), 3427-3436.

Wang, J., Hassan, F., Chigada, P.I., Rigby, S.P., Al-Duri, B. and Wood, J., 2009. Coke formation and characterization during 1-hexene isomerization and oligomerization over H-ZSM5 catalyst under supercritical conditions. *Industrial and engineering chemistry research*, 48 (17), 7899-7909.

Ward, J.W., 1968. The nature of active sites on zeolites: VI. The influence of calcination temperature on the structural hydroxyl groups and acidity of stabilized hydrogen Y zeolite. *Journal of catalysis*, 11 (3), 251-258.

Wei, Y.S., Sadus, R.J., 2000. Equations of state for the calculation of fluid-phase equilibria. *American institute of chemical engineers journal*, 46 (1), 169-196.Weitkamp, A.W., 1968. Stereochemistry and mechanism of hydrogenation

of naphthalenes on transition metal catalysts and conformational analysis of the products. *Advances in catalysis*, 18, 1-110.

Winterbottom, J.M. and King, M.B., eds., 1999. *Reactor design for chemical engineers*. Cheltenham: Stanley Thornes LTD.

Wolf, E.E. and Alfani, F., 1982. Catalysts deactivation by coking. *Catalysis reviews: Science and engineering*, 24 (3), 329-371.

Xu, Z. and Sandler, S.I., 1987a. Temperature-dependent parameters and the Peng-Robinson equation of state. *Industrial and engineering chemistry research*, 26 (3), 601–606.

Xu, Z. and Sandler, S.I., 1987b. Application to mixtures of the Peng-Robinson equation of state with fluid-specific parameters. *Industrial and engineering chemistry research*, 26 (6), 1234-1238.

Zhan, X. and Guin, J.A., 1994. High-Pressure Hydrogenation of Naphthalene Using a Reduced Iron Catalyst. *Energy and fuels*, 8 (6), 1384- 1393.

CHAPTER 8

APPENDICES

8.1 Papers published

8.2. Equation of state verification

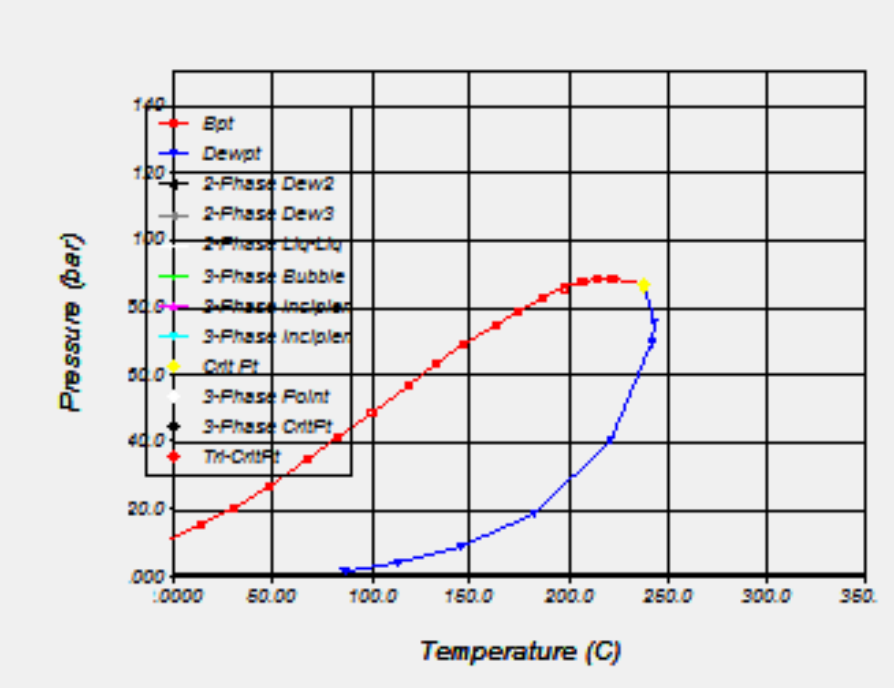

Figure 8.1. Phase diagram for benezene-ethane.

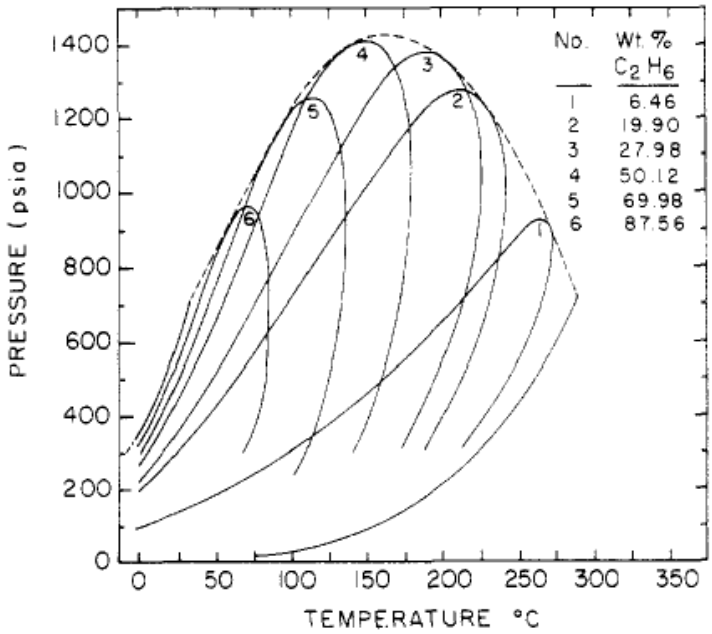

Figure 8.2. Phase diagram for benezene-ethane system by Kay and Nevens, 1952 (Figure taken from Subramaniam and McHugh, 1986).

8.3. Gas chromatograph calibration curves

8.3.1. Gas chromatograph

Peak	Ret. Time (min)
1. 1-hexene	1.75
2. trans(cis)-3-hexene	
trans-2-hexene	1.80
3. cis-2-hexene	1.84
4. dimers (C12)	10-15
5. *	20-25
6. *	25-30

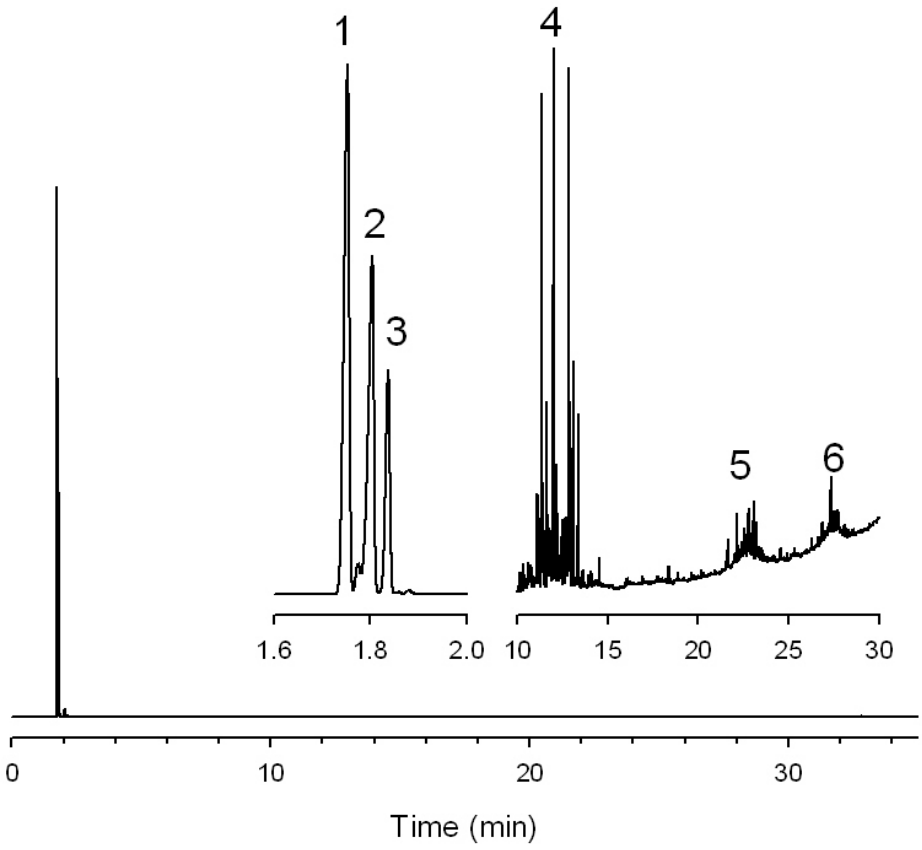

Figure 8.3. GC-Chromatogram (1-hexene and its isomers).

8.3.2. GC calibration curves

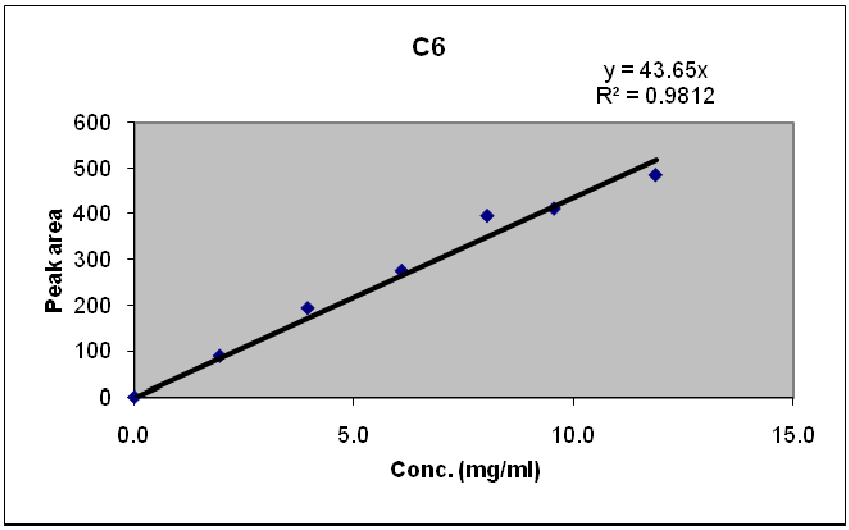

Figure 8.4. Calibration curve for 1-hexene C_6 isomer.

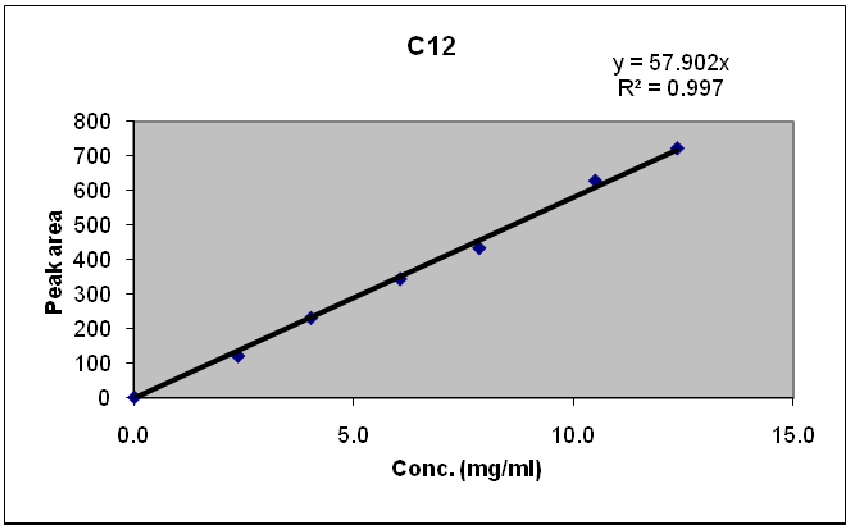

Figure 8.5. Calibration curve for 1-hexene, C_{12}.

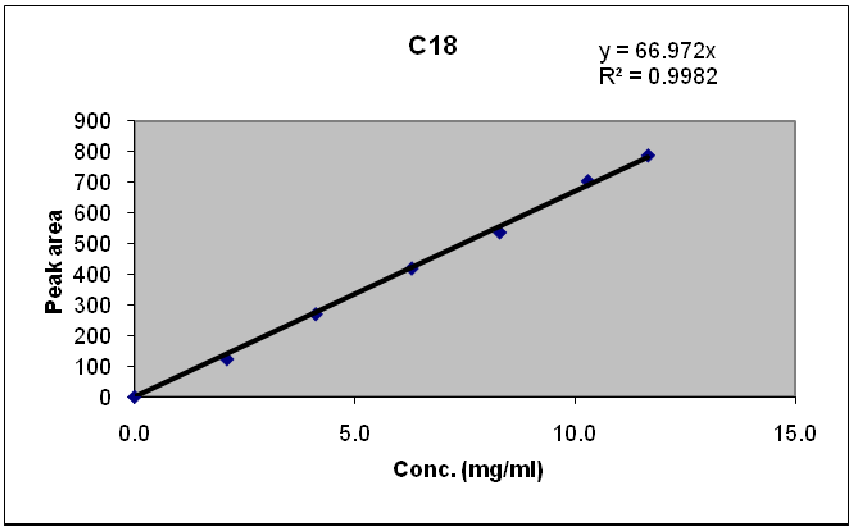

Figure 8.6. Calibration curve for C_{18} (1-hexene isomerisation).

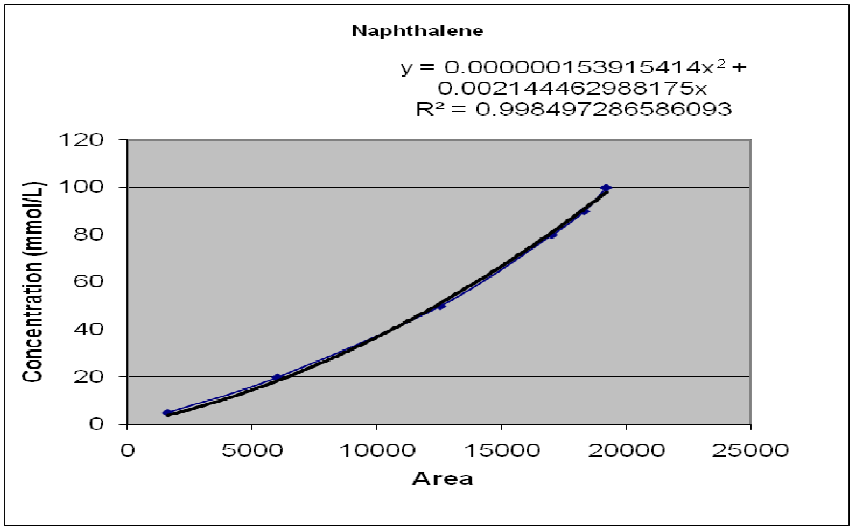

Figure 8.7. Calibration curve for naphthalene hydrogenation.

8.4. HYSYS flash calculation

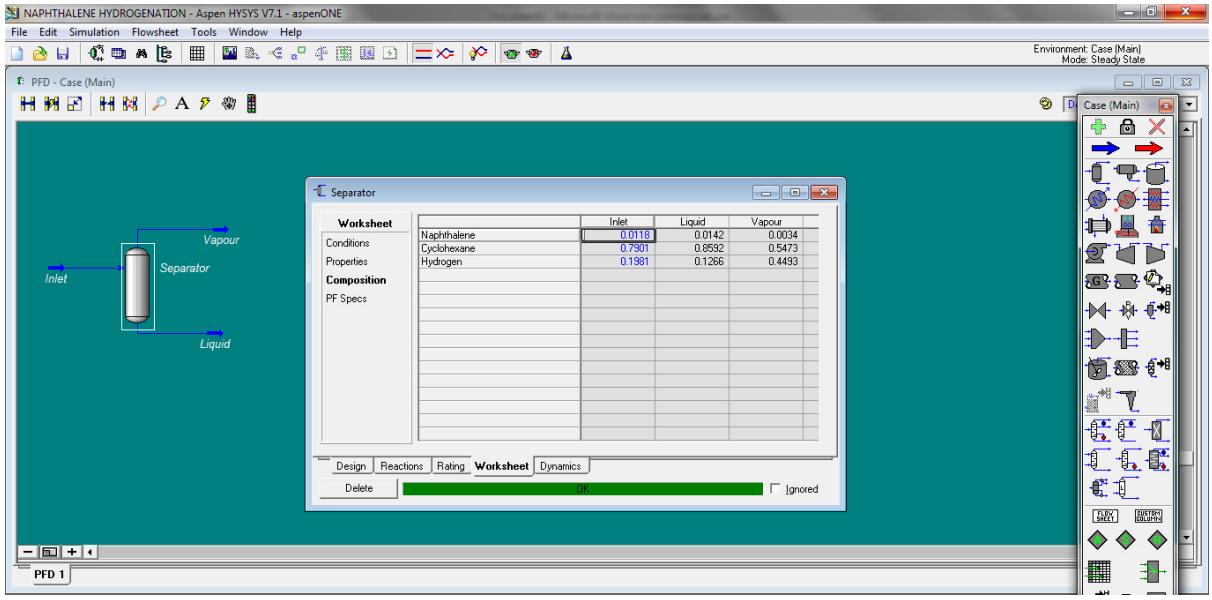

Figure 8.8. Screen shot of HYSYS naphthalene hydrogenation case.

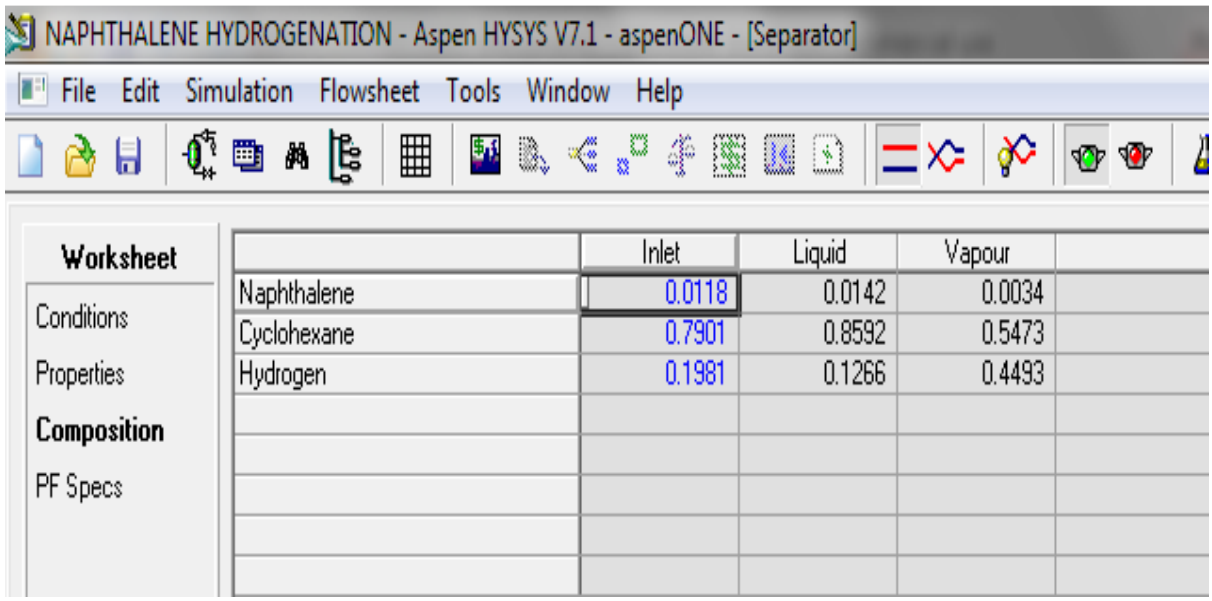

Figure 8.9. Screen shot of HYSYS flash calculation.

8.5. N_2 bubbeling graph

N_2 was bubbled through the 1-hexene feed tank for 45 minutes and 2 hours prior to commencing the experiment. The results in Figure 8.10 shows that similar conversions were achieved.

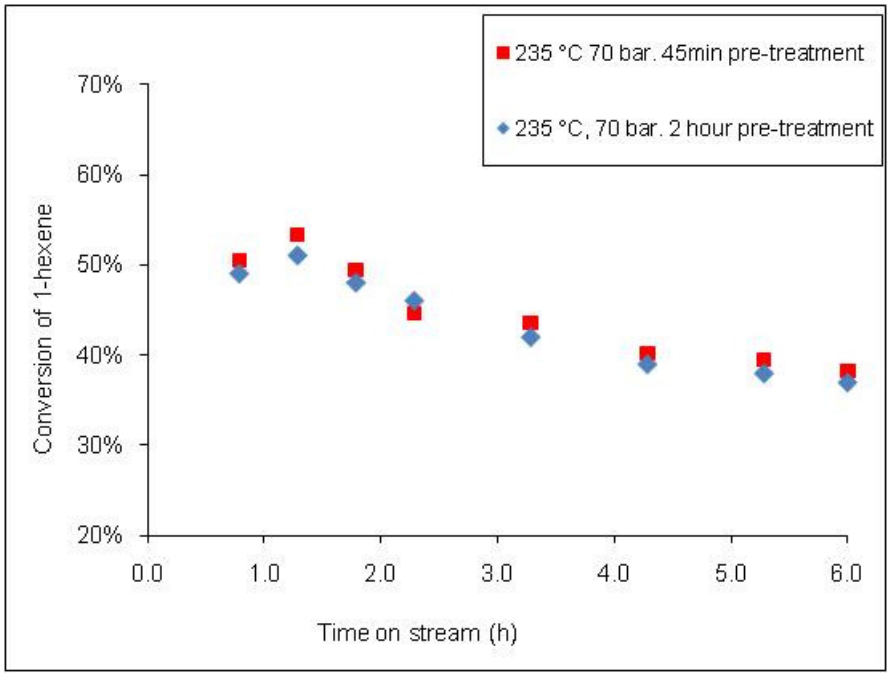

Figure 8.10 N_2 bubbling results for Y zeolite catalyst

8.6 Example diffusion calculation

According to Lee and Thodos correlation the self diffusivity of n-hexane at the critical point is

$$D_c = \frac{0.77*10^{-5}}{\delta}$$

$$= 0.77 * \frac{10^{-5}}{0.01242}$$

$$= 6.19 * 10^{-4}\,\text{m}^2/\text{s}$$

8.7. TPD example calculation for fresh Y zeolite catalyst

$$Number\ of\ acid\ sites\ \left(\frac{mmol}{g}\right) =$$

$$= 0.137 * \frac{A_{with\ TBA}}{(1-c)\ W_1} - \frac{A_{without\ TBA}}{(1-c)\ W_2}$$

$$= 0.137 * \frac{0.869692}{(1-0)*0.0888} - \frac{0.326348}{(1-0)*0.071}$$

$$= 0.712 mmol/g$$

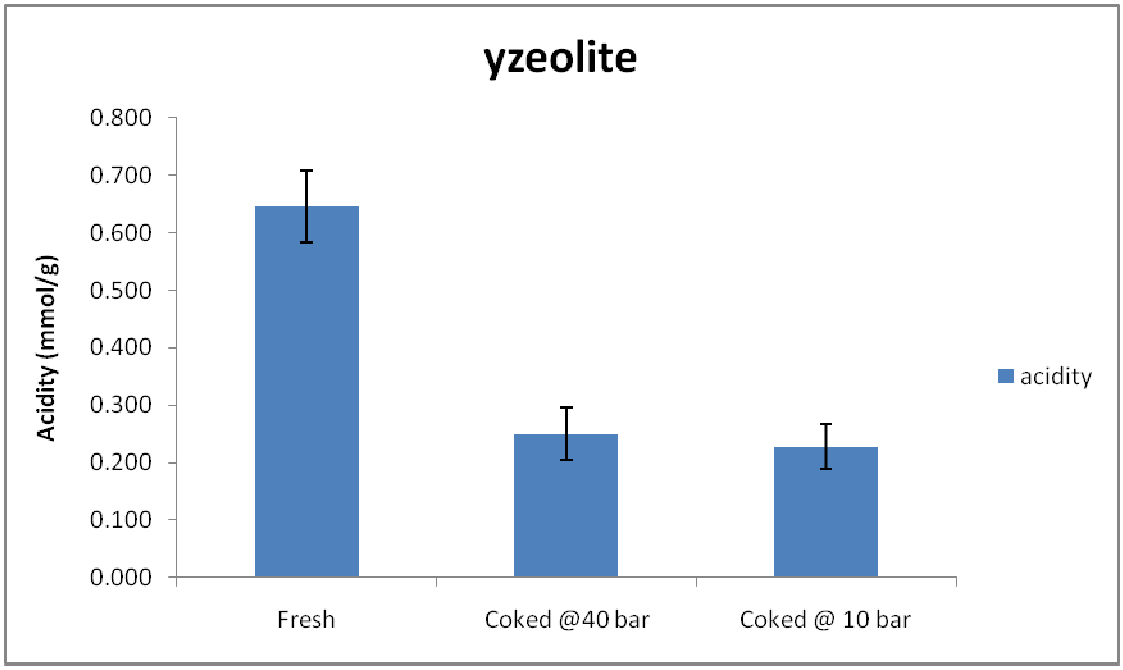

Figure 8.11. Zeolite Y mean acidity.

8.8. Chapter 6 additional data

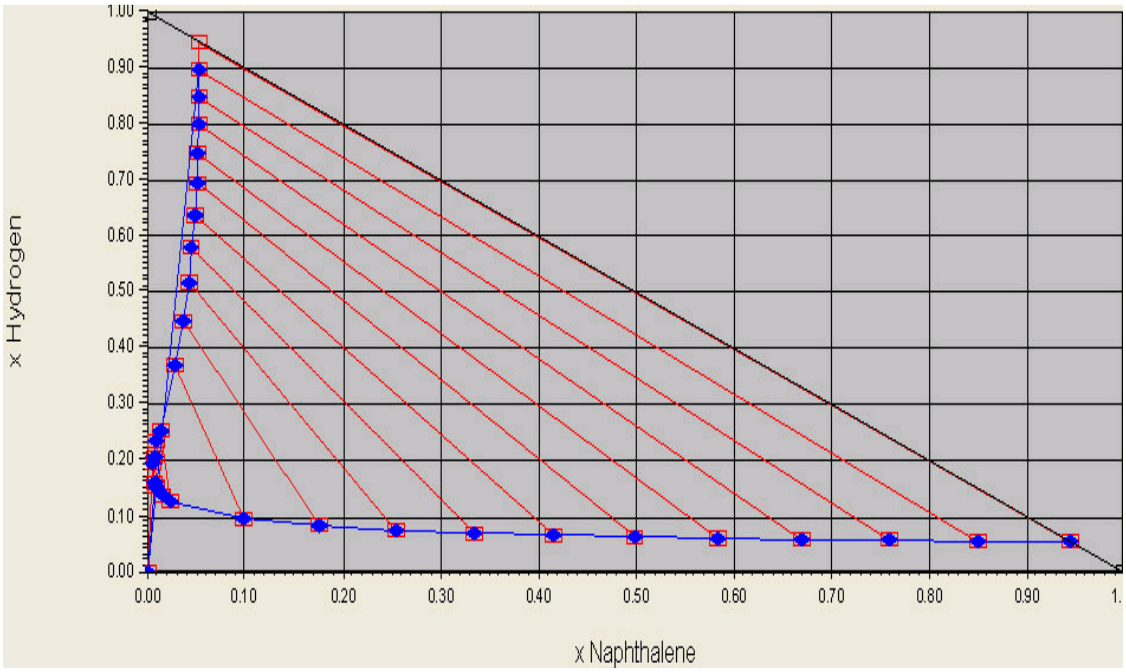

Figure 8.12. Phase diagram for 270 ℃, 80 bar.

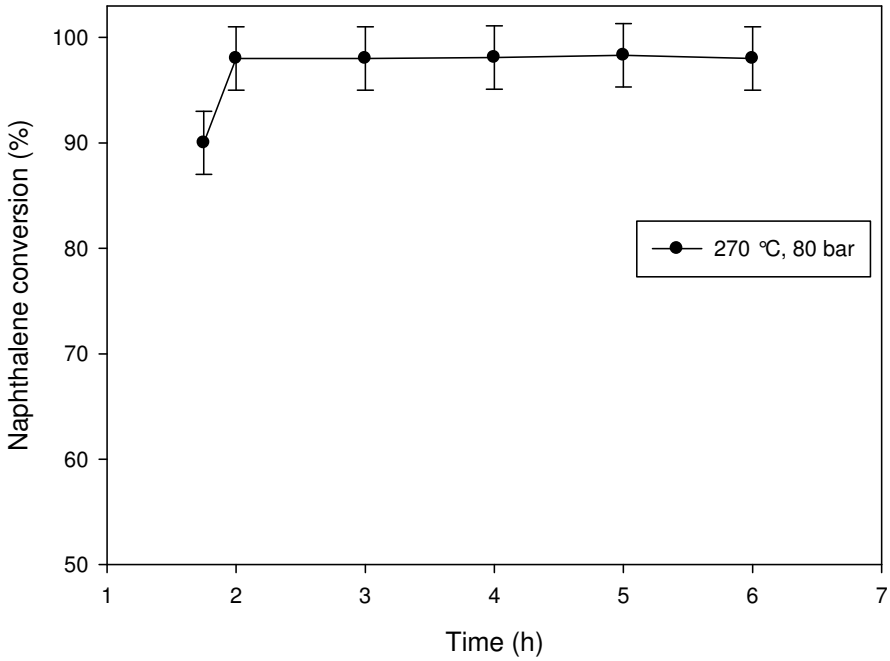

Figure 8.13. Napthalene conversion again time on stream at 270 ℃, 80 bar.

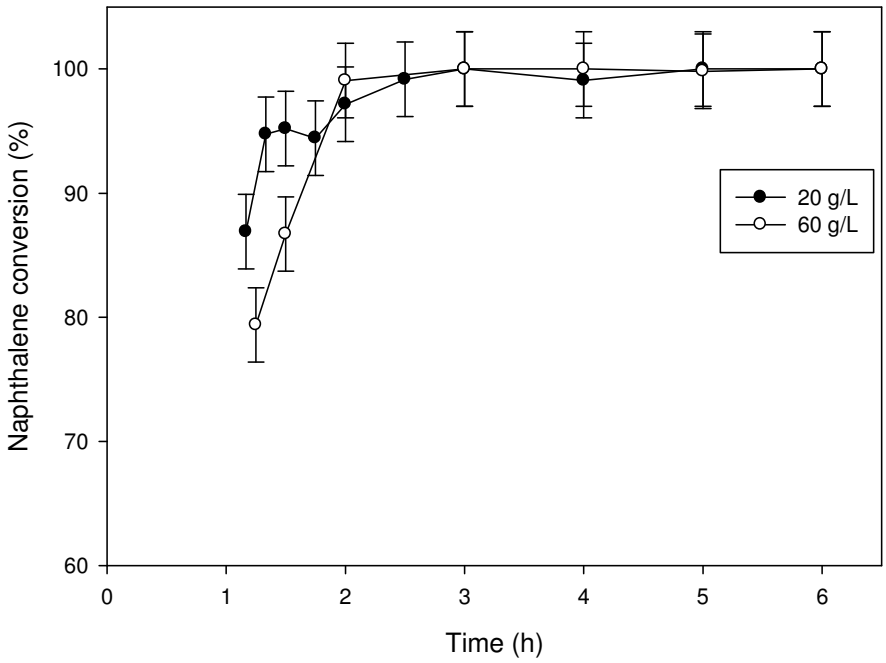

Figure 8.14. Napthalene conversion again time on stream at 20 and 60 g/L naphthalene feed concentration at 300 ℃, 80 bar reaction conditions.

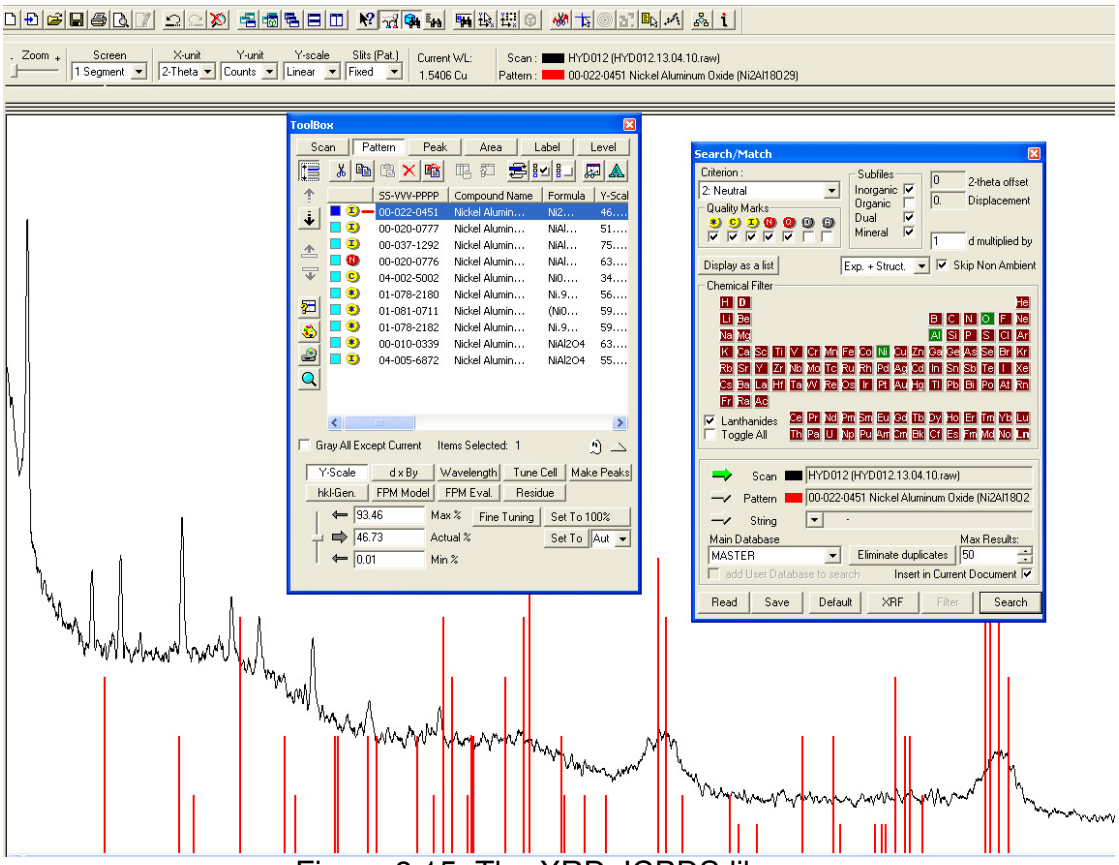

Figure 8.15. The XRD JCPDS library

8.9 BET plot typical fit

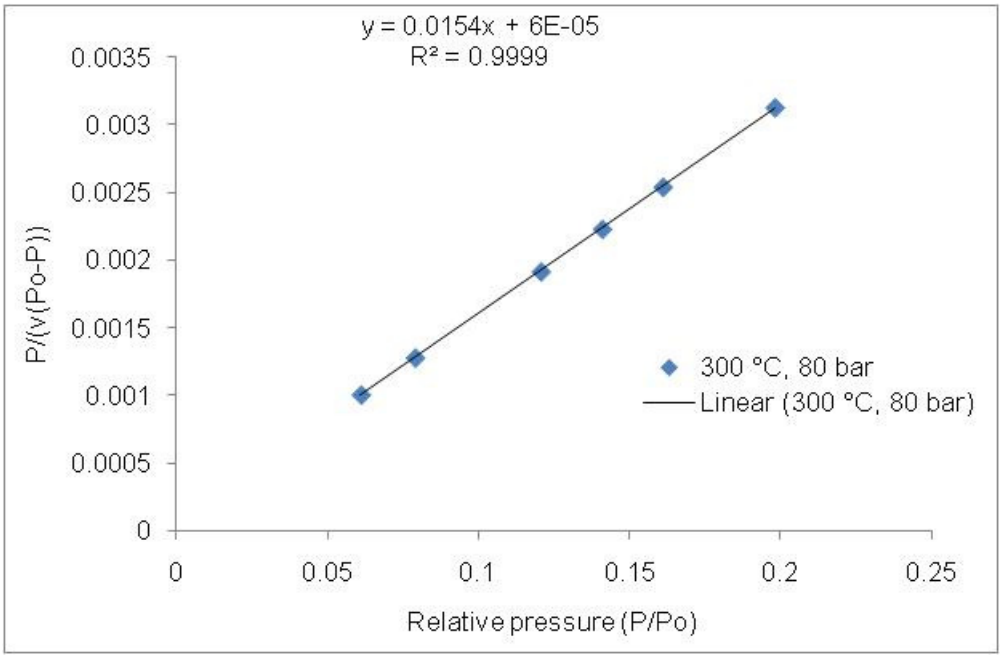

Figure 8.16 Typical fit for the BET plot

Paper 1:

Coke Formation and Characterization During 1-Hexene Isomerization and Oligomerization over H-ZSM-5 Catalyst under Supercritical Conditions.

Jiawei Wang, Faiza Hassan, Peter I. Chigada, Sean P. Rigby, Bushra Al-Duri, and Joseph Wood.

Ind. Eng. Chem. Res., 2009, *48* (17), pp 7899–7909.

DOI: 10.1021/ie801466d

Paper 2:

Deactivation during 1-Hexene Isomerization over Zeolite Y and ZSM5 Catalysts under Supercritical Conditions.

Faiza Hassan, Jiawei Wang, Peter I. Chigada, Bushra Al-Duri, Sean P. Rigby, and Joseph Wood.

Ind. Eng. Chem. Res., 2011, *50* (12), pp 7161–7171.

DOI: 10.1021/ie101876f